CDF Study Report

NG-CryoIRTel

Assessment of Next Generation Cryogenic Infra Red Telescope
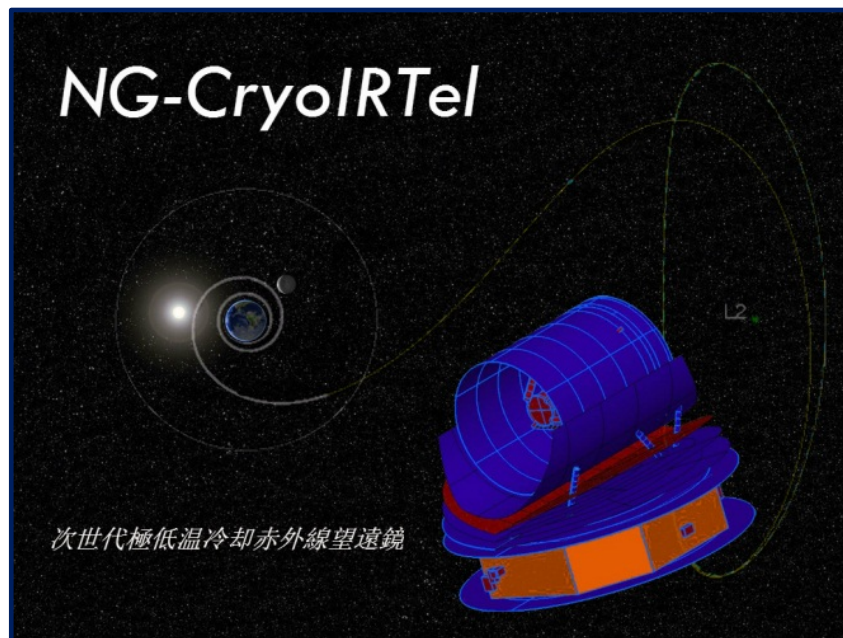
Further information and/or additional copies of the report can be requested from:

Martin Linder
ESA/ESTEC/SRE-FMI
Postbus 299
2200 AG Noordwijk
The Netherlands
Tel: +31-(0)71-5654463
Fax: +31-(0)71-5655985
Martin.Linder@esa.int

Munetaka Ueno
Institute of Space and Astronautical Science, JAXA
3-1-1 Yoshino-dai, Chuo-ku
Sagamihara, Kanagawa 252-5210
Japan
Tel: +81 (0)50-33624758
Ueno@stp.isas.jaxa.jp

For further information on the Concurrent Design Facility please contact:

M. Bandecchi
ESA/ESTEC/TEC-SYE
Postbus 299
2200 AG Noordwijk
The Netherlands
Tel: +31-(0)71-5653701
Fax: +31-(0)71-5656024
Massimo.Bandecchi@esa.int

FRONT COVER

Artistic impression of Next Generation
Cryogenic IR Telescope used as study logo

TABLE OF CONTENTS

1 INTRODUCTION

1.1 Background

The **N**ext **G**eneration **Cryo**genically cooled **I**nfra**R**ed **Tel**escope CDF Study is an instrument study, but is a follow on to the JAXA/ESA SPICA mission extensively studied by JAXA, together with ESA, providing the cooled telescope.

Internal assessments performed at JAXA and ESA have shown that the proposed SPICA mission does not fit within the budget allocation at JAXA and ESA and this new study will support the European and Japanese Science community in defining a post-SPICA mission for the M5 call.

The study was requested by ESA Science Directorate SRE-FM and funded by the General Studies Programme GSP. The study was carried out in 8 sessions, starting with a kick off on the 13th November 2014 and ending with an Internal Final Presentation on the 18th December 2014 by an interdisciplinary team of specialists from ESTEC and ESOC and supported by SPICA/SAFARI experts from JAXA and SRON.

Some background information on the SPICA mission is included below:

- SPICA is a 3.2m class IR telescope (already downscaled from the originally foreseen 3.5m telescope)
- The SPICA telescope is actively cooled down to 6K
- SPICA requires an active cooling system down to 1.7/6K and a demanding verification campaign to validate the passive cooling below 50K
- Even considering international contribution, SPICA is an L-class mission.

1.2 Scope

The purpose of this CDF study is to carry out an assessment of a smaller Next Generation- Cryogenic cooled IR Telescope (NG-CryoIRTel), trying to meet a set of science achievements similar to the ones proposed for the previous SPICA mission. Some pre-conditions and assumptions relating to the study are listed below:

- The main focus will be on the payload module (including telescope) and will include some support from JAXA
- For the purpose of this CDF study, it is assumed that the NG-CryoIRTel will be launched on a Japanese H-II/H-X launcher and perform a free-insertion into a large amplitude Halo around L2
- In addition to course correction manoeuvres during transfer, periodic (~monthly) orbit maintenance manoeuvres will be required in order to maintain the S/C on station during the operational phase
- The operational mission is 3 years in duration + 2 years potential extension, observing core and observatory targets within +/- 10deg viewing zone.
- A 2m class (tbc) cryogenically cooled telescope shall provide astronomical background limited observation between 20-200µm

- The proposed S/C concept is based on a passive cooling using V-Grooves (similar to Planck and EChO) down to 40K and active cooling of the telescope down to 6K, mounted on a SVM comparable to the one used on Herschel/Planck
- The overall mission architecture is the classic one for an L2 mission, with some additional complexity due to the cryogenic cooling required.

1.2.1   Area of Focus

Particular areas of focus during the CDF study were:

- The effective area (and other) requirements and operating temperature on the telescope, compatible with a M-size mission (with JAXA support)
  - Baseline design for a 2m telescope at 6K during the first part of the study, exploration of growth potential or required reduction in the second part as the optional design
- The accommodation of the instruments and the available resources (e.g. dissipation at cryogenic temperatures, cryoharness...)
- The structural design, particularly the thermal impact. To minimise the conductive load to the telescope, a de-coupling mechanism similar to the one applied on GAIA was considered
- Identifying sensible Japanese contribution possibilities on the basis of technical and programmatic interfaces

1.3   Document Structure

The layout of this report of the study results can be seen in the Table of Contents. The Executive Summary chapter provides an overview of the study; details of each domain addressed in the study are contained in specific chapters.

Due to the different distribution requirements, only cost assumptions and main related conclusions excluding figures are given in this report.

2 EXECUTIVE SUMMARY

2.1 Study Flow

Requested by SRE-FM and funded by the General Studies Program (GSP) the NG-CryoIRTel study was performed in the Concurrent Design Facility (CDF) in eight sessions with participation of JAXA and SRON, starting with a kick-off on 13 November 2014 and finishing with an internal final presentation on 18 December 2014. The sessions were supplemented with various smaller working sessions and meetings.

2.2 Objectives

The main science objectives to be covered by the NG-CryoIRTel mission are:

- How do stars and galaxies form and evolve over cosmic ages?
- Observe thousands of obscured, far away galaxies and determine what processes govern their evolution
- How does our solar system relate to other planetary systems and could life evolve elsewhere?
- Characterise oxygen, water, ice and rock in young planet forming systems and study their relation to the rocks and ice in our own Solar System
- We want to understand the physical characteristics, and link the different size-scales.

2.3 Requirements and Design Drivers

The detailed mission requirements for the NG-CryoIRTel study are listed in Appendix A.

The main design drivers for the NG-CryoIRTel spacecraft and mission are the following

- Requirement TR-010 states that "All elements in direct view (or through reflections on mirror surfaces) of the instruments' focal plane detectors shall be cooled to ≤ 6 K" which drives the design and required performance from the cryo-cooling system and sets important constraints on the overall configuration of the S/C, i.e. no surface in direct view of the telescope can have a temperature over 6 K.
- Launcher: The launcher is one of the potential contributions to the mission made by JAXA. For the purpose of the study the use of the H-IIA-204 launch vehicle specifications, using the extended 5S fairing, and launched from the Tanegashima Space Centre is assumed. The actual rocket to be used is the evolution of the H-II currently under conceptual design phase. This evolution, currently named H-X, will offer a fairing volume and a maximum launch capacity into L2 transfer orbit which are higher than for the current H-IIA-204(JP) provided by JAXA. For more detailed information see RD[10].
- The telescope mirror size is 2 m.
- For budgetary reasons it is required to have compatibility with an M-size mission
- Additionally to the baseline design with the 2 m telescope, an optional design accommodating an elliptical main mirror of 3m x 2.6 m, is analysed.

2.4 Mission Architecture

The mission phases and timeline are specified in requirements MR-MIS-230 to 290, and they are shown in Table 2-1 and Table 2-2.

Mission Phase	Event	Start day	End day	Duration	Mode	Assumption
Launch&Early Operation LEOP		0.00	24.00	24.00		assumed 3 days Leop
Commissioning		24.00	93.00	69.00		3 months completed during transfer MR-MIS-130, mostly conducted after decontamination
Transfer		3.00	93.00	90.00		maximum 3 months transfer MR-MIS-180, mostly conducted after decontamination
Instrument performance verification and Science Demonstration		183.00	243.00	60.00		After maximum 6 months of cooling starting right after LEOP, finishes 8 months, MR-MIS-150
Nominal Operations		243.00	1080.00	837.00		completing 3 years of mission lifetime, MR-MIS-230
Extended Operation		1080.00	1800.00	720.00		2 years extension, MR-MIS-240
Decommissioning		1800.00	1814.00	14.00		assumed 2 weeks
						decontamination 1 week after launch lasting minimum 3 weeks

Table 2-1: Mission Phases
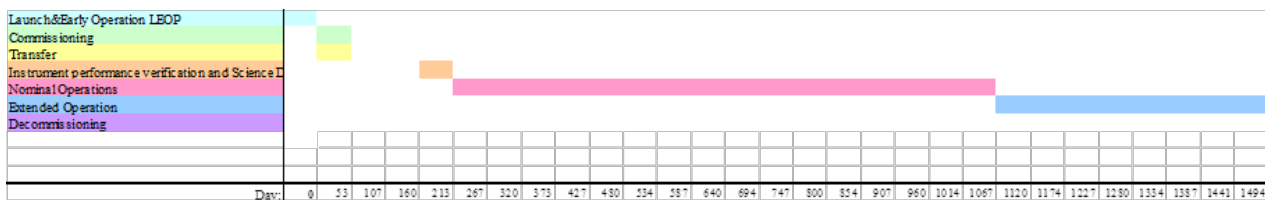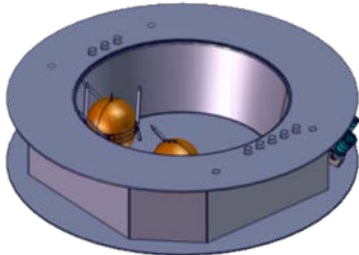
Table 2-2: Mission Timeline

The baselined system characteristics are outlined in Table 2-3.

NG-CryoIRTel System Characteristics

Service Module – System Characteristics

Service Module (SVM)

SVM Mass *(w. margin)*	Dry mass	1332 kg
	Total	1644 kg (*excluding adapter*)
Structure	Service Module: thrust cone and SVM panels, both made of a sandwich structure with CFRP face sheets and an aluminium honeycomb core	
	Isolation of the cryo-cooler panels: 12 dampers , 12 brackets	
Mechanisms	Antenna Pointing Mechanism	
	HDRM for Antenna Pointing Mechanism	
	12 Launch-locks for Cryo-cooler Isolators	
	12 Mechanical INTegration parts (MINT)	
AOCS	1 Attitude Anomaly Detector	
	2 Coarse Rate Sensors	
	2 Sun Acquisition Sensors	
	1 Fine Gyro	
	2 Star Trackers	
	1 Fine Attitude Sensor	
	4 Reaction Wheels	
Propulsion	3 Pseudo-spherical tanks of hydrazine, 173.8 litres each	
	12 Thrusters (20N)	
	Other Propulsion Equipment including service valves, latch valves, evacuation vales and pressure transducers	
Power	Solar Array	14.2 m² of "useful" solar array surface, Triple-junction GaAs cells
	Battery	ABSL 18650HC Li-ion battery
	PCU	S3R regulated 28V bus
Communications	1 X-Band High Gain Antenna	
	2 X-Band Low Gain Antennas	
	2 X-Band Transponders	
	2 Travelling Wave Tube Amplifiers	

	2 Electric Power Conditioner (EPC)
	X-Band Radio Frequency Distribution Unit
Data Handling	Off-the-shelf CDMU solution, based on SCOC3 or other similar SOC
	Remote Terminal Unit as an ad-hoc development for the mission
	Solid State Mass Memory (SSMM) based on flash memory technology
Thermal	8 x 20K-class 2-stage Stirling Coolers
	2 x 4K-class Joule-Thomson Coolers
	2 x 1K-class Joule-Thomson Cooler
	Cryo-cooler Electronics
	Thermal equipment including radiators, MLI, heaters, thermistors, and heat pipes
Instruments	SAFARI Instrument Warm Electronics Box
	SMI Instrument Warm Electronics Box

Payload Module – System Characteristics

Payload Module (PLM)

PLM Mass *(w. margin)*	Total	920 kg (*no propellant in PLM*)
Structure	3 thermal shields: CFRP sandwich with aluminium honeycomb core	
	Thermal Shell: aluminium shell or full aluminium sandwich panel	
	Bipod structure: 2 x 2 bipods, one made of GFRP to be decoupled in later stage and one made of CFRP parallel to the main GFRP one	
	TOB: SiC Plate stiffened by ribs on the back side	
	IOB: milled stiffened aluminium plate	
	Telescope: composed of Primary Mirror (M1) and Secondary Mirror (M2), a hexagonal barrel structure holding M2 and a hexapod structure connecting the barrel to M1.	
	All elements are made of SiC except the interface elements which are made of INVAR.	
	Baffle: cylindrical structure made of CFRP sandwich aluminium honeycomb core	

Mechanisms	1 Refocusing mechanism for M2
	1 Shutter mechanism
	6 Bipod hold-down & release mechanisms and latches
AOCS	2 Fine Attitude Sensor cold unit
Instruments	SAFARI Instrument: Far Infrared Instrument
	SMI Instrument: Mid-Infrared Instrument

Table 2-3: NG-CryoIRTel baseline design

2.5 Technical Conclusions and Options

The NG-CryoIRTel study concluded that from a technical stand-point, no show-stoppers are to be expected with respect to the feasibility of the mission. The share of contributions and responsibilities between ESA and JAXA drives the design and will influence the overall cost share. While the ESA M-call cost envelope remains a challenging target, the study outcomes provide a good starting point for M-class call preparations.

A delta design with a larger telescope of 3x2.6 m^2 was also analysed to fully exploit the mass and volume available in the launcher. Only aspects related to configuration, structure, thermal, telescope design and cost were considered. The major identified technical drawback of this option is that it is not possible with the current instruments and active cooling chain to cool the telescope down to 6K.

This Page Intentionally Blank

3 MISSION OBJECTIVES

3.1 Background

European participation in SPICA – a SPace Infrared telescope for Cosmology and Astrophysics – was first proposed in response to a call in 2007 for missions for the ESA Cosmic Vision 2015-2025 programme. SPICA was selected for study as a candidate M-class mission, with the character of "Mission of Opportunity". The assessment phase ran from November 2007 to August 2009. An updated proposal for European participation in SPICA, based on the outcome of the ESA assessment study, was put forward in late 2009/early 2010 for consideration by the ESA advisory structure by whom it was well-received. The proposal called on ESA to assume a partner agency role in SPICA by making the following contributions: (1) provision of the SPICA cryogenic telescope assembly, (2) use of a European ground station, (3) collaboration on science operations and (4) management of interfaces between JAXA and the European instrument, SAFARI. The SAFARI instrument itself would be procured by ESA from the European Consortium. SPICA entered an extended study phase in early 2010, with the decision on whether to move to implementation phase to be taken on a timescale compatible with the decision by JAXA to take SPICA from the pre-project to project phase.

Discussion between ISAS/JAXA and ESA in 2013 concluded that the scheme for SPICA was not compatible with a timely and robust implementation of the mission. Both JAXA and ESA believe that a more balanced sharing of responsibilities, with an enhanced ESA participation to the mission, would lead to a lower risk and to a more robust mission implementation. Any significant extension of the ESA-contributed elements would bring the mission into the medium mission range, however, with the implication that the mission would need to be proposed by the interested scientific community to an ESA call for missions where it would be peer-reviewed together with other proposals submitted to the same opportunity.

To support the European and Japanese Science community in defining a post-SPICA mission for the M5 call, a smaller Next Generation- Cryogenic cooled IR Telescope (NG-CryoIRTel) has been assessed in this CDF study, without preempting any future proposal that could be made by the science community in response to a future ESA Call for Mission proposals.

3.2 Mission Justification

To reveal the origin and evolution of galaxies, stars and planets is one of the ultimate goals of astronomy. To achieve the goal, observations in the mid- and far-infrared are essential, since it is in this range that astronomical objects emit most of their radiation as they form and evolve in regions where obscuration by dust prevents observations in the visible and near infrared.

Over the past quarter of a century successive space infrared observatories (IRAS, IRTS, ISO, Spitzer and AKARI) have revolutionised our understanding of the evolution of stars and galaxies. Mid- to far-infrared observations have led to stunning discoveries such as the Ultra Luminous Infrared Galaxies (ULIRGS), the basic processes of star formation from "class 0" pre-stellar cores through to the clearing of the gaseous proto-planetary

discs and the presence of dust excesses around main sequence stars. The Herschel Space Observatory launched in 2009 extends this work in the far-infrared and sub-mm and JWST, due for launch in 2018, will provide a major boost in observing capability in the 2 − 28 µm range. Although Herschel and JWST are powerful missions, they have some constraints for the observations in the mid- and far-infrared. Figure 3-1 shows the comparisons of celestial diffuse radiation (natural background radiation) and those of thermal radiation from space missions. The thermal radiation of telescopes onboard Herschel and JWST (if it is used for the far-infrared) is brighter than natural background radiation by a factor of one million in the far-infrared. Hence their sensitivity in the far-infrared could be degraded by a factor of one thousand from that of the natural background limited observations. On the other hand, previous cryogenically cooled missions (e.g. IRAS, IRTS, ISO, Spitzer, and AKARI) had a telescope smaller than 1m. Hence, if a 3-m-class space telescope is to be cooled below 6K, huge sensitivity improvement can be expected from that of Herschel.
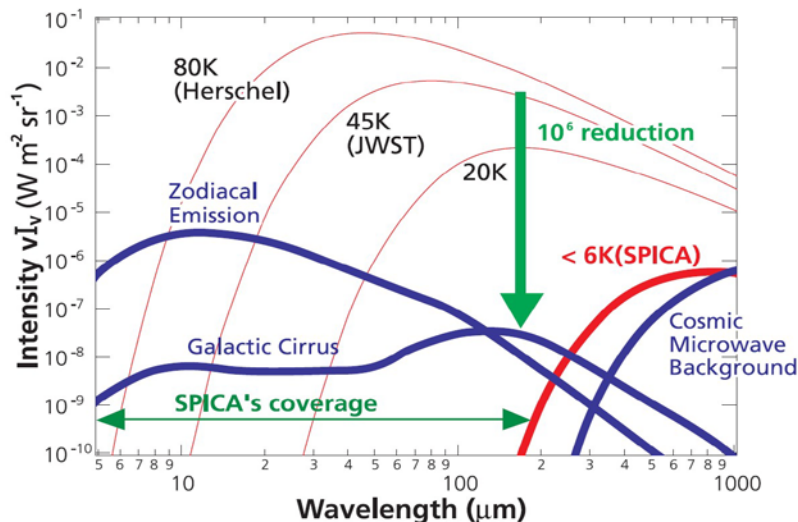
Figure 3-1 Comparison of natural background (zodiacal emission, Galactic cirrus, and cosmic microwave background radiation) with those of thermal radiation from telescopes as a function of temperature

SPICA, which is cooled below 6K, can achieve superior sensitivity by reducing the background radiation by a factor of a million from previous missions.

Hence SPICA was proposed in this context and is optimised for mid- and far-infrared astronomy with a cryogenically cooled, large telescope. SPICA was an observatory that was to provide imaging and spectroscopic capabilities in the 5 to 210 µm wavelength range with a 3.2 m telescope cooled to a temperature less than 6 K. In combination with a new generation of highly sensitive detectors, the low telescope temperature would allow us to achieve superior sensitivity over the full 5 to 210 µm band. This unique capability means that SPICA was supposed to be between one and two orders of magnitude more sensitive than Herschel in the far-infrared band.

NG-CryoIRTel will cover the full 20 to 210 µm wavelength range, including the missing 28 µm to 55 µm octave which is out of the Herschel and JWST domains with

unprecedented sensitivity and spatial resolution. Hence, NG-CryoIRTel will be the only observatory of its era to bridge the wavelength gap between JWST and ALMA, and carry out unique science programs.
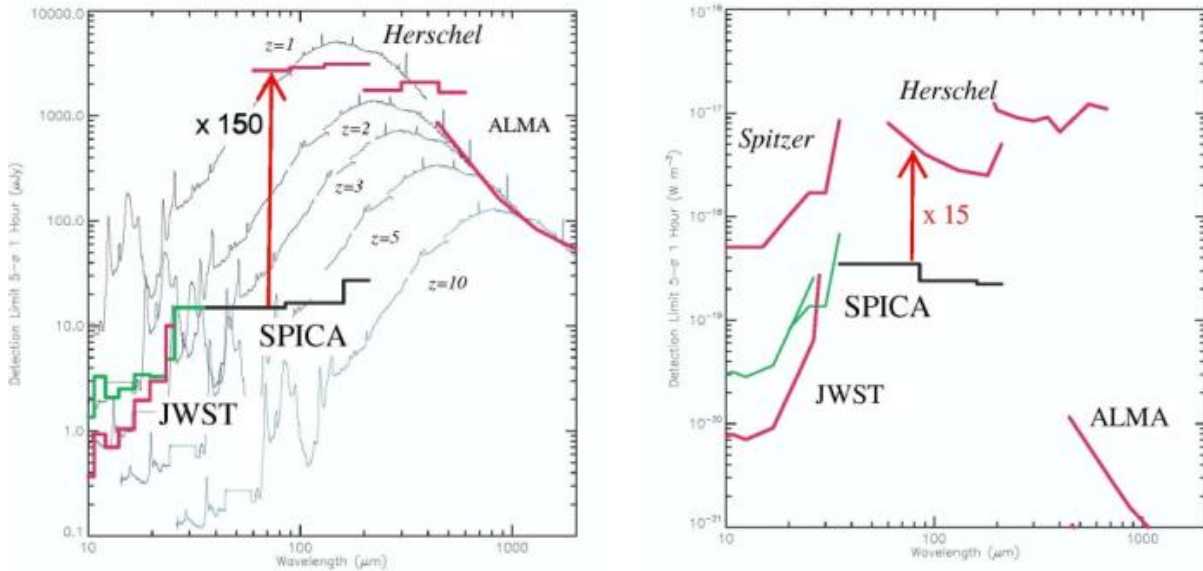
Figure 3-2 Left panel: Photometric performance expected for SPICA (without confusion), compared to Herschel, ALMA and JWST (black), for a point source (in μJy for 5σ in 1 hour) using the goal sensitivity detectors on SPICA (NEP = 2 ×10−19 WHz−1/2). Note the ~ 2 orders of magnitude increase in FIR photometric sensitivity compared to Herschel-PACS. For illustrative purposes the SED of the starburst galaxy M82 as redshifted to the values indicated is shown in the background. Right panel: Spectroscopic performance expected for SPICA compared to predecessor and complementary facilities for an unresolved line for a point source in Wm−2 for 5σ in 1 hour. For ALMA 100 km s−1 resolution is assumed

3.3   Science Objectives

The main science objectives, derived from the previous SPICA study and which NG-CryoIRTel tries to enable are:

- How do stars and galaxies form and evolve over cosmic ages?
- Observe thousands of obscured, far away galaxies and determine what processes govern their evolution
- How does our solar system relate to other planetary systems and could life evolve elsewhere?
- Characterise oxygen, water, ice and rock in young planet forming systems and study their relation to the rocks and ice in our own Solar System
- We want to understand the physical characteristics, and link the different size-scales.

Besides these objectives, the NG-CryoIRTel as studied during this CDF might also be suitable for other science cases requiring a large cryogenically cooled telescope.

3.4 Mission Requirements

The main mission requirement for this study is to accommodate a 2m class telescope, operating below 6K, on a spacecraft maximising the re-use of Planck V-Groove technology for the passive cooling and considering active coolers provided by JAXA for the purpose of this CDF. In addition, it is assumed for this CDF study that the launcher and fine attitude sensor mounted on the instrument optical bench is also provided by JAXA.

In addition, other main requirements which have been considered as part of this study are presented in the Annex.

3.5 Options

As an option, this CDF study will also investigate the growth potential of the selected architecture assessing the maximum telescope size that can be accommodated on the selected V-Groove configuration.

4   MISSION ANALYSIS

4.1   Requirements and Design Drivers

SubSystem requirements		
Req. ID	**STATEMENT**	**Parent ID**
MA-010	Residual acceleration during operational phase $< 6 \cdot 10^{-11}$ km/s^2 required to validate station-keeping ΔV budget	

4.2   Assumptions and Trade-Offs

The operational orbit for NGCryoIRTel was a-priori defined as an orbit about the Sun-Earth Libration Point 2 (SEL2). Other orbit options were not considered for the mission during this CDF study.

For this CDF study, the launch is envisioned on a Japanese H-X launch vehicle from the Tanegashima spaceport in Japan. The H-X launcher can lift more than 3,700 kg (payload excluding payload adapter) into the transfer orbit towards SEL2. The initial ascent is into a circular parking orbit with an inclination of 30 Deg RD[4]. The drift duration in the circular parking orbit until the final upper stage burn for a transfer towards SEL2 determines the final argument of perigee of the departure orbit. The drift duration can be selected to optimise the yearly launch window duration. The powered ascent phase is followed by an upper stage re-orientation phase in case a specific separation attitude is required, e.g. Sun pointing of the solar panels prior to separation.

Illumination constraints of the S/C can prohibit some combinations of argument of perigee values and launch days/hours or might require specific upper stage attitude orientation during the drift phase to protect the payload. Such constraints can also be a driving factor for the AOCS design, since the S/C must be able to reduce the residual tip-off rates such that the payload is always protected from the Sun within the given illumination constraints.

The ΔV values presented in this chapter are so called geometric or impulsive ΔV values. They do not take any losses into account, e.g. manoeuvre decomposition losses, ramping losses or gravity losses are not accounted for. The so called effective ΔV depends on the propulsion system design. On spacecraft with attitude limitations such a loss in efficiency can be drastic, e.g. some manoeuvre direction on Gaia had efficiencies as low as 30 %. If some manoeuvre directions are not possible, biasing strategies must be applied to avoid these directions altogether. Such a strategy usually doubles the ΔV budget for the manoeuvres involved.

4.3   Baseline Design

The baseline orbit for NGCryoIRTel is a large amplitude quasi-Halo orbit about the collinear Sun-Earth Libration Point 2 (SEL2). A typical example of such an orbit is shown in Figure 4-1. Libration Point orbits are best depicted in a rotating coordinate frame. Here the x-axis is along the Sun-Earth line, the z-axis is normal to the ecliptic

plane and the y-axis supplements the system to be a right-hand coordinate system. The origin of the system is located in the Earth's centre.
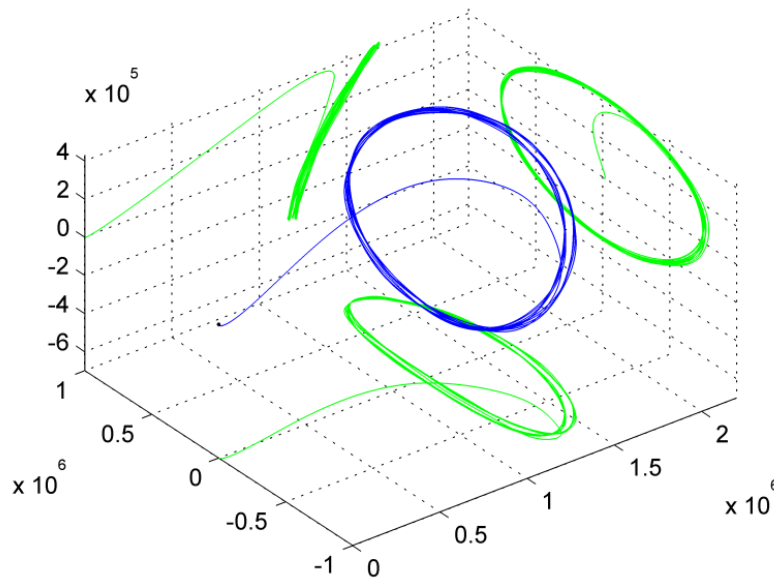
Figure 4-1 : Example of a large amplitude quasi-halo orbit about the Sun-Earth Libration Point 2

The advantages of orbits about SEL2 are a constant thermal environment, since they can be designed to be eclipse free, and a limited communication distance. Another advantage for astronomy missions is that the Sun, Earth and Moon are all located in one hemisphere as seen from the S/C.

Such an orbit can be reached via a so called "free" transfer trajectory, not requiring any deterministic orbit insertion manoeuvre after Earth departure. The S/C travels on the so called stable manifold toward its operational orbit about SEL2. A typical transfer trajectory on the stable manifold of the target orbit is depicted in Figure 4-2. The full stable manifold of the target orbit is shown. Some parts of the manifold intersect with the near-Earth environment (the Earth is at the origin), where the launcher can place the S/C on the stable manifold of the target orbit.
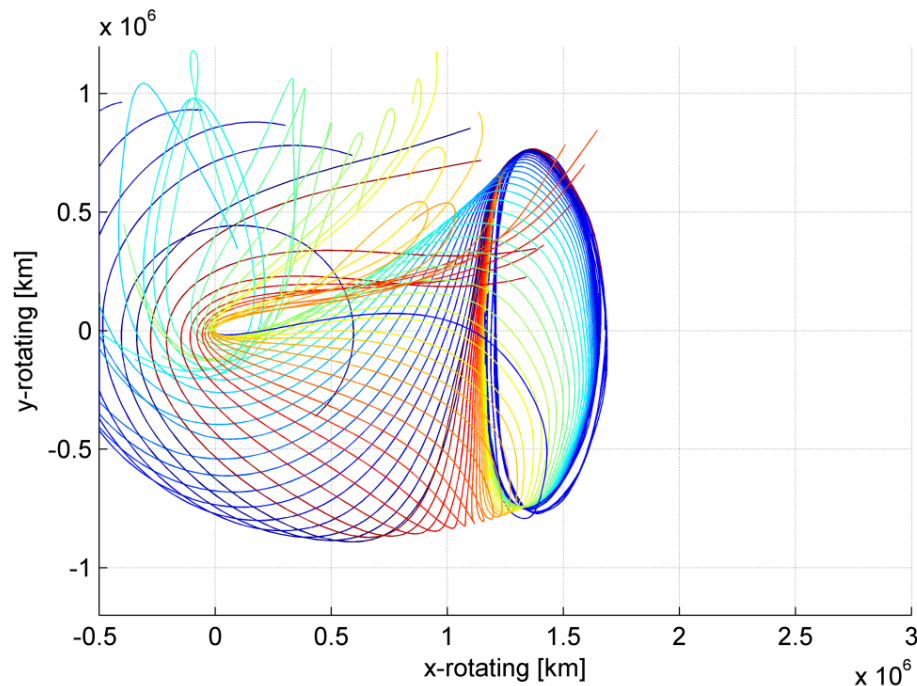
Figure 4-2: Stable manifold and free transfer option to an SEL example orbit. The free transfer trajectory is the single blue line passing through the inner libration point orbit region

It is assumed that after the ascent sequence containing a drift of the upper-stage-S/C stack in the circular parking orbit, the upper stage of the launch vehicle will directly insert the spacecraft on the transfer trajectory towards SEL2. The in-and out of-plane amplitudes (Ay and Az) of the SEL2 orbit are then not prescribed, but depend on the launch date, launch hour and drift duration in the circular parking orbit. The size of a SEL2 orbit is often described by the so called Sun-S/C-Earth angle (SSCE). The minimum SSCE is defined by the free transfer condition and is near 28 Deg. If smaller SSCE angles are required for operational reasons, an orbit insertion manoeuvre must be performed. This is usually required for spinning S/C, where the Earth has to be kept close to the antenna beam (e.g. Planck and Gaia). For 3-axis stabilised missions as NGCryoIRTel there is usually no constraint, however, for NGCryoIRTel an upper limitation of 33 Deg SSCE has been proposed to limit design parameters as e.g. the maximum declination with respect to the Earth's equator, which is important to ensure visibility from ground stations (GS) in the northern and southern hemisphere.

Solutions with an eclipse in the transfer trajectory are excluded from the launch window. The reached SEL2 orbit is eclipse free for the mission duration.

With a fixed launcher program the perigee velocity of the transfer orbit is also fixed. However, for each day of the year the free transfer requires a specific perigee velocity. An example evolution of a required perigee velocity for stable manifold insertion is provided in Figure 4-3. In addition the launcher has a certain dispersion in the final osculating perigee velocity. The spacecraft will therefore initially not travel on the stable manifold of the libration point orbit and thus a small manoeuvre is required to correct the spacecraft state and put it onto the stable manifold.
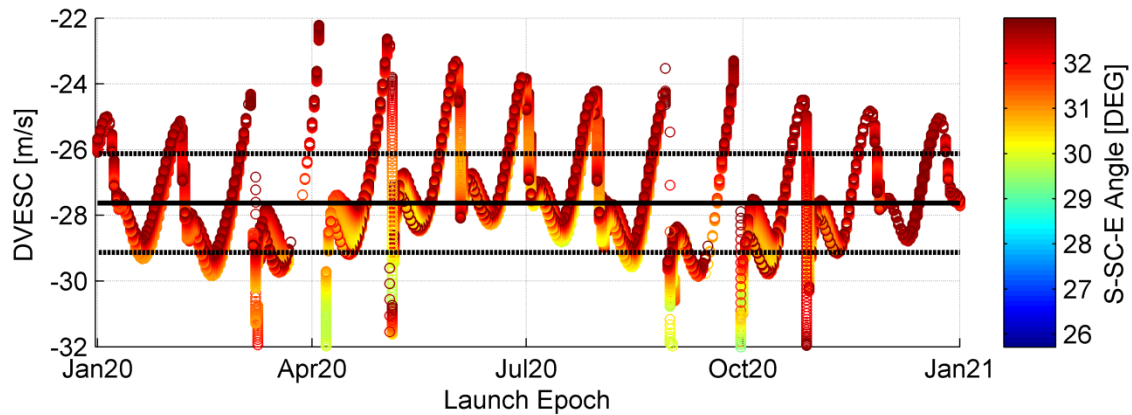
Figure 4-3: Example of perigee velocity delivered by the launcher (solid black bar) compared to the one required for stable manifold insertion (coloured markers). The perigee correction capability is assumed with ±1.5 m/s (dashed black bars) from the one delivered by the launcher

This manoeuvre is time critical and is thus performed as soon as possible after the launch. In order to have enough time to track the spacecraft and estimate the state vector an execution 24 hours into the mission is envisioned, but to account for any problems with the S/C or ground segment an execution on day-2 (48 hours into the mission) is budgeted. Inaccuracies in this manoeuvre will be corrected on day-5 and day-20. The third manoeuvre concludes the transfer. The S/C can now be assumed to be on the SEL2 orbit, where station-keeping continues.

The SEL2 operational orbit is inherently unstable and requires regular but small maintenance manoeuvres. The total ΔV allocated for the orbit maintenance manoeuvre depends on the station-keeping interval and the capability of the AOCS to deliver pure torque or torque only together with a change in the spacecraft's velocity.
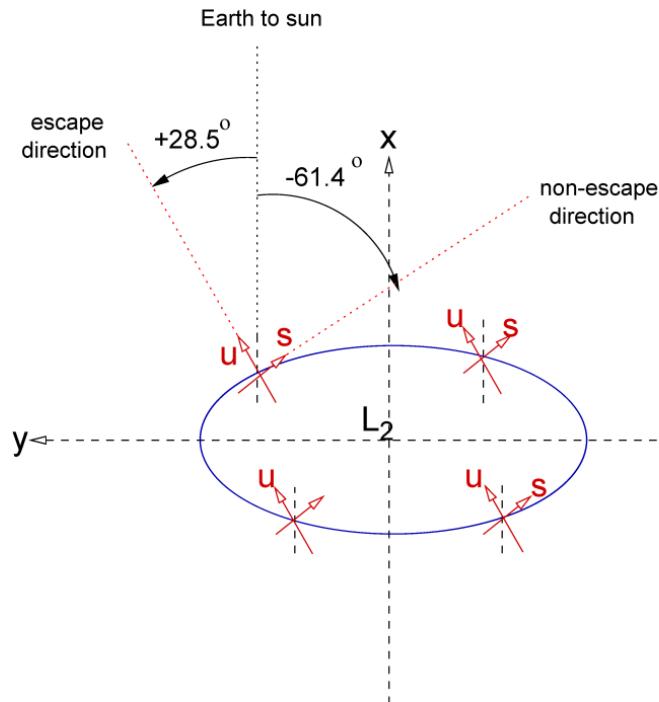
Figure 4-4: Stable and unstable direction derived from linear theory for station-keeping considerations

Station-keeping manoeuvres are assumed in the unstable direction of the linear theory. This direction is depicted in Figure 4-4.

A typical station-keeping ΔV evolution example is provided in Figure 4-5. The yearly station-keeping ΔV highly depends on the residual accelerations of the S/C. To be more precise, it depends on the unknown residual acceleration of the S/C, since known components can be taken into account, similar to the solar radiation pressure. The difference in the allocation can easily be different by orders of magnitude. E.g. the largest station-keeping manoeuvre of Herschel was larger than the station-keeping allocation of Gaia for an entire year. Gaia, being a spinning S/C, had well predictable residual acceleration, while the attitude of 3-axis stabilised Herschel could by definition not be known a-priori.
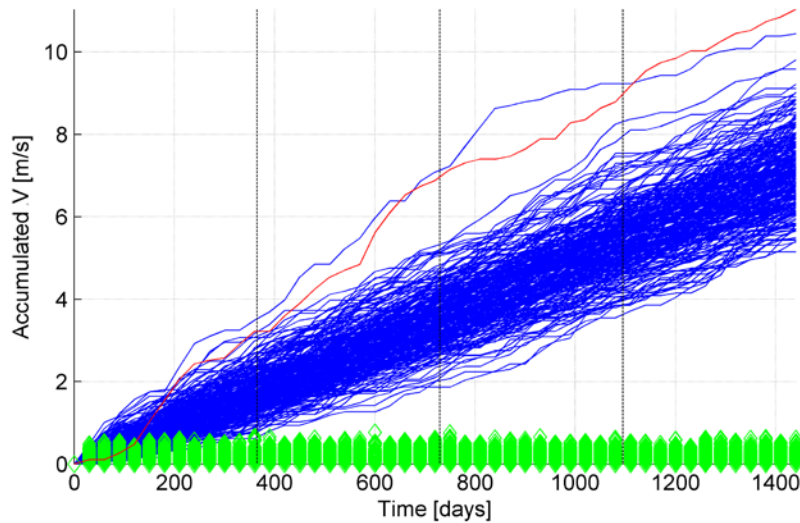
Figure 4-5:Example Station-Keeping ΔV evolution for four years. The blue curve shows the accumulated ΔV and the green diamonds indicate the size of each individual station-keeping manoeuvre. The red curve depicts the worst case trajectory out of the monte carlo simulation set

Another important aspect during the operational phase is the visibility of the S/C from ground stations around the world. Figure 4-6 shows the elevation of the S/C with respect to different ground stations around the world for minimum, maximum and zero declination cases.
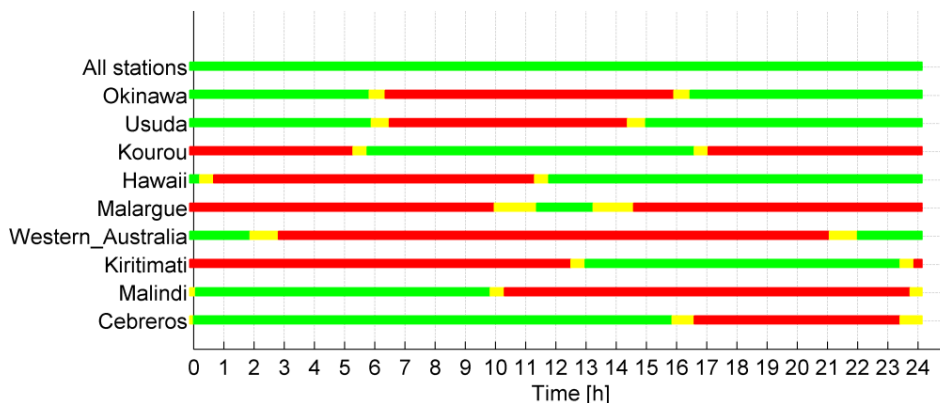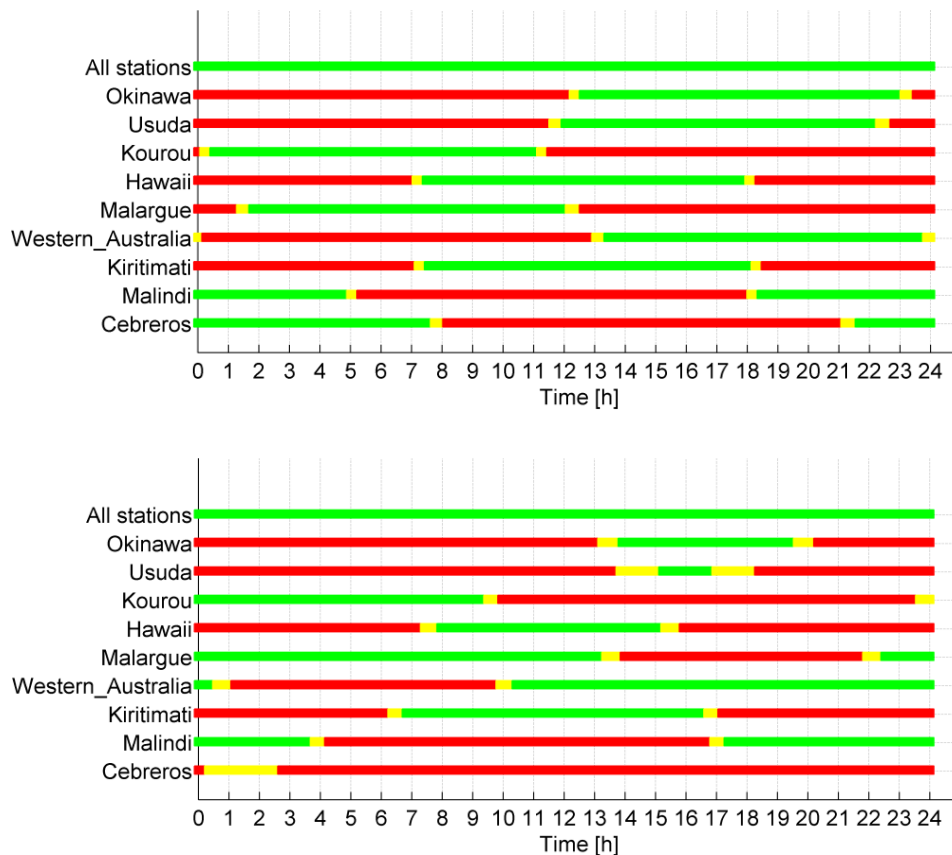
Figure 4-6: S/C visibility from ground stations around the world for maximum declination (top), zero declination (middle) and minimum declination (bottom). Elevations above 10 deg are marked in green, between 5 and 10 Deg in yellow and elevations with less than 5 Deg are marked in red

After the scientific operational phase the S/C must be disposed of. A standard disposal strategy for libration point missions has not been defined yet. In general three different kinds of disposal strategies are possible:

- Heliocentric disposal

- Earth return

- Lunar impact.

The heliocentric disposal has been applied to the Herschel and Planck missions and is currently still the baseline for Gaia. A lunar impact had been studied for Herschel. The Earth return option can either be controlled or uncontrolled. An uncontrolled re-entry can only be performed if the parts of the S/C possibly reaching the ground do not exceed the on-ground casualty risk, as defined in the Space Debris Mitigation Policy for Agency Projects.

For NG-CryoIRTel a heliocentric disposal is currently considered. An allocation for the disposal manoeuvre of 10 m/s has been made. This manoeuvre of up to 10 m/s is to ensure a fast departure into the solar system. A second, later manoeuvre can decrease the likelihood of a return to the Earth-Moon system. No additional allocation beyond

the remaining part of the 10 m/s is made for this manoeuvre, however, the remaining fuel on board can be used to increase this (so called Jacobi raise manoeuvre). This manoeuvre is more efficient at greater distances. The initial manoeuvre ensures that a larger distance is reached reasonably fast to limit operations time for the disposal.

4.3.1 Trajectory Biasing

The design of the NG-CryoIRTel propulsion system is such that all thrusters have a thrust component in the direction of the normal vector of the solar array, pointing away from the Sun. Together with the attitude constraints of the S/C (Telescope line-of-sight should have an angle of 90±15 Deg with the Sun) this leads to the situation that the S/C has no thrust vector component into the Sun direction. The S/C can only be accelerated away from the Sun. This requires the trajectory to be biased to ensure that all required manoeuvre ΔVs are directed away from the Sun. E.g. for the launcher this means that the nominal apogee altitude is selected lower than the one for an optimal transfer trajectory. An example for this is shown in Figure 4-7.
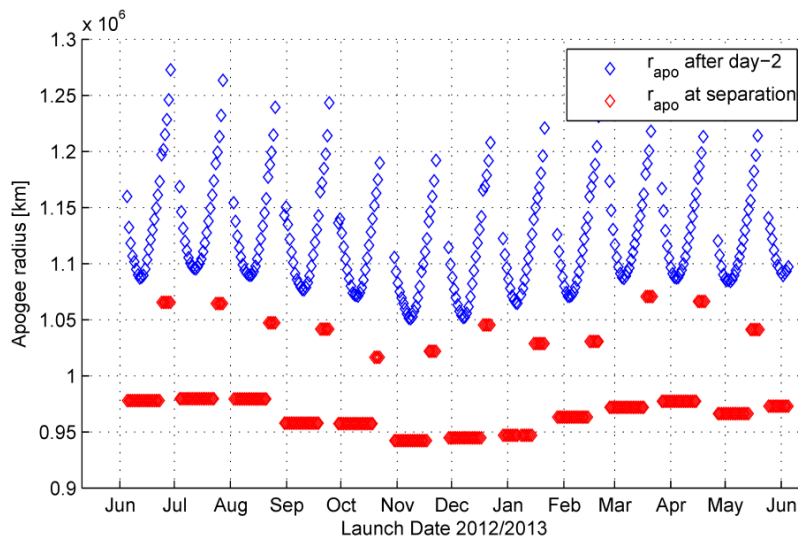
Figure 4-7: Example of a biased launcher injection. The apogee altitude targeted by the launcher is depicted in red, the one required for an optimal transfer is depicted in blue. The example shown is from the Gaia mission, which had a similar propulsion system constraint

In case of a nominal injection the S/C then has to perform a manoeuvre to accelerate to the required apogee altitude. In case of a launcher over-performance, the S/C now does not have to decelerate by braking into the Sun direction, but the first manoeuvre gets smaller than in the nominal injection case (on the best case launch day a 3σ over performance will require no correction manoeuvre). The problematic case with respect to the ΔV is now the launcher under-performance case. In case of a launcher under-performance the S/C has to provide the ΔV to recover from the launcher under-performance and in addition it has to provide the ΔV for the nominal under-shooting of the trajectory. This essentially doubles the ΔV allocation. The same procedure must be applied to all manoeuvres. Any manoeuvre must be undershot in order to ensure that even in case of a manoeuvre over-performance the next manoeuvre is not required to

accelerate the S/C into the Sun direction. E.g. in the station-keeping case the S/C must be constantly kept on the unstable direction falling back towards the Earth.

A S/C with a similar constraint was Gaia, where the tank design did not allow for a prolonged acceleration into the Sun direction, however, smaller manoeuvres were possible such that e.g. the station-keeping allocation did not need to be doubled.

4.4 Budgets

The main Mission Analysis budget is the ΔV budget. With almost no deterministic ΔV, the budget strongly depends on the assumptions for the launcher dispersion and the residual acceleration of the S/C while in the operational orbit.

It should be noted that the budget for the station-keeping is assuming very pessimistic residual accelerations on the S/C. The allocation for the station-keeping ΔV can be significantly reduced if the actual residual acceleration levels are less or in case the residual acceleration can be predicted. In the latter case it can be accommodated in the trajectory design. It should also be mentioned that for current libration point missions in planning the margin on the station-keeping ΔV is 50% compared to the 100 % required in the CDF (RD[5]).

ΔV Requirements					
Manoeuvre	Value [m/s]	Margin [%]	With margin [m/s]	With bias [m/s]	Comment
Perigee velocity correction	13.5	5 %	14.175	28.35	Assuming 1.5 m/s perigee velocity correction capability
TCM#1 (mainly launcher dispersion correction)	27	5 %	28.35	56.7	H-X expected launcher dispersion considered RD[4]
TCM#2 & #3 Transfer correction	4.5	100 %	9	18	
Station-keeping	30.1	100 %	60.2	120.4	Budget is for 2 years and 4 months nominal mission and 2 years mission extension. The given value is only valid for residual accelerations of less than $6 \cdot 10^{-11}$ km/s²
Moon eclipse avoidance	N/A	N/A	N/A	N/A	Not required due to orbit design
Decommissioning (Heliocentric Disposal)	10.0	5 %	10.5	21.0	
Safe Mode ΔV	N/A	N/A	N/A	N/A	Two safe modes per year assumed with residual acceleration level < $6 \cdot 10^{-11}$ km/s²
Operational contingency	10.0	5 %	10.5	21.0	Depends on contingency scenarios to be covered – Save modes are assumed to be covered by this allocation
Sum	95.1	N/A	132.73	265.5	

Table 4-1: ΔV summary table. The total ΔV strongly depends on the station-keepings assumptions. This table is only valid for a S/C with a residual acceleration of less than $6 \cdot 10^{-11}$ km/s²

4.5 Options

Two alternative options with respect to the transfer and the operation orbit are briefly discussed, a small size Lissajous orbit with limited Sun-S/C-Earth angle and the indirect transfer, reducing the criticality of the day-2 manoeuvre.

4.5.1 Small Lissajous Orbit

In case a constraint on the amplitude sizes is added, a small Lissajous orbit could be an alternative to the large amplitude orbit reachable via the free transfer trajectory. Then an orbit insertion ΔV is required at SEL2 arrival. The size of this orbit insertion manoeuvre depends on the maximum Sun-S/C-Earth angle allowed. The transfer is then similar to the one of GAIA RD[3].

4.5.2 Indirect Transfer via HEO

The indirect transfer option removes the criticality of the day-2 manoeuvre described above by inserting the spacecraft into an intermediate HEO prior to the insertion onto the stable manifold of the destination orbit. Dependant on the propulsion system layout an increase in payload mass could also be achieved RD[2]. Such an intermediate HEO transfer scenario is depicted in Figure 4-8. The S/C is not injected directly towards SEL2, but only into an intermediate HEO (blue/magenta) and performs the injection towards SEL2 during its next perigee pass.
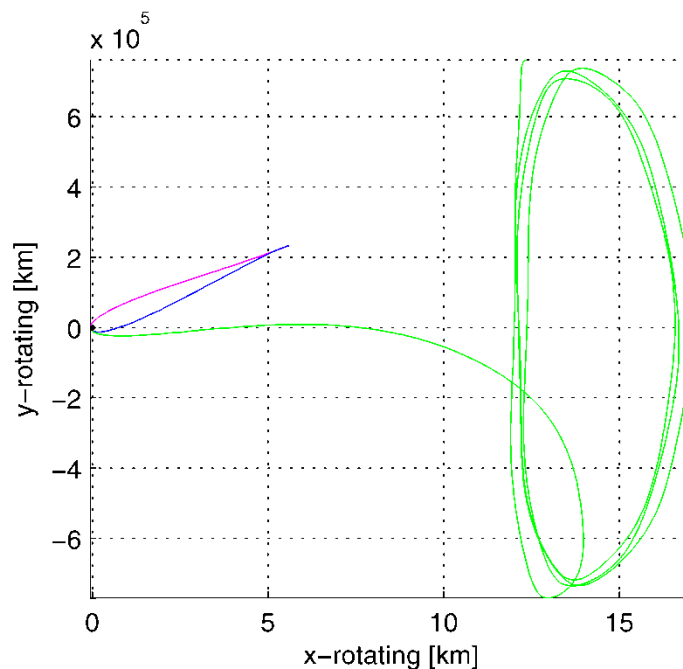
Figure 4-8: Example SEL2 transfer with intermediate HEO.

5 SYSTEMS

5.1 System Requirements and Design Drivers

A detailed list of mission and spacecraft requirements is available in Appendix A. These include requirements on the launch vehicle, site and date, on the injection, transfer and operational orbits, on the mission phases, on the mission lifetime, on the ∆V, on the operation and modes, on science performance, on design requirements, on operations and ground segment and on programmatic.

The main design drivers for the NG-CryoIRTel spacecraft and mission are the following:

- Requirement TR-010 states that "All elements in direct view (or through reflections on mirror surfaces) of the instruments' focal plane detectors shall be cooled to ≤ 6 K" which drives the design and required performance from the cryo-cooling system and sets important constraints on the overall configuration of the S/C, i.e. no surface in direct view of the telescope can have a temperature over 6K.

- Launcher: The launcher is one of the potential contributions to the mission made by JAXA. For the purpose of the study the use of the H-IIA-204 launch vehicle specifications, using the extended 5S fairing, and launched from the Tanegashima Space Centre is assumed. The actual rocket to be used is the evolution of the H-II currently under conceptual design phase. This evolution, also known as H-X, will offer a fairing volume and a maximum launch capacity into L2 transfer orbit which are higher than for the current H-IIA-204(JP) provided by JAXA. For more detailed information see RD[6].

- The telescope mirror size is 2 m.

- For budgetary reasons it is required to have compatibility with an M-size mission

- Additionally to the baseline design with the 2 m telescope, an optional design accommodating an elliptical main mirror of 3m x 2.6 m, is analysed, mainly focussing on the spacecraft's configuration, structural and thermal aspects.

5.2 System Assumptions and Trade-Offs

5.2.1 Assumptions

As a starting point, the CDF team used the Mission Definition Document from SPICA, RD[7], and the results of the previous instrument studies on SPICA/SAFARI, **Error! Reference source not found.**.

The Service Module (SVM) is based on the SVM of Herschel-Planck The modifications required for NG-CryoIRTel were analysed by the CDF team, with particular attention to thermal and structural aspects as well as the interfaces between platform and payload.

5.2.2 Trade-Offs

5.2.2.1 Baseline telescope design

The main trade-off conducted in the study was about the choice of the baseline telescope design.

The design options used included Ritchey-Chrétien on- and off-axis, three mirror anastigmats (TMA) and Korsch configurations. The on- and off-axis refer to the entrance pupil being either on- or off-axis. The terms flat and curved refer to larger or smaller radii of curvature for the image surfaces.

These options were traded-off using a set of 16 different evaluation criteria as shown in Table 5-1. These criteria covered performance aspects, complexity of the design w.r.t. several disciplines, manufacturing, interfaces, accommodation and cost. Weights and scores were discussed and agreed in several meetings and sessions with the participation of experts from all involved disciplines.

Parameter	Weight	RC on-axis flat image surface		RC on-axis curved image surface		RC off-axis flat image surface		RC off-axis curved image surface		Korsch		TMA flat image surface		TMA curved image surface	
		m	wm	m	wm	m	wm	m	wm	m	wm	m	wm	m	wm
Effective area x throughput	15%	7.6	1.1	9.5	1.4	10.0	1.5	10.0	1.5	9.4	1.4	9.4	1.4	9.4	1.4
FoV	7%	5.0	0.4	5.0	0.4	5.0	0.4	5.0	0.4	6.0	0.4	5.0	0.4	6.0	0.4
Optical quality	12%	0.7	0.1	6.9	0.8	3.3	0.4	4.5	0.5	3.4	0.4	1.8	0.2	8.7	1.0
Impact of/on thermal background and straylight	10%	5.0	0.5	5.0	0.5	3.0	0.3	3.0	0.3	4.0	0.4	3.0	0.3	3.0	0.3
Complexity of interfaces and impact on the instrument design	8%	10.0	0.8	2.0	0.2	5.0	0.4	2.0	0.2	5.0	0.4	5.0	0.4	0.0	0.0
Alignment tolerances and stability sensitivity	5%	9.7	0.5	5.0	0.3	9.7	0.5	6.7	0.3	9.5	0.5	10.0	0.5	9.4	0.5
Accommodation in PLM / on SVM	5%	8.2	0.4	8.2	0.4	0.0	0.0	9.1	0.5	9.9	0.5	10.0	0.5	9.2	0.5
Complexity/feasibility/technology readiness of optical design	5%	5.0	0.3	5.0	0.3	4.0	0.2	4.0	0.2	3.0	0.2	3.0	0.2	3.0	0.2
Complexity/feasibility/technology readiness of thermal design	5%	5.0	0.3	5.0	0.3	7.0	0.4	7.0	0.4	6.0	0.3	6.0	0.3	6.0	0.3
Complexity/feasibility/technology readiness of structural design	5%	7.0	0.4	7.0	0.4	10.0	0.5	10.0	0.5	5.0	0.3	5.0	0.3	5.0	0.3
Telescope manufacturing/procurement (polishing)	5%	6.1	0.3	9.9	0.5	5.2	0.3	4.9	0.2	7.0	0.4	1.9	0.1	5.0	0.3
System assembly/verification/testing/calibration	4%	5.0	0.2	5.0	0.2	4.0	0.2	4.0	0.2	3.0	0.1	3.0	0.1	3.0	0.1
Cost	10%	3.7	0.4	5.0	0.5	1.5	0.2	4.0	0.4	3.0	0.3	1.0	0.1	1.8	0.2
Complexity and accommodation of re-focussing and tip-tilt mechanisms	4%	8.8	0.4	7.0	0.3	5.0	0.2	8.6	0.3	10.0	0.4	9.7	0.4	8.7	0.3
Total weighted			5.86		6.24		5.25		5.83		5.88		5.08		5.70

Table 5-1: Results of baseline telescope design trade-off

As a result of this trade-off, a Ritchey-Chrétien on-axis telescope with a curved image surface was selected as baseline for the CDF study.

5.2.2.2 X-band vs. K-band

The trade-off between X and K-band for the communication subsystem is also addressed in chapter 15.2.2.1 and it is shown that, regardless of the important differences in data rate, K-band has only a small advantage, in terms of operation time of the payload, over the X-band.

Safari, which cannot operate during communication takes advantage of the long communication time to recycle the last stage cooler whereas SMI can continue the observations thanks to an antenna pointing mechanism (which will not be required for K-Band).

The procurement cost of the K-band system would be about 10 % more expensive than the equivalent X-band one, as shown in Table 5-2. It should be noted that the operation cost due to the ground stations required time and the required upgrade for the X-Band system is not considered in this analysis, but is comparable to the cost difference.

Additionally a K-band antenna would be larger (0.7 m. diameter compared to 0.4 m. diameter of the X-band antenna) which would put some constraints on its accommodation on the bottom of the SVM and simultaneously reduce the available surface for the solar array.

Therefore X-band communications were baselined for the CDF study. However this choice could be modified in future phases of the missions because the K-band system would also fulfil all mission requirements.

An overview of the cost trade-off is provided in Table 5-2.

CDF NG-Cryo IR Telescope	
TT&C Trade-off	
K/X combined	**Full X band**
Subsystem level activities	Subsystem level activities
Management	*Management*
PA	*PA*
Engineering	*Engineering*
AIT/V	*AIT/V*
GSE	*GSE*
Equipment	Equipment
Deep space transponder	*Deep space transponder*
Tx modulator Ka	*TWTA X band*
TWTA Ka band	*RFDA*
SSPA X band	*HGA X band (0.4)*
RFDA	*APM*
HGA dual band (0.7)	*APM Electronics*
LGAs(2)	*LGAs (2)*
1.09	**1.00**

Table 5-2: X-band vs. K-band equipment list and relative cost

5.3 Mission Architecture

5.3.1 Mission Phases and Mission Timeline
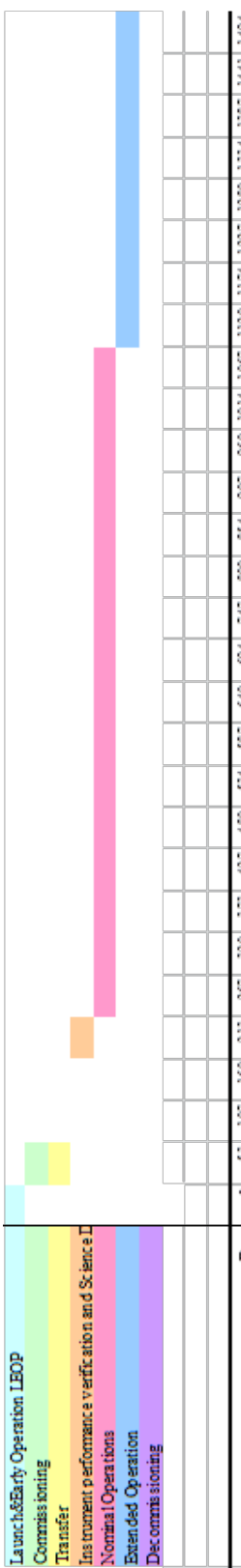
The mission phases and timeline are specified in requirements MR-MIS-230 to 290, and they are shown in Table 5-3.

One week after a LEOP, the decontamination phase lasting a minimum of three weeks is performed. Its objective is to ensure that water released during the initial out-gassing and cooling of the platform cannot freeze out on the telescope optics and instruments.

The commissioning of the S/C and its transfer to the operational orbit should be completed within the first three months. And before starting the nominal operations phase, the S/C needs to finish its cooling process and go through a two months Instrument Performance Verification and Science Demonstration phase.

Following all the above phases, the nominal operations will start and last until three years in the nominal lifetime of the mission. An operation extension phase of two years is also planned.

Mission Phase	Event	Start day	End day	Duration	Mode	Assumption
Launch&Early Operation LEOP		0.00	24.00	24.00		assumed 3 days Leop
Commissioning		24.00	93.00	69.00		3 months completed during transfer MR-MIS-130, mostly conducted after decontamination
Transfer		3.00	93.00	90.00		maximum 3 months transfer MR-MIS-180, mostly conducted after decontamination
Instrument performance verification and Science Demonstration		183.00	243.00	60.00		After maximum 6 months of cooling starting right after LEOP, finishes 8 months, MR-MIS-150
Nominal Operations		243.00	1080.00	837.00		completing 3 years of mission lifetime, MR-MIS-230
Extended Operation		1080.00	1800.00	720.00		2 years extension, MR-MIS-240
Decommissioning		1800.00	1814.00	14.00		assumed 2 weeks
						decontamination 1 week after launch lasting minimum 3 weeks

Table 5-3: Mission Phases and Timeline

5.3.2 System Modes

Several system modes have been identified. Among these, the focus was put on those system modes that were found to be sizing with respect to the design of the thermal and / or power subsystem. It was agreed to have the same system modes for both Elements (Service Module & Payload Module). These ten sizing modes are depicted in Table 5-4.

It should be noted that these system modes should not be confused with the operational modes described in section 1.6 of the Mission Requirements in Appendix 1 Table A-1.

Mode Name	Mode Description
Launch Mode	From launcher umbilical separation to spacecraft separation. All equipment is OFF, except for essential equipment. Battery fully charged.
Initialisation Mode/ Sun Pointing Acquisition	From spacecraft separation to Sun pointing. No energy produced by the S/A. Use of the batteries. TT&C Up/Downlinks. AOCS Actuators are ON.
Stand-by	No Science Operations. SMI and SAFARI Instruments are in STAND-BY. TT&C Up/Downlinks. Rest of the on-board equipment is ON. Cryogenic System is ON.
SAFARI Science	Nominal Operations of SAFARI instrument. SAFARI Instrument is ON. SMI Instrument is in STAND-BY. Rest of the on-board equipment is ON. Cryogenic System is ON.
SMI Science	Nominal Operations of SMI instrument. SMI Instrument is ON. SAFARI Instrument is in STAND-BY. Rest of the on-board equipment is ON. Cryogenic System is ON.
SMI Science with Communications	Nominal Operations of SMI instrument plus Communications. SMI Instrument is ON. SAFARI Instrument is in STAND-BY. Rest of the on-board equipment is ON. TT&C Up/Downlinks. Science Data Downlink. Cryogenic System is ON.
Recycling and Communications	Recycling of SAFARI cooler plus Communications. SAFARI Instrument Recyling Mode is ON. SMI Instrument is in STAND-BY. Rest of the on-board equipment is ON. TT&C Up/Downlinks. Science Data Downlink. Cryogenic System is ON.
Manoeuvres	Manoeuvres. SAFARI Instrument is in STAND-BY. SMI Instrument is in STAND-BY. Rest of the on-board equipment is ON. TT&C Up/Downlinks. AOCS Actuators are ON. Cryogenic System is ON.
Survival Mode	Failure Recovery Mode. Minimum number of units is ON to ensure S/C Survival Conditions (S/C Sun pointing, Thermal Conditions, Power Conditions). Instruments are switched OFF. TM/TC equipment is ON. TM/TC access to DHS is guaranteed to enable failure detection and reconfiguration. Cryogenic System is OFF.
Decontamination Mode	During cruise phase and potentially during observation phase (if required). SAFARI Instrument is OFF. SMI Instrument is OFF. Rest of the on-board equipment is ON. TT&C Up/Downlinks. Out-gassing System is ON. Cryogenic System is OFF.

Table 5-4: System Modes

5.4 System Baseline Design

5.4.1 Overview

The NG-CryoIRTel study was done in two stages. The main part of the study was dedicated to the baseline design of a 2 m size telescope at 6K and the corresponding assessment of all its subsystems.

In a later stage, and in order to explore the growth potential, an optional design was assessed. The objective of this delta design assessment was to find out how much the primary mirror could be enlarged (e.g. higher throughput) without exceeding the available volume allocation for the telescope, and its impact from a structural, thermal and accommodation perspective. The mass budget and equipment list for the optional design are provided in chapter 5.5.

Table 5-5 and Figure 5-1 show the main system characteristics of NG-CryoIRTel baseline design along with its associated reference frames.

NG-CryoIRTel System Characteristics		
Service Module – System Characteristics		
SVM Mass *(w. margin)*	Dry mass	1332 kg
	Total	1644 kg (*excluding adapter*)
Structure	Service Module: thrust cone and SVM panels, both made of a sandwich structure with CFRP face sheets and an aluminium honeycomb core	

	Isolation of the cryo-cooler panels: 12 dampers , 12 brackets	
Mechanisms	Antenna Pointing Mechanism	
	HDRM for Antenna Pointing Mechanism	
	12 Launch-locks for Cryo-cooler Isolators	
	12 Mechanical INTegration parts (MINT)	
AOCS	1 Attitude Anomaly Detector	
	2 Coarse Rate Sensors	
	2 Sun Acquisition Sensors	
	1 Fine Gyro	
	2 Star Trackers	
	1 Fine Attitude Sensor	
	4 Reaction Wheels	
Propulsion	3 Pseudo-spherical tanks of hydrazine, 173.8 litres each	
	12 Thrusters (20N)	
	Other Propulsion Equipment including service valves, latch valves, evacuation vales and pressure transducers	
Power	Solar Array	14.2 m² of "useful" solar array surface, Triple-junction GaAs cells
	Battery	ABSL 18650HC Li-ion battery
	PCU	S3R regulated 28V bus
Communications	1 X-Band High Gain Antenna	
	2 X-Band Low Gain Antennas	
	2 X-Band Transponders	
	2 Travelling Wave Tube Amplifiers	
	2 Electric Power Conditioner (EPC)	
	X-Band Radio Frequency Distribution Unit	
Data Handling	Off-the-shelf CDMU solution, based on SCOC3 or other similar SOC	
	Remote Terminal Unit as an ad-hoc development for the mission	
	Solid State Mass Memory (SSMM) based on flash memory technology	
Thermal	8 x 20K-class 2-stage Stirling Coolers	
	2 x 4K-class Joule-Thomson Coolers	
	2 x 1K-class Joule-Thomson Cooler	
	Cryo-cooler Electronics(part of payload but mounted on SVM)	

	Thermal equipment including radiators, MLI, heaters, thermistors, and heat pipes
Instruments	SAFARI Instrument Warm Electronics Box
	SMI Instrument Warm Electronics Box

Payload Module – System Characteristics		

Payload Module (PLM)

PLM Mass *(w. margin)*	Total	920 kg (*no propellant in PLM*)
Structure	3 thermal shields: CFRP sandwich with aluminium honeycomb core	
	Thermal Shell: aluminium shell or full aluminium sandwich panel	
	Bipod structure: 2 x 2 bipods, one made of GFRP to be decoupled in later stage and one made of CFRP parallel to the main GFRP one	
	TOB: SiC Plate stiffened by ribs on the back side	
	IOB: milled stiffened aluminium plate	
	Telescope: composed of Primary Mirror (M1) and Secondary Mirror (M2), a hexagonal barrel structure holding M2 and a hexapod structure connecting the barrel to M1.	
	All elements are made of SiC except the interface elements which are made of INVAR.	
	Baffle: cylindrical structure made of CFRP sandwich aluminium honeycomb core	
Mechanisms	1 Refocusing mechanism for M2	
	1 Shutter mechanism	
	6 Bipod hold-down & release mechanisms and latches	
AOCS	2 Fine Attitude Sensor cold unit	
Instruments	SAFARI Instrument: Far-Infrared Instrument	
	SMI Instrument: Mid-Infrared Instrument	

Table 5-5: NG-CryoIRTel system characteristics for baseline design
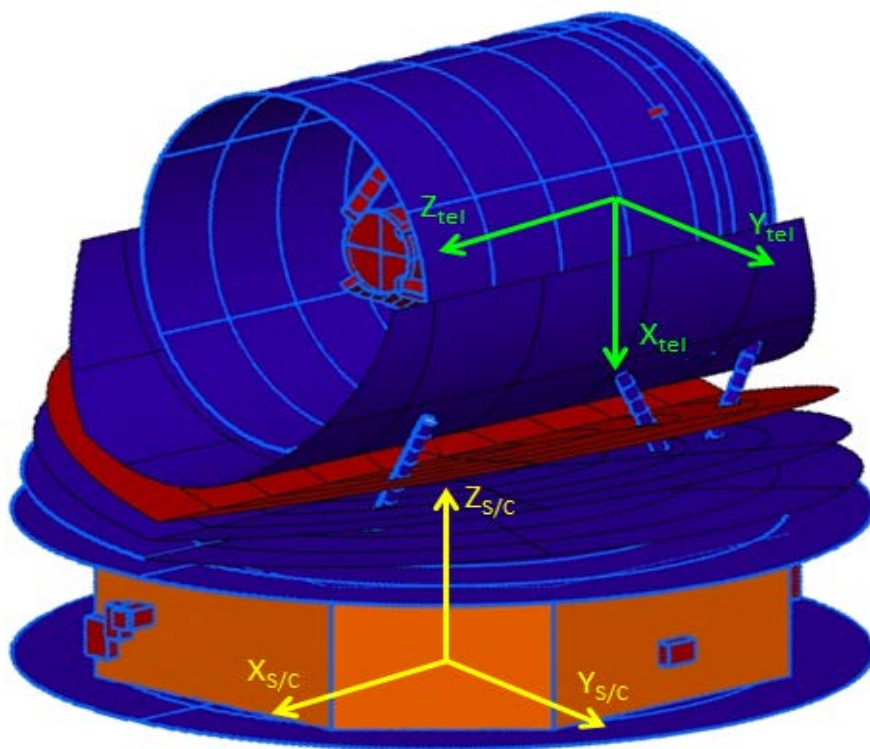
Figure 5-1: NG-CryoIRTel reference frame

5.4.2   Mass Budget

The mass budgets for the Service Module, the Payload Module and the overall spacecraft of the baseline design are provided in Table 5-6, Table 5-7 and Table 5-8. It can be seen that the overall spacecraft wet mass of the baseline design remains below the assumed maximum launch capacity of 3.5 t.

Service Module					
Dry mass contributions	**Without Margin**	**Margin** %	kg	**Total** kg	**% of Total**
Structure	248.10 kg	20.00	49.62	297.72	26.83
Thermal Control	300.00 kg	18.07	54.20	354.20	31.92
Mechanisms	10.84 kg	8.87	0.96	11.80	1.06
Communications	20.20 kg	10.94	2.21	22.41	2.02
Data Handling	29.50 kg	10.00	2.95	32.45	2.92
AOCS	66.03 kg	8.18	5.40	71.44	6.44
Propulsion	82.08 kg	8.18	6.71	88.79	8.00
Power	81.70 kg	10.00	8.17	89.87	8.10
Harness	82.20 kg	0.00	0.00	82.20	7.41
Instruments	49.00 kg	20.00	9.80	58.80	5.30
Total Dry(excl.adapter)	969.65			1109.67	kg
System margin (excl.adapter)		20.00 %		221.93	kg
Total Dry with margin (excl.adapter)				1331.61	kg
Propellant	312.61 kg	N.A.	N.A.	312.61	19.01
Total wet mass (excl.adapter)				1644.22	kg

Table 5-6: Baseline Design – Service Module Mass Budget

Payload Module					
	Without Margin	**Margin**		**Total**	**% of Total**
Dry mass contributions		%	kg	kg	
Structure	445.10 kg	20.00	89.02	534.12	69.68
Thermal Control	10.00 kg	10.00	1.00	11.00	1.43
Mechanisms	24.50 kg	13.27	3.25	27.75	3.62
AOCS	14.00 kg	20.00	2.80	16.80	2.19
Harness	56.78 kg	0.00	0.00	56.78	7.41
Instruments	100.10 kg	20.00	20.02	120.12	15.67
Total Dry(excl.adapter)	**650.48**			**766.57**	**kg**
System margin (excl.adapter)		**20.00** %		**153.31**	**kg**
Total Dry with margin (excl.adapter)				**919.89**	**kg**
Total wet mass (excl.adapter)				**919.89**	**kg**

Table 5-7: Baseline Design – Payload Module Mass Budget

NG-CryoIRTel Baseline Option					
	Mass w/o Margin [kg]	**Margin [%]**	**Margin [kg]**	**Total Mass [kg]**	
Dry mass contributions					
Service Module	**1109.7**	**20.0**	221.9	**1331.6**	
Payload Module	**766.6**	**20.0**	153.3	**919.9**	
Total Dry with Margin				**2251.5**	**kg**
Wet mass contributions					
Propellant	**312.6**	**0.0**	0.0	**312.6**	
Total Wet Mass				**2564.1**	**kg**
Adapter mass (including sep. mech.)	**0.0**	**0**	0.0	**0.0**	
Launch mass				**2564.1**	**kg**
Target Launch Mass				**3500.0**	**kg**
Below Mass Target by:				**935.9**	**kg**

Table 5-8: Baseline Design – Total Mass Budget Without Adapter Mass

5.4.3   Equipment List

The equipment list for the Service Module and the Payload Module of the NG-CryoIRTel baseline design are provided in Table 5-9 and Table 5-10.

Element 1 - Service Module						
FUNCTIONAL SUBSYSTEM	nr	Mass (kg) per unit	Total Mass (kg)	Margin (%)	Margin (kg)	Mass (kg) with Margin
Structure			**248.10**	**20.00**	**49.62**	**297.72**
Thrust cone	1	56.60	56.60	20.00	11.32	67.92
Bottom sunshield	1	30.70	30.70	20.00	6.14	36.84
Top sandwich panel	1	16.40	16.40	20.00	3.28	19.68
Exterior shear panels	1	22.70	22.70	20.00	4.54	27.24
Interior shear panels	1	9.10	9.10	20.00	1.82	10.92
Thrust cone top ring	1	12.00	12.00	20.00	2.40	14.40
Thrust cone bottom ring	1	20.40	20.40	20.00	4.08	24.48
Tank struts and brackets	1	40.00	40.00	20.00	8.00	48.00

Cryo-cooler support panels	1	16.60	16.60	20.00	3.32	19.92
Isolators	1	9.20	9.20	20.00	1.84	11.04
Isolator brackets	1	14.40	14.40	20.00	2.88	17.28
Thermal Control			**300.00**	**18.07**	**54.20**	**354.20**
2ST Cryocooler	8	9.50	76.00	20.00	15.20	91.20
4K JT Cryocooler	2	15.00	30.00	20.00	6.00	36.00
1K JT Cryocooler	2	28.00	56.00	20.00	11.20	67.20
Cryocooler Electronics	1	80.00	80.00	20.00	16.00	96.00
Thermal Equipment	1	58.00	58.00	10.00	5.80	63.80
Mechanisms			**10.84**	**8.87**	**0.96**	**11.80**
APM	1	6.00	6.00	10.00	0.60	6.60
Launch-lock for Cryocoolers Isol.	12	0.12	1.44	5.00	0.07	1.51
MINT	12	0.20	2.40	10.00	0.24	2.64
HDRM for APM	1	1.00	1.00	5.00	0.05	1.05
Communications			**20.20**	**10.94**	**2.21**	**22.41**
X-TRASP	2	3.20	6.40	5.00	0.32	6.72
X-TWT	2	1.00	2.00	5.00	0.10	2.10
X-EPC	2	1.40	2.80	5.00	0.14	2.94
X-LGA	2	0.50	1.00	5.00	0.05	1.05
X-HGA	1	3.00	3.00	20.00	0.60	3.60
X-RFDU	1	5.00	5.00	20.00	1.00	6.00
Data Handling			**29.50**	**10.00**	**2.95**	**32.45**
CDMU	1	5.50	5.50	10.00	0.55	6.05
SSMM	1	12.00	12.00	10.00	1.20	13.20
RTU	1	12.00	12.00	10.00	1.20	13.20
AOCS			**66.03**	**8.18**	**5.40**	**71.44**
SAS	2	0.16	0.32	5.00	0.02	0.34
AAD	1	0.21	0.21	5.00	0.01	0.22
CRS	2	2.00	4.00	5.00	0.20	4.20
STR	2	3.15	6.30	5.00	0.32	6.62
RWL	4	8.60	34.40	5.00	1.72	36.12
GYR	1	6.80	6.80	5.00	0.34	7.14
FAS Warm Electronic	1	14.00	14.00	20.00	2.80	16.80
Propulsion			**82.08**	**8.18**	**6.71**	**88.79**
Propellant tank	3	15.07	45.21	10.00	4.52	49.73
Service Valves	6	0.07	0.39	5.00	0.02	0.41
Pressure Transducer	4	0.27	1.06	5.00	0.05	1.12
Propellant filters	1	0.29	0.29	5.00	0.01	0.30
Latch Valve	2	0.69	1.39	5.00	0.07	1.46
Thrusters	12	1.32	15.87	5.00	0.79	16.67
Piping	50	0.03	1.55	20.00	0.31	1.86
Bracketing & fittings	1	3.32	3.32	20.00	0.66	3.98
Pressurant Gas	1	5.19	5.19	0.00	0.00	5.19
Propellant Residuals	1	6.47	6.47	0.00	0.00	6.47

Passivation valve	3	0.45	1.34	20.00	0.27	1.60
Power			**81.70**	**10.00**	**8.17**	**89.87**
Solar PVA & wiring	1	26.30	26.30	10.00	2.63	28.93
Battery	1	29.40	29.40	10.00	2.94	32.34
PCDU	1	26.00	26.00	10.00	2.60	28.60
Instruments			**49.00**	**20.00**	**9.80**	**58.80**
SAFARI Instrument	*1*		*25.00*	*20.00*	*5.00*	*30.00*
Warm Electronics 1 - ICU	1	25.00	25.00	20.00	5.00	30.00
SMI Instrument	*1*		*24.00*	*20.00*	*4.80*	*28.80*
Warm Electronics	1	24.00	24.00	20.00	4.80	28.80
Propellant						**312.61**

Table 5-9: Baseline Design – Service Module Equipment List

Element 2 - Payload Module						
FUNCTIONAL SUBSYSTEM	nr	Mass (kg) per unit	Total Mass (kg)	Margin (%)	Margin (kg)	Mass (kg) with Margin
Structure			**445.10**	**20.00**	**89.02**	**534.12**
Bipods -X	1	40.30	40.30	20.00	8.06	48.36
Bipods +X	1	3.50	3.50	20.00	0.70	4.20
TOB	1	68.80	68.80	20.00	13.76	82.56
Metering structure	1	6.80	6.80	20.00	1.36	8.16
M1	1	59.70	59.70	20.00	11.94	71.64
M1 bipods	1	0.50	0.50	20.00	0.10	0.60
M2	1	0.30	0.30	20.00	0.06	0.36
Baffle	1	28.50	28.50	20.00	5.70	34.20
Hexapod	1	9.80	9.80	20.00	1.96	11.76
Barrel	1	1.80	1.80	20.00	0.36	2.16
Shield 1	1	20.80	20.80	20.00	4.16	24.96
Shield 2	1	20.40	20.40	20.00	4.08	24.48
Shield 3	1	20.40	20.40	20.00	4.08	24.48
Shield support struts	1	30.00	30.00	20.00	6.00	36.00
Thermal shell	1	18.00	18.00	20.00	3.60	21.60
IOB	1	115.50	115.50	20.00	23.10	138.60
Thermal Control			**10.00**	**10.00**	**1.00**	**11.00**
Cryocooler Thermal Equipment	1	10.00	10.00	10.00	1.00	11.00
Mechanisms			**24.50**	**13.27**	**3.25**	**27.75**
Refocusing M2 mechanism	1	8.00	8.00	20.00	1.60	9.60
Bipods HDRM and Latches	6	2.50	15.00	10.00	1.50	16.50
Shutter mechanism	1	1.50	1.50	10.00	0.15	1.65
AOCS			**14.00**	**20.00**	**2.80**	**16.80**
FAS Cold units	2	7.00	14.00	20.00	2.80	16.80

Instruments			100.10	20.00	20.02	120.12
SAFARI Instrument	*1*			*55.00*	*20.00*	*11.00*	*66.00*
Instrument	1	55.00	55.00	20.00	11.00	66.00
SMI Instrument	*1*		*45.10*	*20.00*	*9.02*	*54.12*
Cam Fore + Rear Optics	1	18.20	18.20	20.00	3.64	21.84
Spec. Fore-Optics	1	12.80	12.80	20.00	2.56	15.36
Spec. Rear Optics	1	14.10	14.10	20.00	2.82	16.92

Table 5-10: Baseline Design – Payload Module Equipment List

5.5   System Optional Design

During a later stage of the CDF study, it was agreed to assess the possibilities to accommodate a larger telescope on the NG-CryoIRTel spacecraft. Hence, an optional design for the telescope was analysed and its impact on the platform assessed.

The optional design of the telescope is an eccentric design but not completely off-axis and it has an obscuration due to the secondary mirror. The objective while establishing this optional design was to minimise the manufacturing complexity of the primary mirror while keeping the centre of gravity of the telescope system as low as possible.

The optional telescope design consists of a 3x2.6m elliptical primary mirror and a 0.81 m secondary mirror with a M1-M2 distance of 1.95 m.

The mass budgets for the Service Module, the Payload Module and the overall spacecraft of the optional design are depicted in Table 5-11, Table 5-12 and Table 5-13. It is highlighted that the overall spacecraft wet mass of this design option remains below the assumed maximum launch capacity of 3.5 t.

Service Module						
	Without Margin		**Margin**		**Total**	**% of Total**
Dry mass contributions		**%**	**kg**	**kg**	
Structure	312.20 kg	**20.00**	62.44	**374.64**	31.41
Thermal Control	300.00 kg	**18.07**	54.20	**354.20**	29.70
Mechanisms	10.84 kg	**8.87**	0.96	**11.80**	0.99
Communications	20.20 kg	**10.94**	2.21	**22.41**	1.88
Data Handling	29.50 kg	**10.00**	2.95	**32.45**	2.72
AOCS	66.03 kg	**8.18**	5.40	**71.44**	5.99
Propulsion	82.08 kg	**8.18**	6.71	**88.79**	7.44
Power	81.70 kg	**10.00**	8.17	**89.87**	7.53
Harness	88.35 kg	**0.00**	0.00	**88.35**	7.41
Instruments	49.00 kg	**20.00**	9.80	**58.80**	4.93
Total Dry(excl.adapter)	1039.90			1192.75	**kg**
System margin (excl.adapter)		**20.00** %		238.55	**kg**
Total Dry with margin (excl.adapter)				1431.30	**kg**
Propellant	312.61 kg	N.A.	N.A.	312.61	17.93
Total wet mass (excl.adapter)				1743.91	**kg**

Table 5-11: Optional Design – Service Module Mass Budget

Payload Module					
	Without Margin	Margin		Total	% of Total
Dry mass contributions		%	kg	kg	
Structure	671.20 kg	20.00	134.24	805.44	76.01
Thermal Control	10.00 kg	10.00	1.00	11.00	1.04
Mechanisms	24.50 kg	13.27	3.25	27.75	2.62
AOCS	14.00 kg	20.00	2.80	16.80	1.59
Harness	78.49 kg	0.00	0.00	78.49	7.41
Instruments	100.10 kg	20.00	20.02	120.12	11.34
Total Dry(excl.adapter)	898.29			1059.60	kg
System margin (excl.adapter)		20.00 %		211.92	kg
Total Dry with margin (excl.adapter)				1271.52	kg
Total wet mass (excl.adapter)				1271.52	kg

Table 5-12: Optional Design – Payload Module Mass Budget

NG-CryoIRTel Delta Design				
	Mass w/o Margin [kg]	Margin [%]	Margin [kg]	Total Mass [kg]
Dry mass contributions				
Service Module	1192.7	20.0	238.5	1431.3
Payload Module	1059.6	20.0	211.9	1271.5
Total Dry with Margin				2702.8
Wet mass contributions				
Propellant	312.6	0.0	0.0	312.6
Total Wet Mass				3015.4
Adapter mass (including sep. mech.)	0.0	0.0	0.0	0.0
Launch mass				3015.4
Target Launch Mass				3500.0
Below Mass Target by:				484.6

Table 5-13: Optional Design – Total Mass Budget

For the optional design, the differences in equipment and design appear to be in the structure of the Service and Payload Module. Therefore, Table 5-14 and Table 5-15 provide the equipment list for the structure only.

Element 1 - Service Module						
FUNCTIONAL SUBSYSTEM	nr	Mass (kg) per unit	Total Mass (kg)	Margin (%)	Margin (kg)	Mass (kg) with Margin
Structure			**312.20**	**20.00**	**62.44**	**374.64**
thrust cone	1	76.10	76.10	20.00	15.22	91.32
bottom sunshield	1	41.00	41.00	20.00	8.20	49.20
top sandwich panel	1	21.90	21.90	20.00	4.38	26.28
exterior shear panels	1	30.30	30.30	20.00	6.06	36.36
interior shear panels	1	12.20	12.20	20.00	2.44	14.64
thrust cone top ring	1	20.00	20.00	20.00	4.00	24.00
thrust cone bottom ring	1	30.50	30.50	20.00	6.10	36.60
tank struts and brackets	1	40.00	40.00	20.00	8.00	48.00
cryo cooler support panels	1	16.60	16.60	20.00	3.32	19.92
isolators	1	9.20	9.20	20.00	1.84	11.04
isolator brackets	1	14.40	14.40	20.00	2.88	17.28

Table 5-14: Optional Design – Service Module Structure Equipment List

Element 2 - Payload Module						
FUNCTIONAL SUBSYSTEM	nr	Mass (kg) per unit	Total Mass (kg)	Margin (%)	Margin (kg)	Mass (kg) with Margin
Structure			**671.20**	**20.00**	**134.24**	**805.44**
PLM truss struts	1	47.90	47.90	20.00	9.58	57.48
hexagonal platform	1	16.00	16.00	20.00	3.20	19.20
TOB	1	141.10	141.10	20.00	28.22	169.32
TOB support struts	1	14.90	14.90	20.00	2.98	17.88
M1	1	116.40	116.40	20.00	23.28	139.68
M1 bipods	1	1.00	1.00	20.00	0.20	1.20
M2	1	1.60	1.60	20.00	0.32	1.92
baffle	1	36.80	36.80	20.00	7.36	44.16
hexapod	1	19.80	19.80	20.00	3.96	23.76
barrel	1	2.70	2.70	20.00	0.54	3.24
shield 1	1	20.80	20.80	20.00	4.16	24.96
shield 2	1	20.40	20.40	20.00	4.08	24.48
shield 3	1	20.40	20.40	20.00	4.08	24.48
shield support struts	1	30.00	30.00	20.00	6.00	36.00
thermal shell	1	18.00	18.00	20.00	3.60	21.60
IOB	1	115.50	115.50	20.00	23.10	138.60
PLM truss struts	1	47.90	47.90	20.00	9.58	57.48

Table 5-15: Optional Design – Payload Module Structure Equipment List

This Page Intentionally Blank

6 OPTICS

6.1 Introduction

The optics design challenge for the NG-CryoIR Telescope mission study has been principally to find an optimum configuration which could fit within the mechanical envelope defined by the interface requirements of the service module while enabling the delivery of a compliant optical field of view to the suite of instruments, at an operational temperature consistent with the scientific objectives of the mission.

6.2 Initial Requirements and Design Drivers

These requirements are flown down from the mission level requirements in chapter 3.

Optical Subsystem Requirements			
Req. ID	Statement	Parent ID	Comment
OR-001	The S/C shall be able to accommodate and operate the following instruments: - The SAFARI FIR instrument - The SMI MIR instrument - The FAS, to meet the needs of the Fine pointing mode (MR-MIS-370)	MR-PERF-060	SAFARI: SPICA Far-IR Instrument SMI: SPICA Mid-IR Instrument FAS: Focal plane Attitude Sensor, i.e. Fine Guidance Sensor. This constrains the optical bench accommodation.
OR-005	The telescope and instrument fore-optics shall cover the 3 to 210 μm wavelength range.	MR-PERF-070	SAFARI and SMI are both above 20 μm. Lower wavelengths are for the FAS.
OR-010	The telescope FoV (defined as a circular radius) shall be at least 15 arcmin.	MR-PERF-080	
OR-015	The telescope FoV (defined as a circular radius) should be at least 18 arcmin.	MG-PERF-090	This is a goal.
OR-020	The telescope and instrument fore-optics figure of merit, defined by the product of the effective area and the throughput (A_{eff} x η), shall be $\geq 0.95*(2m)^2/4*\pi$, over the entire wavelength range defined in MR-PERF-070 and over the entire FoV defined in MR-PERF-080.	MR-PERF-100	
OR-025	Effective aperture (baseline): $\geq$ 3.1m^2 (as defined in OR-020) Effective aperture (goal): $\geq$ 6m^2 [equivalent 2.8m diameter un-obscured aperture]		SAFARI minimum science case for goal

Optical Subsystem Requirements

Req. ID	Statement	Parent ID	Comment
OR-030	The telescope and instrument fore-optics shall be diffraction limited at all wavelengths above $\lambda = 20\ \mu m$ within the entire FoV defined in MR-PERF-080.	MR-PERF-110	
OR-040	The telescope and instrument fore-optics shall have a WFE < 1.43 µm rms.	MR-PERF-110	Marechal criterion: 20/14 (this requirement is effectively redundant with OR-30)
OR-050	The telescope and instrument fore-optics mirrors' roughness shall be ≤ 143 nm rms. (Spatial frequency bandwidth TBD).	MR-PERF-110	1) Allocation: 1/10th of OR-050 2) More stringent requirement from FAS (30 nm rms) is probably achievable.
OR-060	Distance primary-secondary mirrors: 1.8m for on axis and 2.3m for off-axis designs		Initial mechanical envelope constraint
OR-065	Back focal length from 30 to 50 cm behind primary mirror vertex		Initial mechanical envelope constraint
	Background radiation and noise contributions outside of the SAFARI and SMI instruments shall be lower than the astronomical limiting source flux density. i.e. the complete system should be limited by the astronomical photon noise limit or the instruments noise. This drives: - The PLM thermal design requirements - The pointing stability requirements - The straylight requirements - etc.	MR-PERF-120	Derived straylight optical requirements follow below.
OR-070	Straylight (in- and out of field) levels shall be negligible compared to the astronomical noise floor.	MR-PERF-120	
OR-080	The telescope shall have a mechanism on the secondary mirror for in-orbit adjustment of the focus and the alignment (3 DoF TBC).	MR-PERF-110	3 DoF to be confirmed by further analysis.
OR-090	Straylight from out of field astronomical sources scattered onto mirror surfaces into the focal plane instruments shall be ≤ PST is defined as $PST(\theta) = Es(\theta)/E0$. Where the *Es* is the irradiance from an off axis stray-light (point) source at the entrance aperture of the telescope, and *E0* the corresponding irradiance incident at the focal surface of the telescope for any point in the field of view.		Straylight from in-field S/C thermal background sources is negligible when considering TH-010. Active telescope cooling to 6K.

Off-axis angular range	0.25 ~ 3 deg	3 ~ 30 deg	30 ~ 45 deg	> 45 deg
Max PST level	< 5 x 10-4	< 1 x 10-5	< 1 x 10-6	damping to 10-8 @ 90 deg

6.3 Initial Designs and Trade-Off

Telescope concepts used in the trade off include Ritchey-Chrétien on and off-axis, three mirror anastigmats (TMA) and Korsch configurations. All these designs are based on conic surfaces (no aspheric coefficients) and mirror configurations in which the axis of symmetry and vertices of the conical surfaces are on the same line, only the entrance pupil (hence the area of the mirrors illuminated/used) is off-axis.

The influence of the radius of curvature on other design parameters was analysed: "flat" and "curved" in Table 6-1 make reference to larger or smaller radii of curvature for the image surfaces. Image quality was evaluated using the Strehl ratio for each of the designs, and used as one of the trade-off criteria for baseline selection.

To improve image surface flatness (i.e. increase the image surface radius of curvature) in Cassegrain-like systems, the radii of curvature of M1 and M2 need to become similar. The implications are; for on axis systems either a larger secondary mirror (i.e. central obstruction increases) or a larger M1-M2 separation, and for off-axis systems a larger off-axis distance is required.

In TMAs, the correction of field curvature can only be achieved when the balance of radii of curvature of the three mirrors, are not the only degrees of freedom for the correction of other aberrations. In this case the correction relies more heavily on the conic constants. The result can be a large conic constant for the tertiary mirror (see Table 6-1) or high order aspherics. Manufacturing and testing of surfaces with either large conic constants or high order aspheric coefficients is equally challenging.

In Korsch systems, the correction of field curvature becomes easier than in TMAs. The Korsch design in Table 6-1 below shows similar conic constants for M1, M2 and M3 mirrors as compared with the RC On-Axis-Flat telescope and this design yields a significantly flatter image surface with a much larger radius of curvature than available with TMAs.

Telescope concept	EFL (m)	Clearance* (m)	Entrance pupil Size (m)	M1 radius (m) K	M2 radius (m) K	M1-M2 distance (m)	Image radius of curvature (m)	Remarks
Ritchey-Chretien On axis Flat image	9.95	0.5	2	4.68 -1.034	1.42 -2.934	1.8	0.572	
Ritchey-Chretien On axis Curved image	23.00	0.5	2	4.00 -1.002	0.44 -1.442	1.8	0.215	Chosen baseline
Ritchey-Chretien Off-axis Flat image	13.57	2.2	2.5x1.7	4.85 1.030	1.76 -2.245	1.7	0.977	
Ritchey-Chretien Off-axis Curved image	23.00	0.7	2.5x1.7	4.00 -1.002	0.44 -1.442	1.8	0.215	
TMA Flat image	9.77	1.7	2.5x1.7	4.53 -1.060	1.23 -1.828	1.7	0.136	**M3** R = 5.78m K = -14.374

TMA Curved image	13.91	1.9	2.5x1.7	4.53 -1.013	0.74 -1.215	1.9	0.596	**M3** R = 4.57m K = -2.851
Korsch	12.79	0.7	2.5x1.7	3.95 -0.95	0.72 -2.346	1.7	51.947	**M3** R = 0.96m K = -0.507

(*) Clearance is the distance from back of primary to focus for two mirror systems and from tertiary to focus for three mirror systems.

Table 6-1: Basic data of the telescope designs used in the trade off

One of the parameters used in the trade-off for a telescope baseline design selection was the manufacturability and testing of the primary mirror. This drives the development schedule. No large manufacturability differences were found between the different primaries due to their similar radii of curvature, conic constants, and overall dimensions. However it was possible to rank the telescopes using the SESO criterion RD[8], which is a quantitative measure of the polishing difficulty used by telescope manufacturers, and this is presented in Table 6-2 below. The information presented in the second column includes comments on other aspects of the telescope development which were used in the evaluation. During the trade-off additional engineering parameters were also considered in order to reach a balanced selection.

The optimised baseline and the delta study telescopes are also included in this table for completeness.

Telescope type	Primary Mirror Manufacturability (Ranked in order of decreasing difficulty)	Collecting area (m^2)	Strehl ratio (S) (lowest value in FoV)
Design requirements		**7 m^2 (SAFARI)**	**Diffraction limit @ 20 μm (S > 0.8)**
Off-axis Ritchey-Chrétien curved image surface	AIT more complex than for on axis	3.14	0.889
Off-axis Ritchey-Chrétien flat image surface	AIT more complex than for on axis	3.14	0.866
Three mirror TMA curved image surface	Difficult AIT	3.14	0.973
On axis Ritchey-Chrétien flat image surface		2.95	0.815
Three mirror TMA flat image surface	Difficult AIT, challenging tertiary	3.14	0.837
Three mirror Korsch flat image surface	Difficult AIT	3.14	0.868
On axis Ritchey-Chrétien curved image surface	Chosen Baseline concept	3.1	0.937

On axis Ritchey-Chrétien curved image surface	Optimised Baseline (adapted to instruments interface)	3.02	0.896
Eccentric off-axis Ritchey-Chrétien (Delta study)	Larger (asymmetric) primary	5.89	0.922

Table 6-2: Summary of all telescopes evaluated during the study

A basic sensitivity analysis relating the mechanical tolerances of the secondary mirror (e.g. accuracy of its position) and the telescope focus shift was carried out to estimate the required accuracy and range of a focussing mechanism. Not derived from the work carried out during this CDF study but based on lessons learnt from previous projects, shims at the secondary mirror are recommended to be used during the integration and alignment. Additionally, the implementation of a focussing and alignment mechanism on the secondary mirror would also be beneficial (possibly required) for the telescope both at integration but also to correct residual errors due to the cool down process. ESA is currently running a technology development of a cryogenic alignment mechanism optimised for the secondary mirrors of low temperature applications similar to that required for the NG-Cryo telescope. Further details on this are in section 10.1.

It was agreed with JAXA and SAFARI teams that the telescope would have both, an opto-mechanical configuration and layout and optical field of view compatible with existing designs of the instruments. This was done to avoid losing the advantage of the maturity and heritage of the designs as driven by the top level science requirements.

6.4 Selected Baseline Design and Optimisation

Based on an analysis of these designs which included an evaluation of manufacturing complexity and cost, the baseline chosen for further optimisation and use by the other engineering teams was the On axis Ritchey-Chrétien, with curved image surface.

Using the starting data as presented in Table 6-1 this design was then optimised optically to comply with and match as closely as possible the optical interface requirements for the instruments.

The design data for the optimised baseline telescope is given in the following table:

Baseline Telescope	EFL (m)	Clearance* (m)	Entrance pupil Size (m)	M1 radius (m) K	M2 radius (m) K	M1-M2 distance (m)	Image radius of curvature (m)
Optimised Ritchey-Chrétien On axis	10.8	0.5	2	4.00 -1.017	0.96 -2.2279	1.6	0.6

(*) Clearance is the distance from back of primary to focus for two mirror systems and from tertiary to focus for three mirror systems.

Table 6-3: Optical design data of the optimised baseline telescope

This design has the aperture stop on M2, a central obscuration greater than 4% and an f/no of 5.4.
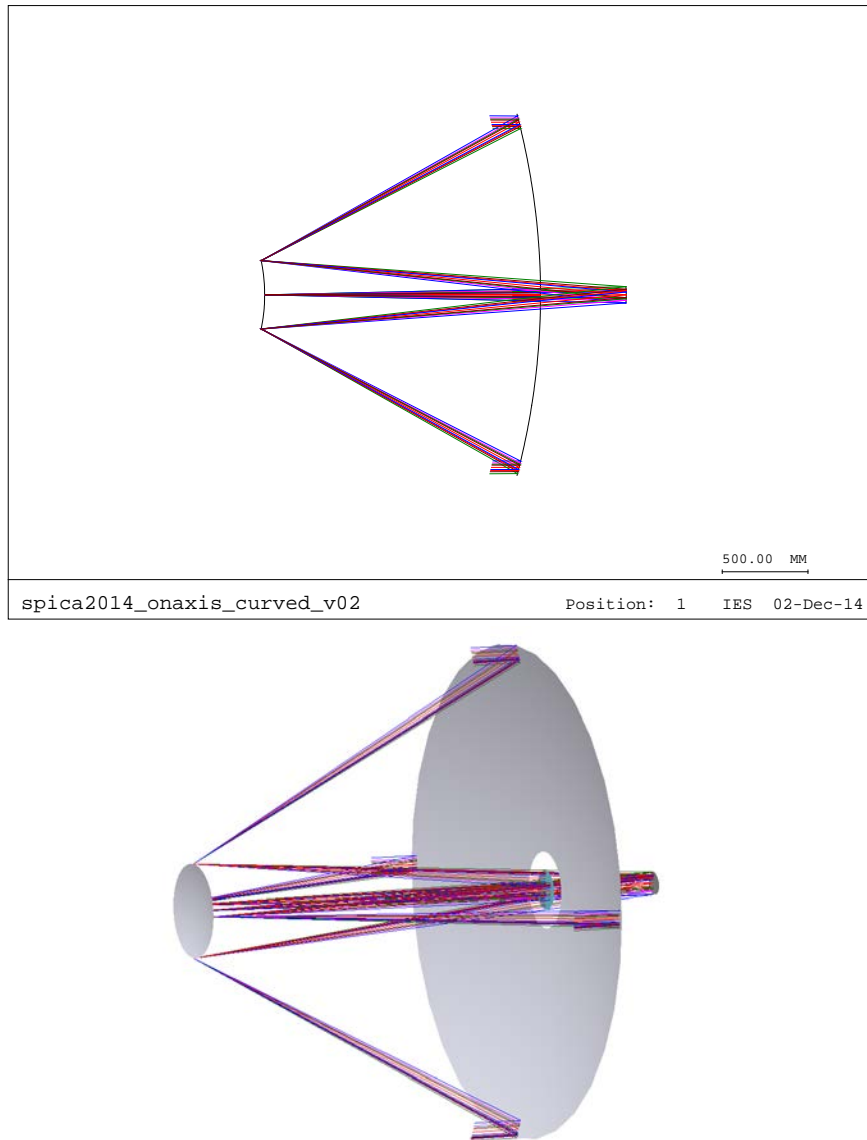

Figure 6-1: Scaled drawing and 3-d view of the telescope baseline

The image quality of the system presented here is analysed for two cases (see Figure 6-2): a curved image surface of radius 600 mm with a FoV of ±15 arc min, and a flat image surface with a square FoV of 3 x 3 arc min (the central object is 10.2 arc min off-axis) tilted at 4.45 degrees. The design is diffraction limited as shown by the spot diagrams (Figure 6-3) and Strehl ratios.
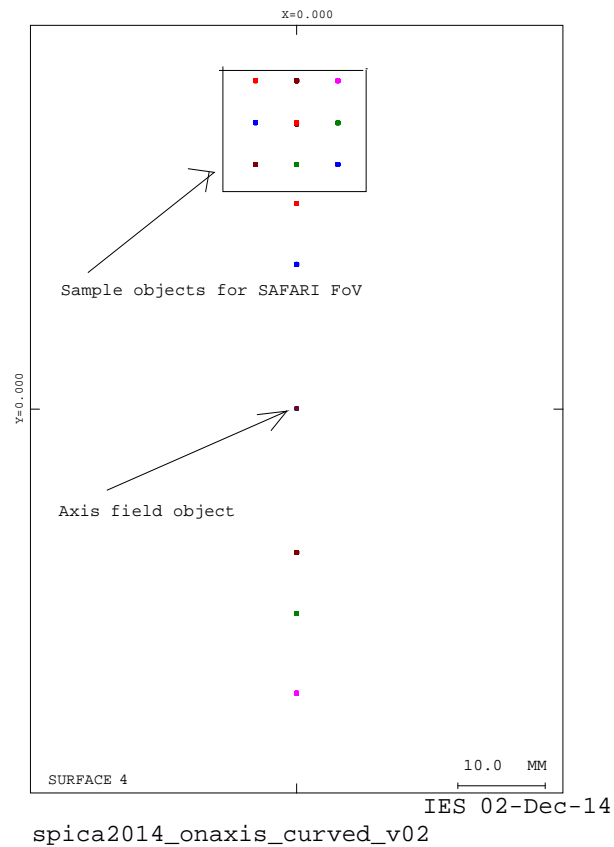
**Figure 6-2: Sample field objects used for image quality analysis**
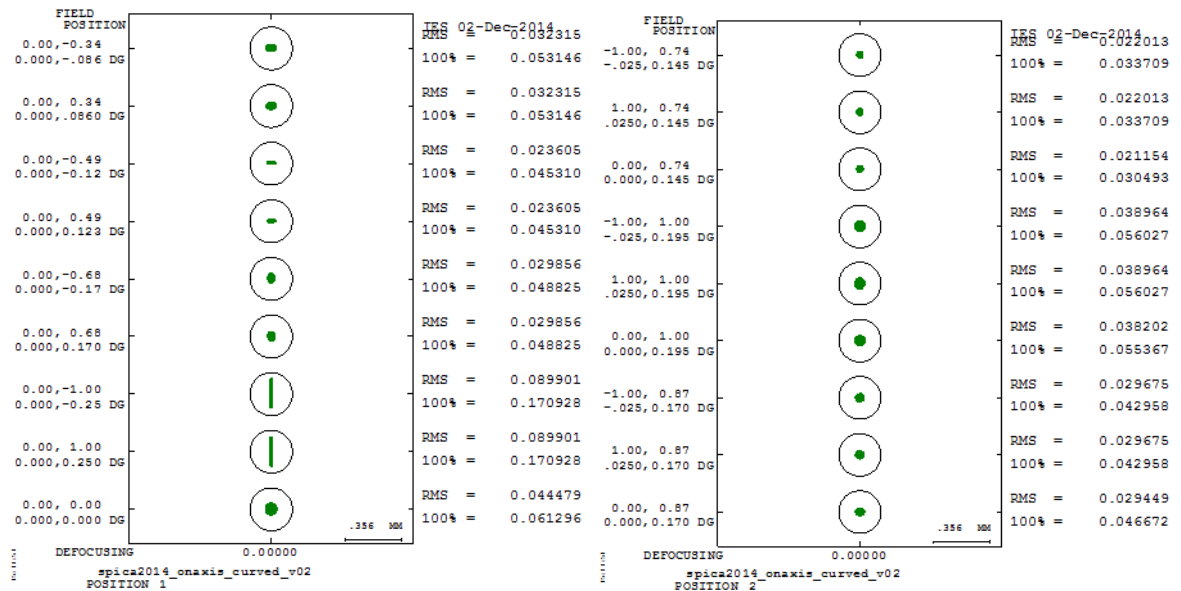
Figure 6-3: Spot diagrams with Airy disc; Left: for a circular FoV of 15 arc min radius with a curved image surface (600 mm radius of curvature); Right: for a square FoV of 3x3 arc min with the central object at 10.2 arc min from axis on a flat image surface

Object points (degrees)		RMS WFE (waves)	Strehl ratio	Object points (degrees)		RMS WFE (waves)	Strehl ratio
X	0.00	0.0215	0.982	X	0.00	0.0197	0.985
Y	0.00			Y	0.17		
X	0.00	0.0529	0.896	X	0.03	0.0200	0.984
Y	0.25			Y	0.17		
X	0.00	0.0529	0.896	X	-0.03	0.0200	0.984
Y	-0.25			Y	0.17		
X	0.00	0.0198	0.985	X	0.00	0.0258	0.974
Y	0.17			Y	0.19		
X	0.00	0.0198	0.985	X	0.03	0.0262	0.973
Y	-0.17			Y	0.19		
X	0.00	0.0134	0.993	X	-0.03	0.0262	0.973
Y	0.12			Y	0.19		
X	0.00	0.0134	0.993	X	0.00	0.0143	0.992
Y	-0.12			Y	0.14		
X	0.00	0.0161	0.990	X	0.03	0.0147	0.991
Y	0.09			Y	0.14		
X	0.00	0.0161	0.990	X	-0.03	0.0147	0.991
Y	-0.09			Y	0.14		

Table 6-4: Image quality in terms of RMS WFE and Strehl ratio for the field objects of Figure 6-2; Left: curved image surface; Right: flat off-axis field *Note that WFE is given in units of waves for 20 µm

Compliance with all interfaces is not possible: e.g. image quality, image surface curvature and f/no are compliant, but location of telescope exit pupil is not. This implies that the optics used in SAFARI would need a re-design.

6.5 Optional Design Study – Optimisation of Throughput vs. Envelope

A delta study including a larger primary mirror was carried out with the aim of finding how much the primary could be enlarged (e.g. higher throughput) without exceeding the available volume allocation for the telescope. Because of the envelope shape (a cone), the main direction of growth for the primary mirror was vertical (that is, orthogonal to the V-grooves) and the distance between the primary and secondary mirrors was not changed noticeably. Although the baseline was an on-axis telescope, a different approach was used for the delta study: it is an eccentric design but not completely off-axis and it has an obscuration due to the secondary. The design approach taken in this case was to minimise the manufacturing complexity of the primary while keeping the centre of gravity of the telescope system as low as possible. Due to the limited time available, no trade-off's similar to the baseline telescopes have been performed.

The design data of the resulting design and its performance are included in the following table:

Delta study Telescope	EFL (m)	Clearance* (m)	Entrance pupil Size (m²)	M1 radius (m) K	M2 radius (m) K	M1-M2 distance (m)	Image radius of curvature (m)
"Eccentric" Ritchey-C Off-axis	16.8	0.6	2.6 x 3.0	4.6 -1.007	0.81 -1.810	1.95	0.38

(*) Clearance is the distance from back of primary to focus for two mirror systems and from tertiary to focus for three mirror systems.

Table 6-5: Optical design data of delta study telescope

This design also has the aperture stop on M2, a central obscuration greater than 2.5% and an f/no of 6.4 x 5.6.

The radius of curvature of the image surface in the above table is indicative only. The image quality is analysed for three flat surfaces with different tilts, corresponding to image locations of the instruments. The field of view locations and sizes are as follows:

- F1: 6 arc min off-axis, 5 x 5 arc min
- F2: 10.2 arc min off-axis, 5 x 5 arc min
- F3: 10.2 arc min off-axis, 2.4 x 2.4 arc min
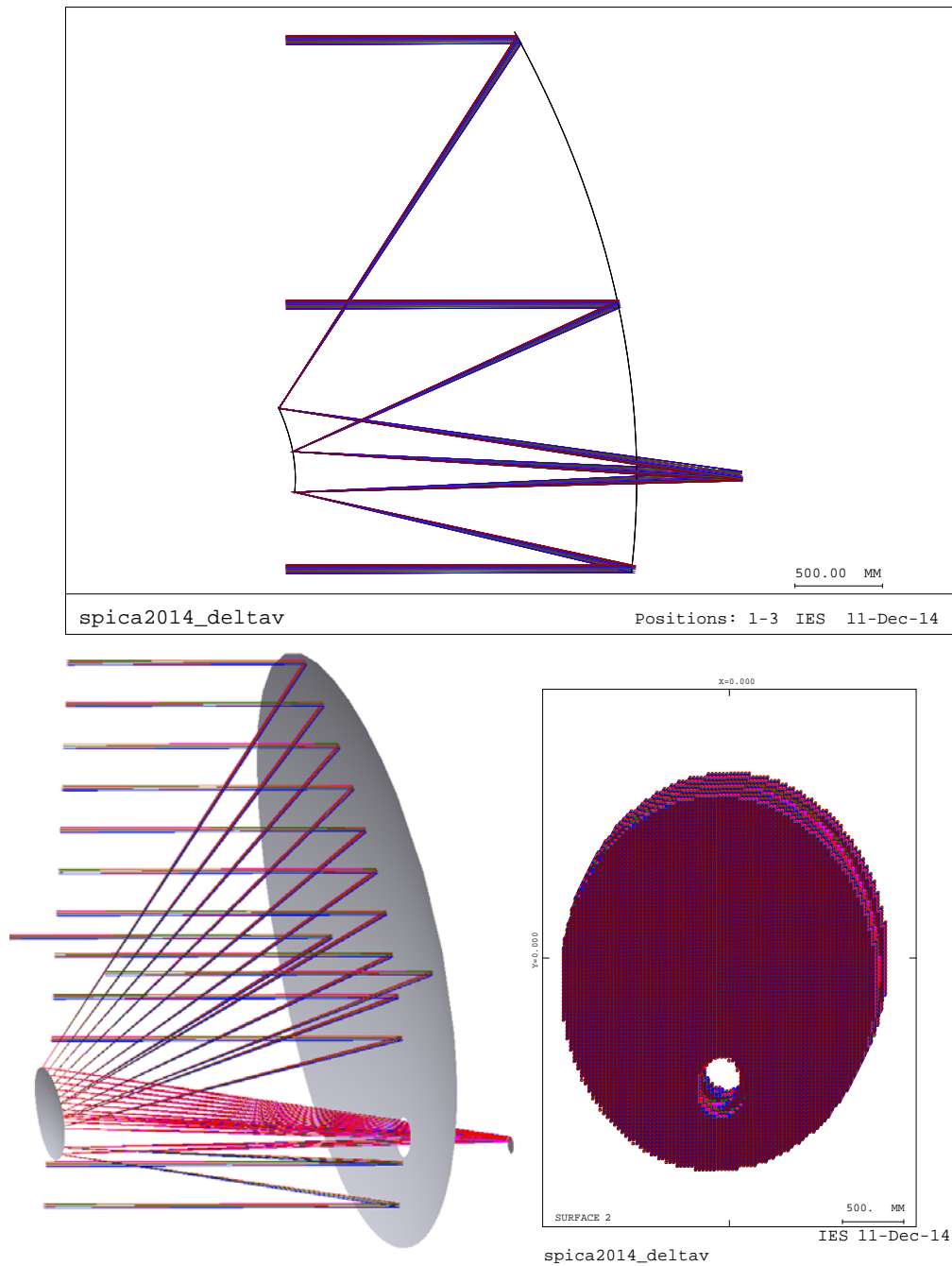
Figure 6-4: Scaled drawing and 3-d view of the telescope for the delta study. A footprint of the beam at the entrance pupil is included on the right showing the shadow of the secondary mirror
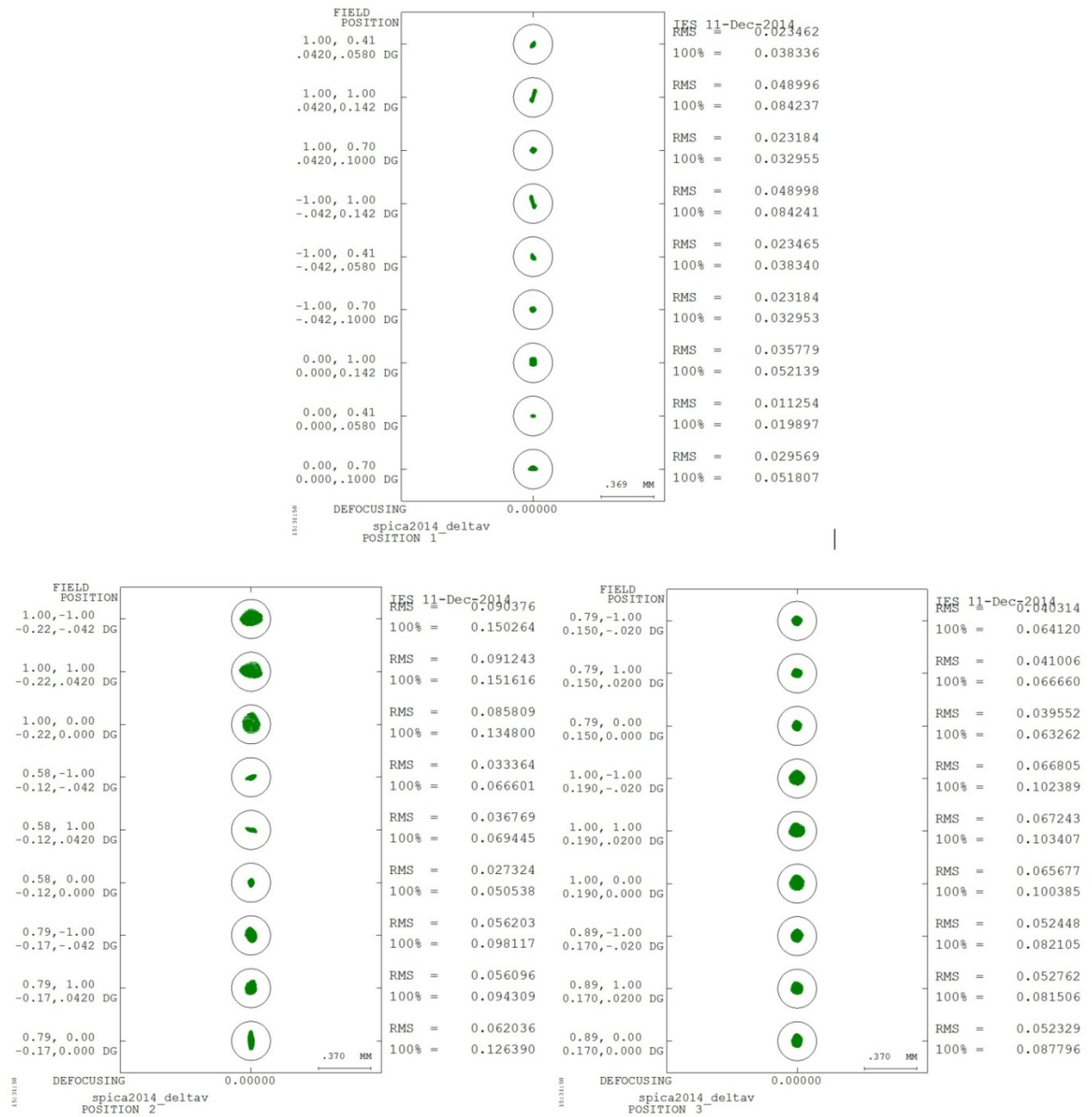
Figure 6-5: Spot diagrams with Airy disc for the field object positions shown in Figure 6-6; Left: FoV F1; Centre (top): FoV F2; and Right: FoV F3

X=0.000

F1

F2

F3

Y=0.000

M1 & M2 optical axis

SURFACE 13

30.0   MM

IES 15-Dec-14

spica2014_deltav
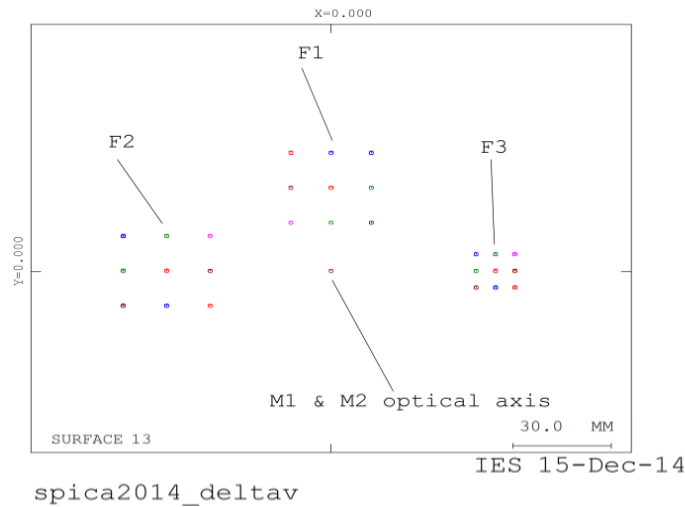
Figure 6-6: Location of the three fields of view with object points used in the analysis of the delta study telescope

Object points for FoV F1 (deg)		RMS WFE (waves)	Strehl ratio	Object points for FoV F2 (deg)		RMS WFE (waves)	Strehl ratio	Object points for FoV F3 (deg)		RMS WFE (waves)	Strehl ratio
X	0.00	0.0125	0.994	X	0.79	0.0353	0.952	X	0.89	0.0306	0.964
Y	0.70			Y	0.00			Y	0.00		
X	0.00	0.0075	0.998	X	0.79	0.0326	0.959	X	0.89	0.0307	0.964
Y	0.41			Y	1.00			Y	1.00		
X	0.00	0.0252	0.975	X	0.79	0.0317	0.961	X	0.89	0.0299	0.965
Y	1.00			Y	-1.00			Y	-1.00		
X	-1.00	0.0158	0.990	X	0.58	0.0150	0.991	X	1.00	0.0366	0.948
Y	0.70			Y	0.00			Y	0.00		
X	-1.00	0.0160	0.990	X	0.58	0.0196	0.985	X	1.00	0.0369	0.948
Y	0.41			Y	1.00			Y	1.00		
X	-1.00	0.0329	0.958	X	0.58	0.0177	0.988	X	1.00	0.0358	0.951
Y	1.00			Y	-1.00			Y	-1.00		
X	1.00	0.0158	0.990	X	1.00	0.0454	0.922	X	0.79	0.0222	0.981
Y	0.70			Y	0.00			Y	0.00		
X	1.00	0.0329	0.958	X	1.00	0.0442	0.926	X	0.79	0.0228	0.980
Y	1.00			Y	1.00			Y	1.00		
X	1.00	0.0160	0.990	X	1.00	0.0404	0.938	X	0.79	0.0225	0.980
Y	0.41			Y	-1.00			Y	-1.00		

Table 6-6: Image quality in terms of RMS WFE and Strehl ratio for the field objects of Figure 6-6; Left: for field objects in FoV F1; centre: for field objects in FoV F2; and right: for field objects in FoV F3 *Note that WFE is given in units of waves, to convert to μm multiply by 20

6.6 Straylight

The straylight properties or performance of the telescope was not analysed or evaluated during the study. However three main sources can be identified:

1. Thermal self-emission – it is critical to control this in order to achieve the desired background limited mission, and it is driven principally by the temperature and emissivity of the innermost surface of the telescope external thermal baffle facing the optics. This needs to be at or below 10 K.

2. In-field (Galactic, Zodiacal, Cosmic Infra-red Background and bright point sources)

3. Out of field (Same as above, but including Sun, Earth, Moon & solar system objects)

A careful analysis is required leading to a deterministic baffling design, with particular emphasis on thermal shielding temperature and emissivity of all surfaces which have a view factor towards the telescope optical surfaces.

6.7 Initial Tolerancing Considerations of NGCryo CDF Baseline Telescope

This section contains initial considerations for a tolerance analysis of the NGCryo baseline telescope. The purpose is to estimate the effect of the secondary mirror (M2) tolerances on the telescope performance and assess the possible use of an aligning and focussing mechanism on this mirror.

It should be noticed that a proper tolerance analysis requires information of a detailed opto-mechanical design. The information here can only be regarded as initial estimates to decide on an alignment and integration strategy. Additionally, it can help to assess the resolution and adjustment range required by an in-flight M2 aligning and focussing mechanism, but it cannot be used to decide if it is necessary since no detailed mechanical design exists yet.

The baseline design used in the CDF (Code V file spica2014_onaxis_curved_v02.seq) is an on axis two mirror telescope. It is an f/5.4 system as required to fit the instrument interfaces.

A separate annex is available on request which contains the results of the wave front error analyses carried out with Code V for possible future reference and information.

6.7.1 Analysis of Results

A complete tolerance analysis of the telescope should include the following error sources:

- Design inherent error
- Telescope manufacturing errors (both mirrors manufacture and mechanical structure)
- Integration and alignment errors (including the effect of cooling)
- Launch settling effects
- In orbit gravity release and stability errors.

To keep the analysis manageable at this early stage a reduced set of criteria types have been identified and used, they are:

- Image quality (e.g. using PSF, Encircled energy or Wavefront Error)
- Line of sight and vigneting effects
- Alignment with the instruments.

For each criteria, two analyses are necessary and are part of the error budget for each:

- One including compensators which represents manufacture (mirror surface form errors, mechanical metering and optical surface support structures and opto-mechanical integration) in which either shims or a mechanism can be used to compensate other errors. The variables used in this analysis are called tolerances or <u>manufacturing tolerances</u> in this document.
- The other in which no compensators are used represents the effects of launch vibrations and in orbit effects (e.g. gravity release and thermal stability). The variables used in this analysis are called <u>stabilities</u>.

The criteria types are discussed in the subsections below together with estimates of the contribution of M2 tolerances (manufacturing and stabilities) for each of them.

6.7.2   Image Quality

The parameter selected to evaluate image quality is RMS WFE. The requirement of a diffraction limited image at the instruments detector (e.g. SAFARI) translates into an overall (during operations) WFE of 1.4 μm ($\lambda/14$ with $\lambda=20$ micron). A preliminary RMS WFE error budget is assumed to make provision for all sources of error (manufacturing, integration, cooling, instrument, etc.) as follows:

Error source # and type	Error source contribution
1 (M2 positioning)	0.3 μm
2 (Telescope as designed)	1.06 μm (worst field object)
3 (All other error sources)	0.86 μm
Total RMS WFE: 1.4 μm	

Table 6-7: Image quality error budget

6.7.3 Manufacturing Tolerances

The set of M2 positioning tolerances which yields increments of the RMS WFE smaller than 0.3 micron for all the field objects included in the analysis are given in the next table. Tolerances used are the M2 "x", "y" (lateral) and "z" (axial) displacements and the tilts in x and y "a" and "b" respectively:

M2 Tolerance variable	Value
z	0.05 mm
x	0.1 mm
y	0.1 mm
a	0.0005 rad
b	0.0005 rad
Compensator (telescope focus shift)	1.6 mm

Table 6-8: All values in the above table are half of the range, the total tolerances are ±"value"

The axial focus shift has been used as compensator and requires a range of ±1.6 mm. This would be equivalent to using axial shims during integration of the instrument. Because of the use of the compensator, the analysis does not give information about the stabilities (vibrations at launch, thermal effects and other in orbit contributions), but only about the effects of the errors in the mechanical structure and cooling. The complete set (tolerances plus compensator) would yield a diffraction limited system (telescope plus instrument). Margins for uncertainties would also need to be added for a final value used during development.

6.7.4 Stabilities

Stabilities are part of the error sources type 3 in Table 6-7. They should yield an error smaller than the total $0.86\mu m$ considered for all other sources (e.g. also instrument errors contribute to this part). Note that other variables such as changes in the mirrors shape due to temperature are also stabilities although are not included in the analysis, therefore a smaller error has been allocated for the set of stabilities used in this analysis: $0.18\mu m$. This set, as before, consists of the displacements of M2 (z-axis is axial displacement, x and y are lateral) and the tilts in x (a) and y (b), now without compensator:

Stability variable	Value
z	0.005 mm
x	0.01 mm
y	0.01 mm
a	0.00005 rad
b	0.00005 rad

Table 6-9: Stabilites: mechanism resolution

If the mechanical design is such that post-integration effects (such as launch vibrations or thermal stability) cause changes in the structure larger than the stabilities, the values given in this section could be interpreted as the required resolution of a focusing/aligning mechanism on M2 to be used in orbit. In case the opposite situation happens, then a compensator in orbit would not be strictly required, though it would

reduce risks against unknown or unanticipated effects (e.g. Hubble type). It would appear, however, that 5µm could be quite a tight value for the axial positioning stability of M2, so, unless the error budget could be changed, this indicates the need of an in orbit focusing mechanism.

6.7.5 Vigneting and Line of Sight

The secondary mirror tilts could yield vigneting (if the primary is not sufficiently oversized) and also change the direction of the FoV of the instrument. The latter is just an offset which can be compensated for. The lateral shift of the light footprint on the primary mirror due to an M2 tilt of 0.0005 rad is less than 1 mm, so the set of tolerances used in image quality seems more stringent than would be required to avoid vigneting. The stabilities obtained in image quality are smaller and so would be their effect on vigneting.

6.7.6 Alignment with the Instrument

Lateral displacements of M2 are in fact displacements of the telescope exit pupil (equal to instrument entrance pupil) whose diameter is 390 mm. The tolerance used in image quality analysis is equivalent to a displacement of the exit pupil of 2.6 per thousand, which does not appear very critical. So once again image quality requirements yield a more stringent tolerance for these variables. Finally, as before, the stabilities obtained in image quality are smaller and so it would be their effect on vigneting.

6.8 Tolerancing Summary

Initial considerations for a tolerance analysis have been discussed and preliminary tolerances and stabilities (these represent launch and other in orbit effects) of the secondary mirror positioning have been obtained in the previous sections. A preliminary tolerancing strategy is explained and followed which includes three possible aspects to be considered during a more complete tolerance analysis.

Estimates of ranges for an M2 mechanism with 5 degrees of freedom which could be used during integration of the telescope and the instrument have been obtained. The need for this mechanism is not derived from the values of these tolerances but justified by the anticipated structural and optical cool down effects. Preliminary stability values are also given. Some of them seem to indicate that an M2 focusing mechanism for in orbit corrections might be necessary.

6.9 Conclusions

Several telescope configurations have been traded off in this study. These configurations included on and off-axis designs, as well as two and three mirror systems. A full parametric analysis of the design parameters versus telescope performance with respect to the driving requirements (image quality, curvature of the image surface, throughput, etc.) was not carried out, but useful conclusions could nevertheless be drawn by careful comparison of the designs. Also a basic sensitivity analysis relating the mechanical tolerances of the secondary mirror (e.g. accuracy of its position) and the telescope focus shift was carried out to estimate the required accuracy and range of a focussing mechanism. The final down-selection was based not only on optical performance but

also on criteria related to manufacturing, volume, focussing mechanism, and other aspects.

The baseline design selected for the study was a Ritchey-Chretien on axis configuration. An initial tolerancing analysis was performed on the baseline telescope which supports the need for a secondary mirror focusing and alignment mechanism.

During the study a further iteration of the baseline telescope configuration (delta design) was carried out to fully use the mechanical volume envelope available to the telescope.

Although the baseline was an on-axis telescope, a different approach was used for the delta study: it is an eccentric but not completely off-axis configuration.

A preliminary optimisation of this delta design allowed a useful increase of the primary mirror with respect to the baseline design, which was highly desired scientifically. The ability to achieve this with a two mirror design is important from a cost effectiveness perspective.

The baseline telescope design presented is compliant with both the available volume envelope and the image quality required for the scientific case. However, this design cannot comply with all the interface requirements for the existing SPICA instrument designs or achieve the desired useful collecting area of 7 m² corresponding with the SPICA 3.2 m telescope.

The delta telescope design developed in this study, however, shows clearly that it is possible to include a larger primary without exceeding the available volume, while providing a sufficient image quality similar to the baseline, and having the distinct advantage of being able to achieve a scientifically useful collecting area of 6 m².

This Page Intentionally Blank

7 INSTRUMENTS AND DETECTORS

7.1 Requirements and Design Drivers

The science case, as detailed in the sections hereunder, calls for photometry and medium to high resolution spectroscopy between 20 and 210 µm. Detectors operating at these wavelengths require active cooling to 6K and 2K (Si:As and Si:Sb technology) and to 50mK (TES Transition Edge Sensor technology).

The wavelength range is covered by two instruments:

- SMI - a camera and grating spectrometer: 20 - 37 µm
- SAFARI - a Fourier-Transform imaging spectrometer: 34 - 210 µm

7.2 Assumptions and Trade-offs

The instrument suite has extensively been studied during early phases, in the framework of the SPICA mission study, and various trade-offs and re-scopes, on the science requirements side as well as on the instrument design side were carried out.

The present instrument concepts are the results of this study and are geared towards the science requirements detailed hereafter.

7.3 Baseline Design

The far-infrared, is a truly unique wavelength domain; a major fraction of the starlight in the universe is processed through dust and gas and subsequently reemitted there, providing measurement tools to assess the physical state and energy balance of cool matter. Following the successes of earlier space missions – IRAS, ISO, Spitzer, AKARI, and Herschel – with warm(ish) or small(ish) size telescopes, the next step in far-infrared research can be made only with a mission with a large cold telescope, as only that will provide a uniquely low background emissivity environment (like the JAXA proposed SPace Infrared telescope for Cosmology and Astrophysics – SPICA). On such a platform the background radiation from the telescope and platform itself are significantly less than or on the order of the background radiation from celestial sources; the zodiacal light and galactic cirrus emission, and the cosmic microwave background – on such a platform a new generation of highly sensitive detectors can be used to observe the universe without being blinded by the telescope.

7.3.1 Instruments

7.3.1.1 SPICA Mid-Infrared Instrument (SMI)

The mid-infrared (20 to 37µm) range of the mission is to be covered by the SPICA Mid-Infrared Instrument (SMI). SMI consists of one imaging channel and two spectroscopic channels (grating spectrometer). The imaging channel has both a wide-band (R=several) and a series of narrow-band (R=20) imaging capability. The latter is to be used for efficient mapping of PAH features at various redshift. The spectroscopic channels are designed to have high spectroscopic survey efficiency for extragalactic studies.
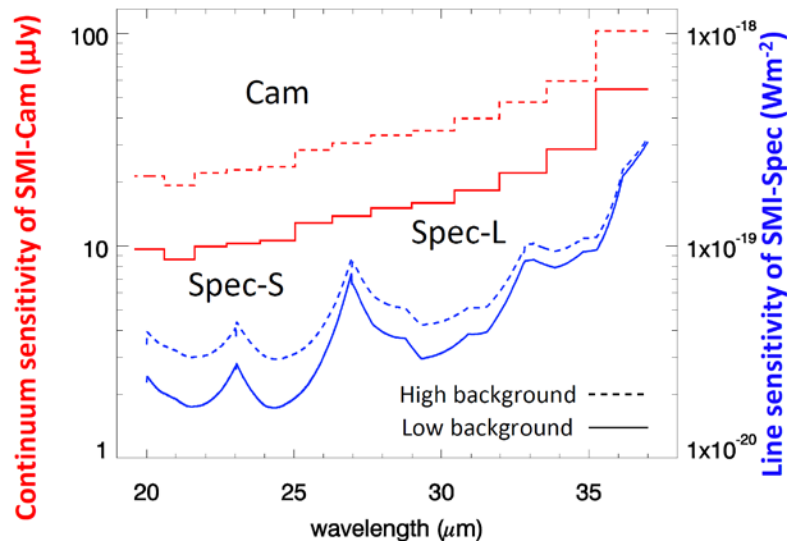
Figure 7-1: Sensitivity (5 sigma in one hour) lot of the SPICA Mid-Infrared Instrument (SMI) based on the baseline 3.2 meter SPICA telescope

Parameter		Function		
		Cam	Spec-S	Spec-L
Wavelength range		20-37 μm	20-27 μm	27-37 μm
Spectral resolution		20 [a]	1000-2000 [b] (point source), 1000 [c] (diffuse)	
Field of View		5' x 5'	150" x 3" (slit)	
FWHM		1."4 (20 μm) - 2."6 (37 μm)		
Pixel scale		0."52 x 0."52	0."52	
Detector		Si:Sb 1K x 1K	Si:As 1K x 1K	Si:Sb 1K x 1K
	Cont. sensitivity (1 hr, 5 sigma)	$(9 - 50)$ μJy	$(0.1 - 0.5)$ mJy	$(0.2 - 1)$ mJy
	Line sensitivity (1 hr, 5 sigma)	$(6 - 15)$ x 10^{-20} W/m^2	$(2 - 7)$ x 10^{-20} W/m^2	$(3 - 10)$ x 10^{-20} W/m^2
	Survey speed [d]	~ 7 arcmin^2/hr	~ 4 arcmin^2/hr	~ 2 arcmin^2/hr
	Sensitivity [e] (1 hr, 5 sigma)	Continuum	Line	
		$(0.2-1)$ MJy/sr	$(1 - 4)$ x 10^{-9} W/m^2/sr	$(2 - 5)$ x 10^{-9} W/m^2/sr
Saturation limit		~ 1 Jy	~ 100 Jy	~ 400 Jy

Table 7-1: Specification of SPICA Mid-Infrared Instrument (SMI) based on the baseline 3.2 meter SPICA telescope

7.3.1.2   SPICA Far-Infrared Instrument (SAFARI)

The far-infrared part (34-210μm) part of the mission is to be covered by the SPICA Far-Infrared Instrument (SAFARI), which is to be developed by the SAFARI consortium led by SRON, Netherlands. SAFARI is an imaging Fourier-Transform spectrometer with very sensitive Transition Edge Sensors (TES).

The basis of the design is a Fourier Transform Spectrometer in a Mach-Zehnder optical configuration. In such a configuration the incoming signal is split in two beams which are relayed via a set of movable mirrors onto a beam combiner from where the signal is forwarded to the detectors. When the mirrors are moved the path length difference along the two arms gives rise to an interference pattern in the re-combined beam, corresponding to the Fourier transform of the incoming spectrum. By utilising this FTS in combination with detector arrays each pixel measures such an interference pattern for a different position on the sky, thus making such an instrument an efficient imaging spectrometer. The instrument has continuous spectroscopic capability from 34-210 μm with three bands, being limited in sensitivity only by the natural background.

	Parameter	Waveband		
		SW	MW	LW
General	Band Center	47 μm	85 μm	160 μm
	Wavelength Range	34−60 μm	60−110 μm	110−210 μm
	Band Center FWHM	5″	7″	13″
	Number of Detectors	43 X 43	34 X 34	18 X 18
	FOV	2' X 2'	2' X 2'	2' X 2'
Photometry	Limiting Source Flux Density (5σ − 1hr)	14 μJy	21 μJy	32 μJy
	Confusion Limit	0.015 mJy	0.5 mJy	5 mJy
	Time to reach confusion limit (1σ)	123 s	0.3 s	0.006 s
Spectroscopy	Limiting Line Fllux (5σ − 1hr)	3.7 X 10^{-19} W m^{-2}	3.4 X 10^{-19} W m^{-2}	2.9 X 10^{-19} W m^{-2}

Table 7-2: Specifications of SPICA Far-Infrared Instrument (SAFARI) based on the baseline 3.2 meter SPICA telescope
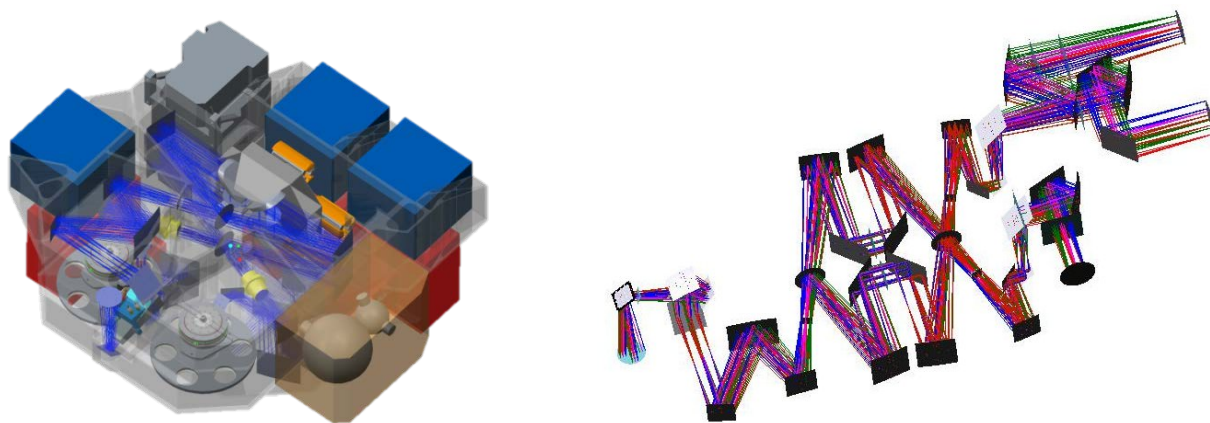

Figure 7-2: right panel - the SAFARI optics design, unfolded, showing in the centre the two moveable rooftop mirrors forming the heart of the FTS. Left panel - the SAFARI cold Focal Plane Unit containing all optical elements and the three detector units, each covering one octave of the total 35-210 μm wavelength range. In the centre the top part of the physical stage containing the FTS rooftop mirrors is visible. The detector arrays are housed in the red boxes, two of which are just

visible on the lower left and right. EMI filtering circuits for each detector array are housed in the blue boxes. The grey structure at the top is the milli-kelvin cooler

7.3.2   Science Objectives

There are many fields of astronomy that can and will be addressed with the SPICA instruments, from nearby to very far away objects and from small to very large – we will be able to characterise many of the small Trans Neptunian Objects in our own solar system, but also observe the very earliest galaxies whose emission is amplified through gravitational lensing by foreground clusters, and many objects in-between. The following sections present those research areas which have been identified by the joint SPICA science team as the main science drivers for the mission; 1) galaxy formation and evolution over cosmic times, 2) the gas and dust properties of nearby galaxies and 3) planet forming disk systems. As such these are the drivers for the instrument design and give guidance when design or implementation trade-offs need to be made.

7.3.2.1   The formation and evolution of galaxies

Over the last decade it has been well established that the bulk of the galaxy star formation and supermassive black hole (SMBH) accretion in the Universe occurred from redshift z~1 to z~3 (Figure 7-2). Also it has become apparent that the evolution of galaxies – at variance with what occurs in dark matter structure formation – proceeds in a "top-down" fashion, with most massive galaxies being the first to form (the cosmic downsizing). At the same time the presence of a SMBH at the centre of local galaxies, reminiscent of a QSO phase, and the tight relations between their mass and the properties of the stellar spheroidal component indicate a past mutual interaction between the black hole growth and the build-up of the mass in stars. The details of this interplay, its effect on cosmic downsizing, as well as the mechanism behind the star formation in massive galaxies are still far from being understood and several crucial questions remain unsolved:

- What are the major physical processes shaping the galaxy mass functions?
- What are the key processes regulating galaxy formation and evolution and the position of galaxies along the star forming sequence?
- What governs the interplay between star formation and AGN accretion in galaxy formation and evolution?

The answers to these questions require a detailed investigation of the physical processes in large samples of cosmic sources, which only can be achieved with sensitive spectroscopic observations. Since both star formation and black hole accretion are characterised by severe dust obscuration around the peak of their cosmic evolution, the mid- to far-infrared wavelength window is the most suited to study the formation and evolution of galaxies.
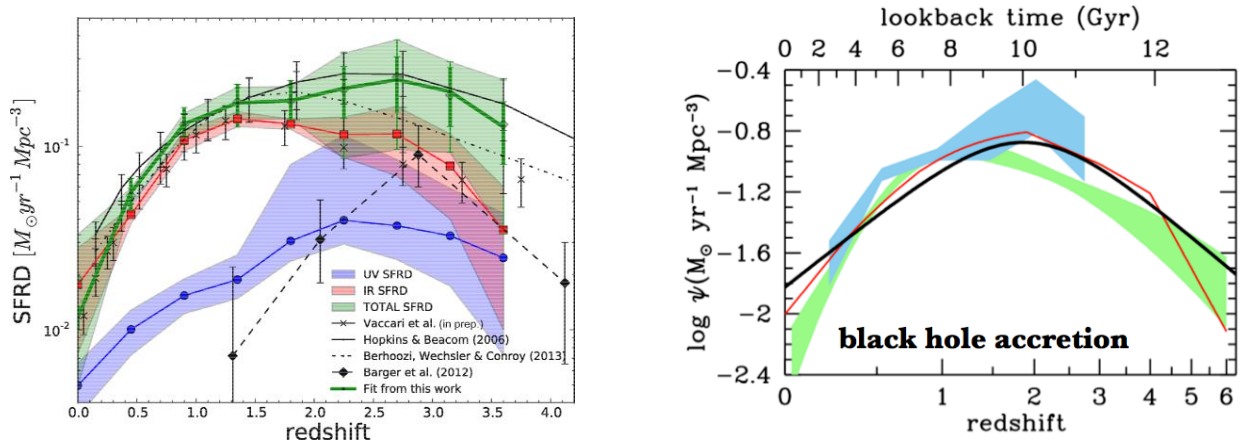
Figure 7-3: Left panel: SFR densities in the UV, uncorrected for dust extinction, in blue, in the far-IR in red, and in total (i.e., UV + far-IR) in green. The lines are the mean values, while the lighter colours show the uncertainties. Right panel: massive black hole accretion history inferred from X-ray (red curve and green shading ref.) and infrared data. The co-moving rates of black hole accretion have been scaled up by a factor of 3300 to facilitate visual comparison to the star formation history (solid black line)

The evolution of star formation and SMBH accretion power with time (Figure 7-3) shows that they were both ~20 times higher at z~1-3 than today, strongly supporting their co-evolution. Similarly, the average dust opacity in star-forming galaxies has a large maximum at about z~1-2, and decreases at higher and lower z, clearly demonstrating that the evolution of star formation in galaxies can only be fully addressed from an infrared perspective, insensitive to dust absorption and where the dust has its emission peak. Fine-structure MIR/FIR lines are direct tracers of the physical conditions (gas excitation, density, ionization, hardness of the primary radiation field, metallicities, etc.), allowing us to e.g. quantify AGN vs stellar power sources inside evolving objects. These tracers provide a large number of tools to address the issue of co-evolution in various ways. For example the star formation in the hosts of QSOs can be studied via PAH features and other star formation tracers like [Ne II], and as an alternative to X-rays, in particular for Compton thick sources, luminosity functions to be used as a means to study the accretion rate history of the universe can be also constructed from high ionization IR lines like [OIV]. Additionally such spectroscopic observations will provide us with essential information on the kinematics of the line emitting media, either induced by the SMBH gravitational potential or by AGN feedback effects. This can be used to determine the SMBH masses and mass functions for obscured AGNs out to redshift of 4, e.g. by using the [OIV] line. Note that this science is a very strong sensitivity driver – the typical line strength of an [OIV] line for a typical galaxy at z ~ 3-4 will be of order a few 10^{-20} Wm^{-2}.

The physical drivers of this co-evolution will be studied. Possible controlling mechanisms providing positive feedback, for instance, are common feeding (e.g. in mergers), secular disk instabilities and clumps, bars, nuclear spiral structures, or triggered star formation through winds/shocks from AGN and/or stars. Negative feedback could come from the quenching of star formation and starvation of SMBHs via strong (e.g. radiation pressure driven) winds/outflows from AGN and/or stars. In order

to reproduce quantitatively the winding down behaviour at redshifts of z=0-1, and explain the discrepancy of the observed baryonic galaxy mass function with the dark matter mass distribution, many galaxy evolution models indeed include such a negative feedback component.

All these issues can be directly addressed only by utilising a platform like SPICA to execute very deep – required line sensitivity ~ 2-5×10^{-20} Wm^{-2} - spectroscopic surveys covering a wavelength range from 20 to 210 µm with a spectral resolution of up to a few thousand. The spectra resulting from such a survey will allow us to measure the basic properties of the star formation process in a large number of galaxies as they evolve over cosmic time.

7.3.2.2 The lifecycle of gas and dust in galaxies near and far

The cycling of gas between stars and the interstellar medium is a major driver of the evolution of galaxies, but its dependence on local conditions is poorly understood. In particular, the rate of star formation varies by orders of magnitude within galaxies, and even more between galaxies of different types. By imaging galaxies in diagnostic lines and features, the conditions of dust and gas such as temperature, density, and radiation field can be characterised in unprecedented detail. This will provide spatially resolved estimates of the local temperature, the gas density. Other star formation rate estimates may be obtained from the [C II] 158 µm line or from the [O I] line for comparison. Complementary information on the magnetic field will come from ground-based facilities such as CCAT, information on the neutral atomic gas distribution from the SKA, on the stellar distribution from EUCLID, on the CO from the LMT, while the cold dust is known from Herschel. By comparing these local ISM conditions with the spatially resolved estimates of the local star formation rates, it will be possible to unravel the origin of cosmic variations in the star formation rate and the stellar mass distribution.

A key question in modern astronomy is how galaxies evolve, and from Spitzer and Herschel research it is now understood that dust grains most certainly play a major role in their evolution. Dust grains are one of the major energy emitters in the galaxy, radiating up to 90% of the total energy from extensively star-forming galaxies. Furthermore, dust grains are the major cooling process during star formation in galaxies. Although dust is important for the galaxies' underlying physical and chemical processes, it is still poorly understood how galaxies have acquired their dust grains within their interstellar medium. By surveying a large number of spatially resolved galaxies the chemical and physical conditions where dust grains are formed, processed, destroyed and lost can be characterised in unprecedented detail.

7.3.2.3 Planet forming disks

The study of protoplanetary disks provides the missing link between planet formation models and extrasolar planetary systems. Stars are born with flat rotating disks in which planets form over timescales ranging from a few Myr (gas giants) to 100 Myr (terrestrial planets). Planet formation must be very efficient since the Kepler mission surveying roughly 150 000 stars found so far more than 2700 planets, roughly half of them in multiple systems. One of the big questions still is how protoplanetary disks evolve into planetary systems and whether there exist multiple pathways to planetary systems.

To improve our understanding of these systems measurements of the strong cooling lines in the 12 – 210 μm domain will provide a complete view of the gas and ice involved in planet formation processes by connecting the inner and outer disk. In particular, SPICA will be the only facility which can investigate for the first time the relation between ices and dust mineralogy, but also between disk structure and the presence of ices for stars similar to our Sun. Several areas of research can be addressed well only in this wavelength domain:

- Which processes drive the gas evolution of planet forming young disks?
- How do the main water reservoirs (gas, ice) evolve during the planet forming process?
- What is the thermal and chemical history of the building blocks of planets (dust and ice)?
- What is the composition (gas, dust, ice) and architecture of nearby resolved debris disks?
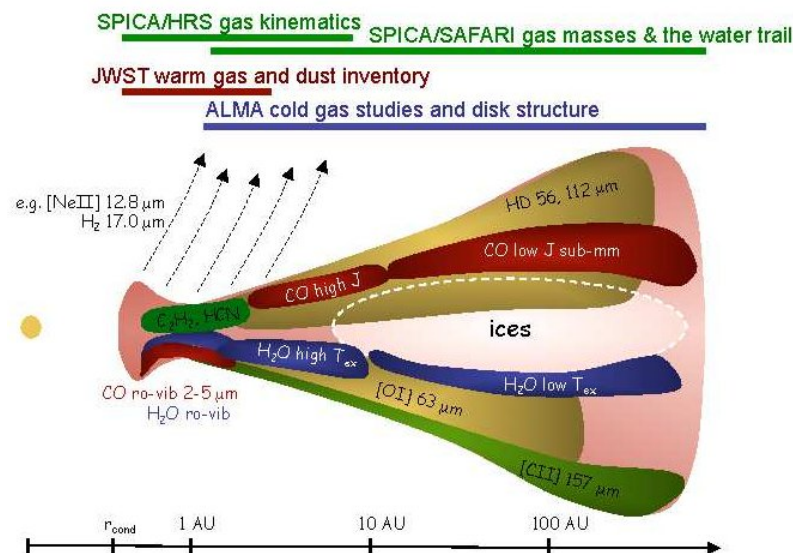
Figure 7-4: Gas emission from planet forming disks as observed with ALMA, JWST and SPICA at different wavelengths

How does the Kuiper belt compare dynamically and chemically to debris disks?

The HD rotational lines provide the most direct method for measuring disk gas mass. The abundance of HD depends only on the local H/D ratio. In cold regions of the disk, cosmic ray dissociation of HD could drive some fraction of HD into HDO ice. The 112/56 μm line ratio provides a reliable gas temperature estimate, and SAFARI is unique in providing access to both these lines. An independent gas temperature probe and key to characterise disk evolution are the [O I] fine-structure lines at 63 and 145 μm. These oxygen lines can extent the disk gas mass estimates into the lower mass regime. It is estimated that both lines should be detected in roughly half of the disks down to disk gas masses of 10−4 M0.

Additionally SPICA instruments are unique in assessing the ice/vapour fraction in disks, studying the link of dust and ice crystallinity through evolutionary/transport processes. Water line emission at mid-IR wavelength together with the ice features will give an in-depth view of the entire water trail in protoplanetary disks.

Debris disks, the remainders from the planet formation process, have been studied in large numbers only via photometric imaging due to their intrinsically faint nature. Indeed the various unbiased surveys conducted in the FIR using facilities such as IRAS, Spitzer and Herschel, failed to detect true Kuiper belt (KB) analogues, i.e. a disk with fractional luminosity (f = Ldisc/L*)~10−7. For unresolved sources the calibration uncertainties have always been too high to confidently detect a disk of such low fractional luminosity. With the SPICA high sensitivity true KB analogues become detectable around a range of stars.

Finally in our own outer Solar System beyond Neptune, more than a thousand objects have been discovered since 1992, including the previously theorized Kuiper Belt. These trans-Neptunian objects (TNOs) are essentially unchanged leftovers of the planetesimal disk around the early Sun and are therefore uniquely valuable tracers of the formation and evolution of the Solar System and of planetary systems in general. SPICA will allow the characterisation of all 40,000 TNOs expected to be discovered by the mid 2020'ies and will for the first time explore properties of small TNOs that can be directly linked to dust and gas properties from a large population of debris disks.

7.4 Technology Requirements

7.4.1 SMI

The instrument design, including cooling chain, and detector arrays are based on the AKARI and Spitzer payload.

Main upgrade is the development of the Si:Sb detector array from 128 x 128 to 1k x 1k.

7.4.2 SAFARI

Flight heritage (Herschel instruments) exists for the main instrument components such as the FTS and the cryocoolers.

The main new developments are the detector arrays, the Transition Edge Sensor (TES) bolometers.

7.5 Instrument Budgets

7.5.1 Mass

[kg]	FPU	Cryo Harness	Warm Electronics	Margin (%)	Total
SMI	45	tbc	24	20	83
SAFARI	55	tbc	25	20	96
P/L	100		89		189

7.5.2   Power (peak)

[W]	Warm Electronics	Margin (%)	Total
SMI	35	20	42
SAFARI	125	20	150
P/L	160		192

7.5.3   Thermal - Operating Temperatures

	FPU		Warm Electronics	
	Tmax [K]	Tmin [K]	Tmax [C]	Tmin [C]
SMI	4-10	0.8	+50	-10
SAFARI	5	0.2	+50	-10

7.5.4   Data Rate

[kbps]	ON	STBY
SMI	2000	1
SAFARI	4000	4

This Page Intentionally Blank

8   CONFIGURATION

8.1   Requirements and Design Drivers

Req. ID	STATEMENT	Parent ID
SubSystem requirements		
CFG-010	The spacecraft configuration shall be designed to fit within the available useable volume of the H-X launch vehicle	
CFG-020	The spacecraft shall interface to the launcher by means of a ring with 2360 mm diameter	
CFG-030	The configuration shall accommodate the telescope, Instruments and equipment in order to comply with the mission objectives, power, thermal, propulsion and communication requirements.	
CFG-040	The configuration shall take into account the limitations due to AIV constraints.	
CFG-050	The configuration shall provide an unobstructed field of view for all instruments and equipment.	
CFG-060	The configuration shall provide unobstructed position for the thrusters to fulfil the mission requirements without contamination of relevant parts of the spacecraft.	
CFG-070	Mission orbital and attitude constraints shall be taken into account to provide the required thermal and stray-light shielding	

8.2   Assumptions and Trade-Offs

It has been assumed that the spacecraft interface with the launch vehicle is defined by the diameter of 2360 mm.

8.3   Baseline Design

8.3.1   Baseline Design

The spacecraft configurations have been based on a modular approach. Two separate modules, the Payload Module (PLM) and the Service Module (SVM), have been conceived to keep the interfaces between the SVM and the PLM simple and clear, simplifying the development and then the integration and testing activities.
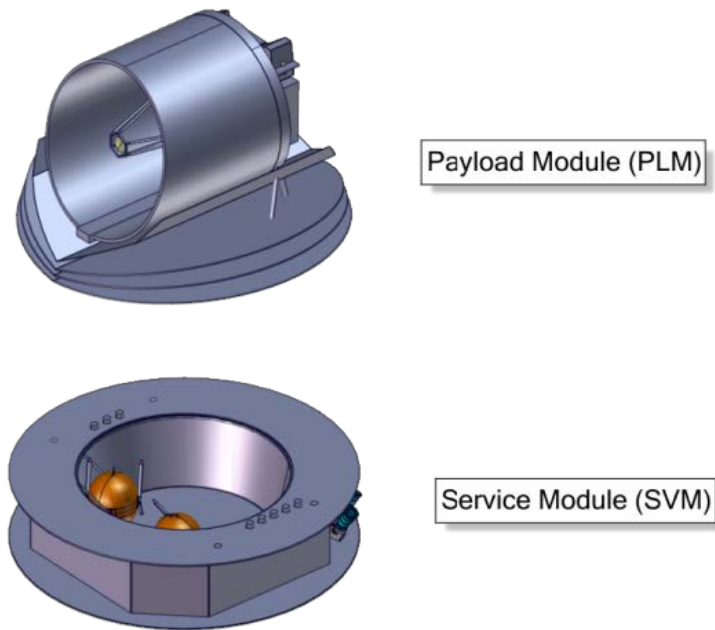
Figure 8-1: NGCryoIRTel modules

During the study 3 spacecraft configurations have been considered as shown in the following table.

	SVM	PLM
Baseline configuration	CryoCooler units inside SVM, H=940mm	Circular mirror Ø2m
Option 1	CryoCooler units inside SVM, H=940mm	Elliptical mirror 2mx3m
Option 2	CryoCooler units on top part of SVM, H=1540mm	Elliptical mirror 2mx3m

Table 8-1: NGCryoIRTel – Configurations

8.3.2 Baseline Configuration

Figure 8-2 shows the baseline configuration of the NG-CryoIRTel Spacecraft inside the fairing volume of H-X Launcher
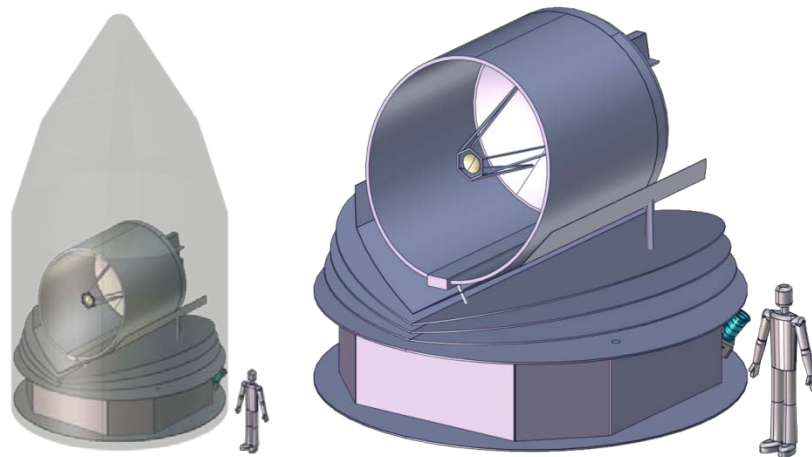
Figure 8-2: NGCryoIRTel spacecraft (1.8m tall dummy)

8.3.3 Service Module (SVM)

The primary structure of the SVM is composed of a thrust cone which also constitutes the load path between the PLM and the launcher, and shear panels. The thrust cone structure will interface the H-X launcher interface at 2360mm diameter. The secondary structure made by the upper and lower platform and side panels accommodates all spacecraft equipment and the cryo-cooler units. The lower platform serves as sunshield and solar panels. Solar cells are mounted on the panel in- and out-side the thrust cone. The octagonal shaped spacecraft body has 940mm height dimension. The upper diameter of the thrust cone of 3m diameter is mainly driven by the optical design dimension. The thrust cone will then have an inverted shaped cone. The outer diameter of the upper and lower platform dimensions is limited to 4.5m by the H-X fairing (which allows a max. diameter of 4.6m). The SVM height is driven by propellant tank size and partly also by the Cryo-Cooler unit panel in the baseline design. Three propellant tanks are accommodated inside the thrust cone by means of struts. Main structural elements of the SVM are illustrated in Figure 8-3.
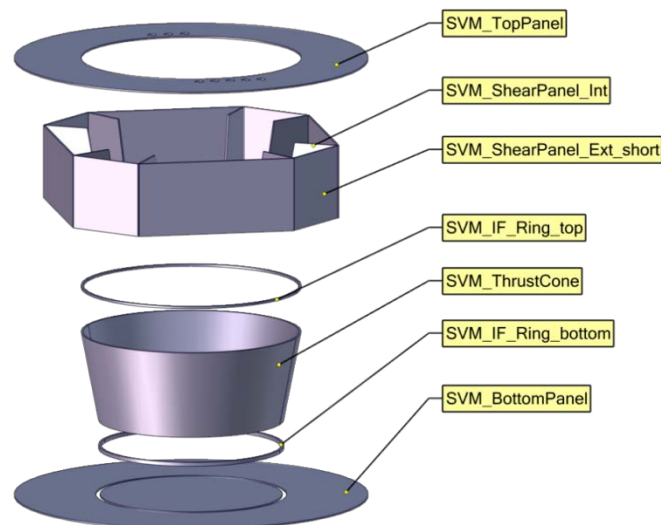
Figure 8-3: SVM main elements

The internal accommodation of the SVM is illustrated in Figure 8-6.

8.3.4   Payload Module (PLM)

To minimise interface loads from integration and cryo-temperature between the SVM and PLM, a 3-points bipod configuration is designed to support the PLM assembly. Each interface point will be connected with 2 sets of bipods. CFRP bipods will provide launch survivability and the GFRP bipods mounted parallel to the CFRP bipods will decouple the instrument from the thermal and thermo-elastic perturbations. The concept is similar to the bipod concept used on the GAIA spacecraft. During the study only one connection beam was modelled to illustrate the bipod.

PLM is composed of thermal shields, telescope, Telescope Optical Bench (TOB), Instrument Optical Bench (IOB) and baffle. The PLM baseline design is driven by the 2 m diameter primary mirror M1. One of the requirements that needs to be fulfilled is that the PLM has to fit within a cone with 15° half-angle, see Figure 8-9.

Planck's passive cooling system concept that used three thermal shields is used for NG-CryoIRTel PLM to passively reduce the temperature from the SVM towards the telescope assembly. In addition to Planck, a thermal shell – which is actively cooled down to 21K – is placed between the V-Groove and the telescope baffle.

TOB and integrated metering structure are PLM parts that have direct connection to the SVM through the 3-point bipods. The TOB gives support to Mirror M1, IOB and the telescope by means of isostatic mounts. M2 supporting structure interfaces the TOB by means of a hexapod structure. The telescope structure that is composed of M1, M2, and M2 support structure is similar to the one used on Herschel.

Figure 8-4 shows the PLM elements:
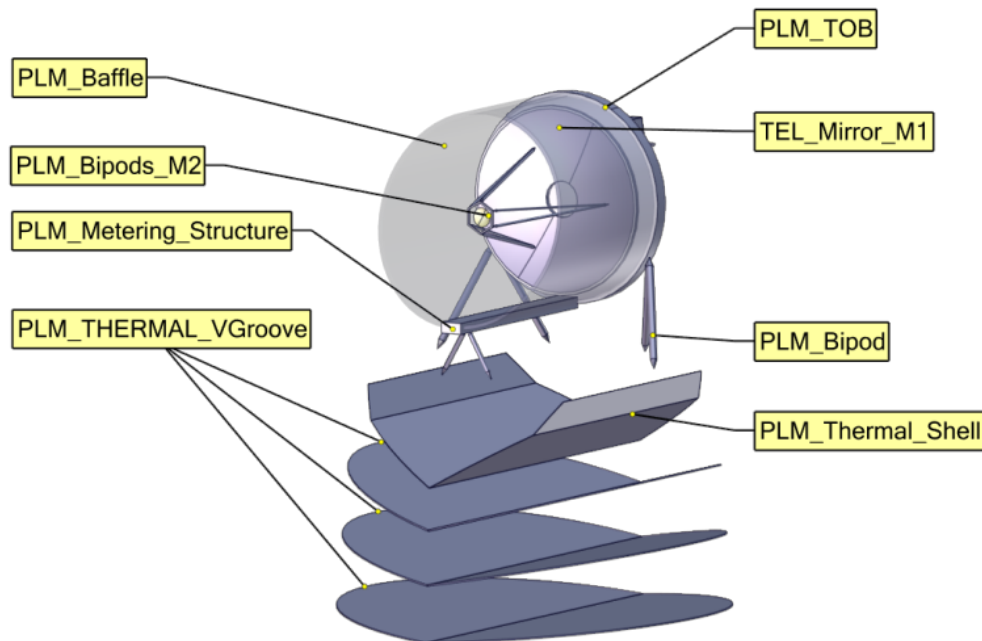
Figure 8-4: PLM elements

8.4 Internal and External Accommodation

There are 8 compartments available inside the SVM as shown in Figure 8-5 to accommodate the electronic boxes and the cryo-cooler units.

All units are accommodated as such that CoG lies around the central launcher axis.
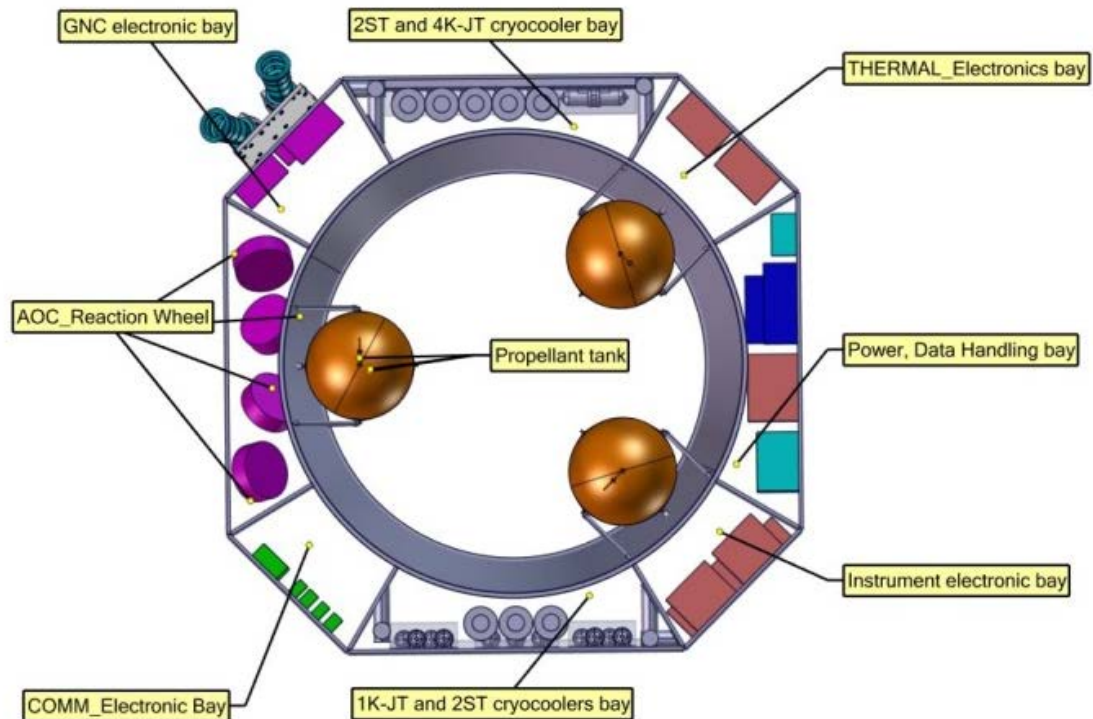

Figure 8-5: SVM compartments
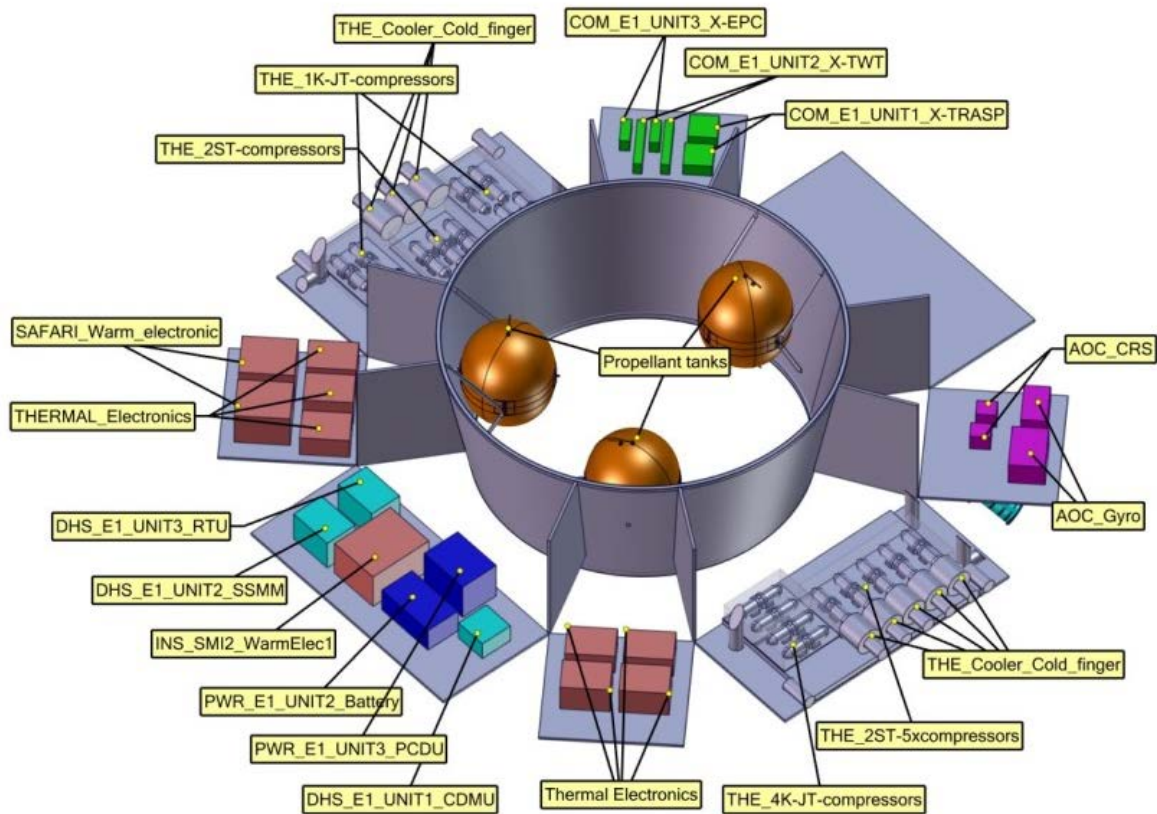
Figure 8-6: SVM internal accommodation

There are 4 units accommodated on the external part of the bottom plate, sun sensors and a high gain antenna as shown in Figure 8-7. Four reaction wheels are mounted on the internal part of the bottom plate as shown in Figure 8-5.
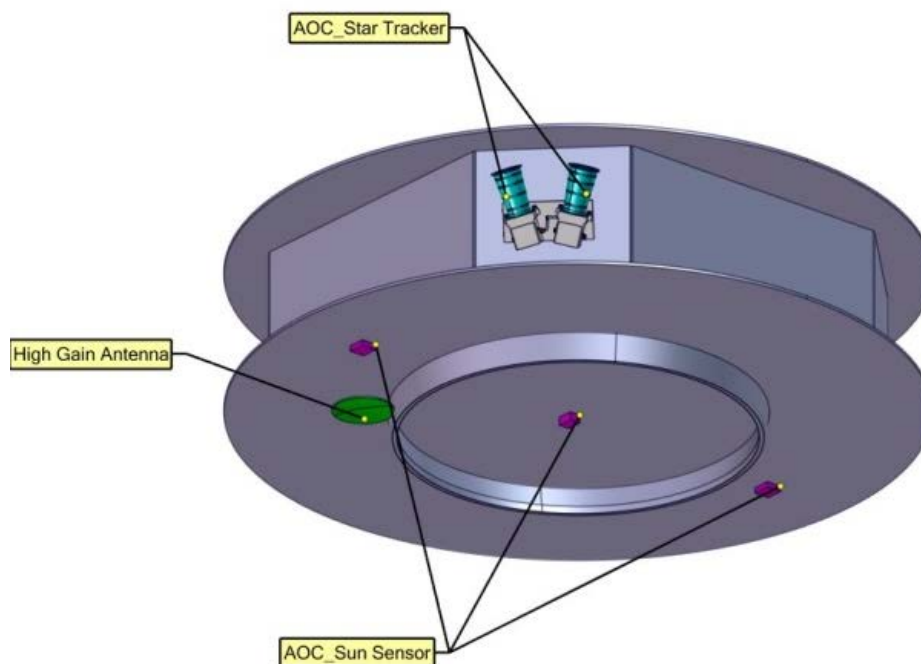
Figure 8-7: SVM external accommodation

PLM accommodation is shown in Figure 8-8.
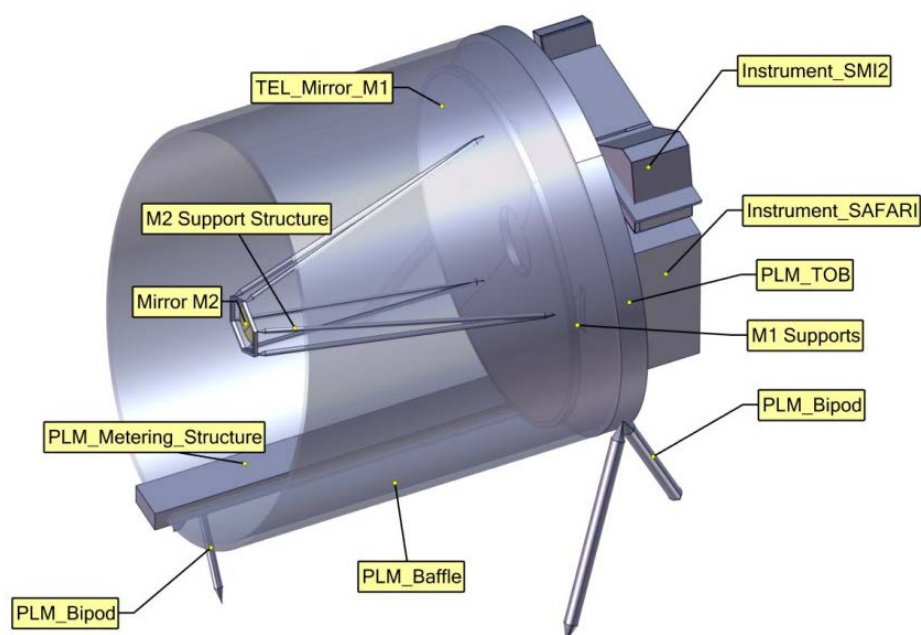
Figure 8-8: PLM accommodation

8.5 Overall Dimensions

The overall dimension of the baseline NG-CryoIRTel spacecraft can be seen in Figure 8-9 to Figure 8-13
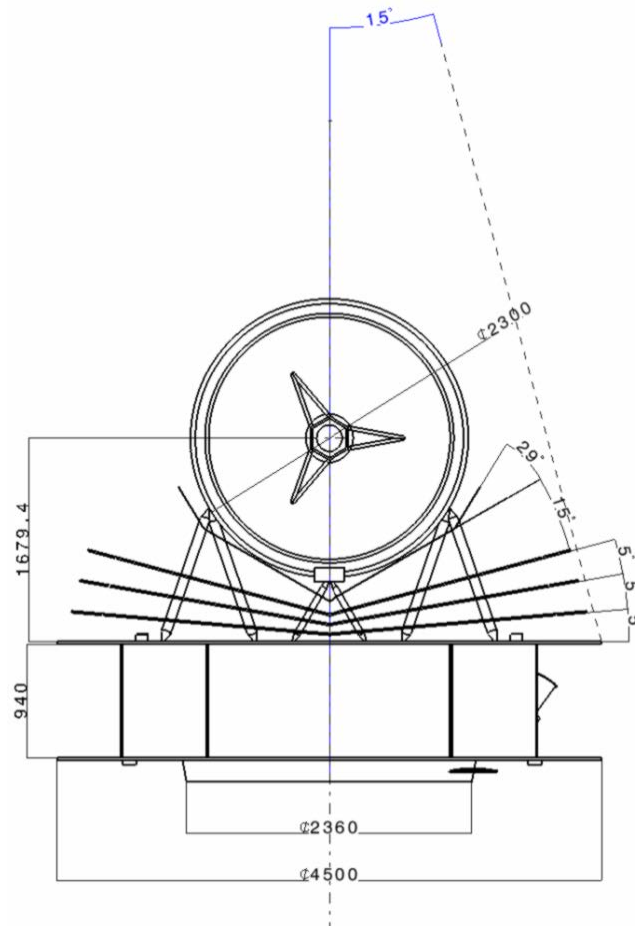
**Figure 8-9: NG-CryoIRTel overall dimension (perpendicular to M1)**
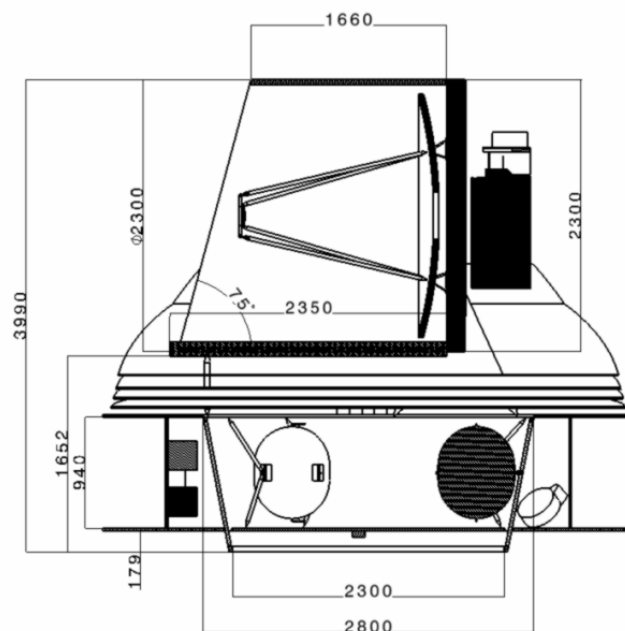
**Figure 8-10: NG-CryoIRTel overall dimension parallel to M1-M2 direction**
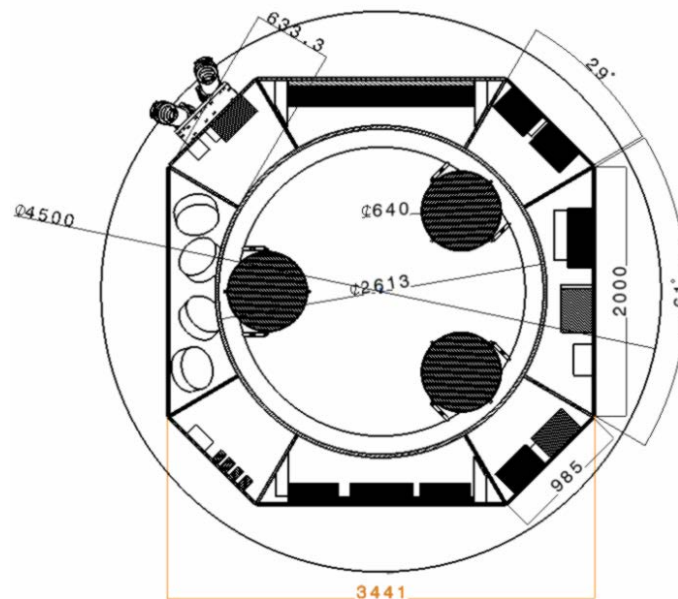
**Figure 8-11: NG-CryoIRTel SVM main dimension**
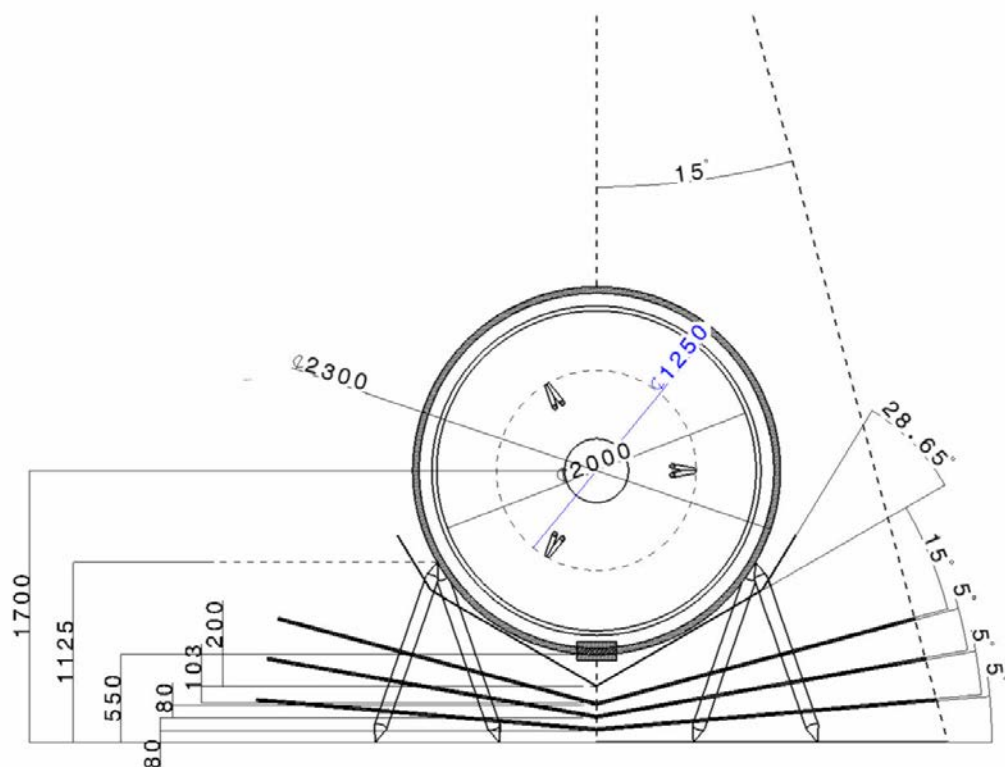
**Figure 8-12: NG-CryoIRTel PLM dimension (perpendicular to M1)**
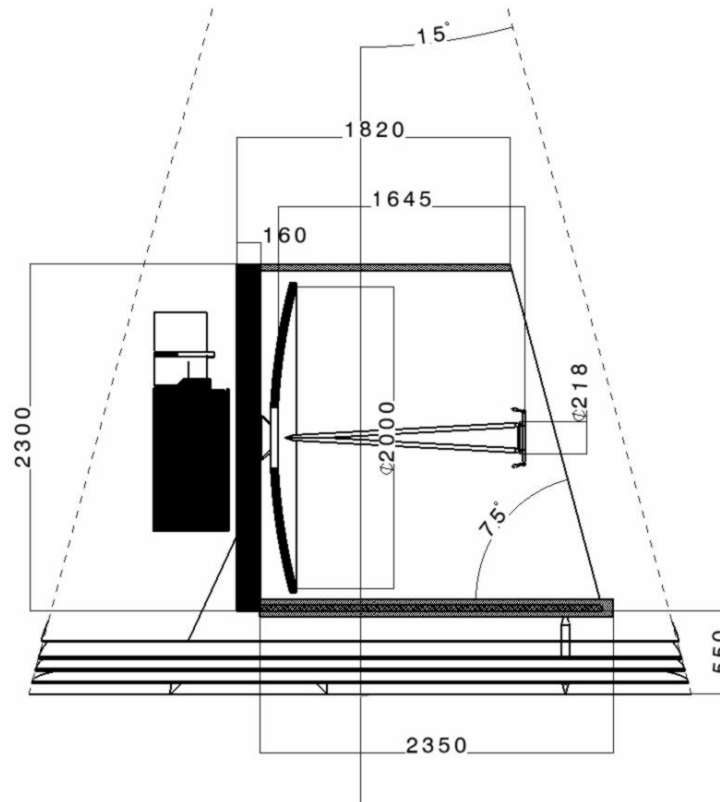
Figure 8-13: NG-CryoIRTel PLM dimension (parallel to M1-M2 direction)

8.6 Options

Configuration option 1 is composed of the SVM from baseline design and PLM for an elliptical mirror M1.

Configuration option 2 is composed of an SVM with an additional module that accommodates the cryo-cooler units including their electronics and the PLM from option 1. This allows integration and testing of a functional PLM (i.e. including compressors, coolers, cooler drive electronics and instrument electronics at room temperature) independently from the SVM.

8.6.1 SVM Option

Figure 8-14 shows an additional module added to the baseline SVM. This module accommodates the cryo-cooler units. The cryo-cooler units with their electronic boxes and the instrument electronic boxes are mounted on the cylindrical wall of around 2.85 m diameter and 600mm height. The thermal shields and thermal shell need to be adjusted to fit inside elliptical cone. The elliptical cone is composed using 15◦ half angle in one direction and 2◦ half angle in the other direction. Figure 8-14 and Figure 8-15 show the SVM for configuration option 2.
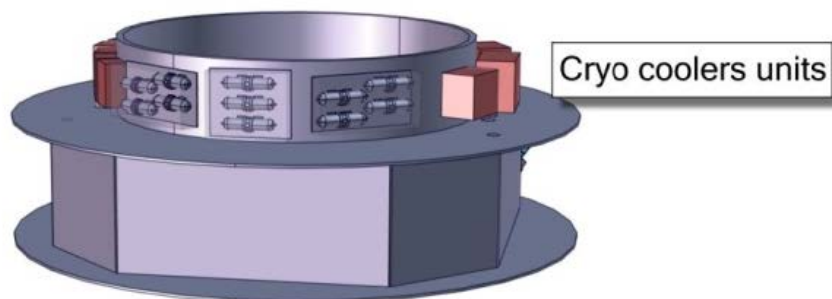
Figure 8-14: SVM design option
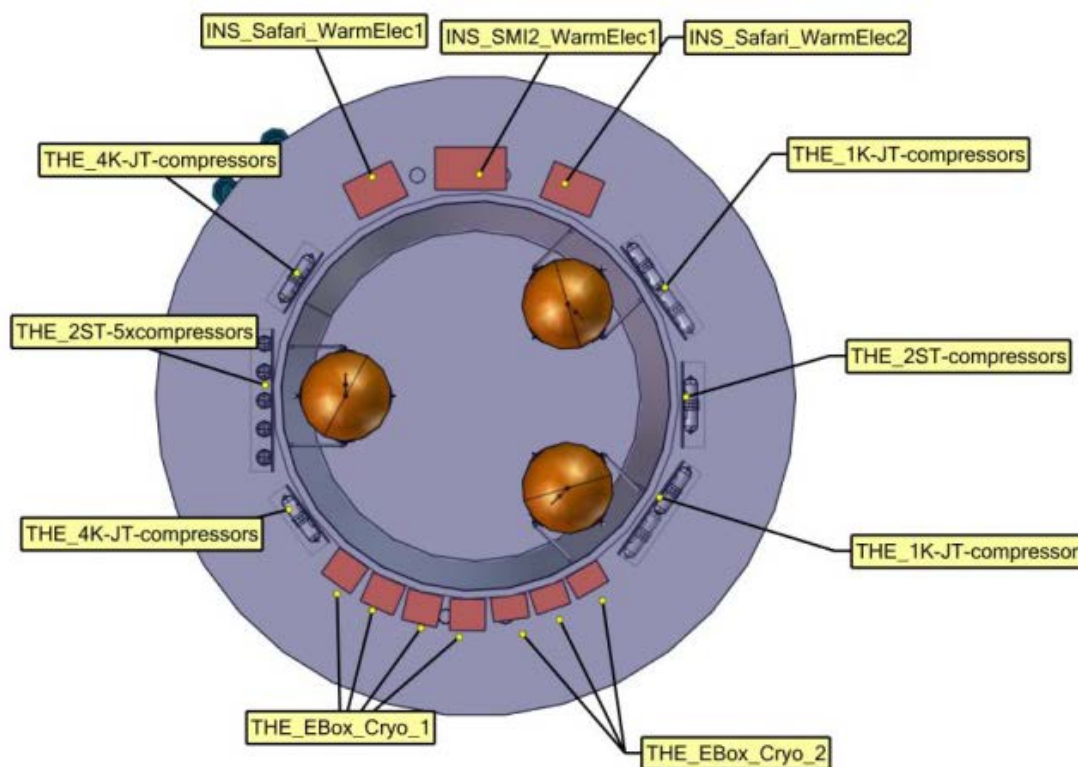
Figure 8-15: Accommodation option of the cryo-cooler units

8.6.2   PLM Option

Telescope supporting structure of the PLM option is derived from the PLANCK spacecraft. There are 6 point interface between the SVM and the PLM. Truss element design for the option using large mirror is shown in Figure 8-16 and Figure 8-17.
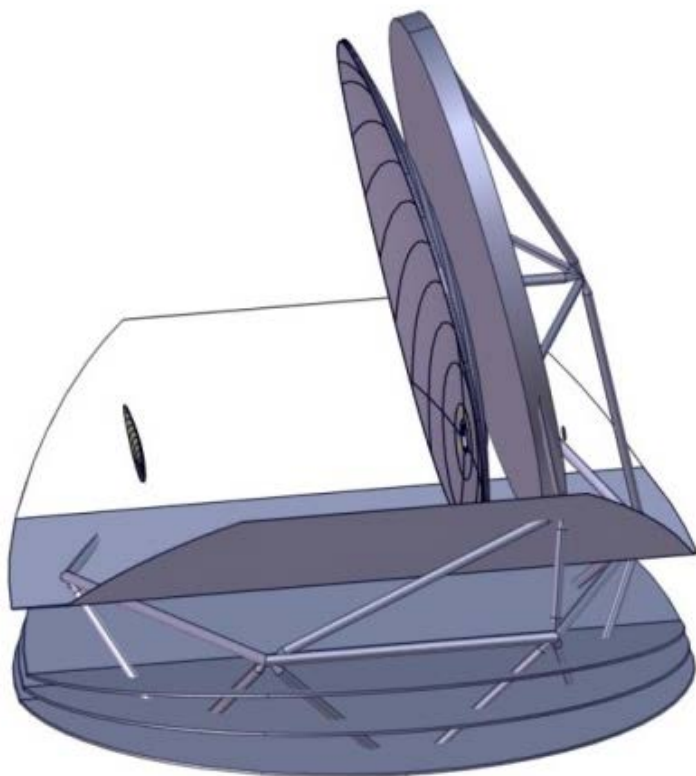
Figure 8-16: PLM design option
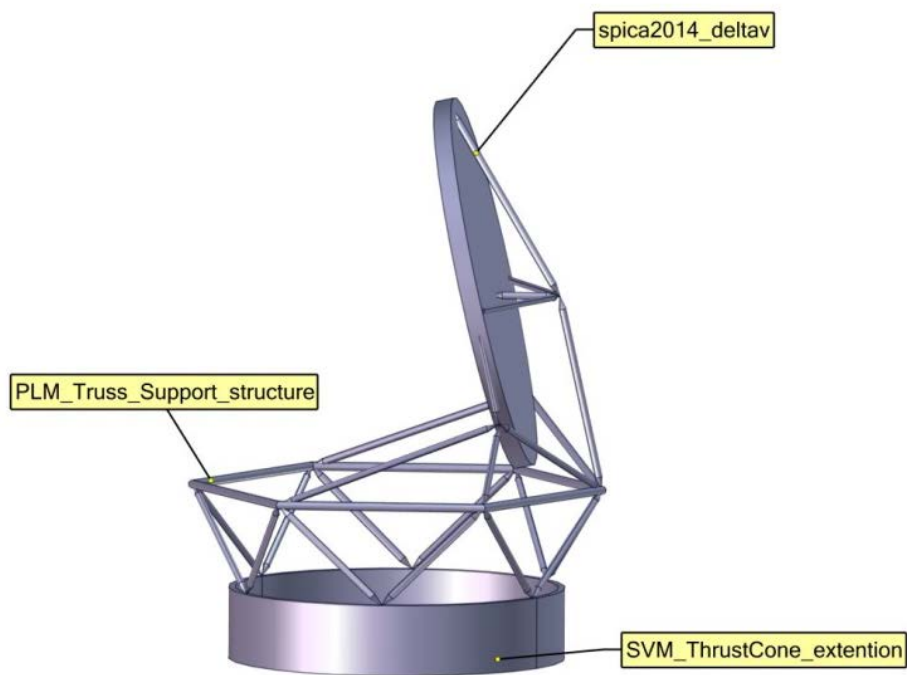
Figure 8-17: Large telescope supporting structure

9 STRUCTURES

9.1 Requirements and Design Drivers

SubSystem requirements		
Req. ID	**STATEMENT**	**Parent ID**
STR-010	Spacecraft/launcher interface: The spacecraft structure shall have a circular interface to the launch vehicle adaptor with a diameter of 2360 mm (RD[9])	
STR-020	Available useable volume: The spacecraft configuration/ structure shall be designed to fit within the available useable volume of the H-X launch vehicle. The useable volume takes into account the dynamic displacement of spacecraft which satisfies the spacecraft stiffness requirements defined by STR-040. (RD[9])	
STR-030	Spacecraft static unbalance: the spacecraft lateral CoM position shall be less than 25 mm from the launch vehicle centre axis in radial direction (RD[9],RD[10])	
STR-040	Spacecraft stiffness requirements for H-X launch vehicle (RD[9])*: - Lateral: 12 Hz - Axial: 35 Hz	
STR-050	PLM stiffness requirements**: - Lateral: 16 Hz - Axial: 49 Hz	

* the spacecraft stiffness requirements proposed by JAXA for the H-X launch vehicle were increased by 15%

** the PLM stiffness requirements have been derived from the spacecraft stiffness requirement by using a frequency separation factor of $\sqrt{2}$.

9.2 Assumptions and Trade-Offs

9.2.1 Launch Vehicle Assumptions

Since the H-X launcher is still under development and will enter service after 2020, the assumed spacecraft stiffness requirements and loads requirements were based on the current H-IIA launch vehicle and were specified by JAXA in RD[9]. The launch vehicle adaptor (2360S) and its dimensions are depicted in Figure 9-1. It has been assumed that the spacecraft interface with the launch vehicle is defined by the diameter of 2360 mm on which the centre points of the separation pusher springs are located. This defines requirement STR-010.
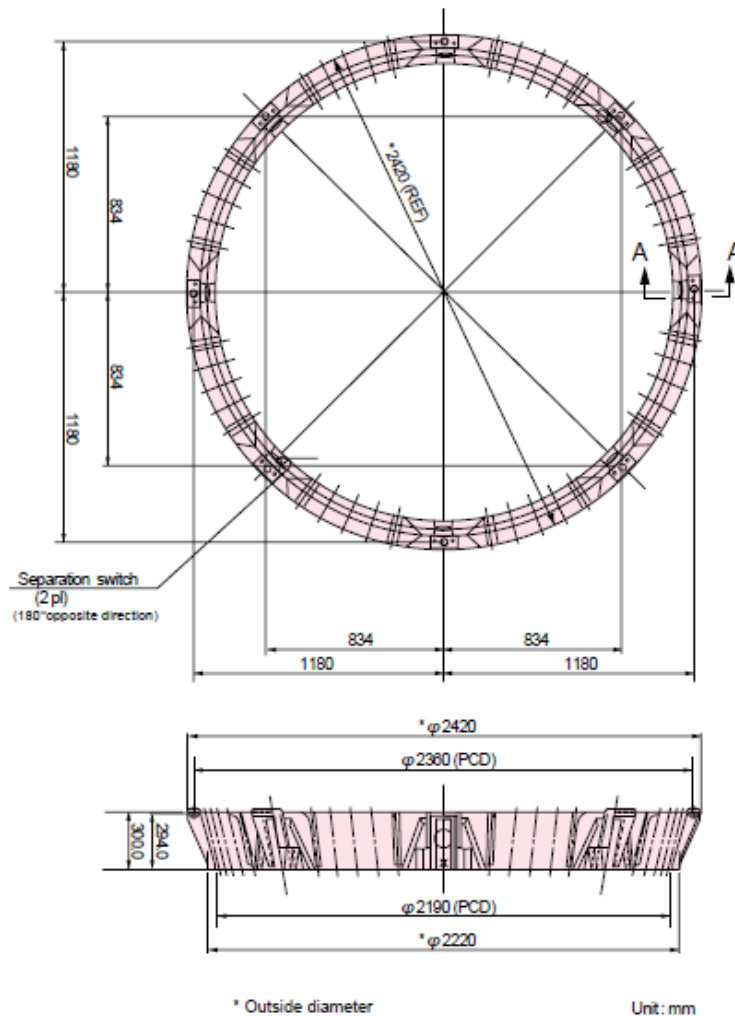
Figure A3.8.2 General view of 2360S adapter

Figure 9-1: H-X/IIA 2360S payload adaptor (RD[9])

9.2.2 Configuration Options

During the CDF study two configurations were proposed to be studied:

- Ritchey-Chrétien On-Axis Telescope with 2m diameter entrance pupil (baseline design)
- Ritchey-Chrétien Off-Axis Telescope with 2.6m x 3.0m elliptical entrance pupil (design with large size telescope).

The first configuration, the baseline design, is described in section 9.3. The second configuration, the design with the large size telescope, is described in section 9.4. The baseline design is described in more detail than the design with the large size telescope. The latter configuration was mainly studied in terms of optical, structural and thermal feasibility.

9.2.3 Materials

The properties of the materials used for the spacecraft structural elements are given in Table 9-1.

MATERIAL PROPERTIES	E [Gpa]	G L/W [Mpa]	rho [kg/m3]	nu [-]	CTE [ppm/K]	S_yield [Mpa]
CFRP (M55J/EX1515)	150		1700	0.30	1.5	n.a.
Ti	110		4500	0.30	8.8	800
Hexcel 5052/F40 - .0019 Alloy Al Flexcore			50			
Al alloy	70		2700	0.30	23.0	240
GFRP	49		2500	0.30	4.9	n.a.
SiC	420		3770	0.17	1.1	270
INVAR	144		9760	0.25	1.4	270
Hexcel 1/8 - 5056 - .0007 Alloy Al honeycomb			50			

Table 9-1: Material properties

9.3 Baseline Design

9.3.1 Structural Architecture

The structural architecture is depicted in Figure 9-2. The main dimensions are given in Figure 8-9. The sizing of the structural elements of the SVM and PLM is presented in sections 9.3.2 and 9.3.3 respectively.
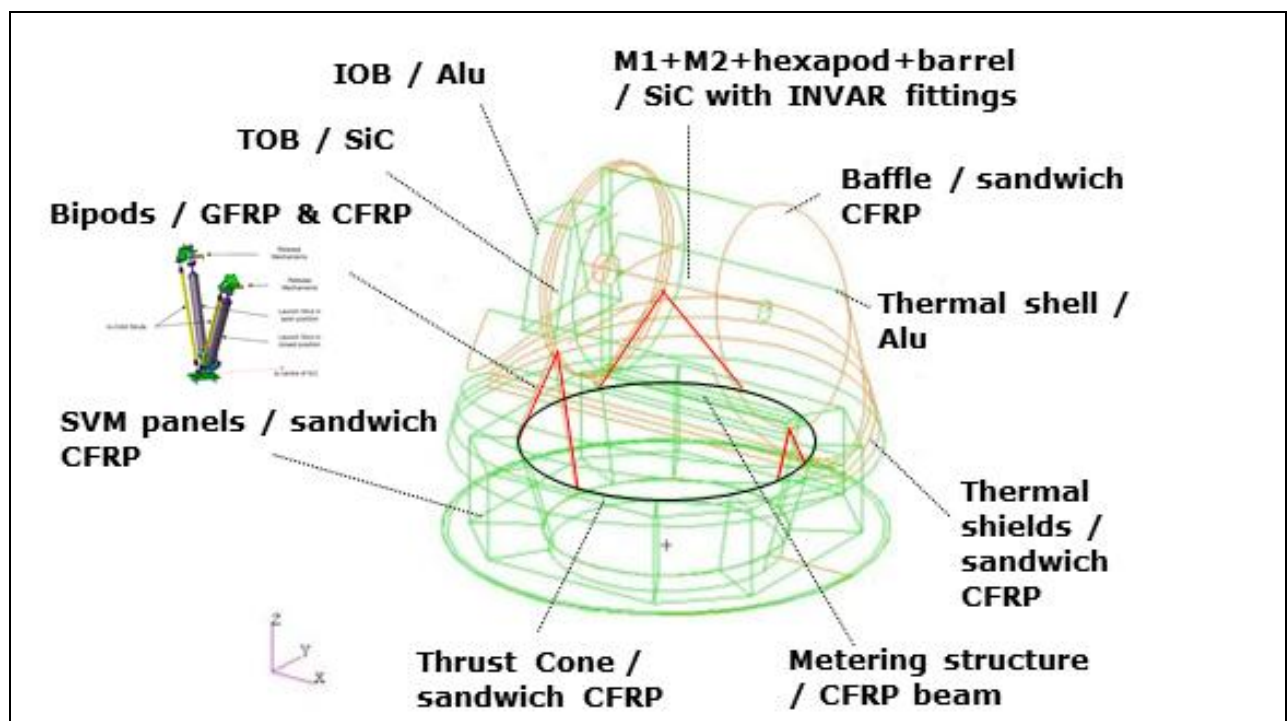

Figure 9-2: Structural architecture of baseline design

9.3.1.1 Thrust cone

The thrust cone forms the backbone of the spacecraft structure and is made of a sandwich structure with CFRP face sheets and an aluminium honeycomb core. On the bottom side it connects to the 2360S adaptor. On the upper side it connects to the PLM. As can be seen, the cone angle of the thrust cone has been adapted to the cone angle of the payload adaptor to improve the transfer of loads. In addition, the widening cone helps to accommodate the PLM, since the bipod legs can be mounted directly to the upper side of the cone. On this side a stiff ring is placed to introduce the PLM bipod interface point loads into the cone structure. The tanks are accommodated on the inside of the thrust cone and attached to the thrust cone by means of struts and honeycomb inserts.

9.3.1.2 SVM panels

At a distance of 200 mm above the spacecraft to launch vehicle interface the sunshield panel is mounted horizontally to the thrust cone. In fact this panel consists of two parts, one positioned outside of the thrust cone and one positioned inside the thrust cone. The sunshield is also used as a solar panel and therefore its entire area is equipped with solar cells. On the upper side of the thrust cone the SVM top panel is mounted on the outside of the thrust cone. On the inside the thrust cone is open. Shear panels are mounted on the thrust cone in radial direction between the top and floor SVM panel. Equipment panels and cryo-cooler panels are used to close the octagonal SVM structure. The equipment panels can be opened to have access to the electronics boxes. The cryo-cooler panels have a slit on either side of the panel to provide access to the vibration isolators, which mount the cryo-cooler panels to the radially oriented shear panels. All SVM panels are sandwich panels with CFRP face sheets and an aluminium honeycomb core.

9.3.1.3 Bipods, TOB, metering structure, thermal shields, thermal shell

The bipods which hold the PLM assembly are made of GFRP to reduce the conductive heat loads induced by the warm SVM. The length of the large bipod struts that connect to the TOB is 1.43 m. The short bipod struts have a length of 0.53 m and connect to the bottom side of the metering structure. Thin CFRP bipods are placed parallel to the GFRP main bipod struts to hold the PLM in position in orbit when the main bipod struts will be conductively decoupled at the PLM/SVM interface. The concept is similar to the bipod concept used on the GAIA spacecraft (see small picture inset in Figure 9-2). The metering structure itself is a monocoque CFRP beam-type structure which together with the TOB forms the backbone of the PLM telescope structure. It has a rectangular cross-section of 250 mm in width and 125 mm in height. For stiffness as well as thermal reasons (low conductivity at 21K) CFRP has been chosen as a material for the metering structure. The three thermal shields that are used to passively reduce the temperature from SVM towards STA are constructed of sandwich panel with CFRP face sheets and aluminium honeycomb core. They are attached to the bipod legs and in addition are supported by thin GFRP support struts to increase the stiffness of the panels. The thermal shell – which is actively cooled down to 21K – is an aluminium shell or full aluminium sandwich panel and is supported by the bipods.

9.3.1.4 TOB, IOB, baffle

The TOB is made of SiC and is constructed as a plate which is stiffened by ribs on the back side. The TOB has attachment points for mounting the M1, the telescope baffle and the IOB and forms an integral part with the metering structure which is attached to it. The IOB is a milled stiffened aluminium plate on which the instruments are mounted (SAFARI , SMI and FAS). It is attached to the TOB by 3 sets of bipods. The baffle is a cylindrical structure made of a sandwich with CFRP face sheets and aluminium honeycomb core. It is attached by isostatic mounts to the TOB and to the metering structure. TOB, IOB and baffle are actively cooled down to 4.5K.

9.3.1.5 Telescope

The telescope is composed of an M1, an M2, a hexagonal barrel structure that holds the M2 and a hexapod structure that connects the barrel to the M1. All elements are made of SiC except the interface elements which are made of INVAR. The telescope structure is similar to the one used on Herschel that is depicted in Figure 9-3. The M1 bipods are made of titanium and are attached to the same M1 interface points as the hexapod. The entire telescope assembly is cooled down to <5K.
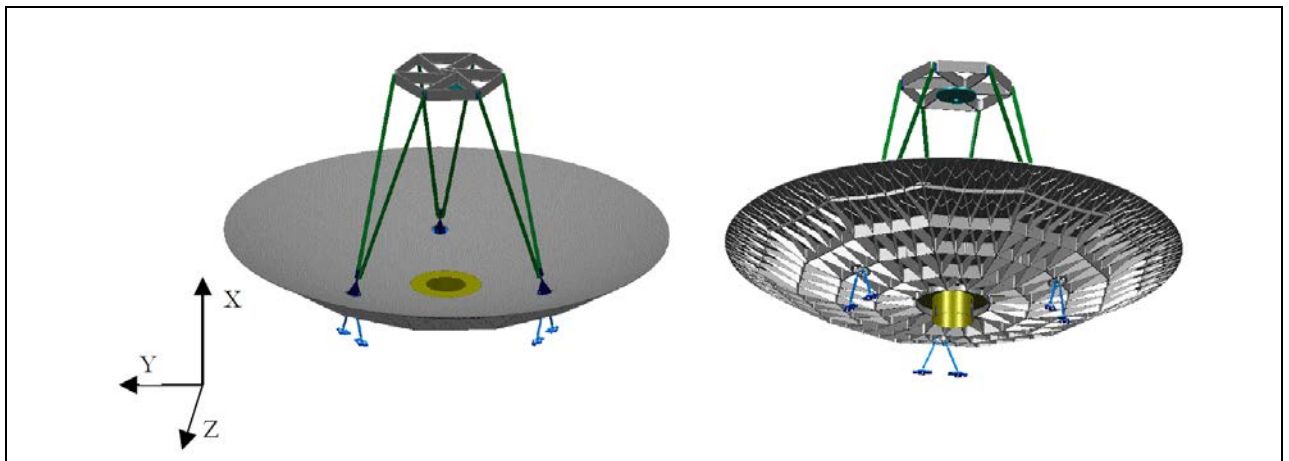

Figure 9-3: Herschel telescope structural architecture

9.3.2 SVM Structural Details

The SVM parts and dimensioning details are presented in Table 9-2. The initial dimensioning/sizing has been performed on the basis of similar spacecraft structural designs. For the material properties the reader is referred to Table 9-1.

Parts SVM	Sub-part	Item type / material
thrust cone		CFRP sandwich with alu core - 1.3 mm / 25 mm / 1.3 mm
bottom sunshield		CFRP sandwich with alu core - 0.3 mm / 20 mm / 0.3 mm
top sandwich panel		CFRP sandwich with alu core - 0.3 mm / 20 mm / 0.3 mm
exterior shear panels		CFRP sandwich with alu core - 0.3 mm / 20 mm / 0.3 mm
interior shear panels		CFRP sandwich with alu core - 0.3 mm / 20 mm / 0.3 mm
cone upper ring		Al ring A=2*100*3 mm2 D=2360 mm
cone lower ring		Al ring A=2*100*4 mm2 D=3000 mm
tank struts & brackets		Al
2 cryocooler panels		CFRP sandwich with alu core - 1.0 mm / 50 mm / 1.0 mm
12 dampers		isolators of cryo-cooler panels
12 brackets		isolator brackets

Table 9-2: SVM parts and dimensioning details

9.3.3 PLM Structural Details

The PLM parts and dimensioning details are presented in Table 9-3. The initial dimensioning/sizing has been performed on the basis of similar spacecraft structural designs. For the material properties the reader is referred to Table 9-1.

Parts PLM	Sub-part	Item type / material
bipods -X		GFRP, L=1430 mm, D=80 mm, t=8 mm + parallel CFRP bipod + NEA + fittings (x 1.4)
bipods +X		GFRP, L=530 mm, D=50 mm, t=6 mm + parallel CFRP bipod + NEA + fittings (x 1.4)
TOB		SiC, D=2.2m, t=4 mm, Surface_Rib_factor=1.2
metering structure		CFRP, L=2300 mm, W=250 mm, H=100mm, t=2.5 mm
IOB		aluminium milled platform with alunium cover (JAXA)
telescope		
	M1	SiC, D=2000 mm, t=3.5 mm, Surface_Rib_fitting_factor=1.2+fittings(x1.2)
	M1 Bipods	Titanium, L=250mm, R=10mm, t=1.0 * fitting_factor=1.2
	M2	D=220 mm, t=1.5 mm, Surface_Rib_fitting_factor=1.2+fittings(x1.2)
	baffle	L=2250 mm, D=2200 mm, sandwich with alu skins & core - 0.2 mm /15 mm / 0.2 mm
	hexapod	SiC, L=1800 mm, H=40mm, W=20 mm, t=2.0mm + INVAR fittings (x1.2)
	barrel	SiC, hexagonal L = 200mm, H=80mm, t=2.5mm
thermal shields		
	shield 1	CFRP sandwich with alu core - 0.10 mm / 15 mm / 0.10 mm
	shield 2	CFRP sandwich with alu core - 0.10 mm / 15 mm / 0.10 mm
	shield 3	CFRP sandwich with alu core - 0.10 mm / 15 mm / 0.10 mm
	supports	L=variable, D=40 mm, t=2 mm, GFRP
	shell	alu shell - 0.5 mm

Table 9-3: PLM parts and dimensioning details

9.3.4 PLM Preliminary Stiffness Verification

In order to make sure that the chosen wall thickness of the struts of the PLM bipods is sufficient to meet the PLM frequency requirements defined by STR-050, a simplified PLM model was constructed in Nastran, refer to Figure 9-4. In this figure the main axial and lateral modes are visualised. All modes meet the frequency requirements defined by STR-050, i.e. f_{lat} > 16Hz and f_{axial}>49Hz.
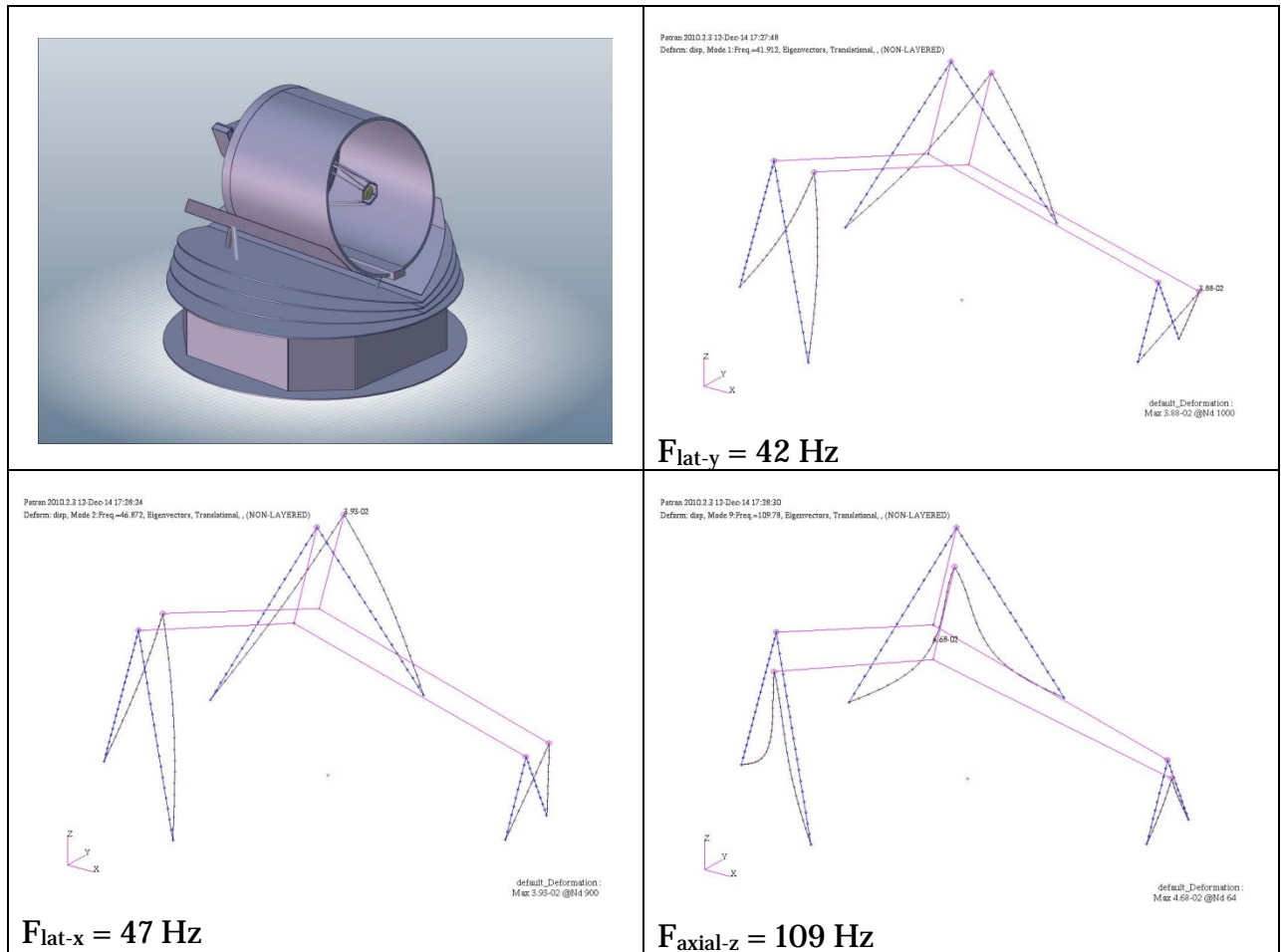
**Figure 9-4: PLM simplified FEM**

9.3.5 Static Unbalance

The CoM position of the spacecraft was estimated for the spacecraft configuration with equipment and system mass margin included. The resulting lateral CoM position satisfies the unbalance requirement STR-030 meaning that no balancing mass is required. The computation is shown in Table 9-4 where it is conservatively assumed that the equipment margin is equal to 1.2 for all equipment and that the system margin is equal to 1.2. Perfect lateral balance is obtained with a balancing mass of 24 kg positioned on the thrust cone at $(X,Y,Z) = (1500,0,940)$ mm. The axial CoM position is equal to 1278 mm for the configuration that includes the balancing mass. The obtained system mass is equal to 2559 kg. For the spacecraft system mass that is fully in line with the less conservative equipment margins the reader is referred to section 5.

		M [kg]	X [mm]	Y [mm]	Z [mm]
SVM	SVM w/o thermal control	927.4	0	0	670
	SVM thermal control	432.0	0	0	952
		1359.4	*0*	*0*	*760*
PROP	propellant (reduced with equipment and system mass margins, 1.2x1.2)	258.9	1150	0	670
		259	*1150*	*0*	*670*
PLM	mechanisms	35.3	0	0	670
	thermal control	14.4	0	0	1740
	AOCS	20.2	0	0	670
	harness	61.6	0	0	670
	instruments	144.1	-852	0	2840
	IOB structure (JAXA:IOB(95/1.1	166.4	-852	0	2840
	bipods -X (2x)	58.0	-522	0	1640
	bipods +X	5.0	1285	0	1380
	TOB	99.1	-522	0	2840
	metering structure	9.9	528	0	1680
	M1	86.0	-322	0	2840
	M1 bipods	0.7	-422	0	2840
	M2	0.4	1197	0	2840
	baffle	41.0	478	0	2840
	hexapod	14.1	367.5	0	2840
	barrel	2.6	1257	0	2840
	shield 1	29.9	0	0	1316
	shield 2	29.4	0	0	1494
	shield 3	29.4	0	0	1675
	shield bipods	43.2	0	0	1407
	thermal shell	26.0	0	0	2025
		916	**-365**	**0**	**2228**
PLM w/o bipods		*853*	*-198*	*0*	*1720*
S/C		**2535**	**-14**	**0**	**1282**
Balancing Mass		**24**	**1500**	**0**	**940**
S/C including Balancing Mass		**2559**	**0**	**0**	**1278**

Table 9-4: CoM position and required balancing mass

9.4 Design with Large Size Telescope

9.4.1 Structural Architecture

The structural architecture of this design is depicted in Figure 9-5. An overview of the spacecraft geometry is given in Figure 9-6. The sizing of the structural elements of the SVM and PLM is presented in sections 9.4.2 and 9.4.3 respectively.
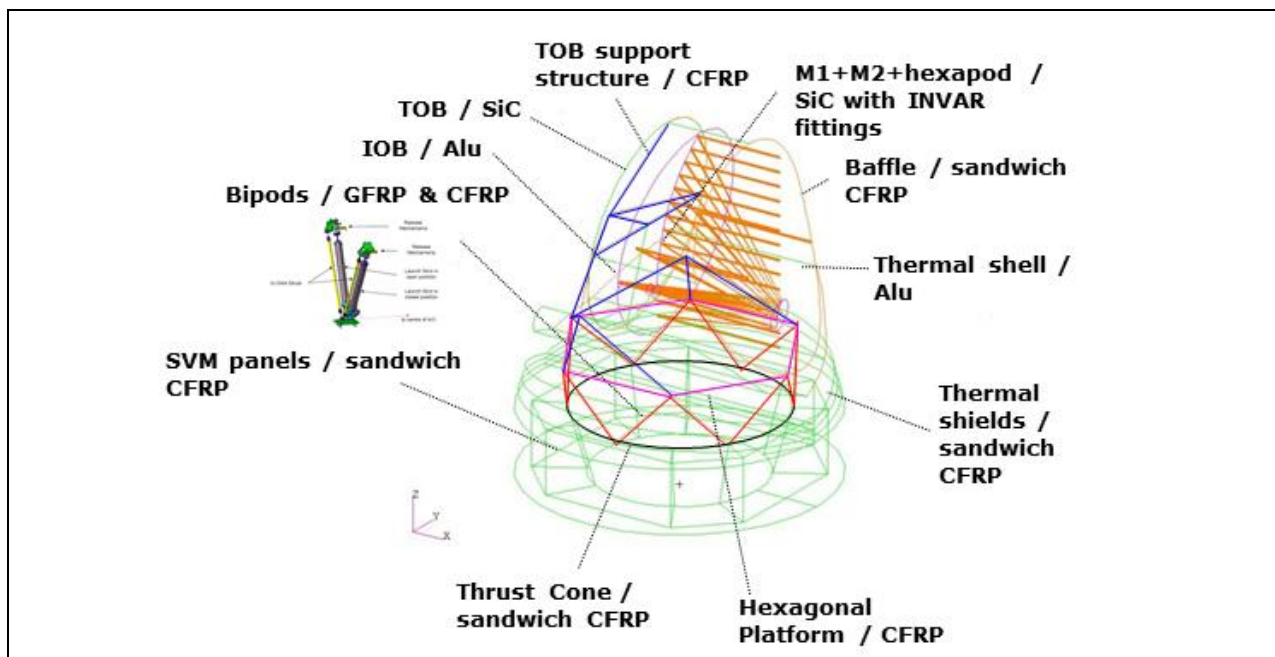
**Figure 9-5: Structural architecture of design with large size telescope**
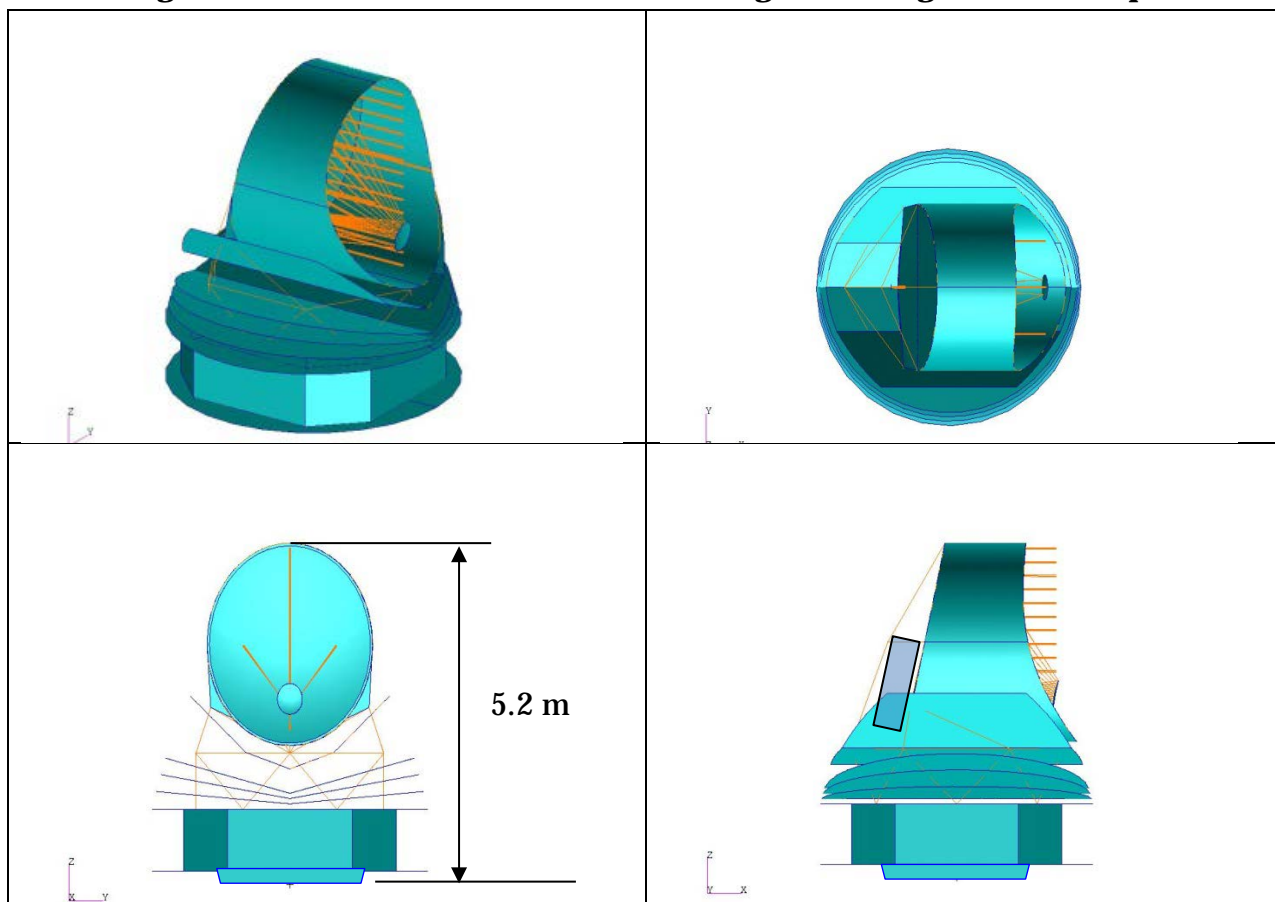
Figure 9-6: Overview spacecraft design

9.4.1.1 SVM

The SVM architecture of the spacecraft was not changed with respect to the baseline design. Only the thickness of the face sheets was increased to sustain the higher loads due to increased mass of the PLM.

9.4.1.2 Bipods, hexagonal platform, thermal shields, thermal shell, TOB support structure

In this design, a hexagonal platform was introduced made of CFRP struts (coloured magenta in Figure 9-5). In conjunction with a set of 6 GFRP bipods (coloured red in Figure 9-5) it forms a stable truss structure which is light-weight and which can serve as a mounting platform for the cold telescope which has increased in mass with respect to the baseline design. After some further optimisation of the hexagonal platform geometry it would be possible to position the entire hexagonal platform between the last thermal shield and the thermal shell. In that case, the hexagonal platform would see a more uniform temperature which would be beneficial to the alignment of the telescope. The GFRP bipods are similar to the main bipods used for the baseline design and can be thermally decoupled from the SVM after launch. In that case the platform is held in position by thin CFRP struts positioned parallel to the main GFRP bipod struts. In order to reduce the thermal load after decoupling even further it might be possible to use a set of only 3 bipods rather than 6. The thermal shields are basically the same as the ones used on the baseline design. Only the attachment positions to the bipod struts have changed. With respect to the baseline design the thermal shield was moved to a higher position and was reshaped. The TOB support structure – the truss structure coloured blue in Figure 9-5 – connects the TOB to the hexagonal platform. The struts of the TOB support structure are made of CFRP.

9.4.1.3 TOB, IOB, baffle

The TOB is made of SiC and basically is constructed as a plate stiffened on the back side with ribs. With respect to the baseline design the dimensions have increased. The TOB has attachment points for mounting the M1, the telescope baffle and the IOB. The IOB structure is identical to one in the baseline design and accommodates the SAFARI and MSI instruments. It is attached to the TOB by 3 sets of bipods. The baffle is a cylindrical structure with an elliptical cross-section which is made of a sandwich with CFRP face sheets and aluminium honeycomb core. On the rear side it is attached by isostatic mounts to the TOB and at the front side to the hexagonal platform by means of a small bipod. TOB, IOB and baffle are actively cooled down to 4.5K.

Telescope

The telescope is composed of an M1, an M2, a hexagonal barrel structure that holds the M2 and an off-axis / eccentric hexapod structure that connects the barrel to the M1. All elements are made of SiC except the interface elements which are made of INVAR. The entire telescope assembly is cooled down to 4.5K.

9.4.2 SVM Structural Details

Like for the baseline design, the SVM parts and dimensioning details are presented in Table 9-5. The initial dimensioning/sizing has been performed on the basis of the established sizing of the baseline design. The thickness of the face sheets of the thrust

cone and shear panels was increased to sustain the higher loads due to increased mass of the PLM. For the material properties the reader is referred to Table 9-1.

Parts SVM	Sub-part	item type / material
thrust cone		CFRP sandwich with alu core - 1.8 mm / 30 mm / 1.8 mm
bottom sunshield		CFRP sandwich with alu core - 0.5 mm / 20 mm / 0.5 mm
top sandwich panel		CFRP sandwich with alu core - 0.5 mm / 20 mm / 0.5 mm
exterior shear panels		CFRP sandwich with alu core - 0.5 mm / 20 mm / 0.5 mm
interior shear panels		CFRP sandwich with alu core - 0.5 mm / 20 mm / 0.5 mm
cone upper ring		Al ring A=2*100*5 mm2 D=2360 mm
cone lower ring		Al ring A=2*100*6 mm2 D=3000 mm
tank struts & brackets		Al
2 cryocooler panels		CFRP sandwich with alu core - 1.0 mm / 50 mm / 1.0 mm
12 dampers		isolators of cryo-cooler panels
12 brackets		isolator brackets

Table 9-5: SVM parts and dimensioning details

9.4.3 PLM Structural Details

The PLM parts and dimensioning details are presented in Table 9-6. The initial dimensioning/sizing has been performed on the basis of similar spacecraft structural designs and on the basis of the established sizing of the baseline design. For the material properties the reader is referred to Table 9-1.

Parts SVM	Sub-part	item type / material
truss struts		GFRP, L=1210 mm, D=60 mm, t=5 mm + parallel CFRP bipod + NEA + fittings (x 1.4)
hexagonal platform		CFRP, L=173 mm, D=60 mm, t=4 mm + fittings (x 1.2)
TOB support struts		CFRP, L=2x1.77/2x1.74/2x0.74/1x1.76/2x1.45/1x0.6/1x1.79, D=50 mm, t=3 mm + fittings (x1.2)
TOB		SiC, A=6.5m2, t=4 mm, Surface_Rib_factor=1.2+fittings(1.2)
IOB		milled aluminium platform with aluminium cover (ref: JAXA)
telescope		
	M1	SiC, D=2000 mm, t=3.5 mm, Surface_Rib_fitting_factor=1.2 + fittings (1.2)
	M1 Bipods	Titanium, L=250mm, R=10mm, t=2.0 * fitting_factor=1.2
	M2	D=500 mm, t=1.5 mm, Surface_Rib_fitting_factor=1.2+fittings(x1.2)
	baffle	A=16.8 m2, sandwich with alu skins & core - 0.2 mm /15 mm / 0.2 mm + uncertainty factor 1.2
	hexapod	SiC, L=2.25 mm, H=50mm, W=30 mm, t=2.5mm + INVAR fittings (factor 1.2)
	barrel	SiC, hexagonal L = 300mm, H=80mm, t=2.5mm
thermal shields		
	shield 1	CFRP sandwich with alu core - 0.10 mm / 15 mm / 0.10 mm
	shield 2	CFRP sandwich with alu core - 0.10 mm / 15 mm / 0.10 mm
	shield 3	CFRP sandwich with alu core - 0.10 mm / 15 mm / 0.10 mm
	supports	L=variable, D=40 mm, t=2 mm, GFRP
	shell	alu shell - 0.5 mm

Table 9-6: PLM parts and dimensioning details

9.5 List of Equipment

9.5.1 Baseline Design

The mass budget for the structures subsystem is shown in Table 9-7. The SVM structures subsystem mass amounts to 248 kg and the PLM structures subsystem mass amounts to 445 kg. The total spacecraft structures subsystem mass equals 693 kg.

S/C STRUCTURE MASS - SUM							693
Module	Parts	Material/Construction	A [m2]	V [m3]	m/S kg/m2	m/V [kg/m3]	m [kg]
SVM							248
	thrust cone	CFRP sandwich with alu core - 1.3 mm / 25 mm / 1.3 mm	10.0		5.7		56.6
	bottom sunshield	CFRP sandwich with alu core - 0.3 mm / 20 mm / 0.3 mm	15.2		2.0		30.7
	top sandwich panel	CFRP sandwich with alu core - 0.3 mm / 20 mm / 0.3 mm	8.1		2.0		16.4
	exterior shear panels	CFRP sandwich with alu core - 0.3 mm / 20 mm / 0.3 mm	11.2		2.0		22.7
	interior shear panels	CFRP sandwich with alu core - 0.3 mm / 20 mm / 0.3 mm	4.5		2.0		9.1
	cone upper ring	Al ring A=2*100*3 mm2 D=2360 mm		4.45E-03		2700	12.0
	cone lower ring	Al ring A=2*100*4 mm2 D=3000 mm		7.54E-03		2700	20.4
	tank struts & brackets	Al					40
	2 cryocooler panels	CFRP sandwich with alu core - 1.0 mm / 50 mm / 1.0 mm	2.82		5.9		16.6
	12 dampers	isolators of cryo-cooler panels					9.2
	12 brackets	isolator brackets					14.4
PLM							445
	bipods -X	GFRP, L=1430 mm, D=80 mm, t=8 mm + parallel CFRP bipod + NEA + fittings (x 1.4)		1.61E-02		2500	40.3
	bipods +X	GFRP, L=530 mm, D=50 mm, t=6 mm + parallel CFRP bipod + NEA + fittings (x 1.4)		1.40E-03		2500	3.5
	TOB	SiC, D=2.2m, t=4 mm, Surface_Rib_factor=1.2		1.82E-02		3770	68.8
	metering structure	CFRP, L=2300 mm, W=250 mm, H=100mm, t=2.5 mm		4.03E-03		1700	6.8
	IOB	milled aluminium platform with aluminium cover (ref: JAXA)					115.5
	telescope						
	M1	SiC, D=2000 mm, t=3.5 mm, Surface_Rib_fitting_factor=1.2+fittings(x1.2)		1.58E-02		3770	59.7
	M1 Bipods	Titanium, L=250mm, R=10mm, t=1.0 * fitting_factor=1.2		1.13E-04		4500	0.5
	M2	D=220 mm, t=1.5 mm, Surface_Rib_fitting_factor=1.2+fittings(x1.2)		8.21E-05		3770	0.3
	baffle	L=2250 mm, D=2200 mm, sandwich with alu skins & core - 0.2 mm /15 mm / 0.2 mm	15.6		1.8		28.5
	hexapod	SiC, L=1800 mm, H=40mm, W=20 mm, t=2.0mm + INVAR fittings (x1.2)		2.59E-03		3770	9.8
	barrel	SiC, hexagonal L = 200mm, H=80mm, t=2.5mm		4.80E-04		3770	1.8
	thermal shields						
	shield 1	CFRP sandwich with alu core - 0.10 mm / 15 mm / 0.10 mm	19.0		1.1		20.8
	shield 2	CFRP sandwich with alu core - 0.10 mm / 15 mm / 0.10 mm	18.7		1.1		20.4
	shield 3	CFRP sandwich with alu core - 0.10 mm / 15 mm / 0.10 mm	18.7		1.1		20.4
	supports	L=? mm, D=40 mm, t=2 mm, GFRP					30
	shell	alu shell - 0.5 mm	13.4	6.68E-03		2700	18.0

Table 9-7: Mass budget structural subsystem – Baseline design

9.5.2   Design with Large Size Telescope

The mass budget for the structures subsystem is shown in Table 9-8. The SVM structures subsystem mass amounts to 312 kg and the PLM structures subsystem mass amounts to 623 kg. The total spacecraft structures subsystem mass equals 936 kg. With respect to the baseline design the SVM structures subsystem mass has increased by 64 kg (26%), the PLM structures subsystem mass has increased by 178 kg (40%) and the total spacecraft structures subsystem mass has increased by 243 kg (35%).

S/C STRUCTURE MASS - SUM							936
Module	Parts	Material/Construction	A [m2]	V [m3]	m/S	m/V	m
SVM							312
	thrust cone	CFRP sandwich with alu core - 1.8 mm / 30 mm / 1.8 mm	10.0		7.6		76.1
	bottom sunshield	CFRP sandwich with alu core - 0.5 mm / 20 mm / 0.5 mm	15.2		2.7		41.0
	top sandwich panel	CFRP sandwich with alu core - 0.5 mm / 20 mm / 0.5 mm	8.1		2.7		21.9
	exterior shear panels	CFRP sandwich with alu core - 0.5 mm / 20 mm / 0.5 mm	11.2		2.7		30.3
	interior shear panels	CFRP sandwich with alu core - 0.5 mm / 20 mm / 0.5 mm	4.5		2.7		12.2
	cone upper ring	Al ring A=2*100*5 mm2 D=2360 mm		7.41E-03		2700	20.0
	cone lower ring	Al ring A=2*100*6 mm2 D=3000 mm		1.13E-02		2700	30.5
	tank struts & brackets	Al					40
	2 cryocooler panels	CFRP sandwich with alu core - 1.0 mm / 50 mm / 1.0 mm	2.82		5.9		16.6
	12 dampers	isolators of cryo-cooler panels					9.2
	12 brackets	isolator brackets					14.4
PLM							623
	truss struts	GFRP, L=1210 mm, D=60 mm, t=5 mm + parallel CFRP bipod + NEA + fittings (x 1.4)		1.92E-02		2500	47.9
	hexagonal platform	CFRP, L=173 mm, D=60 mm, t=4 mm + fittings (x 1.2)		9.39E-03		1700	16.0
	TOB support struts	CFRP, L=2x1.77/2x1.74/2x0.74/1x1.76/2x1.45/1x0.6/1x1.79, D=50 mm, t=3 mm + fittings (x1.2)		8.79E-03		1700	14.9
	TOB	SiC, A=6.5m2, t=4 mm, Surface_Rib_factor=1.2+fittings(1.2)		3.74E-02		3770	141.1
	IOB	milled aluminium platform with aluminium cover (ref: JAXA)					115.5
	telescope						
	M1	SiC, D=2000 mm, t=3.5 mm, Surface_Rib_fitting_factor=1.2 + fittings (1.2)		3.09E-02		3770	116.4
	M1 Bipods	Titanium, L=250mm, R=10mm, t=2.0 * fitting_factor=1.2		2.26E-04		4500	1.0
	M2	D=500 mm, t=1.5 mm, Surface_Rib_fitting_factor=1.2+fittings(x1.2)		4.24E-04		3770	1.6
	baffle	A=16.8 m2, sandwich with alu skins & core - 0.2 mm /15 mm / 0.2 mm + uncertainty factor 1.2	20.1		1.8		36.8
	hexapod	SiC, L=2.25 mm, H=50mm, W=30 mm, t=2.5mm + INVAR fittings (factor 1.2)		5.27E-03		3770	19.8
	barrel	SiC, hexagonal L = 300mm, H=80mm, t=2.5mm		7.20E-04		3770	2.7
	thermal shields						
	shield 1	CFRP sandwich with alu core - 0.10 mm / 15 mm / 0.10 mm	19.0		1.1		20.8
	shield 2	CFRP sandwich with alu core - 0.10 mm / 15 mm / 0.10 mm	18.7		1.1		20.4
	shield 3	CFRP sandwich with alu core - 0.10 mm / 15 mm / 0.10 mm	18.7		1.1		20.4
	supports	L=? mm, D=40 mm, t=2 mm, GFRP					30
	shell	alu shell - 0.5 mm	13.4	6.68E-03		2700	18.0

Table 9-8: Mass budget structural subsystem – Design with large size telescope

9.6 Options

N/A.

9.7 Technology Requirements

The following technologies are required or would be beneficial to this domain:

Equipment and Text Reference	Technology	Suppliers and TRL Level	Technology from Non-Space Sectors	Additional Information
Bipods with detachable main struts	Technology to limit the conductive heat loads from SVM to PLM in operational on orbit condition	Airbus Defence and Space, Toulouse, TRL already high (7-8).	N/A	Technology was used on GAIA, although the struts on GAIA were shorter and the material for the main struts was CFRP and for the on-orbit struts GFRP. For NG-CryoIRTel the material choice is the other way around.
Sintered SiC telescope parts (TOB, M1, M2, hexapod, barrel)	Technology to produce ceramic telescope parts with superior conductivity for cryogenic applications.	Airbus Defence and Space, Toulouse, TRL already very high (8).	N/A	Technology was used on Herschel with a telescope operating at 70K. This time the telescope shall be cooled down to 4.5K for which the technology has not been proven yet for a 2m or 3m class telescope.

This Page Intentionally Blank

10 THERMAL

10.1 Requirements and Design Drivers

The key requirement for the thermal design is an active cooling of the telescope down to 6 K. This requires an active cooling chain.

Furthermore, passive cooling of the payload module has been restricted to temperature levels in the order of 50 K in order to make on-ground thermal system testing feasible.

SubSystem requirements		
Req. ID	STATEMENT	Parent ID
TH-010	Passive cooling shall be limited to ~50K	
TH-020	Active cooling of the telescope down to 6K, considering a 25% system margin on the cooler capability	

10.2 Assumptions and Trade-Offs

The thermal control of the Next Generation Cryogenic Infrared Telescope assumes that all elements in direct view of the instruments' focal plane detectors shall be cooled to < 6 K.

Passive cooling will be restricted to temperature levels above 50 K in order to have a feasible on-ground testability of the assembly.

For the CDF study, it is assumed that the active cooling of the telescope assembly is provided via JAXA coolers (see Figure 10-1 and Figure 10-2) with the following heat lift capabilities:

- 1K-class Joule-Thomson cooler (1K-JT)
  - 10mW heat lift @ 1.7K (EOL) ➔ 7.5mW @ 1.7K including margin
- 4K-class Joule-Thomson cooler (4K-JT)
  - 40mW @ 4.5K (EOL) ➔ 30mW @ 4.5K including margin

- 20K-class 2-stage Stirling cooler (2ST)
  - 200mW @ 20K (EOL) ➔ 150mW @ 20K including margin
  - 1000mW @ 100K

Figure 10-1: JAXA Joule-Thomson cooler
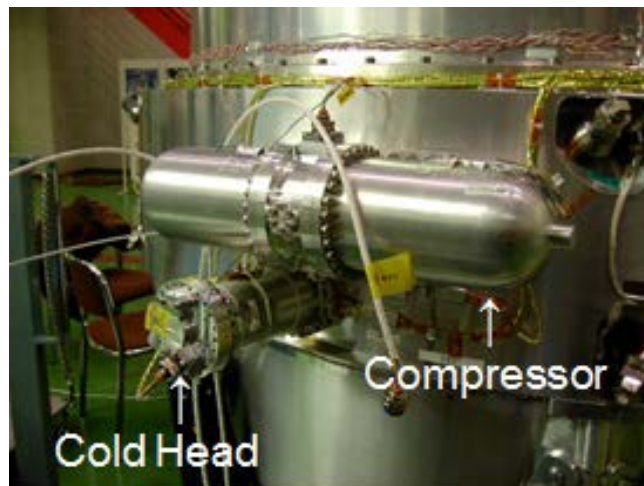
Figure 10-2: JAXA two-stage Stirling cooler

10.3 Baseline Design

The thermal control equipment needs for the service module (SVM) have been derived from the Planck mission design. The total mass for standard thermal control equipment such as MLI, heaters, thermistors, and heat pipes is estimated to be 64 kg.

Regarding the sizing of needed radiator area, the total amount of heat rejection needed is largely driven by the dissipation of the entire cryo-cooler system. A total heat rejection capability of 1585 W is needed.

The radiator panels will reside on the service module and are assumed to be black painted and having no sun incidence. The heat sink temperature of the radiators is set at 273 K (including a 10 K margin). The resulting effective radiator size required is 5.6 m².

The following paragraphs discuss the thermal design of the payload module.

10.3.1 Thermal Heat Shields

The thermal design is based on a cooling concept with heritage from Planck and EChO missions. Three passively cooled V-groove shaped thermal radiation shields are employed. A fourth thermal radiation shield has been shaped to minimise thermal radiation from the third V-groove shield to the telescope baffle. It is actively cooled down to a temperature of 20 K. Finally, the space telescope assembly (STA) including the telescope baffle is actively cooled down below 5 K. Figure 10-3 gives an overview showing the thermal shields and the telescope baffle.
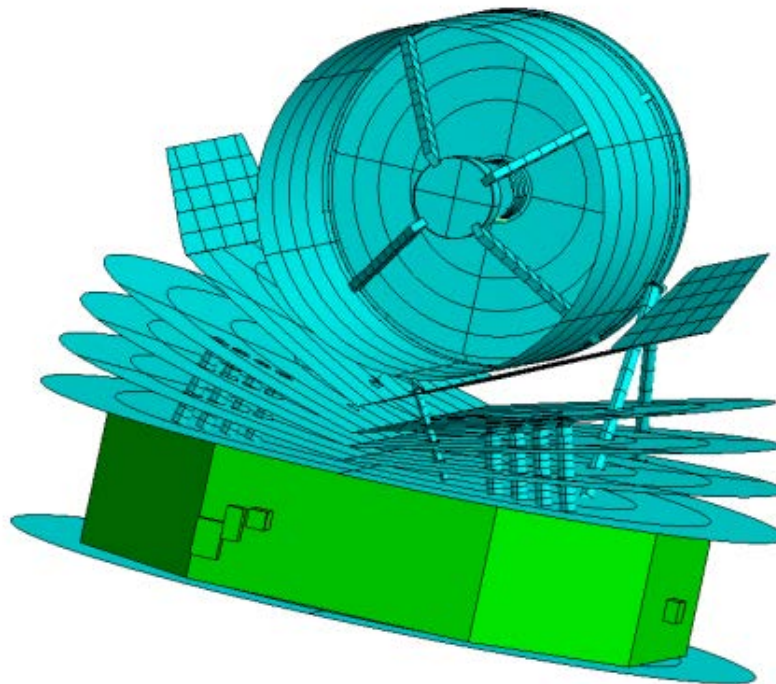
Figure 10-3: Thermal design overview of the four thermal shields and telescope baffle

10.3.2 Mechanical Support Struts

The STA is mechanically supported via six support struts (shown in Figure 10-4) made of GFRP. These struts are thermally disconnected after launch, i.e. they will not have a thermally conductive link to the STA in orbit.

Furthermore, six thin STA support struts (see Figure 10-4) made of CFRP are used, which provide a very low conductive link to the telescope assembly.
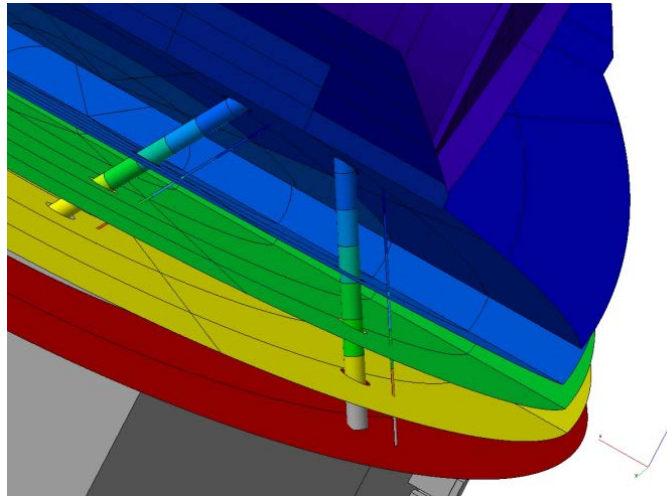
Figure 10-4: two GFRP struts and two thin CFRP struts for STA support

10.3.3 Active Cooling Chain

Regarding the active cooling chain, the JAXA design as used for the SPICA development has been chosen for this study (see Figure 10-5). It consists of 6 two-stage Stirling coolers, two 4K Joule-Thompson coolers and two 1.7K Joule-Thompson coolers. This concept employs hot redundancy of the coolers at each level of the chain, allowing for failure of one cooler at each level without compromising thermal performance.

Additionally, two two-stage Stirling coolers (hot redundant) are employed for active cooling of the fourth thermal radiation shield.
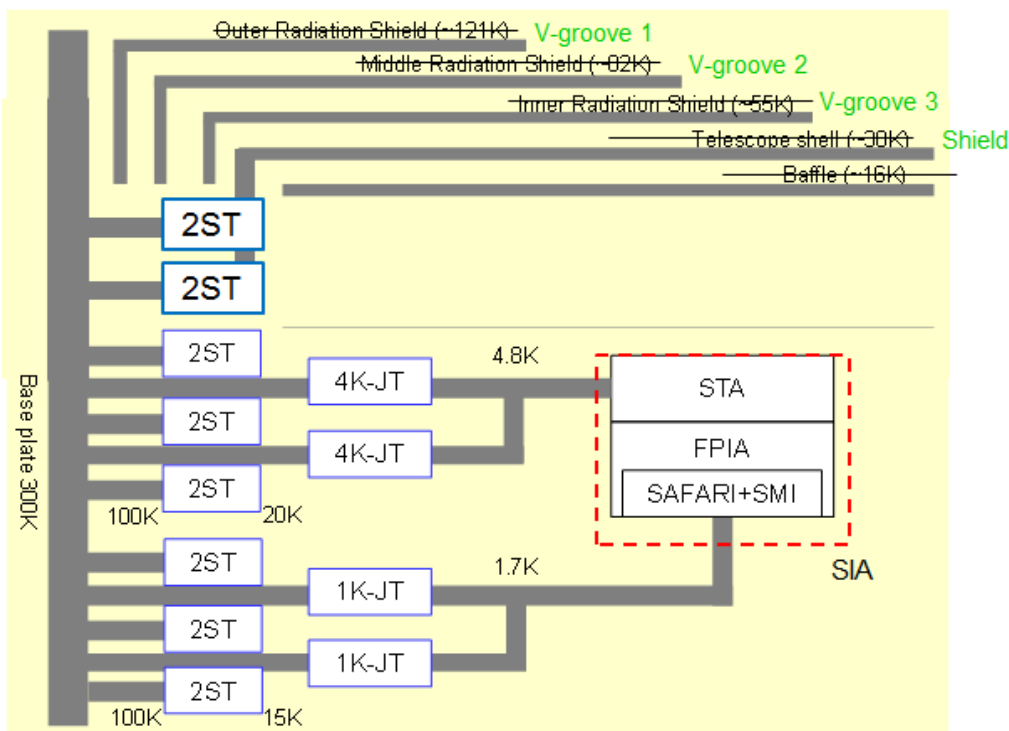
Figure 10-5: Overview of the active cooling chain

10.3.4 Cryocooler Positioning

In order to minimise the parasitic heat fluxes between the warm stages of the Stirling coolers and the Joule-Thompson coolers operating at a much colder temperature level and to minimise the export of micro-vibrations from the coolers, the following configuration has been chosen (see Figure 10-6):

- The 2-stage Stirling cryocooler (2ST) compressors are located inside the SVM, close to the side panel which is acting as a radiator

- The µ-vibration export is inhibited via a dedicated suspension mechanism of the cryocooler compartment

- The cold finger of each two-stage Stirling cooler is thermally shielded by a GFRP tube mounted on the SVM top side and extending through the lower two V-groove shields

- Each Joule-Thompson cooler loop is thermally protected by a smaller Al-tube mounted to the third V-groove shield and extending into the GFRP tube.
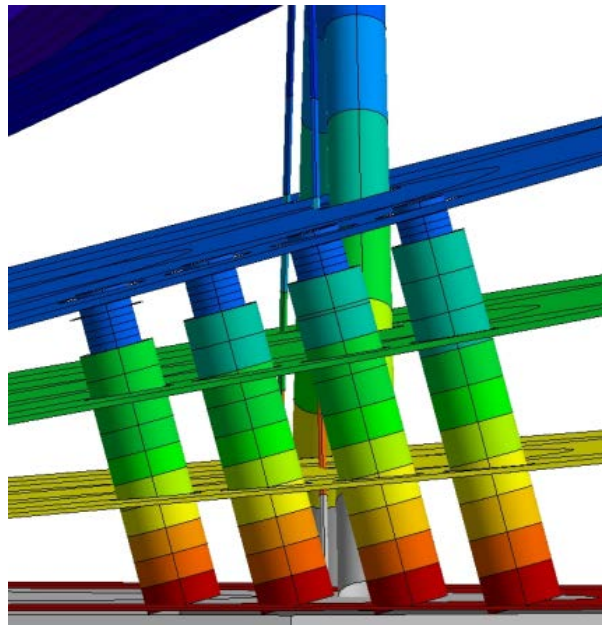
Figure 10-6: Thermal protection of cold cryo-stages: GFRP tubes (extending through the lower shields) and smaller Al-tubes (mounted to third thermal shield)

10.3.5 Parasitic Heat Load from Harness

The allocations are based on latest available SPICA results (ref. H2L2-AS0444), accounting for the difference in temperature levels and taking 100% margin (conservative approach):

- Heat load on 1st V-groove: 1000 mW
- Heat load on 2nd V-groove: 1000 mW
- Heat load on 3rd V-groove: 400 mW
- Heat load on actively cooled shield: 70 mW

10.3.6 Thermal Analysis Results and Discussion

The computed temperature levels of the baseline design are (see also Figure 10-7):

- STA baffle   4.8 K
- 4th shield (cold side)   21 K
- 3rd V-groove shield   54 K
- 2nd V-groove shield   109 K
- 1st V-groove shield   161 K
- SVM (top side)   243 K
- SVM (inner part)   273 K
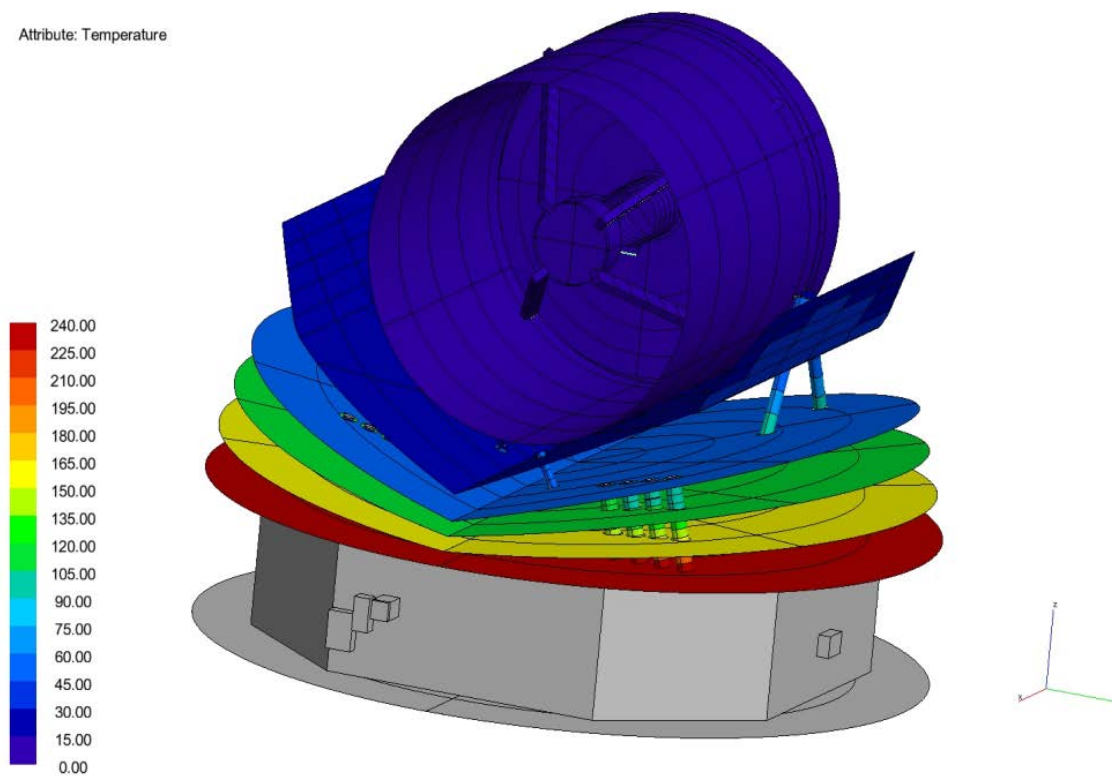
Figure 10-7: Map of Temperature Results

Regarding the heat flow budget, the relevant computed heat fluxes with the Shell actively cooled at 25K are shown in Figure 10-8.
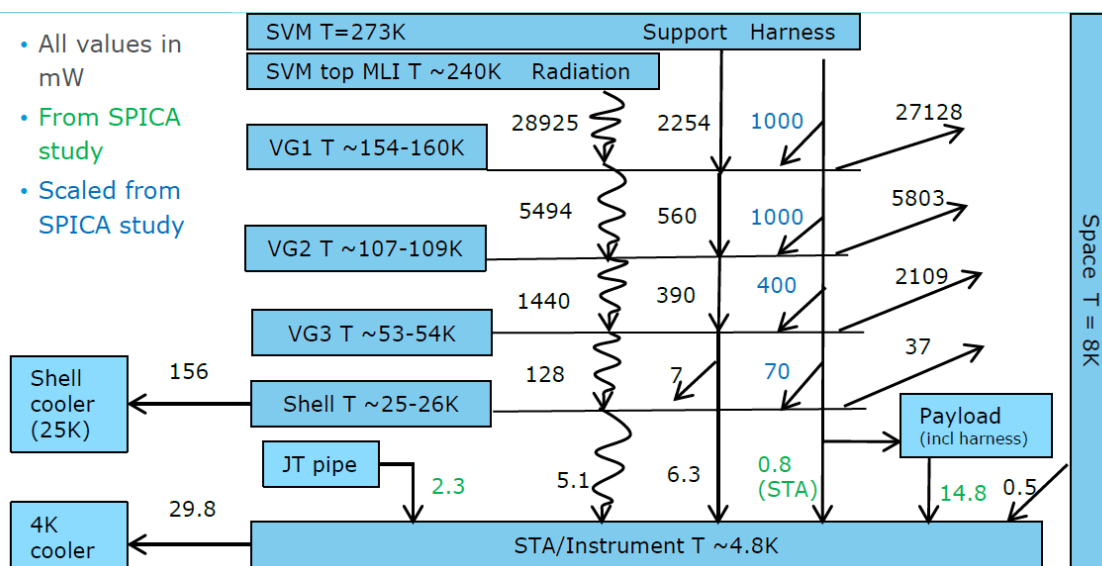
Figure 10-8: Resulting heat fluxes

The heat flow budget takes into the account the conservative assumptions on the parasitic heat flux from the harness (see paragraph 10.3.5). The loads are compliant to the cooler heat lift capabilities mentioned in paragraph 10.2.

The analysed active cooling heat load of the Telescope shell (fourth thermal shield) at a temperature of 25 K is within the JAXA 2-stage Stirling cooler specification. Cooling the shell at 20K, the heatload (including margin) is above the JAXA 2stage Stirling cooler specification)

A possible active cooling of the fourth thermal shield at 25 K (third analysis case) would enable the use of a Neon Joule-Thompson or sorption cryocooler instead of a Stirling cooler. European developments for these types exist, e.g. University of Twente and RAL.

10.4 List of Equipment

Element 1	Service Module				MASS [kg]		
Unit	Unit Name Click on button above to **insert new unit**	Part of subsystem	Quantity	Mass per quantity excl. margin	Maturity Level	Margin	Total Mass incl. margin
1	2ST Cryocooler		8	9.5	To be developed	20	91.2
2	4K JT Cryocooler		2	15.0	To be developed	20	36.0
3	1K JT Cryocooler		2	28.0	To be developed	20	67.2
4	Cryocooler Electronics		1	80.0	To be developed	20	96.0
5	Thermal Equipment		1	58.0	To be modified	10	63.8
-	Click on button below to insert new unit			0.0	To be developed	20	0.0
	SUBSYSTEM TOTAL		**5**	**300.0**		**18.1**	**354.2**

Element 2	Payload Module				MASS [kg]		
Unit	Unit Name Click on button above to **insert new unit**	Part of subsystem	Quantity	Mass per quantity excl. margin	Maturity Level	Margin	Total Mass incl. margin
1	Cryocooler Thermal Equipment		1	10.0	To be modified	10	11.0
2					Fully developed	5	0.0
-	Click on button below to insert new unit			0.0	To be developed	20	0.0
	SUBSYSTEM TOTAL		**1**	**10.0**		**10.0**	**11.0**

Table 10-1: List of thermal equipment and corresponding mass

Element 1	Service Module			
Unit	Unit Name	Part of subsystem	Quantity	Ppeak
	Click on button above to **insert new unit**			
1	2ST Cryocooler		8	400.0
2	4K JT Cryocooler		2	265.0
3	1K JT Cryocooler		2	235.0
4	Cryocooler Electronics		1	560.0
5	Thermal Equipment		1	250.0
-	Click on button below to insert new unit			
SUBSYSTEM TOTAL			5	1710.0

Element 2	Payload Module			
Unit	Unit Name	Part of subsystem	Quantity	Ppeak
	Click on button above to **insert new unit**			
1	Cryocooler Thermal Equipment		1	
2				
-	Click on button below to insert new unit			
SUBSYSTEM TOTAL			1	0.0

Table 10-2: List of thermal equipment and corresponding peak power needs

10.5 Options

The option of having an increased telescope size (elliptical mirror) has been studied from a thermal point of view as well. The main results of this study are summarised below:

A simplified model of the large telescope has been established to verify the performance (see below). The dis-connectible struts have been simulated by either assuming a lower conductivity representative of the small struts or using a reduced I/F conduction between the strut and mounting plane. The cut-outs of the struts and coldfingers have been simulated by assuming a 1% transmissivity of the V-Grooves.
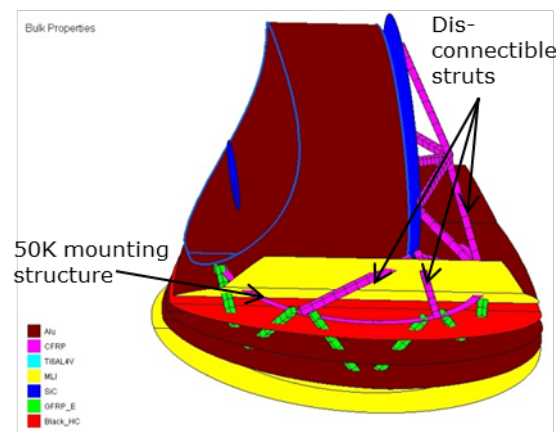
Figure 10-9: Large telescope configuration, materials/coatings used for thermal model

Taking into account a disconnect of the CFRP struts connecting the telescope to the 50K mounting structure, the following cooling power is required from the active cooling system:

- 5K: 20.5mW for conduction through the structure and radiation ➔ total load of ~40mW at 4.8K
- 25K: 360mW (including conduction, radiation and harness).

This assumes that all disconnectable struts have in parallel small struts for ground operation. Depending on the test orientation, this might not be required and reducing the number of small struts might allow to reduce the load by a few mW. This needs to be further assessed in detail in the next Phase.

Since this is above the allocation from the active cooling system for the telescope assembly at 6K, either the cooling power of the instrument needs to be reduced by ~10mW or the performance of the coolers needs to be improved. For the Shell cooler, a Ne-JT would be required since the total load is above the capabilities of the JAXA 2 stage Stirling cooler.

Additional coolers are not an option, due to complexity and power constraints already coming from the large cooling system.

The temperatures of the V-Groove system are shown below:
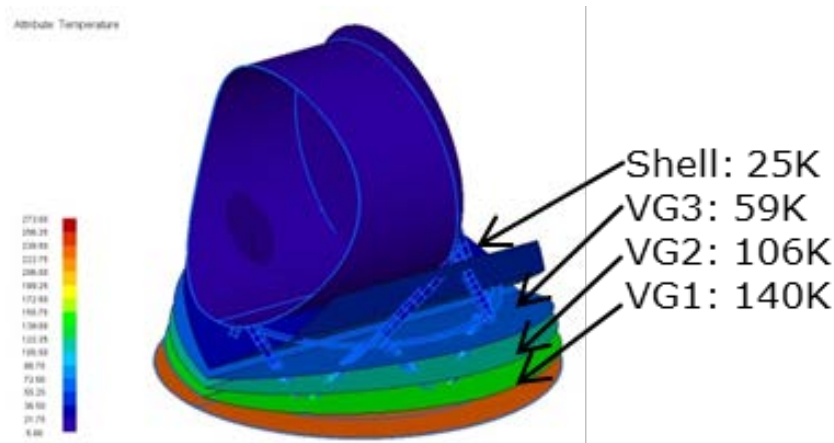
Figure 10-10 Predicted temperatures for the large telescope configuration actively cooled below 6K

10.5.1 Option with Large Telescope at Temperatures Between 15-35K

In addition to a telescope below 6K, which is required to comply with the current science requirements, the feasibility of higher telescope temperatures have been assessed. The results are reported here, since this might be still of interest for future science missions with a different science case.

One configuration has been studied allowing to cool the telescope down to 15-18K, using a hydrogen JT cooler. Due to the reactivity of the hydrogen gas and negative impact on the fatigue behaviour of most materials, mechanical compressors as used for the 4K/2K JT coolers are most likely not suitable. Instead a Hydrogen Sorption cooler currently under development by ESA has been considered. The EChO configuration, providing

70mW at 18K and shown in Figure 10-11, with the following modifications have been assumed:

- Additional cooling at 40-45K (200mW) increases performance by 50-70% ➔ 120mW at 18K

- Split HP and LP cells between VG3 and VG2, 2W each ➔ increase input power by 30% ➔ 160mW at 18K
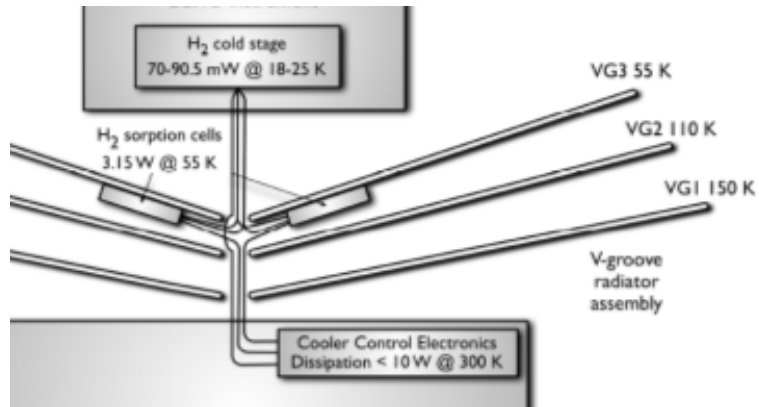

Figure 10-11 EChO sorption cooler configuration

Besides the addition of the sorption cooler, this configuration also allows to merge the Shell and the baffle into one element. As a side effect, the distance between the shell and 3rd V-Grooves increase, further reducing the radiative load onto this stage.
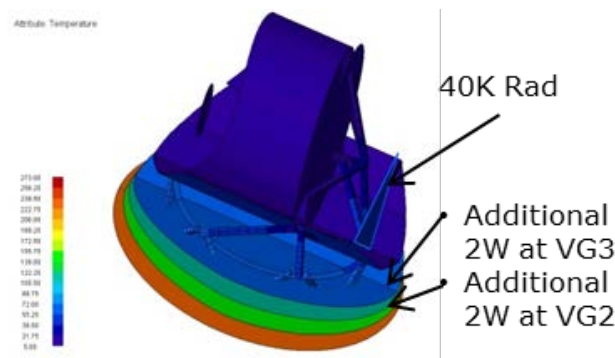
Figure 10-12 Temperature map of the Large Telescope configuration operating at 15-18K

The total load 15-18K stage is 160mW (incl. radiation, conduction and harness) without disconnecting the support structure as for the 6K case. Disconnection should reduce load further, which is considered as margin for now. The same cooling power can also be provided at different temperatures by:

- 20-25K, using JAXA Stirling coolers

- 25-30K, using a modified JT cooler (ESA or JAXA) with Neon

And in a pure passive mode, the telescope would operate below 35K, similar to the JWST.

11 MECHANISMS

11.1 Assumptions and Trade-Offs

11.1.1 M2 Refocusing Mechanism

Special attention in this study is reserved for the refocusing mechanism of the secondary mirror. Functional requirements like operation in cryogenic temperature and high accuracy and stability make its development particularly critical.

The refocusing mechanism provides the motion along multiple degrees of freedom (DoF), in general 5, in order to accurately locate the secondary mirror of the telescope and keep it stable. This refocusing mechanism can therefore correct possible misalignments coming from the assembly residual errors, deformations due to environmental effects from ground to orbit etc. Its main specifications define the resolution, range, accuracy with respect to a reference position, lifecycle (number of full strokes) and operative temperature range. Other important characteristics are the capability to produce a limited heat dissipation, survive launch loads, compactness and light weight.

An overview of similar applications adopted both in ESA and NASA projects is firstly given, with a discussion of the main features developed to overcome the most critical technical issues. Later, the most relevant aspects, like the kinematic layout and the high accuracy measurements in cryogenic environments, and components, like the motors and gearboxes are addressed in more detail, also highlighting innovative aspects. This will allow a thorough selection of the best options.

11.1.1.1 GAIA M2M

The Gaia M2 Mechanisms has three in-series stages layout: the Y motion stage on the bottom, the X stage immediately on top, and finally a tripod (tip-tilt-piston) stage, connected to the mirror structure. In total it controls 5 DoF: two rotations and three translations of the mirror. Figure 11-1 shows an exploded view.
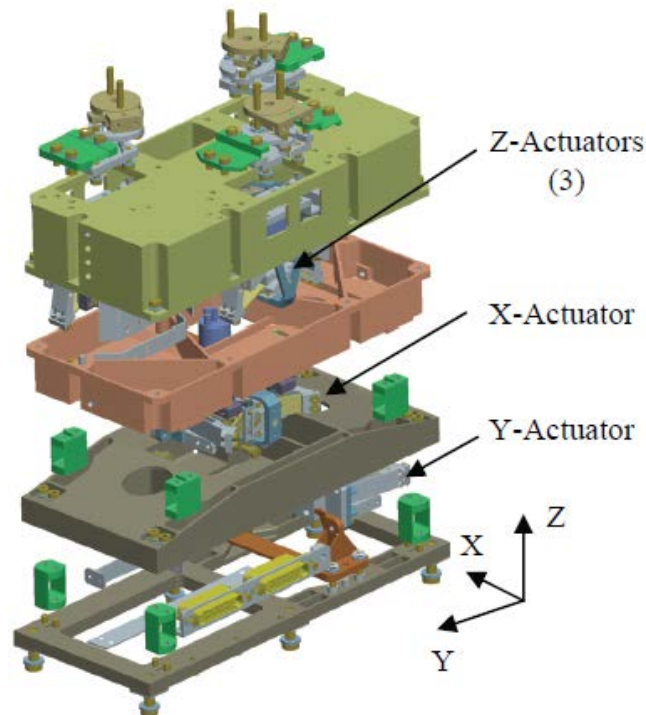
Figure 11-1: Exploded view of the Gaia M2M. The stacked X and Y stages are visible at the bottom, while the tip-tilt-piston stage is realised with the three actuators at the top, oriented along the Z-axis

Each DoF is controlled by a linear actuator, as seen in Figure 11-2. It is based on the following main elements:

- Stepper Motor, with high detent torque to withstand the elastic forces when unpowered.

- Planetary Gearbox: employed to perform the necessary speed reduction in order to obtain a small resolution step from the stepper motor angular step. Due to the cryogenic environment, the teeth shall be dry-lubricated. A supplier from USA was selected, since the technology was not sufficiently mature in Europe.

- Plain screw-nut: used to transform the rotary motion from the planetary gearbox into a linear motion. It needs a preload (play recovery) device, and features sliding motion between screw and nut threads, which need to be dry-lubricated.

- Flexure joints with structural reduction: it realises a further reduction of the linear motion from the nut to the output I/F. Figure 11-3 shows a kinematic scheme of the design concept. The structural reduction also strongly reduces the amount of load that is seen by the input element, when a load is applied at the output, since the majority of the load is diverted through the housing structure. A consequence is the increase of stiffness of the output degree of freedom.

- Guiding flexure joints: they are needed to constrain the motion of the output element of the actuator, by connecting the stages and the mirror in an isostatic manner (kinematic mounting). The isostatic mounting is needed to avoid internal

load path as consequence of assembly misalignments and thermal distortions, hence to reduce uncontrolled deformations.

No position sensors are used in the mechanism. The system works in open-loop, therefore the actuators has to provide the necessary stability throughout the lifetime, and a calibration (mapping) is needed to associate the angular position of the stepper motors to the DoF of the mirror.
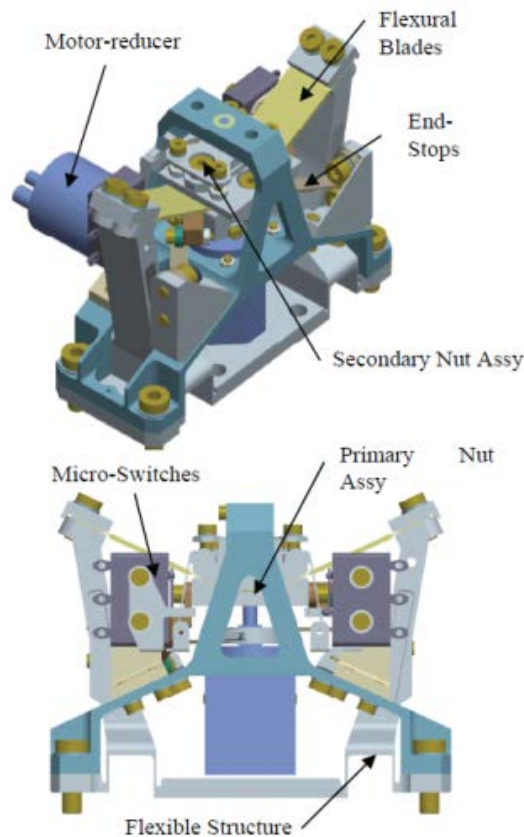
Figure 11-2: Gaia M2M linear actuator. The motor-gearbox and the screw-nut assemblies are indicated in the top view. On the lower view, it is visible the motion reduction realised with the flexural joints in grey and the flexure blades in yellow, partially covered by the micro-switches and the screw-nut assembly. Note that the output element, the grey block at the bottom of the picture, is not guided laterally by the actuator flexure, and needs therefore an external set of flexure guides
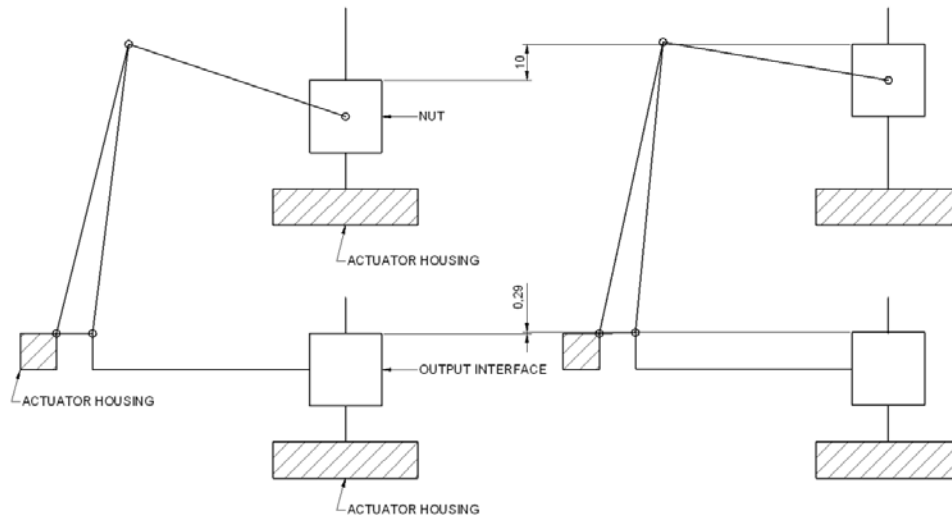
Figure 11-3: Scheme of the structural reduction mechanism for Gaia M2M. Only half is represented. Left side, original position, right side, motion after the nut is translated 10 units upwards. The combination of a horizontal knuckle-lever on the top, and the lever arm of the triangular structure on the bottom, results in a big reduction of the step size
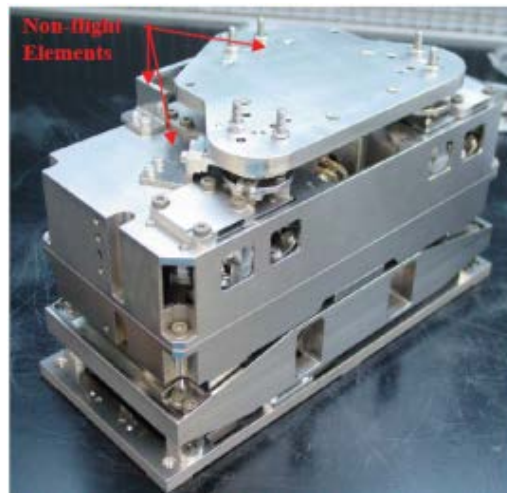
Figure 11-4: Photo of the Gaia M2M assembled

11.1.1.2   JWST Mirror pointing mechanisms

The James Webb Space Telescope (JWST) uses the mirror pointing mechanism for the position control of both the independent segments of the Primary Mirror, and the Secondary Mirror.

The layout of the JWST Mirror Refocusing Mechanism consists of a Hexapod plus an additional curvature actuator, and shown in Figure 11-5. The hexapod consists of six linear actuators, attached to the mirror structure and the telescope structure via suitable flexure joints. See Figure 11-6, on the left.
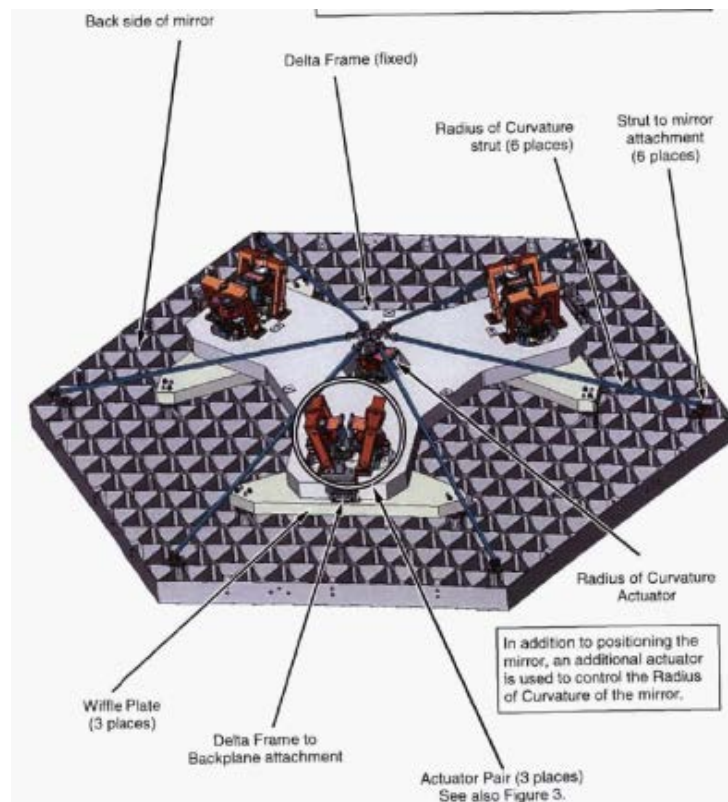
Figure 11-5: Layout of the JWST mirror positioning hexapod mechanism. The six actuators arranged in three pairs (bipods) are shown. An additional seventh actuator is mounted on the centre, to control the mirror curvature

As shown in Figure 11-6 on the right, the actuator employs two motion stages, one for the fine positioning, and one for the coarse. The two stages are integrated in a way that a single motor is used. The coarse chain is coming in motion once the fine stage has reached its range extremes, thanks to the tumbler coupling.

The linear actuator is based on a stepper motor, followed by a planetary gearbox and spur gears.

The fine positioning is realised with an eccentric bearing/cam which reduces the step size. It furthermore provides a linear motion at the output when a rotation in the input shaft is commanded. The step size is further reduced (or the resolution increased) by means of a double knuckle levers structure.

The coarse positioning is based on ball-screw, and spur gear transmissions. The coarse motion is actuated once the two parts of the tumbler coupling come into contact. Otherwise only the fine-motion occurs and the coarse chain remains in its position. A wide range of motion is needed for the JWST since the mirrors are of big diameter and deployable, hence the misalignments to be compensated can be bigger.

The actuator includes a LVDT as coarse position sensor.
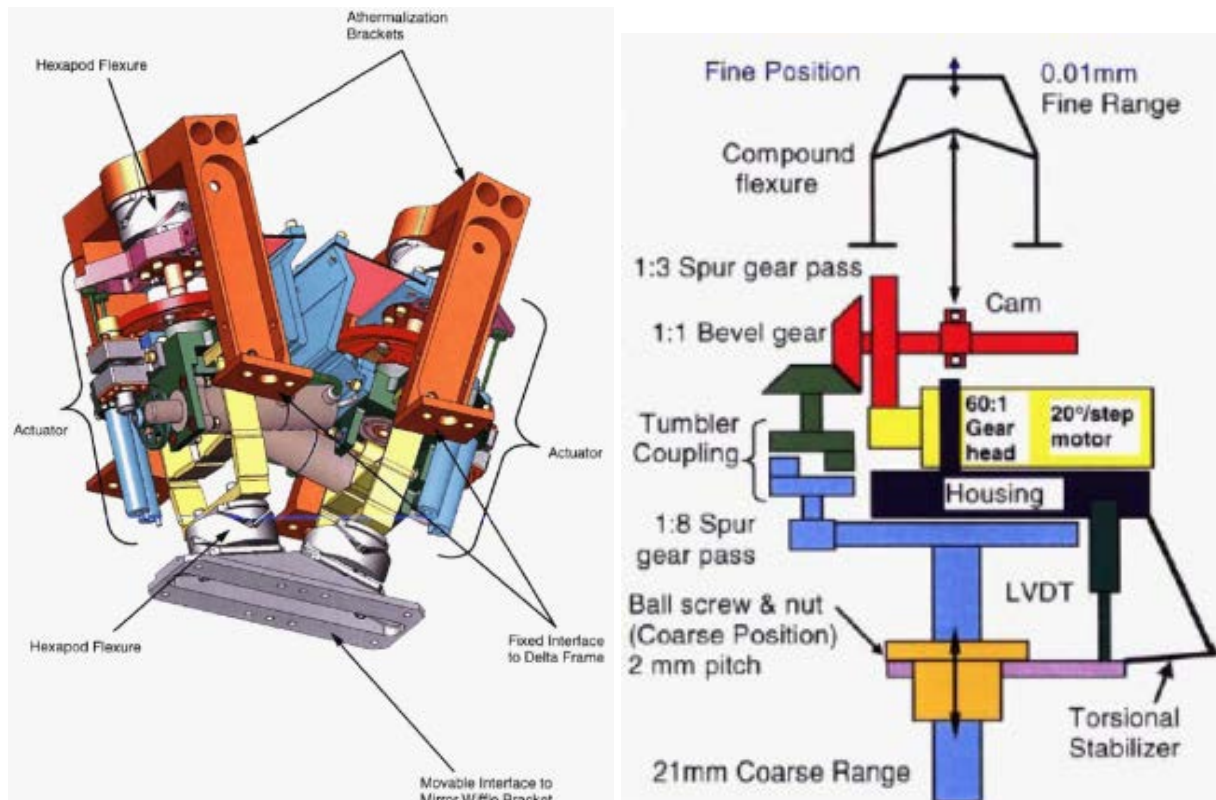
Figure 11-6: On the right, the assembly view of a couple of linear actuators for the hexapod. Note the white hexapod flexure which perform the function of a universal joint. On the left, a conceptual scheme of the actuator. On the upper side, the fine positioning chain, with the red shaft, the eccentric cam and the compound flexure realising a structural reduction via a double knuckle-levers. On the lower side, the coarse positioning chain, with the blue gears and the ball-screw-nut. The Tumbler coupler realises the engagement of the coarse positioning chain, once its two parts come into contact. An LVDT is used as coarse displacement sensor

11.1.1.3 Spica/Echo Cryogenic IR Telescope M2M

An R&D activity has been started for the development of a qualification model of a 6 DoF mirror positioning mechanism. The activity was started with specifications from early Echo and Spica mission studies.

The design is chosen for the baseline of this study, and it will be addressed with more details in the design section of this chapter.

11.1.1.4 Comparison of Mirror Positioning Mechanisms

The table below shows a summary of the main specification for the secondary mirror positioning mechanism discussed before.

		Gaia	JWST	Echo-Spica
Actuators layout		serial + parallel tripod	parallel hexapod	parallel hexapod
Number of DoF		5	7	6
Position measurement		No	Coarse	No
Minimum operative temperature	K	100	20	5
Resolution, translations	um	0.07	0.01	0.1
Range, translations	um	550	20000	1000
Resolution, rotations	urad	1.8	-	2.5
Range, rotations	urad	2000	-	4000
Mass of the mirror	kg	1.8	5	5.4
Launch-locking provisions		No	In lat. Direc.	No
Mass of the mechanism	kg	4.8	4.2	8
Deployable		No	Yes	No

Table 11-1: Comparison of Mirror Positioning Mechanisms specifications for Cryogenic IR-Telescopes

11.1.1.5 Kinematic layout

An evaluation of the two different kinematic layouts seen before is done.

In summary, the chosen hexapod solution has the following advantages over the 3-stage solution:

- High stiffness since, thanks to the 6 actuators working in parallel, the inertia load can reach the base structure via multiple paths through the actuators. The stiffness anyway varies with the orientation of the actuators axes, which also depends on the needed ranges of motion on the mirror DoF.
- Modularity, repeatability of components and operations in manufacturing and assembling, thanks to the use of six identical actuators.
- Partial redundancy: since 6 actuators are used to control 5 DoF, and the mirror have an axial-symmetric shape, in case of the failure of one actuator the 5 DoF motion can still be realised once the rotation of the mirror is accepted.

The main disadvantages are:

- More mathematically-complex direct kinematic: for computing the mirror position from the actuator position, the solution of algebraic equations in closed form is needed. Relationships between input and output DOF need to be computed via calibration and mapping to reduce parasitic motions.
- Six linear actuators have to be used instead of five, one more than what is necessary.

For the current study, the Hexapod solution is selected. The advantages of greater modularity and stiffness have been regarded as particularly attractive.

11.1.1.6 Cryogenic motors

11.1.1.6.1 Stepper Motor

The stepper motor is used in high accuracy applications for its capability to keep a desired angular position (step), also when powered-off. Permanent magnet stepper motors have high detent torque, which has to withstand the elastic reaction forces from preload devices and flexures.

In cryogenic applications, Samarium-Cobalt (SmCo) rare-earth magnets are employed instead of the more common Neodymium-Iron-Boron (NdFeB), for their higher capability to withstand low temperature without substantial loss of magnetic field strength. See p. 223 of RD[14].

It is noted that at very low temperatures the electric resistance of the copper windings decreases by a factor of about 100, see p 123 of RD[14]. This is an advantage for optical-IR applications where temperature control is critical, since it reduces a lot the power consumption and the consequential heating for Joule effect.

Finally, special care must be taken in the mechanical design of the bearings. The wide temperature excursion from assembly to operation environments can cause deformations which lead to overloading on balls and races, or the occurrence of big clearances which can affect the air-gap between stator and rotor. Therefore the CTE of the materials have to be known with sufficient accuracy, and properly matched.

Ball bearings need to be dry-lubricated, typically with sputtered MOS_2.

11.1.1.6.2   Inertia-drive piezoelectric motor

An actuator which has become interesting in recent years for high accuracy positioning is based on the inertia-drive piezoelectric principle, see Figure 11-7. It can realise nanometre-level resolution motions in a very compact volume. Indeed, no dedicated reduction stages are needed compared to the stepper motor solution.
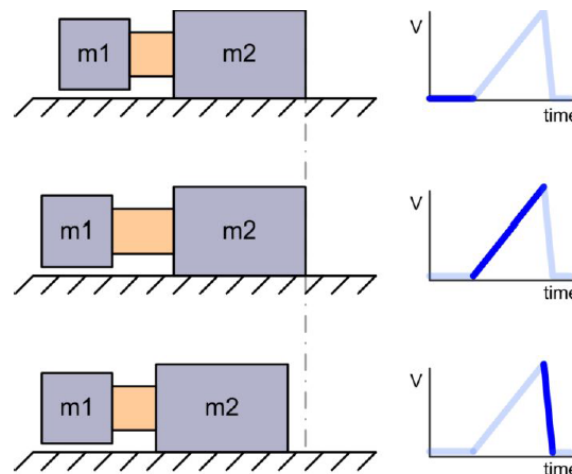

Figure 11-7: Illustration of the working principle of the inertia-drive piezoelectric actuator, from RD[15]. Sequential fast-slow piezoelectric stack motions in combination with a free floating mass M1 cause inertial forces that can break the friction force between M2 and the floor

A special implementation of the inertia-drive is the PiezoKnob actuator, see Figure 11-8. The floating mass becomes a rotating external ring M1, while the actuated mass M2 is a disc at which axis a screw is mounted. The screw then engages into a nut, mounted on

the supporting base. As the disc rotates, the screw advances linearly. The friction between the screw and the nut allows the micro-step motion, and at the same time avoids the backward movement. Since the piezoelectric elements can perform many turns, the electric power has to be transferred by sliding contacts.
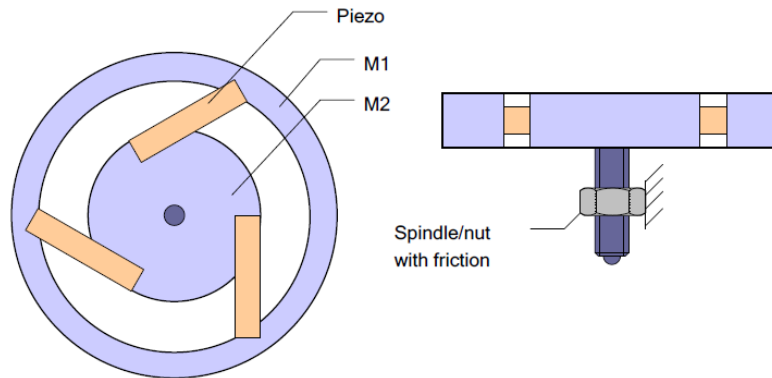

Figure 11-8: Working principle of the PiezoKnob. From RD[15]

Its effective functioning has already been demonstrated for non-space scientific application, such as quantum physics and ground-based large telescopes instruments. For the space environment there are several challenging aspects which need to be verified:

- Suitability for launch vibrations, in particular of the suspended mass
- Friction coefficient stability throughout the whole life, and step size variation
- At cryogenic temperatures, performance of piezoelectric material, in particular with respect to the observed reduction of strain versus voltage characteristic
- Assessment of the effects of the micro-vibrations produced by the step-wise and high frequency motions.

The steps size show less stability and predictability compared to the stepper motor. An accurate position measurement is therefore needed.

The plain-screw-nut element needs a play-recovery element. The backlash can be for example avoided if the output stage is pre-loaded by a spring.

11.1.1.6.3   Cryogenic motor trade-off

The selected solution for this study is the stepper motor. The uncertainty due to the low technological maturity for space applications is considered more critical than the drawback of the stepper motor to necessitate of a relatively complex speed/step reduction system.

11.1.1.7   Cryogenic speed reducers

11.1.1.7.1   Dry-lubricated gearbox

Gearboxes are needed to reduce the angular step size provided by the stepper motor to a value which can be later handled by the guiding flexure joints and further structural reduction stages. Moreover, since the range of motion of the flexure joints is restricted

by the elastic strain limit of the material, the gearbox provides also a reduction of the rotation range.

Usually for such application, 3 or 4 planetary gears stages are needed, with reduction ratios of the order of several hundreds.

A critical aspect in cryogenic environments is the lubrication of the teeth of the gears. Dry-lubricated coatings are needed, among other, MoS_2 coatings are preferred for their numerous applications and very low coefficient of friction. Torque capabilities and lifetime are reduced if compared to the case of liquid-lubricated gearboxes.

In planetary gearboxes, a certain angular backlash exists, which has to be cancelled by a dedicated preload device.

The bearings on the planetary gearbox have also to be dry-lubricated. Wear phenomena are less critical compared to the teeth of the gears, since the micro-sliding speed is much lower. For the small satellite gears, plain bearings are to be used due to the reduced size available. Here, wear can be an issue, and special attention has to be taken in their design and testing.

11.1.1.7.2   Magnetic gears

Instead of using the sliding contact between engaging teeth of the mechanical gears, magnetic gears transfer the motion thanks to the action of magnetic fields in the air-gap.

A major breakthrough of this technology occurred with the introduction of high performance "shutter" or "field-modulated" type magnetic gears. In recent years, progress in development with respect to both torque volume and mass density has been done, and currently they can provide torque values similar to dry-lubricated gearboxes. Improvements were made thanks to the availability of new material with high B*H energy product and coercivity, and enhancements in the capability of Finite Element Analysis software for the magnetic-field domain.

In Figure 11-9, a magnetic gear of the last generation is shown, from RD[16]. A proper combination of the angular frequency of permanent magnets and ferromagnetic pole-pieces on the rotors and stator generates a "modulated" magnetic field wave on the outer air-gap that rotates at a speed lower than the one of the inner (input) rotor. The outer field drags the outer rotor (output) to move at a lower speed.
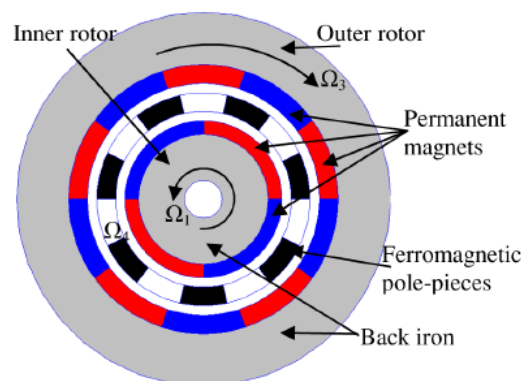

Figure 11-9: Schematic of the magnetic gear "shutter" of "field-modulated" type

Compared to dry-lubricated gearboxes operated in cryogenic environment, the main advantages are:

- Contact-free, no gear lubrication, high durability
- No friction, high energy efficiency
- No backlash
- Intrinsic torque limited: sudden accidental increase in the output torque will not lead to gears damage
- Fewer elements, higher reliability
- Possibility of integration with the electric motor.

While the main disadvantages are:

- Lower stiffness at same max torque capacity
- Still lower torque density, in terms of both volume and mass
- Lower maturity.

11.1.1.7.3 *Cryogenic speed reducers trade-off*

For the baseline of this design, the planetary gearboxes are selected. The main reasons are both the low readiness level of the magnetic gearbox solution for the space environment, and the few applications still existing nowadays in the non-space industry.

11.1.1.8 Position measurement

11.1.1.8.1 *Displacement measurements and calibration on ground*

In order to validate the accuracy requirements, position measurements have to be made during the development, which is a particularly complex and expensive task: Measurements have to be performed in cryogenic environments; the tested unit is placed inside a cryostat; at least as many sensors as the number of DoF have to be employed, and accurate optical instruments have to transmit their laser signal outside the cryostat via suitable windows. At very low temperatures, less than 100 K, the high thermal gradient between the outer and inner environment of the cryostat creates distortions on the windows and produces significant thermal radiation. The first issue has the effect to alter the optical measurement taken with interferometers and auto-collimators, while the second can affect the uniformity of the temperature inside the chamber. Efforts have to be paid to compensate both the problems. Moreover at such low temperature range, the thermal conduction of metals reduces a lot, and the time to be spent to reach stationary temperatures increases, making this test particularly time-consuming.

Efforts should be done to avoid the use of optical sensors which need to transmit a signal from inside to outside of the cryostat. Improvements have been recently made to increase the accuracy of several displacement transducers able to operate in cryogenic environments: LVDT, extensometers (based on strain gauges) and magneto-resistive sensors for example are being used. These transduces are able to fully function between 4 and 300 K, maintaining drift due to temperature effect in a predictable and acceptable range. Some implementations of the extensometers and magnetic-resistive sensors are shown in Figure 11-10, Figure 11-11 and Figure 11-12.

To avoid the use of many sensors inside the cryostat, at least one per DoF, and where it is possible to employ at least one window on the cryostat, a displacement measurement via wavefront sensor could be implemented. Inside the cryostat, the target element is the mirror itself (or an equivalent dummy one). Similar techniques are widely used in adaptive optics for large ground telescopes.
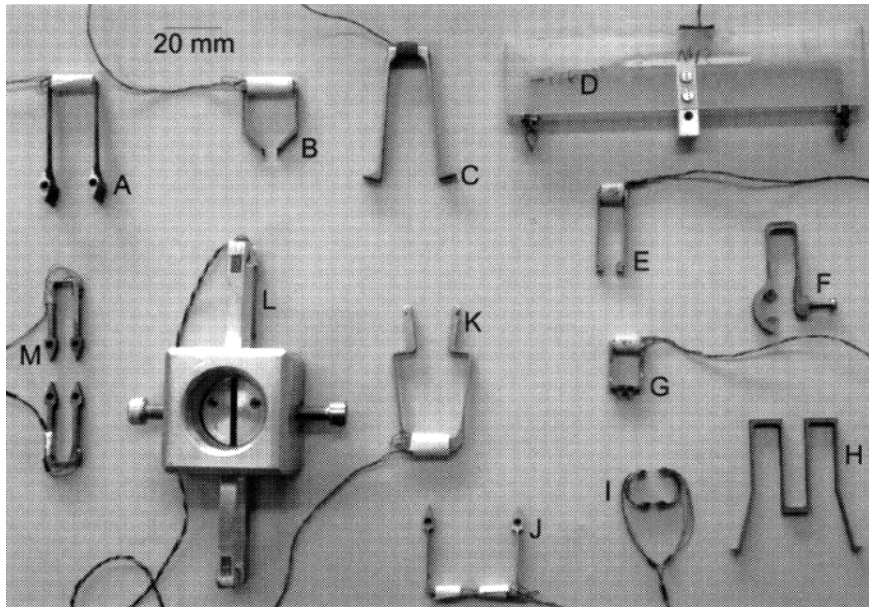

**Figure 11-10: Examples of extensometers form RD[11]**
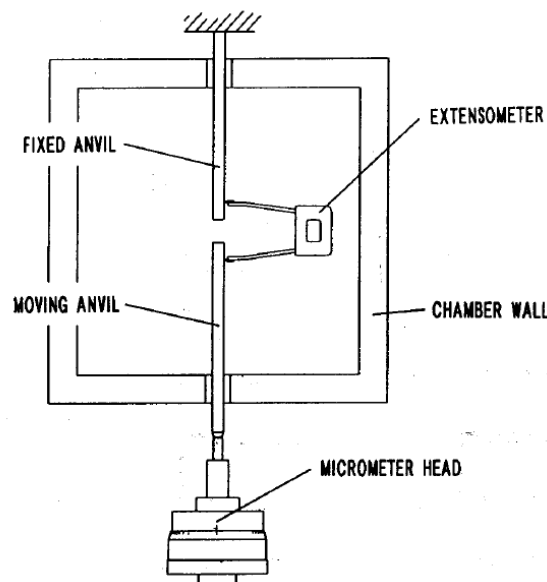

Figure 11-11: Extensometer, principle of operation, from RD[12]
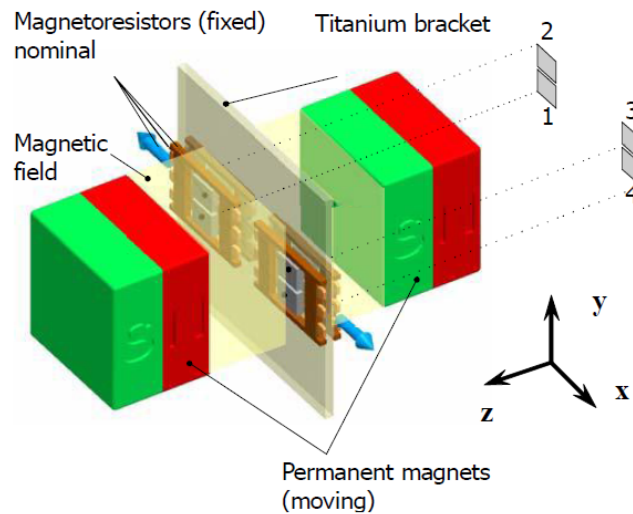
Figure 11-12: Schematic view of the one dimensional magneto-resistive position sensor. Four field plates (1-4) on the same side of the holder are located in the strong magnetic field region between a sensor magnet pair providing the nominal signal. This is a flight solution employed in JWST NIRSPEC instrument, RD[13]

11.1.1.8.2   *Displacement measurements during in-orbit operations*

For certain mechanisms solutions, a further option could be to embed displacement sensors in the mechanism itself, therefore obtaining a system with a position feedback. In this case the sensor, beyond the cryogenic environment of the cryostat, has also to survive the full launch and space environment without losing its accuracy and calibration setup.

Depending on the telescope design, position measurements for the M2 mirror can be indirectly obtained from optical measurements, such as from a wavefront sensing or via analysis of the acquired images. The former case is adopted for example for the fine-motion adjustment of the JWST mirrors. The advantage of this approach is that the real effects of the mirror displacement on the image quality are directly obtained, leaving out a lot of disturbances coming from the assembly and the environment. As a consequence, room is left for simplifying the design and the ground calibration needs, and their costs.

Therefore, from the point of view of the design and development of the mirror pointing mechanisms, the use of on-board image-level measurements system is strongly desired.

11.2 Baseline Design

11.2.1   Introduction

In this section, the design of the mechanisms used in the Service Module and in the Payload Module of the NG-CryoIRTel will be described.

Mechanisms on the Service Module:

- Antenna Pointing Mechanism (APM) and its Hold-Down and Release Mechanism (HDRM)
- Launch-Locks for the Cryo-coolers and MINT (Mechanical INTegration Parts) are assumed to be provided by JAXA, and are not described in this section.

On the Payload Module:

- M2 refocusing Mechanism (M2M)
- Bipods, Hold-Down and Release Mechanism and Latches for the Payload Module
- Shutter mechanism.

11.2.2   Antenna Pointing Mechanism and HDRM

The foreseen High Gain Antenna for this mission has a 40 cm diameter and a mass of about 1 kg. It requires a pointing accuracy of 0.5 deg and 2 DoF motion capability.

The baseline Antenna Pointing Mechanism is made of two stages, one for the azimuth and one for the elevation on the top. The motorisation is provided by a stepper motor for each stage, and a reduction gear to produce the resolution which is compatible with the accuracy requirement.

Similar antenna pointing mechanisms are already used in Earth Observation satellites, but there, required rotation ranges and speeds of motion are higher.
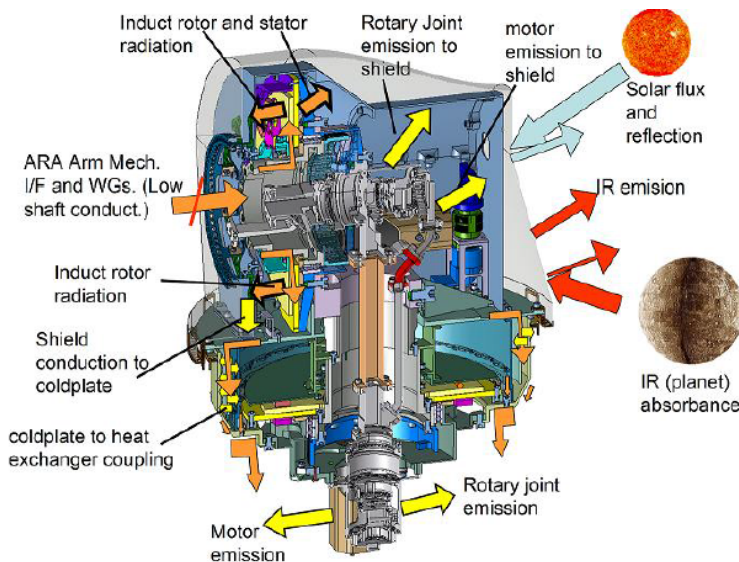
Figure 11-13: Model of the Bepi-Colombo Medium Gain Antenna APM

A peak power consumption of 12 W is estimated, when the two motors are switched on. The mass is approximately 5 kg, excluding the Antenna and HDRM.

Since the size of the antenna is greater than the usual applications for Earth Observation satellites, a specific HDRM is probably needed to hold the antenna during the launch phase, and therefore included in the baseline.

Figure 11-13 shows the 3D model of the APM for the Bepi-Colombo Medium Gain Antenna, from RD[17], which can be a reference for the design of the Ka-band APM foreseen in the baseline.

11.2.3   M2 Refocusing Mechanism

The accuracy and environmental specifications for the M2 refocusing mechanism are fully compatible with those foreseen for the design of a qualification model of M2 Mechanism for the Echo-Spica missions.

Being an activity under development, several details are confidential at this stage. Anyway the main points are addressed in the following description and general approaches for the solution justified.

The mechanisms kinematic layout consists of a hexapod configuration of the actuators, or Steward platform. Compared to the solution adopted in Gaia, a 1+1+3 DoF stacked stages, this is a fully parallel mechanism: All the actuators are connected to the telescope structure at one side, and to the mirror structure to the other.

A number of hinges have to be employed to constrain and guide properly the various internal DoF of the mechanism. Each actuator needs for instance at least a universal joint on one end, and a spherical joint on the other, which are made respectively of 2 and 3 revolute hinges. Sliding and point rolling contacts typically occurring inside the hinges should be avoided as much as possible as they are sources of friction, backlash, wear, all phenomena that affect the accuracy and repeatability. When the needed displacement is low enough, elastic flexure joints can be used instead. Figure 11-14 shows some examples of the implementation of a universal joint with flexure hinges, while Figure 11-15 illustrates their employment in a parallel kinematic mechanism.
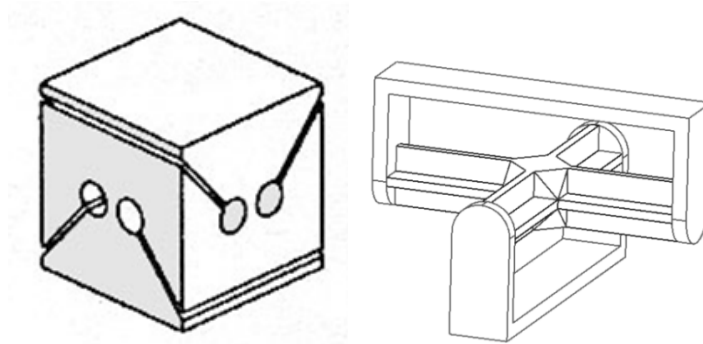

Figure 11-14: Some examples of realisation of a universal joint with flexure joints. On the right, the so called Cruciform type, which allows a greater rotation range. The universal joint allows two rotations while constraining all the other 4 DoF
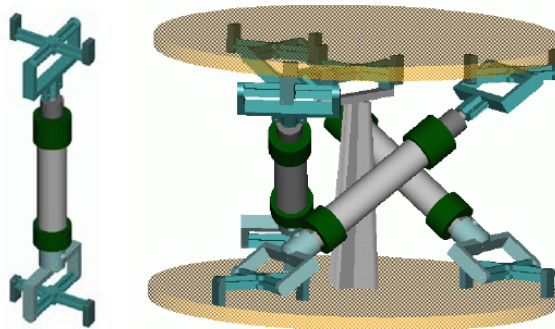

Figure 11-15: On the left, a leg with two universal joints at its ends, an actuator solution which can be used for the hexapod mechanism. On the right is shown its employment on a 3-DoF mechanism

For high accuracy operations in cryogenic environment, it is of paramount importance that the thermo-elastic deformations are minimised. This can be done at best with a structure which uses as much as possible the low CTE Invar alloy. Unfortunately,

structural parts undergoing high stress levels, like thin sections of flexure joints, or components in point contact like rolling bearings and gears teeth, need to be manufactured preferably in titanium alloy and stainless steel respectively. This inevitably leads to mismatch of CTE. However, the effects can be minimised by adopting the following techniques:

a) Reducing as much as possible the length of the element with different CTE along the direction of interest

b) Making the direction of main contraction/elongation of the material with different CTE orthogonal to the direction of interest

c) Using an high reduction ratio between the displacements of the material of different CTE and the output element

d) Introducing compliant elements to absorb the different contractions, so to avoid internal load paths and variation of preloads, of use isostatic (kinematic) mounts

e) Introducing a second element in a backward dimensional path with CTE tailored to balance the effect of targeted dimensional variation (passive athermalization).

When using a rotary actuator such as a stepper motor, its rotation motion has to be transformed into translation via a suitable mechanism, commonly a screw-nut. In high accuracy mechanisms, sliding elements, such as plain screw-nut couplings shall be avoided where possible as they present potential stick-slip behaviour and they need a preload to avoid backlash. Moreover in cryogenic environment they need to be dry-lubricated, and solid coatings are more prone to wear than liquid-lubricated surfaces. The baseline solution features a proper combination of flexure joints and levers. The solution is also effective in decoupling the axial thermal displacement of the motor-gearbox (made of stainless steel and Ti-alloy) from the axial output axial displacement of the actuator assembly.

In Figure 11-16, a conceptual scheme of the linear actuator represents in a simplified manner the principles explained above. The crank-lever 2 together with rocker-arm 3 transforms the rotation of the motor shaft into a horizontal translation. The knuckle levers 4 deform, producing a small displacement in Y direction of the output element 7. A high reduction ratio is realised. Note how this concept is similar to the one described for the fine-motion stage of the JWST mirror actuator, where an eccentric bearing was used in place or the crank-lever 2. The motor-gearbox 1, the shaft-crank 2 and the rocker-arm 3 are made of stainless steel and Ti-alloy, since they need to withstand higher stress than the rest of the structure, made of Invar alloy. The contraction of el. 1 and 2 have very little effect on the vertical displacement Y of the output 7, since it occurs in different direction, or is decoupled by the hinges. The contraction of the rocker-arm 3 has reduced effect thanks to the high reduction of the displacement happening in the knuckle levers 4, and shortening their length will also help. Thanks to the various compliant hinges, the mechanism is always isostatic, so residual internal deformations do not cause major changes in the load paths. Finally, the metering structure 5 is made of the same material as 4, in the dimensional path to the output 7 goes backward wrt the knuckle levers. When they undergo the same temperature change, they compensate each other (passive athermalization), and the output 7 will therefore not displace along Y.
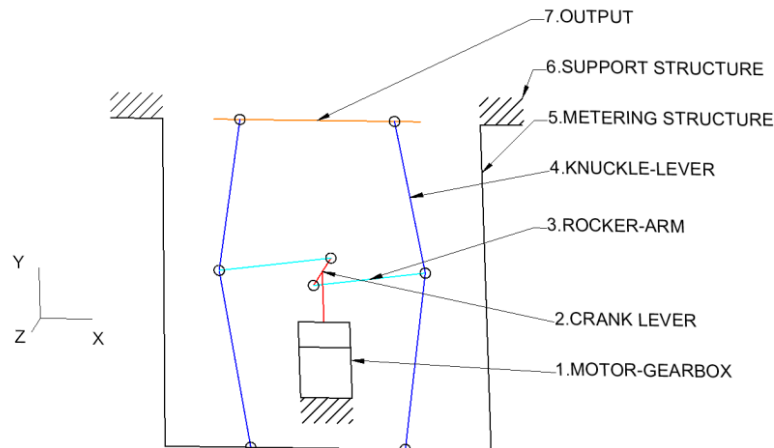
Figure 11-16: Conceptual scheme of a linear actuator implementing several thermo-elastic design guidelines

Each actuator is motorised by a stepper motor with a planetary gearbox, dry-lubricated. The stepper motor provides defined angular positions (steps), which can be held when the power is switched off thanks to the magnetic characteristic of the motor. The motor detent torque is the toque to be applied to the motor to make it lose a step when not energised. All the static reaction forces, coming from the gearbox preloading device and the elastic reaction of the flexure joints shall provide a torque at the motor sufficiently low to avoid step losses. As mentioned, the planetary gearbox has to be provided with a play-recovery device, a rotational spring, which elastically preloads the gearbox to remove the backlash effect when the direction is reversed. The minimum torque provided by the play-recovery device must be higher than the friction of the backward motion. Its maximum torque shall not be too high, the limit is the torque needed by the stepper motor.

The actuator employs limit switches, which have to detect with sufficient accuracy the ends of the range of motion. Their location has to be accurate enough to serve as a reference point, in case a reset of the step-count is needed.

The baseline design does not use displacement sensors. The accuracy is provided by the stability of the steps of the motor, and the position accuracy of the reference points defined by the limit switches.

No HDRM to hold the mirror mass are foreseen in the baseline. Related to this aspect, a small mass of the mirror is highly beneficial for the mechanism design since it allows to reduce the stiffness and stress of the flexure joints, and increase their allowable displacement range. Thanks to this, the elastic reaction forces are also smaller, meaning that the motor and gearbox torque requirements are lower. It is therefore advisable to spend efforts in developing effective technology for reducing as much as possible the mass of the secondary mirror.

11.2.4 Bipods, Hold-Down and Release Mechanism and Latches for the Payload Module

The Payload Module needs to be thermally isolated from the Service module during operations. The stiff bipods structure (Launch Struts) which holds the Payload module attached to the Service Module have to be separated after launch, in order that only a thinner, and less thermally conductive bipod structure remains afterwards (In-Orbit Struts). See in Figure 11-17 the design solution adopted in Gaia.

The separation function is done by six Hold-Down Down and Release Mechanisms (HDRM), one for each strut. Once activated, a spring moves the strut to rotate at a certain angle, till the latch engages, hence firmly keeping the launch struts separated.

The HDRM employed in Gaia can provide a preload of 26 kN, enough to withstand the separation forces foreseen during launch. The axial stiffness of one full strut is higher than $7 \cdot 10^7$ N/m.

During separation, it is important that the HDRM induces a shock level on the Payload that is not harmful for the delicate optical elements and electronic devices accommodated in the vicinity. In the case of Gaia, the induced shocks were less than 2000 g on the Service I/F, and less than 600 g on the Payload I/F.
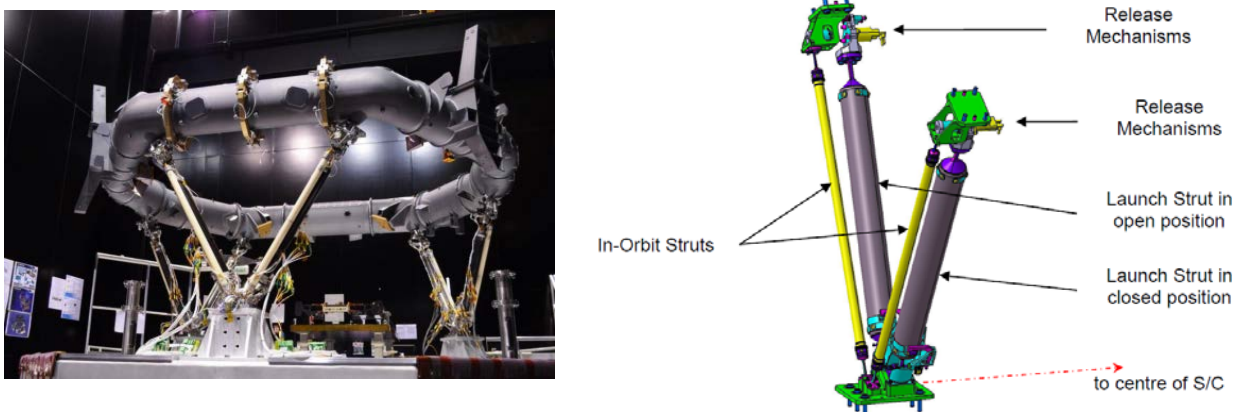

Figure 11-17: On the left, a picture of the Gaia Payload module, suspended by the six struts. On the right, a detail drawing of a bipod made of two stiff (launch) struts, and two in-orbit struts beside

11.2.5 Shutter Mechanism

A shutter mechanism is needed to cover the detector from sunlight, during early mission phases. There is indeed the risk that, due to the launch profile or in case of malfunctioning of the AOCS in the early orbit manoeuvres, the sunlight can accidentally enter the telescope and potentially damage the detectors.

For accommodation reasons, the cover is preferred to rotate around an axis parallel to the optical beam. This solution allows in fact the shortest envelope in the direction of the light beam. The optical beam size at the location of the shutter is about 170 mm diameter.
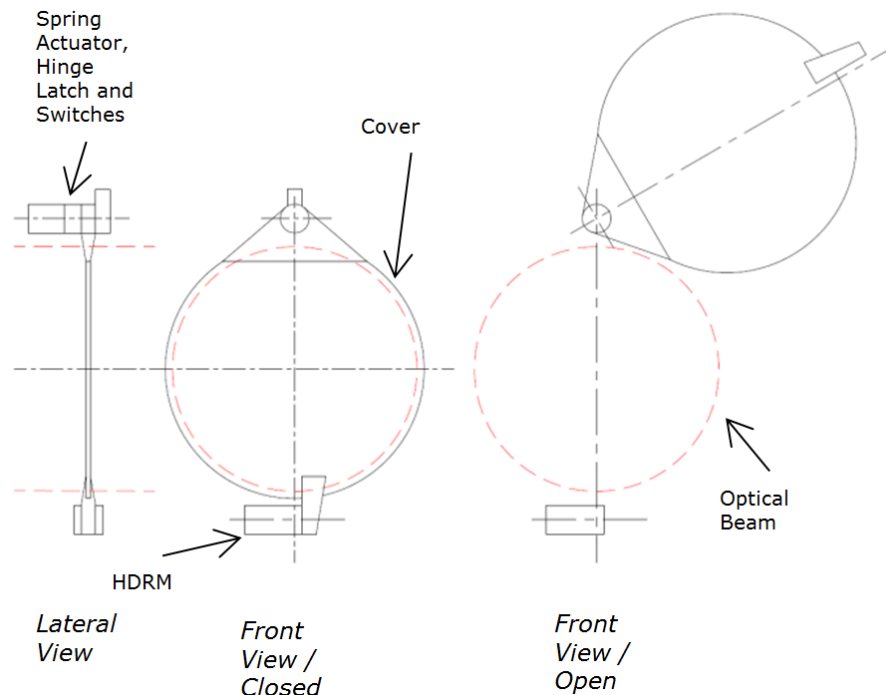
Figure 11-18: View illustrating the conceptual design of the shutter mechanism. On the middle-left, front view, the cover is closed, therefore completely covering the optical beam (traced in a red dashed line). On the right, the cover is in open position. The lateral view of the left shows how limited is the envelope in the optical beam direction

A one-shot mechanism is proposed, and a sketch of the conceptual design is shown in Figure 11-18. The main components are:

- Cover plate: The main functional element of the mechanism, it is a circular disc of aluminium alloy which covers the light beams. It could be necessary to statically balance the cover, see comment later about the spring actuator

- Rotational hinge: It allows the rotation of the cover, and is made of two angular contact ball bearings. They guarantee sufficient accuracy, stiffness for withstanding the launch loads and give a constant friction behaviour

- Spring Actuator: The opening motion is motorised by a spring. The stiffness and initial preload has to be high enough to overcome the friction of the hinge, but not too high to avoid excessive speeds and shock at the end-stop for latching position. If necessary, a viscous damper may be needed. For operation in ground under 1-g gravity, the spring may be required to overcome the cover own weight. An alternative design is to have the cover statically balanced (CoG on the rotation axis), at the expense of increasing the mass

- HDRM: A Hold-Down and Release Mechanism is used to keep the cover in closed position during launch, as well as offering an additional constraint to the cover to increase its stiffness. A low-shock HDRM shall be used to avoid potential damage to sensitive optical and electronics instrumentation accommodated in the vicinity

- Latch: The latch mechanism consists of a pin or a tooth which engages into a slot after the cover reaches its open position, hence ensuring a stable constraint of the cover rotation. The pin or tooth is pushed by a pre-loaded spring. It slides against a surface of the cover shaft during opening. An easily accessible disengagement device is needed to reset the mechanisms for ground testing
- Limit Switches: Two limit switches are used, one at each end of the stroke, to monitor the actual position of the cover.

11.3 List of Equipment

The list of equipment and mass budget for the mechanisms in the Service Module is shown in Table 11-2, while the list for the Payload Module mechanisms is shown in Table 11-3.

Element 1	Service Module			MASS [kg]			
Unit	Unit Name	Part of custom subsystem	Quantity	Mass per quantity excl. margin	Maturity Level	Margin	Total Mass incl. margin
1	APM		1	6.0	To be modified	10	6.6
2	Launch-lock for Cryocoolers Isol.		12	0.1	Fully developed	5	1.5
3	MINT		12	0.2	To be modified	10	2.6
4	HDRM for APM		1	1.0	Fully developed	5	1.1
-	Click on button below to insert new unit						
SUBSYSTEM TOTAL			4	10.8		8.9	11.8

Table 11-2: Equipment in the Service Module

Launch-locks for Cryo-cooler Isolators and MINT (Mechanical INTegration parts, meaning fasteners, brackets etc.) are provided by JAXA.

Element 2	Payload Module			MASS [kg]			
Unit	Unit Name	Part of custom subsystem	Quantity	Mass per quantity excl. margin	Maturity Level	Margin	Total Mass incl. margin
1	Refocusing M2 mechanism		1	8.0	To be developed	20	9.6
2	Bipods HDRM and Latches		6	2.5	To be modified	10	16.5
3	Shutter mechanism		1	1.5	To be modified	10	1.7
-	Click on button below to insert new unit						
SUBSYSTEM TOTAL			3	24.5		13.3	27.8

Table 11-3: Equipment in the Payload Module

11.4 Options

No optional solutions are foreseen for the baseline design.

11.5 Technology Requirements

The following technologies are required or would be beneficial to this domain:

Included in this table are:

- Technologies to be (further) developed
- Technologies available within European non-space sector(s)
- Technologies identified as coming from outside ESA member states.

Equipment and Text Reference	Technology	Suppliers and TRL Level	Technology from Non-Space Sectors	Additional Information
M2 Refocusing Mechanism	3 or 5 Mirror DoF	Ruag, Sener	Many application in modern large ground astronomical telescopes.	On-going R&D activity: Echo/Spica M2M
Bipods, Hold-Down and Release Mechanism and Latches	Separation of stiff struts	Ruag	-	Possible similarity for scale with Athena Mirror HDRM, R&D activity proposed.
Planetary gearboxes, dry-lubricated	Dry-lubricated gearboxes for extended temperature range	TRL-4, Lidax, Ruag	-	R&S activity on-going: "Development of a dry-lubricated gear box"
Ka-Bd APM	2-DoF APM able to steer with the needed accuracy a high gain antenna, and Ka-Bd rotary joints.	TRL-4, various	-	An R&D activity is going on for the application of Metop SG Earth Observation satellite. For a L2 orbiting S/C, slew rate and range will be lower, but probably accuracy need and antenna mass and envelope will be higher.

This Page Intentionally Blank

12 ATTITUDE CONTROL SYSTEM

12.1 Requirements and Design Drivers

12.1.1 Functional Requirements

The following functions are required for the AOCS:

- Three axes stabilisation
- Fine target pointing during science mode. The science pointing shall have the following sub-modes (see following sections):
  - o Fine raster pointing mode with high accuracy pointing direction and stability during observation time
  - o Line scanning with accurate and very slow scanning rate and duration up to several minutes
- Prevention of direct Sun illumination of the payload by keeping safe attitude domain
- Fast Sun acquisition and pointing after separation or major failure
- Periodic orbit correction and station-keeping manoeuvres
- Reaction wheel angular momentum management (biasing and offload).

12.1.2 Main Performance Requirements

The main system performance requirements for this mission to achieve the science observation objectives are defined as system level requirements:

- **Absolute Performance Error** (APE) = 0.8" (3σ)
- **Relative Performance Error** (RPE) = 0.05"over 200s (3σ) NOTE: the susceptibility to pointing stability at different frequencies is reported in Figure 12-1
- **Absolute Knowledge Error** (AKE) = 0.03" (3σ) intended after ground post-processing.
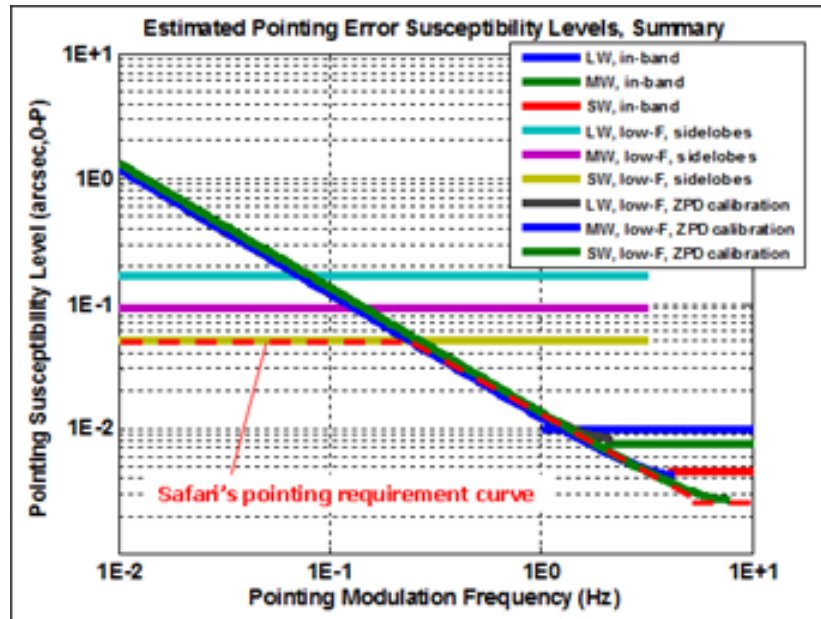
Figure 12-1: RPE susceptibility level

Requirements are intended for Line-Of-Sight (LOS) direction (i.e. about Y_{SC} and about Z_{SC}). Requirements around LOS have not been defined but are known to be much less stringent and therefore not considered drivers for the AOCS design.

It is noted that for RPE the susceptibility in the high frequency domain is very challenging, being the domain where the AOCS has no authority whereas the mechanical design (structure design) through isolation of vibration sources (passive/active dampers) plays the key role.

12.1.3 Understanding of Requirements

For the definitions of the error indices, reference is made to the ESA pointing error engineering handbook (see RD[19] and RD[20]).

The APE is defined as the difference between the target/commanded and the actual attitude in the control reference frame.

The RPE is defined as the difference between the APE at a given time within a time interval Δt and the Mean Pointing Error (MPE) over the same time interval. The time interval corresponds to the duration of single target observation period that in the context of this study has been set up to 200s.

12.1.4 Pointing Requirements Allocation

In terms of allocation to different Pointing Error Sources, very little disturbance should come directly from the instrument. Additionally, the PLM in terms of structure and thermally is expected to be very stable because of the limited excursion wrt the Sun pointing. Therefore the allocation considers the contribution from PLM negligible and assigns the overall error to the SVM.

The **Absolute Pointing Error** budget contributions come from three different main sources: the structure misalignment between instrument and Fine Attitude Sensor

(FAS) (since the FAS is mounted directly on the PLM, this contribution can be considered negligible); Fine Attitude Sensor constant bias; and controller performance including actuator disturbance noise.

The FAS bias performance is estimated below 0.6" (3σ), therefore the remaining budget (0.5", 3σ) is left for controller performance. This value is considered fully within feasibility based on past experience.

The **Relative Pointing Error** budget is instead the real driver of the design. The error sources contribution to such performance come from three main contributors: attitude relative pointing estimation (FAS + GYR); short term controller performance including actuator noise; μ-vibration sources (RWL and Cryo-coolers).

The preliminary estimation of contribution from the relative pointing filter (FAS+GYR) comes from the previous study and is set at 0.03" (3σ). With such, the remaining budget of 0.04" (3σ) shall be split between μ-vibrations and controller performance. In section 12.2.4 an analysis of μ-vibration sources is provided together with some possible solutions to ensure some margin wrt the current budget. Preliminary allocation foresees 0.025" (3σ) assigned to μ-vibration and the remaining 0.03" (3σ) for controller performance.

The **Attitude Knowledge Error** budget as such is linked to the attitude estimation error achievable on board with the possible corrections obtained by post-processing on ground. The performance is not considered a driver by the instrument team, since it is in line with previous experience.

12.2 Assumptions and Trade-Offs

12.2.1 Main Spacecraft Properties

The S/C behaves as a rigid body with regards to the AOCS fine pointing modes, given that the solar panel is body mounted and no additional appendages are present and the AOCS control bandwidth is well decoupled from the sloshing mode natural frequency.

The latter condition could not be true with RCS based control modes, when fast slews are operated. This implies that a certain settling period shall be accounted before nominal operations can be started.

The following mass and inertia properties have been assumed:

- Mass = 2137 kg (*)
- Inertia : J_{xx}=4200kgm², J_{yy}=4000 kgm², J_{zz}= 3500 kgm²
- CoM = [0.04; -0.011; 1.185]m
- (*) Note on mass: increases of mass within allowed launcher capabilities do not affect the overall conclusions, but budgets shall be revised accordingly.

12.2.2 Environmental Disturbance

Solar pressure is the main environmental disturbance in L2. The S/C is nominally lying with the $-Z_{SC}$ axis pointed to the Sun and it is fully symmetric wrt Sun vector incidence. Therefore to get the maximum disturbance torque it is assumed that the S/C stands at

the edge of the pointing domain, when the attitude wrt the Sun is 20deg de-pointed around Y_{SC} axis, where the largest contribution applies.

The overall dimensions of the S/C solar panel are assumed, as conservative case, as a circle of 4.5m diameter, i.e. S=15.9m². Neglecting the contribution from the CoM displacement along X_{SC} and Y_{SC} axes, the maximum Solar disturbance torque can be obtained as: $T_S = A \cdot W_S \cdot (1 + r) \cdot \cos i \cdot \Delta_{CoM\_CoP}$ where A is the SA area, Ws the solar flux, r the reflectance, i the Sun incidence angle and Δ the offset between S/C centre of mass and centre of pressure, calculated at maximum angular displacement as worst case.

	Total Area [m²]	Ca	Cr	Cd
Solar Array	15.9	70%	6%	24%
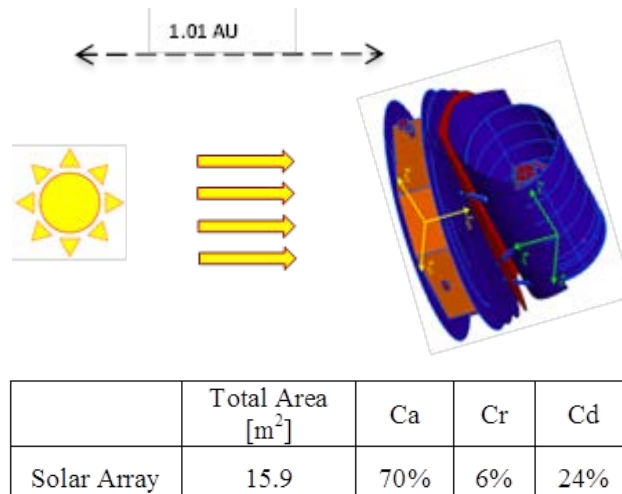
Figure 12-2: Solar pressure disturbance

The exact calculation would lead to 27 µNm. Taking into account simplifications and considering possible changes in the S/C configuration resulting in CoM migrations, an additional margin has been considered leading to 50 µNm as environmental disturbance torque for actuator sizing.

12.2.3 Attitude Domain

The AOCS has to guarantee that the attitude domain with respect to the Sun is never exceeded. The domain is driven by the need to avoid Sun light entering the telescope aperture and to ensure a thermally stable environment to the PLM.

The domain has been defined as the maximum excursion angles about the two orthogonal S/C axes wrt the Sun vector, namely ±15deg about Y_{SCC} and ±1deg about X_{SCC}, and ±180deg about Z_{SCC} being the axis nominally pointing the Sun. The domain is shown pictorially in the figure below.
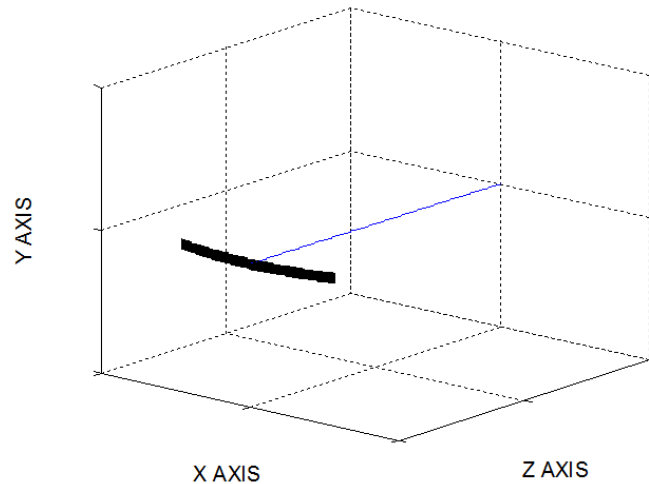
Figure 12-3: Pointing domain

The AOCS shall ensure the S/C will not exceed the pointing domain at any time. Therefore an incremental-severity approach is implemented, with thresholds to be defined such that the domain is never exceeded even in worst case combination of rotational speed and attitude point.

This leads to the definition of the 'Operational', 'Safe' and 'Contingency' Zones as exploited in the figure below.
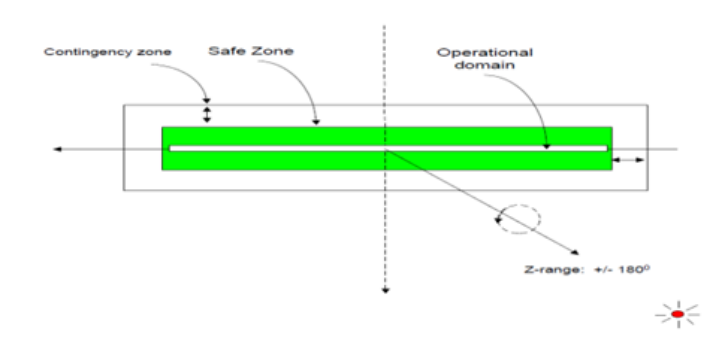

Figure 12-4: Thresholds for Pointing domain

Contingency Zone is defined as the nominal observation Zone.

Safe Zone is where the nominal AOCS FDIR monitors the evolutions and recovers from unwanted excursion outside this Zone.

In the case that the Attitude and Rate Anomaly Detection triggers, the AOCS shall enter in Safe Mode and immediately recover the Sun pointing. This action shall in any case avoid the excursion outside the contingency domain.

The AOCS design implications are the following:

1. Dedicated attitude domain monitoring function composed of Attitude Anomaly Detector and Coarse Rate Sensor to monitor and prevent any excursion outside Safe Zone

2. AOCS path planner shall take into account the limitations driven by pointing zones when calculating the slews between two observation points or to the ΔV direction.

12.2.4 μ-Vibrations

μ-Vibration disturbances generated by RWL and Cryo-Coolers mainly affect the pointing stability (RPE) of the system and therefore their evaluation is considered in the pointing budget to assess the amount of the overall requirement eroded by these effects.

Considering that μ-Vibration disturbances fall in a frequency domain (>10 Hz) outside the reach of the attitude control subsystem, which tends to have bandwidth below 0.1 Hz, the suppression or mitigation of μ-Vibrations has to be pursued by other means, like isolators or dampers between the source of the disturbance and the S/C structure.

The evaluation of the effects for the Cryo-coolers vibrations assumes the mounting on passive isolators with a final maximum effect on RPE estimated as 0.02". This number comes from a previous study (SPICA) where the same Cryo-coolers were considered, with some assumptions made on structure transfer function and mounting isolator performance.

The 4 reaction wheels selected in the baseline are the same as used in Herschel (maximum torque 0.2 Nm at angular momentum range up to 20 Nms). The contribution from the wheels to μ-Vibration has been obtained from the unit (static and dynamic) imbalance specification and assuming they are mounted on lateral panels. The total contribution to RPE of wheels μ-Vibrations, assuming 4 being operated simultaneously, is about 0.028".

These performance error contributions combined with the expected performance contribution from relative estimation coming from AOCS sensors filtering, do not leave any additional room for any other error source (e.g. controller performance and actuator noise).

The conclusions end with one of the following available options:

1. <u>BASELINE:</u> Re-use of standard lubricant RWLs (Herschel like) is possible, pending the mounting on dedicated vibration isolator (developed with appropriate transfer function attenuating the range of frequencies where wheels harmonics are present) and with low residual margin for RPE to be allocated to controller performance. As the most valid in terms of cost, complexity and reliability (TRL), this solution is considered as baseline with the recommendation to investigate all possible optimisations in terms of reaction wheels and Cryo-coolers mounting positions, structure design through dedicated FEM analysis and limitation of reaction wheels operational speed through specific biasing.

2. <u>OPTION#1:</u> Use of Cold-Gas Micro Propulsion system (MPS) during the scientific fine pointing modes, in combination with the wheels used during slews. This solution would improve significantly the RPE performance, but would have

significant drawbacks in terms of cost, complexity and mass (additional system and propellant). The TRL is not an issue considering the on-going activities on EUCLID.

3. OPTION#2: Use of MWI Magnetic Bearing Reaction Wheels instead of standard wheels. Magnetic wheels have the advantage of very low noise and reduced imbalance (up to factor of 20 wrt standard wheels), without significant increase of complexity and cost. The main technical drawback is the increase of power consumption. However, the TRL of these units is considered not yet sufficient to be taken as baseline for this mission. This option remains a valid alternative in the case of future further development of these units.

The trade-off between the baseline and option 1 needs to be confirmed in a follow on study, taking into account the detailed performance of the dampers for the RW and coolers and the de-coupling between the SVM and PLM using the dis-connectible structure

12.3 Baseline Design

AOCS baseline design is full re-use of Herschel SVM architecture, three axes stabilised system based on star tracker and gyro estimation filter for coarse pointing modes and with the fine attitude sensor (mounted on PLM) in the loop to reach stringent requirements during science fine pointing mode.

12.3.1 AOCS Modes

The AOCS modes are presented in the figure below and detailed in the following text. The objective is to establish a simple structure covering all the requested functionalities. Each mode is associated to a well-defined sensor and actuator configuration as summarised in Figure 12-5.
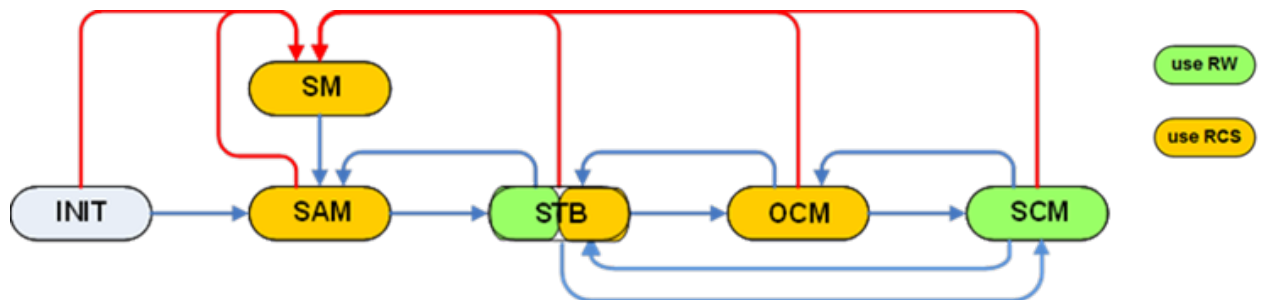

Figure 12-5: AOCS modes and transitions

Initialisation Mode (INIT): Mode used during launch, idle mode. Considering the need to perform the Sun Acquisition as quickly as possible after separation from launcher, this mode shall foresee the GYR, the THR heaters and the OBC to be switched ON.

Sun Acquisition mode (SAM): Provides Sun acquisition and coarse Sun pointing. This mode is entered immediately after separation to quickly point the S/A to the Sun and avoid the illumination of the PLM.

Stand-By Mode (STB): Provides inertial attitude hold mode with coarse pointing performance. This mode is used outside science operations for communication windows

or as an intermediate step for failure investigation. This mode is as well used for wheel unloading manoeuvres.

Orbit Control Mode (OCM): Perform ΔV manoeuvres for orbit maintenance. This mode uses RCS for both attitude control and orbit control.

Science Control Mode (SCM): Provides fine pointing or scanning mode with high accuracy performance. This is the science mode where instruments are used to collect science data. This mode uses the Fine Attitude Sensor located on PLM in the control loop.

Survival Mode (SM): Provides Sun acquisition and stable pointing after major failures. This mode can be entered from any mode and it shall be exited only by ground control.

Table 12-1 shows the set of units (sensors and actuators) used for each AOCS mode.

	INIT	SAM	STB	OCM	SCM	SM
AAD			X	X	X	
CRS		X	X	X	X	X
SAS		X				X
STR			X	X	X	
GYR	Standby	X	X	X	X	
FAS					X	
RWL			X		X	
RCS	Heat	X	(X)	X		X

Table 12-1: AOCS modes configuration

12.3.1.1 AOCS vs System modes

The mapping between the AOCS modes and system level modes is reported in Table 12-2.

	Launch	Init/SAM	Stand-By	Science	Recycling	OCM	Survival	Decont.
INIT	X							
SAM		X						
STB			X		X			X
OCM				X				
SCM						X		
SM							X	

Table 12-2: AOCS modes vs System modes

12.3.1.2 Science Control Mode (SCM)

The science pointing mode foresees different pointing sub-modes, depending on the instrument functionality required.

This section summarises all the pointing/scanning modes with the envelope of the whole step and duration requirements collected for each sub-mode.

A. RASTER MODE:
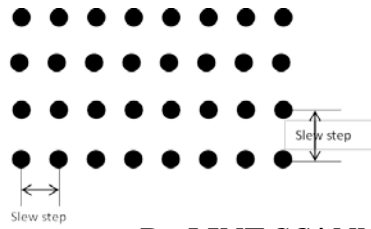
Step amplitude: between 1.5"-282" slew time 30s-100s

SAFARI → 15" to 108", slew time 30s to 100s

SMI → 1.5" to 282", slew time 30s

B. LINE SCANNING MODE:
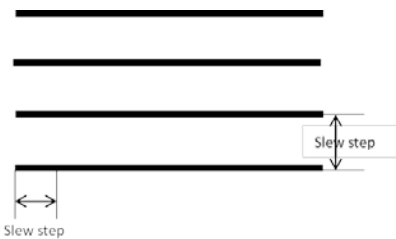
Scan rate: from 0.0025"/s up to 72"/s for several min

SAFARI → 10"/s to 72"/s for several min

SMI → 0.0025"/s to 0.25"/s for 1000s to 10000s

C. SYSTEM OBJECT TRACKING:
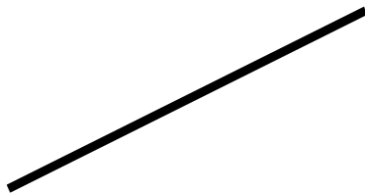
Track rate: 10"/min for several min

SAFARI → 10"/min for several min

SMI → 10"/min for 1200s

12.4 List of Equipment

The following list of equipment is proposed. The list includes also the fine attitude sensor and the reaction control system that are not under AOCS subsystem perimeter, but they are part of the loop. Details of those subsystems are reported in relevant sections.

Attitude Anomaly Detector (AAD): providing simple and reliable information about violation of the allowed attitude domain. Output is a Boolean indicator of the Sun presence in the FoV, which corresponds to the allowed attitude domain. This sensor is used exclusively in the FDIR process in combination with the CRS, as part of ARAD = Attitude and Rate Anomaly Detection.

Coarse Rate Sensor (CRS), 2 units, one unit is used in Safe Mode, the other supports the rate anomaly detection in combination with the AAD as part of ARAD. The unit is used for detection of anomalies in angular rate that could lead to excursion outside attitude domain.

Sun Acquisition Sensor (SAS), 2 units mounted with unit FoV pointed nominally towards the Sun (-Zsc) providing (almost) hemispherical coverage; the SAS are used in both nominal Sun Acquisition and safe Sun pointing mode. The performance shall allow the S/C to keep the Sun within attitude domain with sufficient margin.

Fine Gyro (GYR), 1 unit internally redundant to be used for all nominal modes; the high performance class are driven by the need to be used for target acquisition in

combination with the Fine Attitude Sensor (FAS). The driver performances are the ARW ($1e-4$ deg/h$^{1/2}$) and RRW ($5e-3$ deg/h$^{3/2}$). The GYR is internally redundant, having 4 sensors in hot redundancy mounted in skewed configuration, while 3 are used in the loop.

Star Tracker (STR), 2 units in cold redundancy (requirements around LOS are relaxed); the performances are driven by the pointing requirements for target acquisition by the FAS. The baseline is for full autonomous STR which provides in output the measured attitude in inertial reference frame and angular rate.

Fine Attitude Sensor (FAS), formed by 2 cold elements (for redundancy) mounted on the PLM and representing the optical part and the detector, and redundant warm electronics mounted in the SVM for signal processing. The expected output rate (based on info from SPICA study) is 0.2Hz with an accuracy of 0.53" for absolute pointing and 0.036" for relative attitude.

Reaction Wheels Assembly (RWA), 4 units in skewed configuration delivering fine control torque during the science observations for slews and hold pointing; the sizing of the wheels has to provide reasonably large momentum storage capability (25Nms compatible with estimated disturbance torque and slews planning) and adequate torque for large slews (200mNm compatible with the requested slew rate and durations).

Reaction Control Subsystem (RCS), 6+6 units delivering force and torque on the 3-axes, the thrusters are used for attitude control for slews in nominal Sun Acquisition and safe Sun pointing mode, where either the fast acquisition of the Sun pointing attitude after separation or the quick recovery from not nominal situation in Safe mode respectively are needed. During ΔV and orbit maintenance manoeuvres the same set of thrusters provide the requested force and the attitude control torques to keep constant the direction. Finally during RWL off-loading the thrusters generate the momentum for wheel off-loading.

Element 1	-				MASS [kg]		
Unit	Unit Name Click on button above to **insert new unit**	Part of custom subsystem	Quantity	Mass per quantity excl. margin	Maturity Level	Margin	Total Mass incl. margin
1	SAS	AOCS	2	0.2	Fully developed	5	0.3
2	AAD	AOCS	1	0.2	Fully developed	5	0.2
3	CRS	AOCS	2	2.0	Fully developed	5	4.2
4	STR	AOCS	2	3.2	Fully developed	5	6.6
5	RWL	AOCS	4	8.6	Fully developed	5	36.1
6	GYR	AOCS	1	6.8	Fully developed	5	7.1
7	FAS Warm Electronic	AOCS	1	14.0	To be developed	20	16.8
-	Click on button below to insert new unit						
SUBSYSTEM TOTAL			**7**	**66.0**		**8.2**	**71.4**

Table 12-3: AOCS Equipment List - SVM

Element 2	-			MASS [kg]			
Unit	Unit Name Click on button above to **insert new unit**	Part of custom subsystem	Quantity	Mass per quantity excl. margin	Maturity Level	Margin	Total Mass incl. margin
1	FAS Cold units	AOCS	2	7.0	To be developed	20	16.8
2	FAS Warm Electronic	AOCS	0	14.0	Fully developed	5	0.0
-	Click on button below to insert new unit						
SUBSYSTEM TOTAL			**1**	**14.0**		**20.0**	**16.8**

Table 12-4: AOCS Equipment List PLM

12.5 Technology Requirements

The following technologies are required or would be beneficial to this domain:

Included in this table are:

- Technologies to be (further) developed
- Technologies available within European non-space sector(s)
- Technologies identified as coming from outside ESA member states.

Equipment and Text Reference	Technology	Suppliers and TRL Level	Technology from Non-Space Sectors	Additional Information
FAS (required)	Cold optical unit in PLM and warm electronics in SVM	Performance provided by JAXA, TRL=3	N/A	Alternatives in EU exist under development for other programmes.
MWI RWL (optional)	Magnetic Bearing reaction wheels	ROCKWELL COLLINS, TRL=4/5	N/A	Optimal alternative to micro-thrusters

Table 12-5: AOCS modes configuration

This Page Intentionally Blank

13 PROPULSION

13.1 Requirements and Design Drivers

13.1.1 Requirements

The amount of requirements relevant to the propulsion system was very limited. They are summarised below:

An overall ∆V budget broken down as follows:

Manoeuvre	∆V with margin [m/s]
Perigee velocity correction	28.35
TCM#1 (mainly launcher dispersion correction)	56.7
TCM#2 & #3 Transfer correction	18
Station-keeping	120.4
Moon eclipse avoidance	N/A
Decommissioning (Heliocentric Disposal)	21.0
Safe Mode DeltaV	N/A
Operational contingency	21.0
Sum	**265.5**

Table 13-1: ∆V summary table with margin and assuming an unbalanced spacecraft

The NG-CryoIRTel nominal plus extended science operation phase shall start from the end of the commissioning phase, and shall have a duration of at least 5 years.

13.1.2 Uses of the Thruster

The AOCS strategy with regards to the use of thrusters as an actuator is similar to Herschel-Planck. This includes:

- Safe Mode
- Orbit maintenance manoeuvres
- Reaction wheel off-loading.

In addition, the thrusters shall be used for all transfer orbit manoeuvres during the mission.

As per Herschel, the thruster size selected is the 20N thruster size.

13.1.3 Thruster Configuration

In order to avoid the plume impingement of the thruster into the instrument, all thrusters are pointing opposite to the payload as shown in Figure 13-1 and this therefore results in an unbalanced solution (similarly to Herschel).
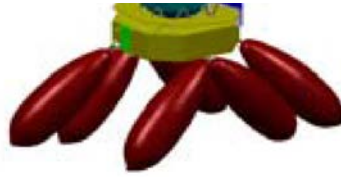
Figure 13-1: Proposed thruster pointing direction

The thruster pointing induces an increased ΔV budget (i.e. almost a factor of 2) and therefore an increased propellant need. The analysis of the plume was outside the scope of work for a such an early phase of the mission and it is recommended to look into it in more advanced phases as this could result in a very significant propellant consumption reduction, the number of propellant tanks needed (i.e. from the current three to only two) and therefore a simplification of the architecture.

13.2 Assumptions and Trade-Offs

Within the frame of this study, due to the similarity of the mission profile, range of spacecraft mass and payload accommodation, similarities with the Herschel-Planck mission were identified. This could induce evident cost benefits if platform re-usability was pursued. A preliminary task was performed to assess if Herschel-Planck propulsion system could accommodate sufficient propellant for the whole NG-CryoIRTel mission.

13.3 Baseline Design

The baseline design system proposed for the NG-CryoIRTel study is a classic monopropellant system. The schematic proposed is depicted below:
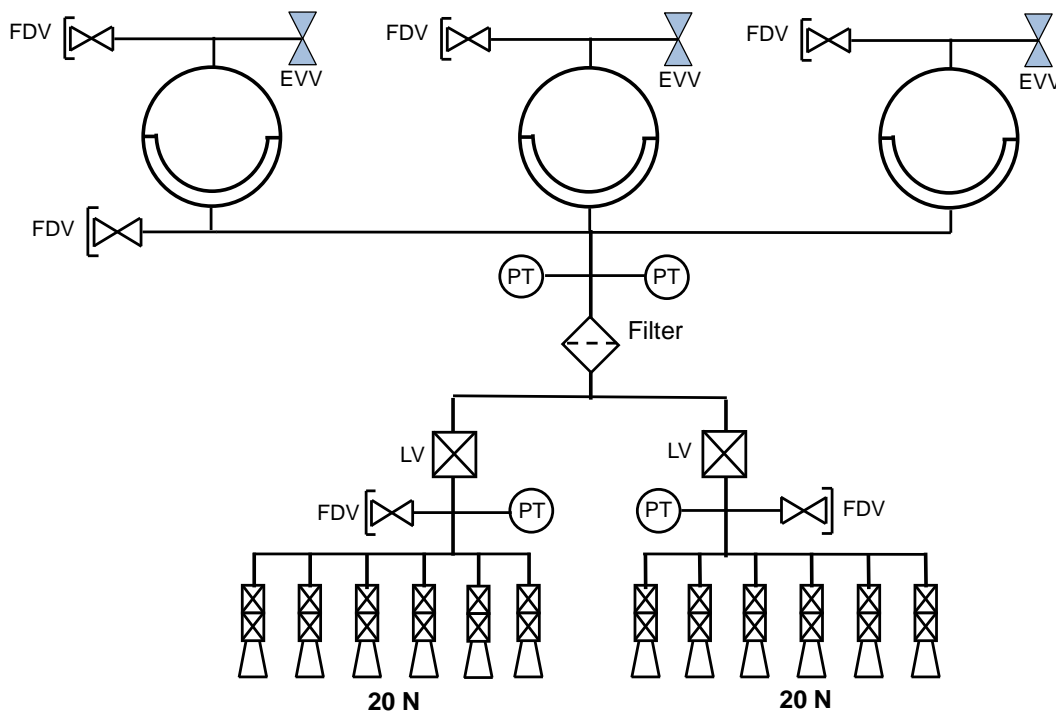
Figure 13-2: Basic architecture proposed for NG-CryoIRTel

The Propulsion system architecture has heritage from Herschel-Planck.

The detailed propellant budget is summarised below.

Mission		ΔV budget [m/s]	Isp [s]	Prop. Consumption [kg]
NG-CryoIRTel	SSF	145.1	230.1	156.7
	PMF	120.4	200	149.9
	Safe Modes (5 for the whole mission)			6.0
	TOTAL	265.5	204.2	312.6
	EOL Propellant Residuals			6.5
	TOTALS			319.1

Table 13-2: Propellant Mass budget Allocation

Based on the current analysis, the propellant tank capacity has a comfortable margin exceeding 20%.

For the calculation of the propellant consumption during safe mode, a table is summarised below:

	Number of pulses	Propellant mass [kg]
5 times Sun Acquisitiion Slew in Safe Mode	1250	0.3
1 times (7days each time) in Safe Mode @ BOL	4500	1.5
2 times (7days each time) in Safe Mode @ MOL	10500	2.6
2 times (7days each time) in Safe Mode @ EOL	11600	1.6
	27850	**6.0**

Table 13-3: 20N Thruster pulse count

The numbers shown in the above table have been extrapolated from figures from Herschel-Planck. These numbers correspond to the accumulated pulse count from all twelve 20N thrusters. It assumes 1 safe mode per year and a mission lifetime of 5 years.

The detailed dry mass budget is shown in Table 13-4

Dry Propulsion Mass	Unit Nominal Mass [kg]	Supplier	Model	Units	Margin Philosophy	Unit Worst Case Mass [kg]
Service Valves	0.07	EADS-ST (D)	3-barrier	6	5	0.07
Propellant tank	15.07	MT-A (DE)	PTD-177s	3	10	16.58
Pressure transducer	0.27	AMETEK (US)	PA4089	4	5	0.28
Propellant Filters	0.29	VACCO (US)	F1D10559-01	1	5	0.30
Latch Valve	0.69	MOOG (US)	52-226	2	5	0.73
Thrusters (20N)	1.32	EADS-ST (DE)	CHT-20N	12	5	1.39
Piping	0.03	tbd	tbd	50	20	0.04
Passivation valve	0.45	EADS-ST (DE)	FCV	3	20	0.53
Bracketing	1.00	tbd	tbd	3.32	20	1.20
Pressurant Gas	5.19	tbd	tbd	1.00	0	5.19
Propellant Residuals	6.47	tbd	tbd	1.00	0	6.47
TOTAL Nominal Mass [kg]				82.09		88.81

Table 13-4: Dry Mass budget Allocation

The detailed power budget is shown in Table 13-5:

	Power Peak [W]	Power ON [P_on, W]	Power Stand-by [P_off, W]
RCS Heaters	45.6	45.6	45.6
RCS Thrusters	0	79.8	0
RCS Latch Valves	0	27.5	0
Evacuation Valves	140	140	0
Pressure Transducers	2	2	2
TOTAL	187.6 W Max	<187.6 W	47.6 W

Table 13-5: Power budget Allocation

13.4 List of Equipment

The list of equipment for the baseline is presented below.

	Baseline Configuration			
	Units	Model	Supplier	Status
Propellant tank	3	PTD-177	MT-A (D)	Under manuf. Modif. (TRL 5)
Pressure transducer	4	PA4089	AMETEK (US)	Flight proven (TRL 9)
Service valves	6	3-barrier	EADS-ST (D)	Flight proven (TRL 9)
Propellant filters	1	F1D10559-01	VACCO (US)	Flight proven (TRL 9)
Latch Valves	2	52-226	MOOG(US)	Flight proven (TRL 9)
Evacuation Valve	3	FCV+PV	EADS-ST (D)	Flight proven (TRL 9)
Thrusters(20N)	12	CHT-20N	EADS-ST (D)	Flight proven (TRL 9)

Table 13-6: List of the baselined propulsion equipment

13.4.1 Propellant Tanks

The propellant tank proposed has an overall volume of 173.8 litres.

The propellant tank used currently for Herschel-Planck is using a membrane from RAFAEL (Israel). The development of a membrane within Europe (by MT-A(DE)) is due to start within 2015. A new chemical formula for the membrane, that is chemically compatible with hydrazine has been identified, successfully tested and manufactured for a smaller propellant tank. MT-A(DE) subsequent task is to validate/qualify the existing manufacturing process of the membrane using the new membrane chemical formulation. The tank shell was developed by MT-A(DE) and it is flight qualified. The activities on the membrane development (currently the tank is at TRL 5) shall be finalised by the end of 2015.

The propellant tank is a pseudo-spherical tank (two spherical domes with a cylindrical section) that uses a polymeric bladder that separates the gas from the liquid propellant. The system operates in blow-down mode with a volume ratio of 4:1. This leads to a propellant capacity of ~130 litres of propellant.

The tank is mounted around its equator by means of four lugs. Each lug is evenly distributed along the equator. Mounting philosophy and main dimensions are shown in Figure 13-3.
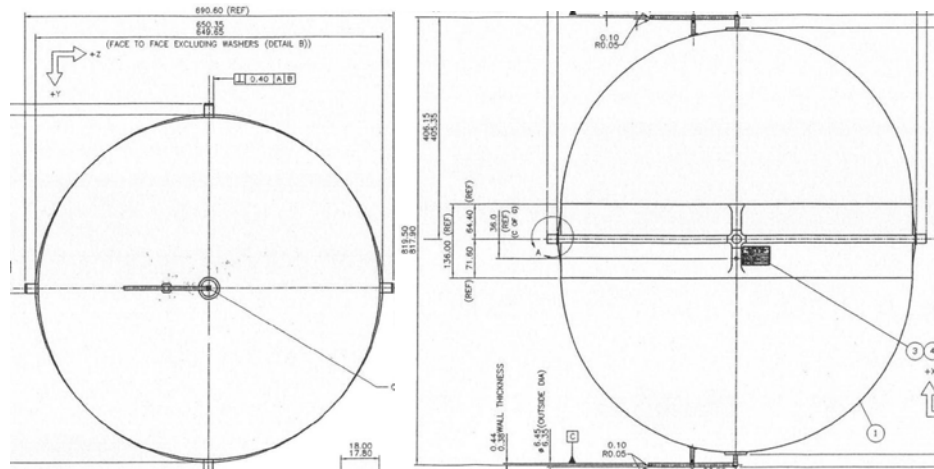
Figure 13-3: Herschel-Planck Propellant tank from MT-A (DE)

13.4.2 Latch Valve

There are no "off-the-shelf" latch valves available in Europe that can cover the needs for NG-CryoIRTel. The American valve from MOOG Model 52-266 has been selected due to its extensive heritage. The valve has been used on various European missions meaning that it fulfils the European standards.

This latch valve is actuated by a bi-stable torque motor and uses a Teflon-base as a seal and is supplied with an inlet filter. The pipe interface is ¼". It has flight heritage on various missions including MCP, DRTS, XMM, Mercury Messenger, A2100, Deep Impact, SELENE-A, WINDS, MT-SAT-2 and Herschel-Planck.

The latch valve wetted areas are made of titanium, stainless steel and teflon and its dry mass is 0.65 kg.
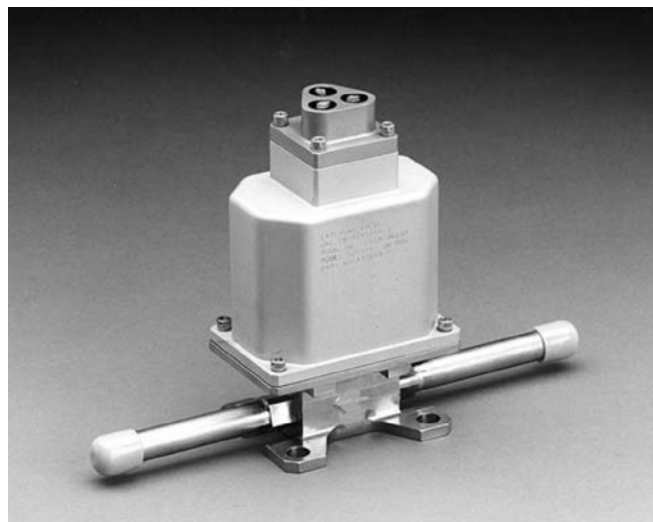
Figure 13-4: Model 52-266 from MOOG (US)

13.4.3 Service Valves

The service valves required for NG-CryoIRTel shall have a pipe interface of ¼". There are a number of options available in Europe (including EADS-ST, AMPAC and RTG).

The AMPAC design has an alert in place which may lead to leakage levels out of specification and the RTG has not shown compliance to ECSS standards. This leads to propose the valves from EADS-ST (Lampoldshausen) for PLATO.

The main design of this valve was developed in the 80's. In the recent years EADS-ST has included a third barrier in order to comply with Launcher authorities requirements. The valve is fully qualified and shall be used in Lisa Pathfinder.

Figure 13-5: 3-barrier model from EADS-ST(D)

13.4.4 Pressure Transducers

The proposed pressure transducer is the same as per Herschel-Planck. It corresponds to the model PA4089 manufactured by Ametek (US). The pressure sensor provides a static accuracy of < 0.2% with a temperature sensitivity shift of < 0.005%FSP/°F which enables a residuals level to minimise the propellant residuals in the tank. They have flight heritage in Eurostar telecommunication platforms, Mars & Venus Express, GAIA and Herschel-Planck.

Figure 13-6: Pressure transducer developed by AMETEK (US)

13.4.5 Propellant Filters

The proposed propellant filter is the same as per Herschel-Planck. The unit is manufactured by VACCO (US). It has been selected based on his low pressure drop, low dry mass and fine filter sizing.

Figure 13-7: Propellant Filter developed by VACCO (US)

13.4.6 Evacuation Valve (EVV)

The proposed evacuation (or passivation) valve is composed of a derivative of an electromagnetic thruster valve + pyrotechnic valve from EADS Airbus GmbH in order to comply with the three safety mechanical barriers required by safety range at launch.

The lifetime for the mission is 5 years total. This shall be taken into account due to the life limit item from the pyrosquibs (i.e. 8 years starting from the manufacturing date). The proposed pyrosquibs should be adequate for the whole mission. Should this not be sufficient the valve could also be activated in flight prior to the end of the life of the mission and rely on the two-mechanical barrier electromagnetic valve.

+

+
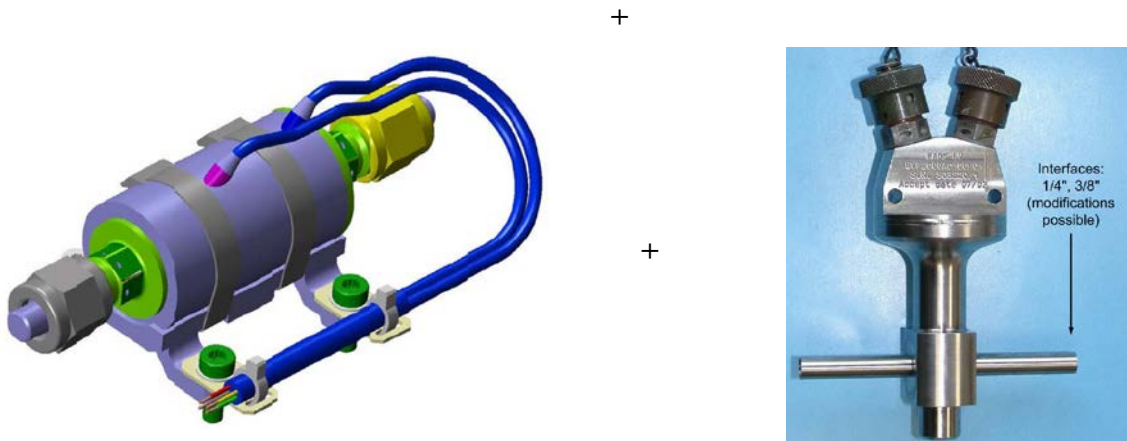
Figure 13-8: Evacuation Valve developed by EADS-ST(D)

13.4.7 Thrusters

There is one European 20N-thruster operated with hydrazine, which is an off-the-shelf product. This corresponds to the model CHT-20N developed by EADS-ST(D). This is the only option available.

The thruster has been qualified over 90000 pulses. It is estimated not to perform more than 200 pulses.

It has one main limitation on the longest continuous burn that the thruster can perform. The thruster has been qualified for a longest burn of 1 hour.

Figure 13-9: Model CHT-20N thruster developed by EADS (DE)

13.5 Options

No options have been considered as the goal of the activity was to re-use as much as possible the Herschel-Planck platform. Only two main differences are worth mentioning:

- The addition of three evacuation valves have been added to show compliance to a requirement of spacecraft passivation at the EOL
- The propellant tank membrane will need to be replaced with a new formulation as the membrane used on Herschel-Planck was supplied by RAFAEL(ISR) as a one-off situation.

13.6 Technology Requirements

As explained in Section 13.4, the components have been selected based on the component availability in Europe. In case the components needed were not available in Europe, alternatives elsewhere have been investigated. The following table summarises all components that are procured outside Europe.

Equipment and Text Reference	Technology	Suppliers and TRL Level	Technology from Non-Space Sectors	Additional Information
Latch Valve	Torque Motor	MOOG (US) (TRL 9)	N/A	Model 52-266
Filter	Etched disk	VACCO (US) (TRL 9)	Unknown	Model F1D10559-01
Pressure sensor	Wheatstone Bridge	AMETEK (US) (TRL 9)	Unknown	Model PA4089

Table 13-7: Technologies procured outside Europe

14 POWER

14.1 Requirements and Design Drivers

14.1.1 Re-use of Planck Heritage

The preferred design concept is to re-use the Planck SVM as far as possible. For the power system, this implies the following baseline configuration:

- Bottom-mounted fixed circular solar array, 5 panels (see Figure 14-1). However it is assumed that the array can be populated with the latest generation of solar cells (triple-junction 3G30%).

- S^3R solar array regulation, supplying a 28V regulated bus.
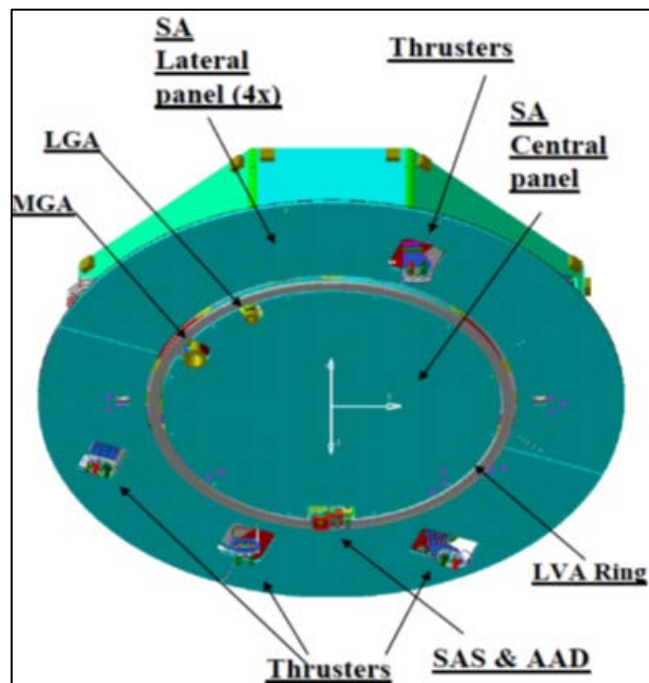
Figure 14-1: Planck SVM, showing the 5-panel solar array mounted on the bottom (-z) of the spacecraft

14.1.2 Solar Illumination Environment

The operational environment is a large halo orbit at the Sun-Earth L2 point. This provides steady illumination conditions with no eclipses.

The spacecraft −z axis will point in the Sun direction, with deviation of ±15° to cover the field-of-regard. Effective solar illumination depends on the cosine of the Sun incidence angle. Cos 15° = 0.966, so the off-pointing effect upon the power generation is very small.

14.1.3   Spacecraft Lifetime

The power system must support the required lifetime of 3+2 years, including initial cool-down phase. (Aging effects need not be considered for the battery, as it will be sized for LEOP energy requirements).

14.1.4   Power & Energy Demand

The power and energy requirements of the spacecraft electrical loads are show in Table 14-1. The requirements are broken down in terms of both subsystem and spacecraft mode. Examination of the values leads to the identification of the important sizing cases:

- <u>Battery sizing case</u>: It is assumed that Sun pointing is achieved at the end of the Initialisation mode. Therefore, the battery must supply all electrical energy during the Launch mode and the Initialisation mode.
  = [192 W for 130 minutes] + [924 W for 90 minutes].

- <u>Solar array sizing case</u>: The highest average power spacecraft mode is Stand-By, with a total demand of 2018 W. Increased demand during peak power will be supplied by the batteries.

Mode		Thermal	AOCS	Comms	Propulsion	DHS	Mech	SAFARI Instrument	SMI Instrument	TOTAL CONSUM.
	Ppeak	1710 W	402 W	0 W	127 W	41 W	27 W	125 W	35 W	2467 W
Launch Mode	Pon	0 W	0 W	116 W	47 W	41 W	0 W	0 W	0 W	204 W
	Pstdby	0 W	0 W	36 W	47 W	0 W	0 W	0 W	0 W	83 W
	Duty Cycle	0 %	0 %	100 %	0 %	71 %	0 %	0 %	0 %	90%
	Paverage	0 W	0 W	116 W	47 W	29 W	0 W	0 W	0 W	192 W
Tref 130 min	Total Wh	0 Wh	0 Wh	251 Wh	102 Wh	63 Wh	0 Wh	0 Wh	0 Wh	416 Wh
Initialisation Mode/ Sun Pointing Acquisition	Pon	700 W	15 W	116 W	128 W	41 W	0 W	0 W	0 W	1000 W
	Pstdby	0 W	15 W	36 W	47 W	0 W	0 W	0 W	0 W	98 W
	Duty Cycle	100 %	0 %	100 %	7 %	100 %	0 %	0 %	0 %	92%
	Paverage	700 W	15 W	116 W	52 W	41 W	0 W	0 W	0 W	924 W
Tref 90 min	Total Wh	1050 Wh	23 Wh	174 Wh	79 Wh	62 Wh	0 Wh	0 Wh	0 Wh	1387 Wh
Stand-by	Pon	1660 W	388 W	116 W	47 W	41 W	0 W	125 W	35 W	2412 W
	Pstdby	0 W	52 W	36 W	47 W	0 W	0 W	125 W	35 W	295 W
	Duty Cycle	92 %	20 %	100 %	0 %	100 %	0 %	0 %	0 %	81%
	Paverage	1535 W	119 W	116 W	47 W	41 W	0 W	125 W	35 W	2018 W
Tref 1440 min	Total Wh	36840 Wh	2851 Wh	2784 Wh	1128 Wh	984 Wh	0 Wh	3000 Wh	840 Wh	48427 Wh
SAFARI Science	Pon	1660 W	402 W	116 W	1 W	41 W	0 W	125 W	35 W	2380 W
	Pstdby	0 W	66 W	36 W	1 W	0 W	0 W	125 W	35 W	263 W
	Duty Cycle	92 %	20 %	0 %	0 %	100 %	0 %	0 %	0 %	78%
	Paverage	1535 W	133 W	36 W	1 W	41 W	0 W	125 W	35 W	1906 W
Tref 1080 min	Total Wh	27630 Wh	2390 Wh	648 Wh	25 Wh	738 Wh	0 Wh	2250 Wh	630 Wh	34312 Wh
SMI Science	Pon	1660 W	402 W	36 W	1 W	41 W	0 W	125 W	35 W	2300 W
	Pstdby	0 W	66 W	36 W	1 W	0 W	0 W	125 W	35 W	263 W
	Duty Cycle	92 %	20 %	0 %	0 %	100 %	0 %	0 %	0 %	81%
	Paverage	1535 W	133 W	36 W	1 W	41 W	0 W	125 W	35 W	1906 W
Tref 1440 min	Total Wh	36840 Wh	3187 Wh	864 Wh	34 Wh	984 Wh	0 Wh	3000 Wh	840 Wh	45749 Wh
SMI Science with Comms	Pon	1660 W	402 W	116 W	1 W	41 W	0 W	125 W	35 W	2380 W
	Pstdby	0 W	66 W	36 W	1 W	0 W	0 W	125 W	35 W	263 W
	Duty Cycle	92 %	20 %	100 %	0 %	100 %	0 %	0 %	0 %	81%
	Paverage	1535 W	133 W	116 W	1 W	41 W	0 W	125 W	35 W	1986 W
Tref 1440 min	Total Wh	36840 Wh	3187 Wh	2784 Wh	34 Wh	984 Wh	0 Wh	3000 Wh	840 Wh	47669 Wh
Recycling and Comms	Pon	1660 W	388 W	116 W	1 W	41 W	0 W	125 W	35 W	2366 W
	Pstdby	0 W	52 W	36 W	1 W	0 W	0 W	125 W	35 W	249 W
	Duty Cycle	92 %	20 %	100 %	0 %	100 %	0 %	0 %	0 %	81%
	Paverage	1535 W	119 W	116 W	1 W	41 W	0 W	125 W	35 W	1972 W
Tref 360 min	Total Wh	9210 Wh	713 Wh	696 Wh	8 Wh	246 Wh	0 Wh	750 Wh	210 Wh	11833 Wh
Manoeuvres	Pon	1660 W	28 W	116 W	128 W	41 W	0 W	125 W	35 W	2132 W
	Pstdby	0 W	52 W	36 W	47 W	0 W	0 W	125 W	35 W	295 W
	Duty Cycle	92 %	0 %	100 %	33 %	100 %	0 %	0 %	0 %	92%
	Paverage	1535 W	52 W	116 W	74 W	41 W	0 W	125 W	35 W	1977 W
Tref 10 min	Total Wh	256 Wh	9 Wh	19 Wh	12 Wh	7 Wh	0 Wh	21 Wh	6 Wh	330 Wh
Survival Mode	Pon	700 W	15 W	116 W	100 W	41 W	0 W	0 W	0 W	972 W
	Pstdby	0 W	15 W	36 W	47 W	0 W	0 W	0 W	0 W	98 W
	Duty Cycle	100 %	0 %	100 %	1 %	100 %	0 %	0 %	0 %	94%
	Paverage	700 W	15 W	116 W	48 W	41 W	0 W	0 W	0 W	920 W
Tref 1440 min	Total Wh	16800 Wh	360 Wh	2784 Wh	1141 Wh	984 Wh	0 Wh	0 Wh	0 Wh	22069 Wh
Decontamination Mode	Pon	700 W	388 W	116 W	109 W	41 W	0 W	0 W	0 W	1354 W
	Pstdby	0 W	52 W	36 W	47 W	0 W	0 W	0 W	0 W	135 W
	Duty Cycle	100 %	20 %	100 %	6 %	100 %	0 %	0 %	0 %	73%
	Paverage	700 W	119 W	116 W	50 W	41 W	0 W	0 W	0 W	1026 W
Tref 1440 min	Total Wh	16800 Wh	2851 Wh	2784 Wh	1212 Wh	984 Wh	0 Wh	0 Wh	0 Wh	24631 Wh

Table 14-1: Power and energy demand

14.2 Assumptions and Trade-Offs

Considering the requirement to re-use the Planck SVM as far as possible, the power system design was not subject to trade-offs, but was initially assumed to be of the Planck configuration. It was then necessary to calculate if the power budget [generation-demand] was positive in the identified sizing cases. In the case that the lower surface fixed solar arrays might prove inadequate, it was planned to introduce additional deployable panels that would fold down to form outer "petals" on the periphery of the fixed circular panels.

The power demand from the spacecraft systems and payloads was gathered using the CDF IDM functionality, and was summarised above in Table 14-1. The sizing of the power system to meet this demand was determined by simulation using the ESA power system modelling tool PEPS. The graphical representation of the NGCryoIR power system model is shown in Figure 14-2. The model elements, from left to right, are explained as follows:

- The environment of Sun-Earth Lagrange point L2 is modelled at the June solstice, corresponding to the maximum sun distance

- The solar array is modelled as body mounted using the current generation of European space-qualified 3G30% triple-junction GaAs cells. The array pointing angle is set at 15° to Sun normal. The simulation is programmed to replicate the Launch mode and the Initialisation mode with darkness until 13200 s (220 minutes), at which time the sun is "activated". Radiation degradation is set to the PEPS option of 15 years GEO EOL (conservative for NGCryoIR Case)

- The PCDU is modelled as S^3R regulated 28V bus, as per Planck

- The battery is modelled as an ABSL unit with Sony 18650HC cells

- Distribution & harness losses are modelled with dedicated "components".

- The model component "Power Table" simulates the load. It is modelled with a sequentially stepped power demand representing the sizing cases of Launch, Initialisation and Stand-By modes, as shown in Table 14-2. A power budget margin of 20% has been added to the sizing case values identified in Section 14.1.4 above.

Time from beginning of simulation (seconds)	Power demanded by load including 20% margin (Watts)
0	230
7800	1109
13200	2421

Table 14-2: Electrical load demand profile used in the PEPS simulation
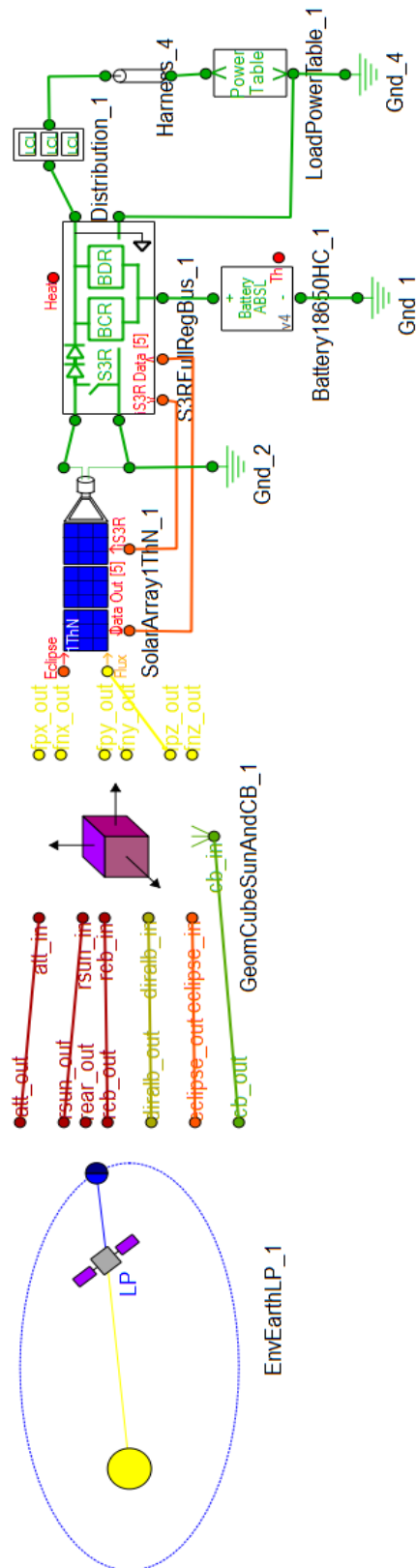
Figure 14-2: Configuration of the PEPS power system model

14.3 Baseline Design

The power system PEPS model was iterated in terms of solar array and battery size until the simulation showed that the pre-Sun LEOP phase was adequately supported without over discharge of the battery, and the sizing case Standby Mode power demand was met without utilising any battery power. Some output plots from the optimally sized simulation case are shown in Figure 14-3.

NOTE: The simulation is designed as a sizing calculation, and therefore represents an artificial situation in which the battery-supported LEOP phase is followed immediately by the maximum power demand. This means that, in the simulation, the battery is charging very slowly in the period after 13200 seconds. In reality, the charging of the battery after first Sun acquisition will be very fast, because the high power Stand-By mode will not be implemented at this point in time.
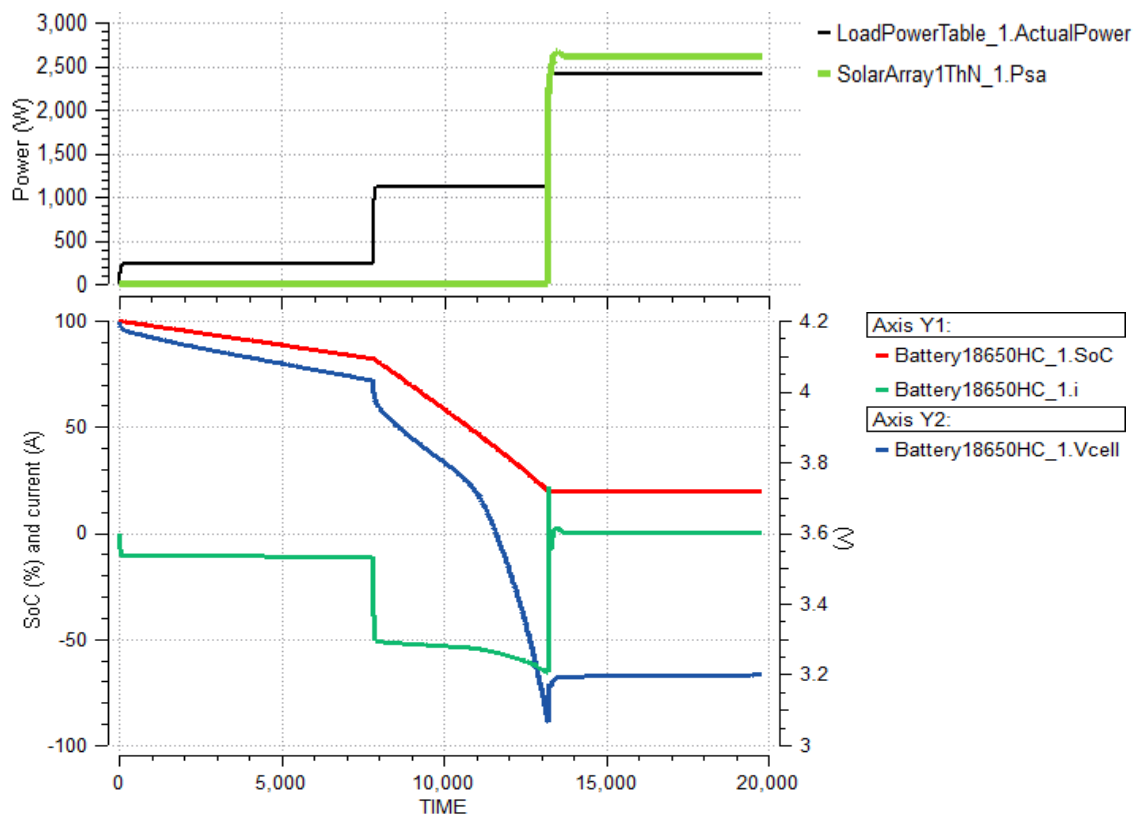
Upper plot:
Black = Load power demand (see Table 14-2.).
Green = Raw power generated by the solar array (note: darkness until 13200 s).

Lower plot:
Red = Battery state of charge (%, left axis).
Green = Battery current (amps, left axis). Negative current represents discharge.
Blue = Battery cell voltage (volts, right axis).

Figure 14-3: Results of the PEPS power system sizing simulation

14.3.1 Sizing Results

Solar array:

18 cells per string. 210 strings. 5 strings are assumed failed.

14.2 m² of "useful" array is needed (after cut-outs are subtracted). 15 m² is available on the lower surface of the NGCryoIR SVM, so no additional deployable panels are needed. PVA and wiring mass is 26 kg.

Mass and area calculations are direct from the PEPS model, accounting for PVA and wiring only in the mass value, and assuming a packing factor of 80% observing cropped corners.

Battery:

6 cells in series, 90 strings in parallel, 2.9 kWh nameplate energy, 810 Ah capacity.

Two strings are assumed failed (but no fading/degradation is included, as the sizing case is at BOL).

The mass and volume are 29 kg and 28 litres, calculated directly from the PEPS model of the ABSL 18650HC Li-ion battery (but others e.g. SAFT are also fully applicable).

PCDU:

PEPS does not yet include mass/volume sizing calculations for PCDUs. Therefore, the mass and volume are best assessed by reference to spacecraft with similar topologies.

In this case, it is clear that the best estimate is to take the case of the Planck PCDU, with a mass of 26 kg.

14.4 List of Equipment

Element 1	Service Module		MASS [kg]				
Unit	Unit Name Click on button above to insert new unit	Quantity	Mass per quantity excl. margin	Maturity Level	Margin		Total Mass incl. margin
1	Solar PVA & wiring	1	26.3	To be modified	10		28.9
2	Battery	1	29.4	To be modified	10		32.3
3	PCDU	1	26.0	To be modified	10		28.6
	SUBSYSTEM TOTAL	3	81.7		10.0		89.9

Table 14-3: Power system equipment list (mass)

Element 1	Service Module		DIMENSIONS [m]		
Unit	Unit Name Click on button above to insert new unit	Quantity	Dim1 Length	Dim2 Width or D	Dim3 Height
1	Solar PVA & wiring	1			
2	Battery	1	0.52	0.27	0.20
3	PCDU	1	0.40	0.30	0.31

Table 14-4: Power system equipment list (dimensions)

This Page Intentionally Blank

15 TELECOMMUNICATIONS

15.1 Requirements and Design Drivers

Communications subsystem requirements		
Req. ID	**STATEMENT**	**Parent ID**
COM-010	The link budget margins shall be as defined in RD[25] • Nominal > 3dB • RSS worst case > 0dB	
COM-020	SAFARI produces 4Mbit/s during 18h/day. SMI produces 1Mbit/s during 24h/day.	
COM-030	Downlink communications interferes with the operation of the SAFARI instrument.	
COM-040	The maximum net daily science data-volume to be downlinked is 260GBit/day.	COM-020
COM-050	A maximum uplink telecommand data rate of 4kbit/s is needed in all modes that need communication.	
COM-060	A maximum downlink housekeeping telemetry data rate of 30 kbit/s is needed during all modes that need communications	
COM-070	Low-rate bidirectional communication shall be possible in every orientation for contingency cases.	

Table 15-1: Communications subsystem requirements

The NGCryoIRTel mission can be classified as a category A (spacecraft-Earth surface distance < $2 \cdot 10^6$ km) mission according to ECSS standards. Furthermore the radio service used for telemetry, tracking and command (TT&C) is classified as Space Research (SR) service.

15.1.1 Requirements

The requirements on the communications subsystem of NGCyroIRTel can be derived from the requirement of telecommandability, reception of housekeeping telemetry by the mission operation centre and reception of scientific telemetry data by the science operation centre. These requirements are accompanied by a number of constraints that restrict the design space such as cost, technical and regulatory constraints. A list of requirements that apply to the telecommunications subsystem can be found in Table 15-1.

15.1.2 Design Drivers

The major design drivers for the communications subsystem of NGCryoIRTel are:

- Cost constraints [MR-PROG-050]
- Relatively high scientific data generation rates [COM-020, COM-040]
- Regulatory constraints for the occupied bandwidth in one of the possible downlink radio bands [RD3]

15.2 Assumptions and Trade-Offs

15.2.1 Assumptions

A number of assumptions were taken in order to design the communications subsystem for this mission.

Since the spacecraft will orbit the Sun-Earth liberation-point SEL2 in a halo orbit, the maximum distance between a viable ground station and the spacecraft will be 1.77 million km.

In order to be able to transmit the large volume of scientific telemetry produced every day one daily communication pass between an Earth ground-station and the telescope of 8 hours is assumed [MR-OGS-140]. Due to high amplitude halo orbit, this can only be guaranteed using at least two ground stations: one on the northern and one on the southern hemisphere. These ground stations will need to be switched on a seasonal schedule.

Due to the long range and associated high path losses on the RF-signals (~225dB in S-Band, ~236dB in X-Band and ~248dB in K-Band), the assumed ground stations must have a diameter of at least 35m in order to guarantee the necessary transmission and reception gains.

The available frequency bands for category-A, SR-type missions are S-, X- and K-Band. Their respective frequency ranges are summarised in Table 15-2.

Band	Frequency range / MHz	Direction	Max. occup. bandwidth
S-Band	2,025 - 2,110 (85)	Earth → Space	N/A
	2,200 - 2,290 (90)	Space → Earth	6 MHz
X-Band	7,190 - 7,235 (45)	Earth → Space	N/A
	8,450 - 8,500 (50)	Space → Earth	10 MHz
K_a-Band	25,500 - 27,000	Space → Earth	N/A
	37,000 - 38,000	Earth → Space	N/A

Table 15-2: Available TT&C frequency bands

Furthermore we assume one of the coding schemes as indicated in Table 15-3 available for TM downlink according to RD[23].

Type	Rate (r)	Comment
Convolutional codes (K=7)	½ = 0.5,	
	2/3 = 0.667	Punctured
	¾ = 0.75	Punctured
	4/5 = 0.8	Punctured
	5/6 = 0.833	Punctured

	6/7 = 0.857	Punctured
Reed-Solomon codes	223/255 = 0.875	
	239/255 = 0.938	
Concatenative codes (Outer: RS, Inner: Convolutional)	0.437, 0.583, 0.656, 0.700, 0.729, 0.750	Combinations of the available RS and Convolutional codes
	0.469, 0.625, 0.703, 0.750, 0.781, 0.803	
Turbo codes	½ = 0.5	
	1/3 = 0.333	
	¼ = 0.25	
	1/6 = 0.167	
Low Density Parity Check (LDPC)	½ = 0.5	
	2/3 = 0.667	
	4/5 = 0.8	
	223/255 = 0.875	

Table 15-3: Available coding schemes and rates according to RD[23]

15.2.2 Trade-Offs

The major trade-off considered in this study was one between an X-Band only communications subsystem versus a combined X-Band and K_a-Band subsystem. An S-Band only system was not considered due to the low achievable downlink data rate. A combined S-/X-Band system would not add anything compared to an X-Band only system and was thus not considered either. A K_a-Band only system would be problematic for LEOP and contingency cases as the antenna pointing requirements are very stringent in this high frequency range. In general the beam-width (the angle of a cone that contains most of the transmitted power or that can receive most transmitted power) is decreased for higher frequencies and increased for larger gain and thus large diameter antennae.

The maximum downlink bitrates and downlink times for the considered options are:

- X-Band: 9.5Mbit/s → TM D/L time: < 8h
- K_a-Band: 75Mbit/s (limited by ground segment) → TM D/L time: < 1h

15.2.2.1 X-Band downlink

Not considering any regulatory restrictions, X-Band would be a good candidate for the system. The telecommand data could be transmitted between a 35m ground-station and two low gain antennae on board of the spacecraft. The high science telemetry volume could be downlinked via a high gain antenna. This option has been the baseline for previous ESA mission stationed on SEL2 like GAIA, Herschel and Plank. The technology needed for this option has a high technological readiness level (TRL) and is well understood.

15.2.2.1.1 Bandwidth

A challenge with X-Band downlink for cat-A SR missions is that only 50 MHz of bandwidth are available for 5 channels resulting in channels of only 10 MHz each (cf. Table 15-2). This effectively restricts the maximum downlink data rate. As an example, the GAIA transponder's 99% occupied bandwidth was 8.7 MHz at a symbol rate of 10 Msym/s using GMSK $BT_b=0.25$. From this figures we get a bandwidth efficiency of 1.15 sym/MHz. We could thus achieve a maximum symbol rate of 10.92 Msym/s considering 0.5 MHz of bandwidth margin.

We could increase the downlink data rate by scaling up the transmitted power in order to increase the received signal-to-noise-ratio (SNR). Increases in bit-rate go hand in hand with an increase in occupied bandwidth. This places us in a regime where the bit-rate can only be increased by increasing either the gain-to-noise-temperature-ratio (G/T) of the G/S receiver or by using more efficient modulation and coding schemes. Since we already assume the best ground stations available from ESTRACK the only degree of freedom for downlink data rate optimisation left, is that of better modulation and coding schemes.

15.2.2.1.2 Coding

From a naïve perspective, increasing the bandwidth efficiency of a RF communication system can be achieved by using either higher-order modulation schemes or by increasing the coding rate of the channel coding scheme used.

Figure 15-1 summarises the allowed modulation schemes with their respective theoretical bandwidth efficiencies achievable with a perfectly linear transmit power amplifier and perfect demodulator RD[24]. From this figure we can see that for a highly bandwidth constrained channel, LDPC 7/8 is the most power efficient solution.

Unfortunately, LDPC 7/8 is not available in ESTRACK yet and its use would thus make a development necessary. Current European on-board computers also do not yet support LDPC 7/8 so there is need for development in that area too. Alternatively the coding hardware could be moved into the transponder which would also necessitate developments.

15.2.2.1.3 Modulation

Next to using efficient channel coding schemes, using a higher-order modulation scheme could also dramatically increase bandwidth efficiency. This theoretical advantage is unfortunately reduced because of the non-linear behaviour of practical power amplifiers. In order to achieve acceptable power efficiency, on-board power amplifiers are usually operated in saturation thus introducing non-linear distortions. Table 15-4 shows that the occupied bandwidth per bit (R_s is the same as our bit-rate in this table) is very similar for both precoded GMSK (order 2) and filtered OQPSK (order 4) when amplified by an SSPA in saturation. Similar figures are to be expected for amplification through a TWTA. This behaviour leads us to choose the very efficient GMSK $BT_b = 0.25$ as modulation scheme.

15.2.2.1.4 Downlink Scheduling and pointing

Requirement COM-030 mandates that no communication can take place during operation of the SAFARI instrument because of interference from the strong electromagnetic field strengths originating from the HGA. At the same time, this

instrument needs a long regeneration period during which the second instrument XFI cannot be operated. These circumstances make it possible to have a period of at least 8h per day available only for D/L. Since the 3dB-beam-width of the proposed solution is only ~6° but the telescope may be observing in directions outside of this cone an antenna pointing mechanism is necessary. The angular drift during a D/L session is <1° which allows us to point the HGA before downlinking in order to avoid micro-vibrations that could disrupt the operation of XFI.

Modulation Type	Two Sided -60 dB Bandwidth [9]	Occupied Bandwidth
Unfiltered BPSK	635 R_S	20.56 R_S
Baseband Filtered OQPSK/PM		
Butterworth 6th order BT_S=0.5 SRRC (α=0.5)	2.70 R_S	0.88 R_S
Bessel 6th order BT_S=0.5	2.68 R_S	0.88 R_S
	3.69 R_S	0.93 R_S
Baseband Filtered OQPSK I/Q Butterworth		
6th order BT_S=0.5 SRRC α=0.5	4.06 R_S	0.86 R_S
Bessel 6th order BT_S=0.5	4.24 R_S	0.88 R_S
	4.95 R_S	1.34 R_S
Precoded GMSK BT_S = 0.25	2.14 R_S	0.86 R_S

Table 15-4: Occupied Bandwidth of Category A Recommended Efficient Modulations after Spectral Regrowth Due to Saturated SSPA (source RD[26])
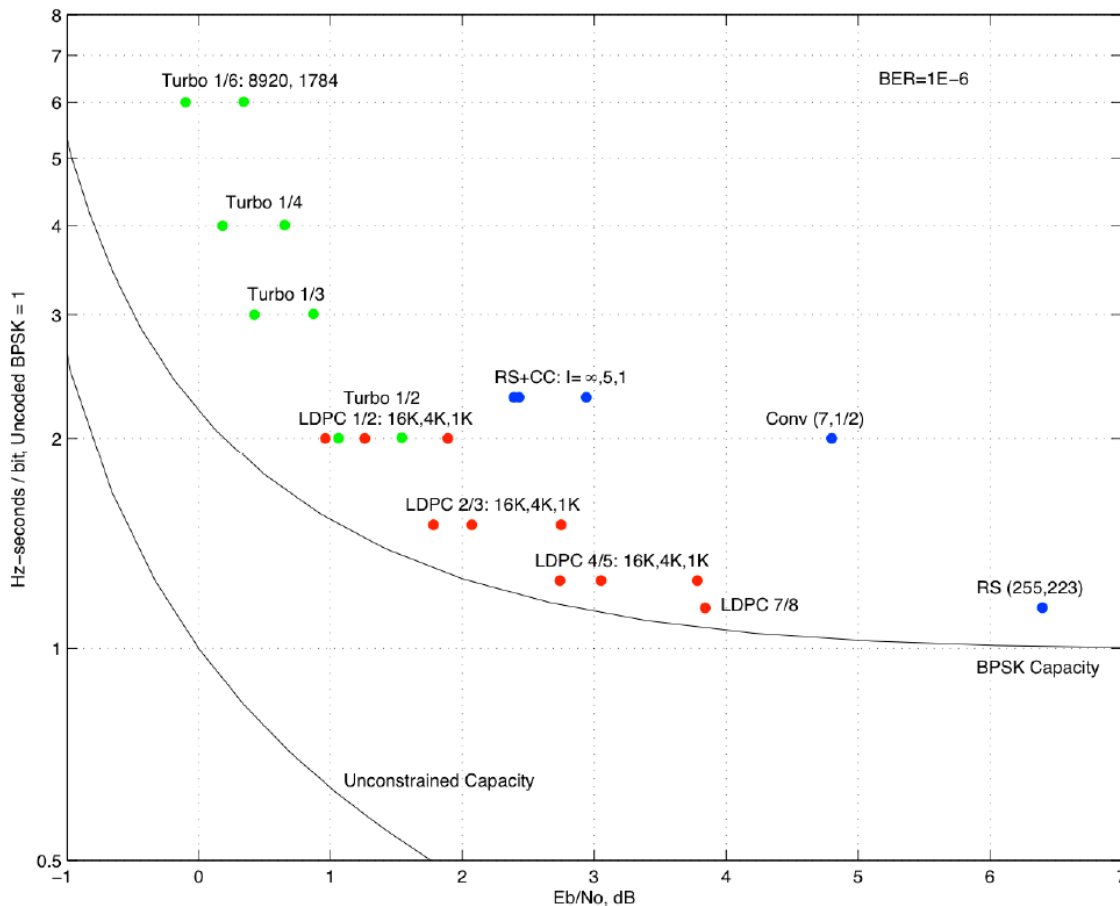
Figure 15-1: Power Efficiency vs. Spectral Efficiency for Several CCSDS Codes

15.2.2.2 K_a-Band downlink

K_a-Band could be used to downlink the science telemetry in very little time. This band is meant to be used for high symbol rate downlink once X-Band cannot provide sufficient bandwidth. An analysis based on another planned ESA SEL2 mission results in a net downlink time of less than one hour.

This short downlink time would allow the S/C to be pointed to the G/S using the attitude and orientation control system thus making an antenna pointing mechanism (APM) unnecessary.

Due to the low antenna efficiency for such high frequency, the HGA would have to have a diameter of ~70 cm as opposed to almost half for X-Band. This would decrease the available area for the solar arrays mounted on the same surface as the HGA.

Surprisingly, the subsystem cost of a K_a-Band solution is not a lot higher than the X-Band solution. This is mainly due to reduced G/S booking times caused by the low transmission time and possibility to omit the APM that is necessary for the X-Band system.

The atmospheric losses in K-Band are highly dependent on the weather in the line of sight between S/C and G/S. Wet weather can highly degrade a K-Band link. Therefore

there is a need for an on-board file system and a file transfer protocol that supports retransmission. A solution to this could be the usage of CFDP, the **C**CSDS **F**ile **D**elivery **P**rotocol.

15.2.2.3 Recapitulation

Table 15-5 has been compiled based on the aforementioned facts about the two candidate bands. The result of this analysis is not definite but there is a tendency towards an X-Band only solution. Based on this fact the X-Band solution was chosen as baseline and the K_a-Band solution is retained as an option.

Aspect	X-Band only	X + K_a-Band
Mass	+	-
Volume	+	-
Power	+	-
Energy	-	+
Antenna size	+	-
Cost	0	0
Mechanisms	-	+
TRL	+	-
New developments	-	+
Weather losses	+	-

Table 15-5: X- vs. X+K_a-Band high level trade-off

15.3 Baseline Design

15.3.1 Architecture

The baseline architecture of the on-board telecommunications subsystem is illustrated in Figure 15-3. Nominal TT&C operation and scientific telemetry downlink are both performed in X-Band. The overall system includes:

- Two redundant X/X transponders
- Two redundant TWTAs each composed of:
  - A Travelling Wave Tube Amplifier
  - An Electric Power Conditioner (EPC)
- One steerable X-Band HGA of 40 cm diameter
- Two fixed X-Band LGAs with hemispherical coverage
- A Radio Frequency Distribution Unit (RFDU)

The LGAs should be positioned in a way such that continuous coverage is achievable. The HGA is mounted on the nadir panel of the S/C so it will be roughly pointed to Earth in nominal attitude. The configuration is illustrated in Figure 15-2.
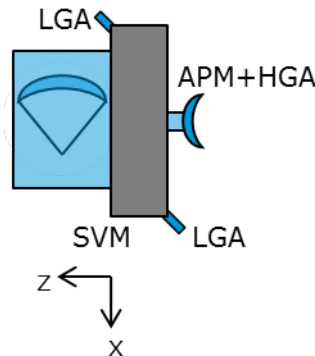
Figure 15-2: Preliminary antenna accommodation
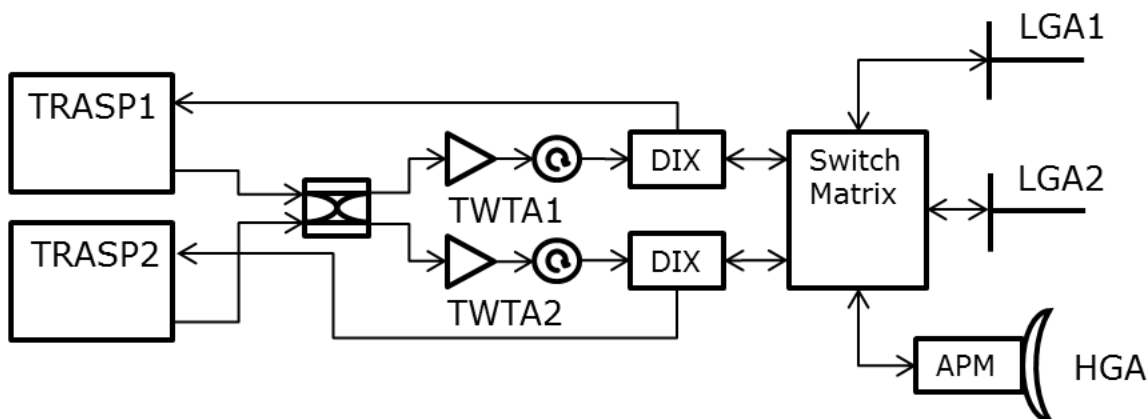
Figure 15-3: Tentative X-Band Architecture. TRASP: X-Band Transponder, TWTA: X-Band Travelling Wave Tube Amplifier, DIX: Diplexer

The proposed architecture features active redundancy for the upstream and passive redundancy for the high data rate downlink. The Switch Matrix is composed of RF-Switches. During nominal operation no switching is necessary so the system is reliable. As a defensive measure against switches getting stuck in non conducting state, the matrix can be designed with backup paths increasing the overall reliability.

15.3.2 Modulation, Coding and Ranging

The preliminary selected modulation schemes have been chosen from the applicable CCSDS standard RD[23]:

- Telecommand uplink: NRZ/PSK/PM(sine), modulation index: 1.0° peak

- Telecommand coding: N/A

- Telemetry downlink: GMSK BT_s=0.25

- Telemetry coding: LDPC 7/8

- Ranging: PN ranging.

Ranging can be performed parallel to GMSK using regenerative Pseudo-noise (PN) ranging. This technology is not standardised yet at the time of writing but it is expected that this will happen soon and the technology has already been well studied RD[27].

15.3.3   List of Equipment

The following paragraphs describe the chosen equipment in detail.

15.3.3.1   High Gain Antenna

A parabolic reflector dish antenna mounted on a 2DoF APM shall be used. The specifications are as follows:

- Efficiency: 60%
- Diameter: 40cm
- Mass: 3kg (excluding APM)
- 3dB-beam-width: ~6°
- Boresight gain: ~29dBi.

15.3.3.2   Low Gain Antennae

The two Low Gain Antennae are in charge of receiving and transmitting data during LEOP or potentially in contingency cases.
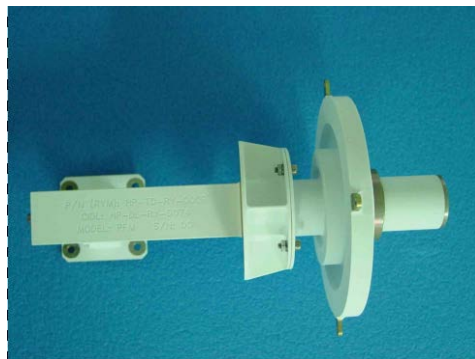
Figure 15-4: Example LGA

Two LGAs are used to provide an omnidirectional radiation. This allows for communication in case the S/C has an uncontrolled attitude. The gain pattern of a stand-alone antenna is shown in Figure 15-5.
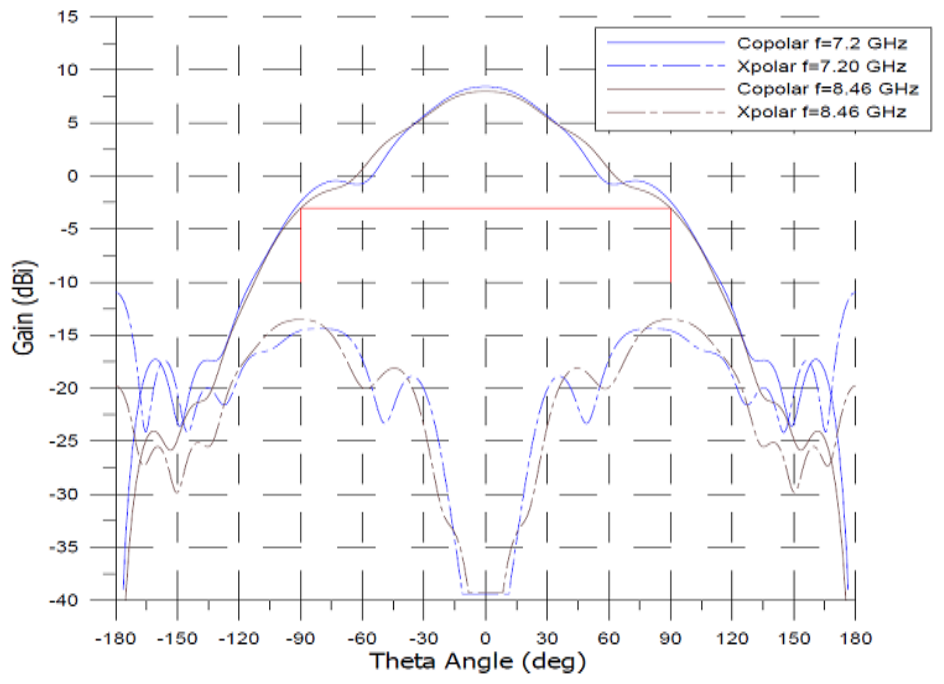
Figure 15-5: Example LGA radiation pattern

The main performance figures of the LGA are given below:

- Antenna type: Choked horn
- Gain: -4 dBi to +6 dBi (in one hemisphere)
- Mass: 0.5 kg.

15.3.3.3   Transponders

The X-Band transponders are in charge of:

- Demodulating the telecommand signal received from either the LGA or HGA
- Delivering the demodulated signal to the On Board Computer (OBC)
- Modulating the telemetry data
- Forwarding the signal to the amplifier and of redirecting the ranging signal to ground.

The proposed transponder has a TRL of 9. It has been developed by TAS-I and has a heritage from GAIA and Herschel-Planck. The receiving part will work in hot redundancy while the transmitter will work in cold redundancy (MR-SYS-150).

A further development is needed in order to support PN ranging. It might also be advisable to implement LDPC 7/8 coding in the transponder.

The main performance details for this equipment are given below:

- Maximum TC uplink data rate 4 kbps
- Telemetry downlink modulation schemes: BPSK, SP-L and GMSK
- Ranging capability simultaneous with low data rate telemetry
- Total mass considering a 10% margin: 3.2 kg

- Consumed power (transmitter OFF/ receiver ON): 18 W
- Consumed power (transmitter ON / receiver ON): 35 W
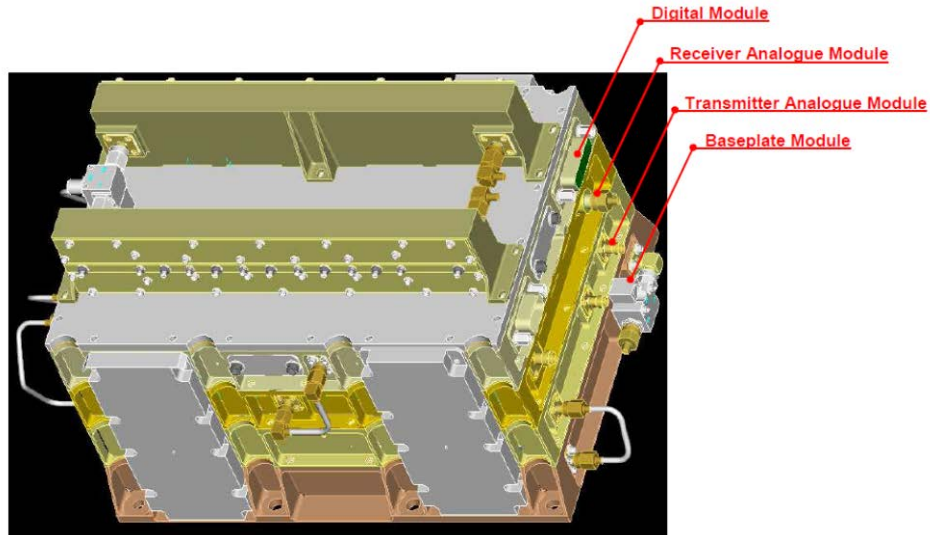
Figure 15-6: Proposed X-Band Transponder

15.3.3.4 Travelling Wave Tube Amplifiers

The Travelling Wave Tube Amplifier (TWTA) is in charge of amplifying the downlink signal to the necessary RF output power. It consists of a travelling wave tube (TWT) supplied by an electrical power conditioner (EPC).

The proposed equipment currently has a TRL of 9. The TWTA has been developed by TAS-B and has flown previously in ESA missions.

Two TWTAs are used to provide equipment redundancy. The operating mode is cold redundancy meaning only one of them is switched on at any time.

The main performance details for this equipment are given below:

- RF output power: 35 W
- Mass: 1 kg (TWT) + 1.4 kg (EPC)
- Consumed power: 60 W (TWT) + 3W (EPC).

Figure 15-7: Travelling Wave Tube Amplifier

15.3.3.5   Radio Frequency Distribution Unit

The RFDU is composed of all elements needed to interconnect the previously discussed pieces of equipment. It is composed of waveguides guiding the RF-power, RF-switches, diplexers separating the up- and downlink signals, isolators reducing reflections and couplers splitting up RF-signals.

15.3.4   Budgets

15.3.4.1   Mass

Element 1	Service Module				MASS [kg]		
Unit	Unit Name Click on button above to **insert new unit**	Part of custom subsystem	Quantity	Mass per quantity excl. margin	Maturity Level	Margin	Total Mass incl. margin
1	X-TRASP		2.00	3.20	Fully developed	5	6.7
2	X-TWT		2.00	1.00	Fully developed	5	2.1
3	X-EPC		2.00	1.40	Fully developed	5	2.9
4	X-LGA		2.00	0.50	Fully developed	5	1.1
5	X-HGA		1.00	3.00	To be modified	20	3.6
6	X-RFDU		1.00	5.00	To be modified	20	6.0
-							
	SUBSYSTEM TOTAL		6	20.2		10.9	22.4

Table 15-6: Subsystem mass budget

15.3.4.2 Power

Unit	Unit Name	Quantity	Pon	Pstby
1	X-TRASP	2.00	53.0	36.0
2	X-TWT	2.00	60.0	0.0
3	X-EPC	2.00	3.0	0.0
4	X-LGA	2.00	0.0	0.0
5	X-HGA	1.00	0.0	0.0
6	X-RFDU	1.00	0.0	0.0
-			116.0	36.0

Table 15-7: Subsystem power budget

15.4 Options

Next to the baseline of an X-Band only design, a combined X-/K_a-Band solution has been considered as an option. The drawbacks of such a solution are the increased mass, volume, HGA antenna diameter and lower technological readiness. The advantage would an increased flexibility with regard to science telemetry generation rate and the possibility to use a non steerable HGA. Additionally, the cost due to G/S booking and management can be reduced and there would be no need implement LDPC 7/8 as the lower rate version LDPC ½ and LDPC 4/5 are already implemented by ESTRACK.

15.4.1 Architecture

15.4.1.1.1 Base architecture

In RD[28], two architectures involving K_a-Band are evaluated for the PLATO mission. The first architecture is depicted in Figure 15-8. It combines an X-Band system equipped with only LGAs for telecommand uplink, LEOP and emergency telemetry downlink and tracking with a dedicated K_a-Band payload data transmitter system equipped with an HGA for science telemetry downlink. In the proposed architecture for PLATO, the HGA is attached to an APM. Since the HGA's 3dB-beamwidth is ~0.8° and the S/C is idle regularly due to SAFARI regeneration, this mechanism can be omitted. The S/C can be pointed to the G/S for each downlink session.

The mass and power figures of the combined X/K_a design are:

- Mass: ~45 kg
- Power: ~160 W (in K_a transmit mode).

15.4.1.1.2 Optimised architecture

The aforementioned document also mentions an alternative, optimised architecture where the HGA is shared between the X- and K_a-Band subsystems. This would make the X-TWTAs unnecessary and would allow replacing them with SSPAs built into the transponder.
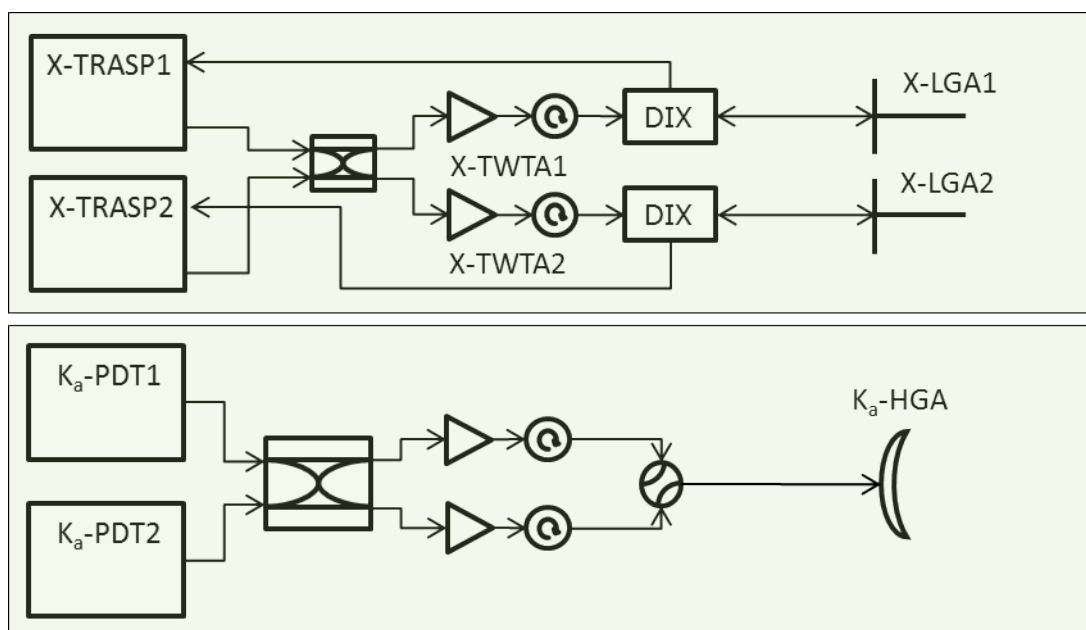
Figure 15-8: Modified (no APM) X/Ka-Band combined architecture as proposed in RD[28]

The mass would be reduced due to the omission of the X-TWTA but the power figure would stay the same in regard to the non optimised version.

15.4.2 Modulation and Coding

The following techniques could be used for a K_a-Band science downlink:

- Modulation: OQPSK (hard keyed or SRRC-OQPSK)
- Coding: LDPC ½
- Ranging: PN

15.5 Technology Requirements

The following technologies are required or would be beneficial to this domain:

Equipment and Text Reference	Technology	Suppliers and TRL Level	Technology from Non-Space Sectors	Additional Information
G/S decoder	LDPC 7/8	ESTRACK		
On-board computer or transponder	LDPC 7/8			

16   DATA HANDLING

16.1 Requirements and Design Drivers

Subsystem requirements		
Req. ID	**STATEMENT**	**Parent ID**
DH-010	The C&DH subsystem shall provide overall SC control: AOCS, Thermal, Power and FDIR	
DH-020	The C&DH subsystem shall acquire and store platform and payload housekeeping data and payload science data	
DH-030	The C&DH subsystem shall process platform housekeeping data to support on-board autonomous functions	
DH-040	The C&DH shall generate and distribute the SC Elapsed Time	
DH-050	The C&DH shall support data transfer from and to ground.	

16.2 Assumptions and Trade-Offs

The scientific instruments generate an average science data rate of 3Mbps and around 15 kbps of instrument housekeeping. Another 15kbps are reserved for platform housekeeping.

The Mass Memory shall be able to acquire and store up to 36 hours of scientific data.

The C&DH subsystem is based on highly recurrent designs with no real need for new technology developments. However, the mission could highly benefit from the use of file based Mass Memory Units and file based operations.

There has been significant work within ESA, with several TRP/GSP activities, in that line. Some ESA missions, such as EUCLID or JUICE, already include CFDP as baseline for the SC commanding and scientific data transmission to ground.

16.3 Baseline Design

The baseline architecture is based on three units, the OBC, the RTU and the SSMM. The detailed configuration and functionality of the C&DH units will depend on the final RF design. Figure 16-1 and Figure 16-2 show the baseline architecture for X-band and K-band scientific data download.

In the proposed architecture for X-band, due to the relatively lower bandwidth of the downlink, the scientific data communication is handled directly by the OBC, implementing LDPC coding scheme.

In the case of K-band, the bandwidth is too large to be handled by the OBC. The SSMM has a direct connection with the K-band transponder and implements the coding scheme and the communication protocol. Typically, the K-band link is quite unreliable, being extremely sensitive to water. Therefore, the use of an automatic retransmission protocol such as CFDP is strongly recommended. This exact same approach has already been taken in missions with similar requirements such as EUCLID.
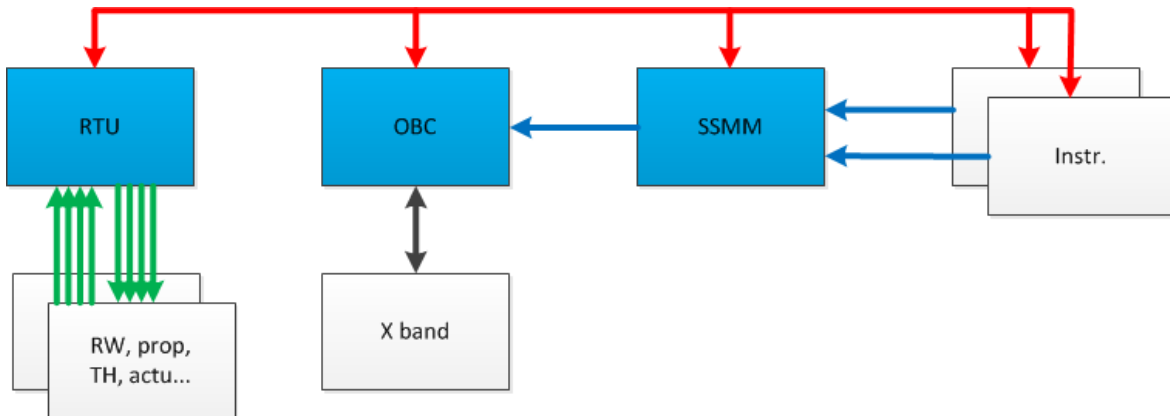
Figure 16-1: DHS architecture with X-band
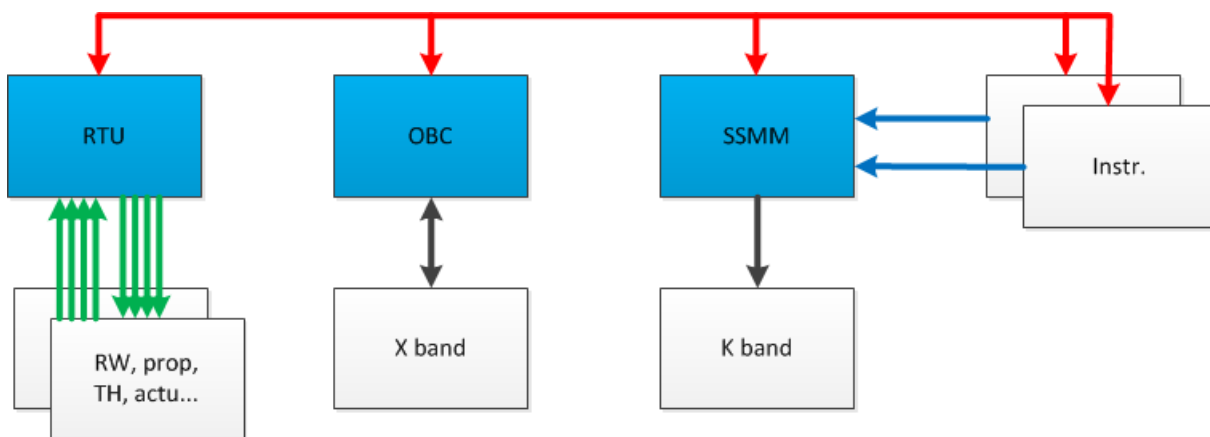
Figure 16-2: DHS architecture with K-band

The C&C bus of the unit is based on CAN or 1553. The payload data is transferred by means of Spacewire, from the instruments to the SSMM and to the OBC if necessary.

16.4 List of Equipment

The OBC is based on an off-the-shelf solution based on SCOC3 or other similar SOC. It contains a small mass memory to store platform housekeeping, SW patches and OBCPs. The OBC acts as a master in the C&C bus and implements spacewire to the SSMM for payload data transfer.

The RTU is an ad-hoc development for the mission, although there is a big heritage from previous mission. It communicates to the OBC using the C&C bus. It is in charge of the platform housekeeping acquisition. It implements the interface to propulsion, reaction wheels, pyro, electrical actuators, HPC and so on.

The SSMM is based on flash memory technology. It is in charge of acquiring and storing the scientific data and housekeeping from the instruments via spacewire. The mission could highly benefit from the use of file systems and file delivery protocols such as CFDP.

If the X-band only solution is taken, the size case for the memory is 36 hours at 3Mbps, which is around 400Gbit. The data is then formatted and transferred to the OBC via Spacewire to be forwarded down to Earth

In the case of K-band data downlink, some measures must be taken to cope with the possible outages of the data transmission. To begin with, 50% margin must be applied to the size of the memory, around 600Gbit EOL memory size. Secondly, an automatic retransmission protocol, such as CFDP, must be implemented. This implementation will likely require a SW/HW co-design to reach around 80Mbps of data transmission. And lastly, a trade-off between the error correction capabilities of the K-band coding scheme and the retransmission capabilities of CFDP must be performed in order to reduce the data overhead and maximise the scientific data download.

Element 1	-			MASS [kg]				
Unit	Unit Name	Quantity	Mass per quantity excl. margin		Maturity Level	Margin		Total Mass incl. margin
1	CDMU	1	5.5		To be modified	10		6.1
2	SSMM	1	12.0		To be modified	10		13.2
3	RTU	1	12.0		To be modified	10		13.2
-	Click on button below to insert new unit							
SUBSYSTEM TOTAL		3	29.5			10.0		32.5

Table 16-1: Mass summary for X-band

Element 1	-			MASS [kg]				
Unit	Unit Name	Quantity	Mass per quantity excl. margin		Maturity Level	Margin		Total Mass incl. margin
1	CDMU	1	5.5		To be modified	10		6.1
2	SSMM	1	20.0		To be modified	10		22.0
3	RTU	1	12.0		To be modified	10		13.2
-	Click on button below to insert new unit							
SUBSYSTEM TOTAL		3	37.5			10.0		41.3

Table 16-2: Mass summary for K-band

Element 1	-			POWER
Unit	Unit Name	Part of custom subsystem	Quantity	Ppeak
1	CDMU		1	15.0
2	SSMM		1	12.0
3	RTU		1	14.0
-	Click on button below to insert new unit			
SUBSYSTEM TOTAL			3	41.0

Table 16-3: Power summary for X-band

Element 1	-			MODE
Unit	Unit Name	Part of custom subsystem	Quantity	Ppeak
1	CDMU		1	15.0
2	SSMM		1	25.0
3	RTU		1	14.0
-	Click on button below to insert new unit			
SUBSYSTEM TOTAL			3	54.0

Table 16-4: Power summary for K-band

17 RISK ASSESSMENT

17.1 Reliability and Fault Management Requirements

The following reliability and fault management requirements were proposed for the NGCryoIRTel mission:

ID	Requirement
MR-SYS-140	The overall reliability of the mission, from after LV separation till the end of the nominal lifetime, shall be ≥ 85%.
MR-SYS-150	Single point failures with a severity of catastrophic or critical (as defined in ECSS-Q-ST-30C) shall be eliminated or prevented by design.
MR-SYS-160	Retention in the design of single point failures of any severity rating is subject to formal approval by ESA on a case-by-case basis with a detailed retention rationale.
MR-SYS-170	A failure of one component (unit level) shall not cause failure of, or damage to, another component or subsystem.
MR-SYS-180	The failure of an instrument channel shall not lead to a safe mode of the S/C.
MR-SYS-190	Any hazardous situation, which will not cause immediate loss of but may develop into the loss of the S/C or instrument, shall be prevented by design or protected against.
MR-SYS-200	The design shall allow the identification of on-board failures and their recovery by autonomously switching to a redundant functional path. Where this can be accomplished without risk to spacecraft and instrument safety, such switching shall enable the continuity of the mission timeline and performance.
MR-SYS-210	Where redundancy is employed, the design shall allow operation and verification of the redundant item/function, independent of nominal use.
MR-SYS-220	For design and analysis purposes, an average of 3 safe mode events of 3 days (plus recovery time) each per year shall be considered.

Table 17-1: Reliability and Fault Management Requirements

The requirements were reviewed during the course of the study and found to be adequate for NGCryoIRTel. An NC with respect to critical single point failures (M-SYS-150) was identified in the baseline design and consequently highlighted in the risk log (see risk ID SPA_07).

17.2 Risk Management Process

Risk management is an organised, systematic decision making process that efficiently identifies, analyses, plans, tracks, controls, communicates, and documents risk in order to increase the likelihood of achieving the project goals. The procedure comprises four fundamental steps RD[30]:

- Step 1: Definition of the risk management policy which includes the project success criteria, the severity & likelihood categorisations, and the actions to be taken on risks

- Step 2: Identification and assessment of risks in terms of likelihood and severity

- Step 3: Decision and action (risk acceptance or implementation of mitigating actions)

- Step 4: Communication and documentation
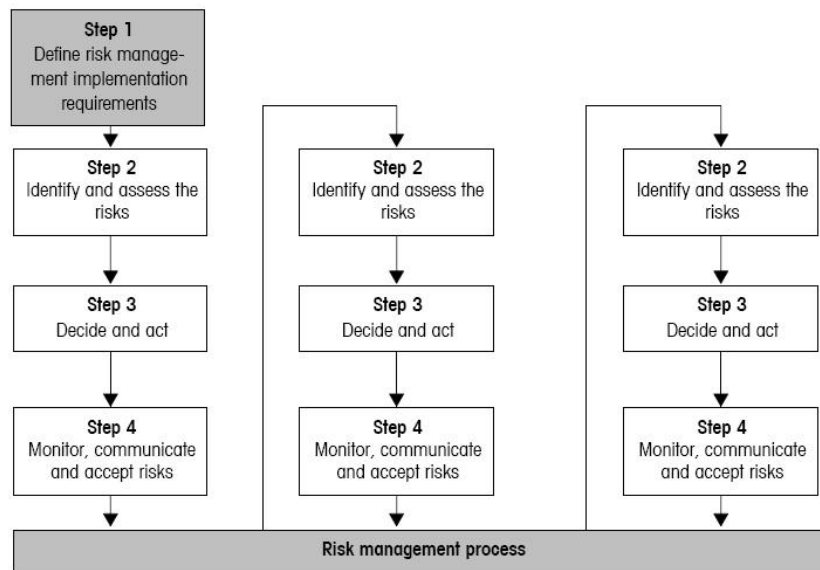
Table 17-2: ECSS-M-ST-80C, 2008 Risk Management Process

17.3 Risk Management Policy

The CDF risk management policy for NGCryoIRTel aims at handling risks which may cause serious science, technical, schedule and/or cost impact on the project.

17.3.1 Success Criteria

The success criteria with respect to the science, technical, schedule, and cost objectives are presented in Table 17-3:

Domain	Success Criteria
Science	SCI01- The mission accomplishes all of the key science goals
Technical	TEC01- The spacecraft performs successfully during the nominal mission lifetime (5 years) with a reliability at EOL of ≥ 85% (ref. MR-SYS-140)
	TEC02- No performance degradation owing to single point failures (ref. MR-SYS-150)
	TEC03- No failure propagation (ref. M-SYS-170)
Schedule	SCH01-The mission launch date is no later than 2028 (ref. MR-MIS-020) SCH02-All mission related units (LV, space and ground segment) reach a TRL of at least 6 by the end of the definition phase (ref. MR-PROG-020)
Cost	COS01-The mission is compatible with the ESA M5 CaC boundary (ref. MR-PROG-050)

Table 17-3: Success Criteria

17.3.2 Severity and Likelihood Categorisations

The risk scenarios are classified according to their domains of impact. The consequential severity level of the risks scenarios is defined according to the worst case potential effect with respect to science objectives, technical performance objectives, schedule objectives and/or cost objectives.

In addition, identified risks that may jeopardise and/or compromise the NG-CryoIRTel mission will be ranked in terms of likelihood of occurrence and severity of consequence.

The scoring scheme with respect to the severity of consequence on a scale of 1 to 5 is established in Table 17-4, and the likelihood of occurrence is normalised on a scale of A to E in Table 17-5.

Score	Severity	Science	Technical	Schedule	Cost
5	Catastrophic	Failure leading to the impossibility of fulfilling the mission's scientific objectives	Safety: Loss of life, life-threatening or permanently disabling injury or occupational illness; Severe detrimental environmental effects. Loss of system, launcher or launch facilities	Delay results in project cancellation	Cost increase result in project cancellation
4	Critical	Failure results in a major reduction (70-90%) of mission's science return	Safety: Major damage to flight systems, major damage to ground facilities; Major damage to public or private property; Temporarily disabling but not life- threatening injury, or temporary occupational illness; Major detrimental environmental effects Dependability: Loss of mission	Critical launch delay (24-48 months)	Critical increase in estimated cost (100-150 M€)
3	Major	Failure results in an important reduction (30-70%) of the mission's science return	Safety: Minor injury, minor disability, minor occupational illness. Minor system or environmental damage Dependability: Major degradation of the system	Major launch delay (6-24 months)	Major increase in estimated cost (50-100 M€)
2	Significant	Failure results in a substantial reduction (10-30%) of the mission's science return	Dependability: Minor degradation of system (e.g.: system is still able to control the consequences) Safety: Impact less than minor	Significant launch delay (3-6 months)	Significant increase in estimated cost (10-50 M€)
1	Minimum	No/ minimal consequences (<10% impact)	No/ minimal consequences	No/ minimal consequences (1-3 month delay)	No/ minimal consequences (<10 M€)

Table 17-4: Severity Categorisation

Score	Likelihood	Definition
E	Maximum	Certain to occur, will occur once or more times per project.
D	High	Will occur **frequently**, about 1 in 10 projects
C	Medium	Will occur **sometimes**, about 1 in 100 projects
B	Low	Will occur **seldom**, about 1 in 1000 projects
A	Minimum	Will **almost never** occur, 1 in 10000 projects

Table 17-5: Likelihood Categorisation

17.3.3 Risk Index & Acceptance Policy

The risk index is the combination of the likelihood of occurrence and the severity of consequences of a given risk item. Risk ratings of low risk (green), medium risk (yellow), and high risk (red) were assigned based on the criteria of the risk index scheme (see Table 17-6). The level of criticality of a risk item is denoted by the analysis of the risk index. By p0licy high risks are not acceptable and must be reduced (see Table 17-7).

Severity					
5	5A	5B	5C	5D	5E
4	4A	4B	4C	4D	4E
3	3A	3B	3C	3D	3E
2	2A	2B	2C	2D	2E
1	1A	1B	1C	1D	1E
	A	B	C	D	E
					Likelihood

Table 17-6: Risk Index

Risk Index	Risk Magnitude	Proposed Actions (during assessment phase)
3E, 4D, 4E, 5C, 5D, 5E	High Risk	Unacceptable risk: implement mitigation actions (either likelihood reduction or severity reduction through new baseline) with responsible party.
1D, 1E, 2C, 2D, 2E, 3B, 3C, 3D, 4A, 4B, 4C, 5A, 5B	Medium Risk	Acceptable risk: Monitor and control. Optional reduction.
1A, 1B, 1C, 2A, 2B, 3A	Low Risk	Acceptable risk

Table 17-7: Proposed Actions

17.4 Risk Drivers

The following risk drivers have been considered in the identification of specific risk items:

- New technologies
- Environmental factors
- Design challenges
- Reliability issues, single point failures (SPFs)
- Major mission events
- Programmatic factors

17.5 Top Risk Log

Top risk items have been identified at the mission (ESA) and spacecraft (prime) levels. Please refer to Table 17-8 for a complete list of identified top risks and their corresponding suggested mitigating actions. Risk index results are summarised in Table 17-9.

Risk Type	Classifica tion	Risk Index	Risk Scenario	Cause	Mitigating Action 1	Mitigating Action 2	Mitigating Action 3
Mission							
MIS_01	Technical	4D	Re-definition of the mission due to uncertainties related to the baseline launch vehicle (H-X) which is a concept design.	H-X launch vehicle uncertainties in: • Launch capability (kg) • Usable volume for S/C • Interface adaptor • Launch environment (loads)	Use the H-IIA 204 launch vehicle specifications until those for H-X are available.	Consider worst case margins in terms of performance to L2, payload fairing volume, and environmental loads to ensure compatibility.	Determine as soon as possible the actual capabilities of the H-X launch vehicle.
MIS_02	Schedule	3C	Delays in international cooperation elements/interface s impact the development cost and/or schedule of the mission.	NG-Cryo IR telescope is proposed as an international cooperation mission with a partner agency.	Establish a close cooperation with partner agency with regular progress meetings. Create a trusting and open environment enabling improved communication flow for quicker problem notification and resolution.	Adequate funding of dedicated ESA interface team with the partner agency.	Establish clearly defined managerial and technical interfaces to minimise complexity.
MIS_03	Science	3D	Radiation environment impact on spacecraft and science return.	• L2 radiation environment: Galactic cosmic rays, solar particle events, and solar and Jovian electrons. • Single event effects and deep dielectric charging and electrostatic discharge effects during transfer to L2.	Build on lessons learnt of radiation environment in L2 thanks to knowledge acquired by Hershel and Plank.	Provide detailed radiation environment assessment and study mitigation options including shielding , rad-hard component selection, etc.	Do not plan any critical manoeuvres during the Van Allen belt pass.
MIS_04	Cost	5D	Risk of exceeding the ESA M-class cost boundary of 470M€.	Telescope and cryo-cooling chain are major cost drivers.	Reconsider scientific return and mission objectives and 1) minimise accordingly to fit an M-class mission or 2) re-evaluate towards an L-class mission.	Re-evaluate work distribution with JAXA.	
MIS_05	Science	3E	Observational efficiency requirement of ≥85% (MR-PERF-040) is not met.	Low efficiency of the SAFARI instrument cooler recycling (6 hour duration every 20	Reconsider observational efficiency requirement.	Optimise operational concept to maximise observational	Optimise cryo-cooler inside SAFARI.

Risk Type	Classification	Risk Index	Risk Scenario	Cause	Mitigating Action 1	Mitigating Action 2	Mitigating Action 3
				hours). There is a need to run a high current through cyro-coolers which has EMI implications for the SMI instrument.		efficiency, e.g. perform payload data transmission during cooler recycling.	
Spacecraft incl. telescope platform							
SPA_01	Science	3D	Impact of micro-vibration disturbances on telescope performance.	Micro-vibrations induced by mechanical equipment particularly the cryo-coolers violate pointing requirements.	Need for mechanical isolation. Place cryo-coolers on appropriate mountings (dampers) .Along the vibration paths, modifications of structural elements or equipment relocation can be attempted with the aim of reducing the mechanical coupling between vibration sources and receivers.	Insert sufficient margins in schedule.	
SPA_02	Schedule	4C	Delays in cryogenic system technology development efforts impact schedule (particularly the 1K JT)	Low technology readiness level (4) of 20K class two stage Stirling cooler (2ST), 4K Joule Thomson (JT) cooler, 1K JT, and cooler driver electronics.	Invest in technology and testing. Insert sufficient margins in schedule.	Development efforts are on-going.	Certain EM developments for the ASTRO-H mission are applicable. There is also additional heritage from AKARI and SMILES.
SPA_03	Science	5C	Detectors direct sun exposure during spacecraft attitude change manoeuvres in failure situations or before launcher separation.	AOCS failure.	Implementation of an autonomous safe shutter. Note this is a critical Item.	Stringent implementation of reliability and fault management requirements for AOCS and propulsion [R-SYS-150 and R-SYS-190]	Reliable safe mode.
SPA_04	Science	5C	Failure in cryo-cooling chain.	Technical complexity. Mechanical (e.g. seal leak) or electronic failure.	Failure tolerant system with cyro-coolers in active (load sharing) redundancy or ideally in cold redundancy.		

Risk Type	Classification	Risk Index	Risk Scenario	Cause	Mitigating Action 1	Mitigating Action 2	Mitigating Action 3
SPA_05	Schedule	3D	Challenging configuration leads to re-design of the spacecraft with impact on schedule.	• Complex structural design of large telescope in horizontal configuration (sun illumination constraints). • CoG off spacecraft centre axis. • Fitting coolers/dampers in appropriate locations within the compact platform is very challenging technically.	Insert sufficient dimensions/mass margins to ensure concept feasibility.	Implement CoG balancing mitigation measures.	Telescope vertical configuration option to be studied and compared.
SPA_06	Schedule	3E	Delays during spacecraft AIVT impact schedule.	Challenging AIVT due to integration of cryo-chain into SVM.	Design SVM for optimised assembly and integration of the cryogenic system.	Plan for late integration of cryo-coolers.	Insert margins in schedule.
SPA_07	Science	5B	Failure in shutter opening mechanism.	Critical single point failure.	Mechanism to be considered as critical item.	Design for reliability and test according to ECSS standards and procedures.	Simple one-shot mechanism is proposed.
SPA_08	Technical, Science	3D	Telescope performance degradation due to optics contamination during manufacturing, assembly, testing, transport, launch campaign or flight.	Optical instruments mounted on space platforms may be subject to performance degradation due to condensation of gases, debris contamination, dust particles or plume impingement from AOCS thrusters.	Appropriate cleanliness requirement specification and cleanliness and contamination control plan covering all project phases.	Configuration layout such that the sources of contamination cannot impact on sensitive surfaces.	Apply previous space telescope experience and lessons learnt.

Table 17-8: Risk Log

Severity					
5		SPA_07	SPA_03, SPA_04	MIS_04	
4				MIS_01	
3			MIS_02, SPA_02	MIS_03, SPA_01, SPA_08, SPA_05	MIS_05
2					
1					
	A	B	C	D	E
					Likelihood

Table 17-9: Top Risk Index Chart

17.5.1 Risk Log General Conclusions

- High risks are typical of a phase A project. Areas with lack of definition or little previous experience pose a-priori more risk to the mission and therefore are the ones with more risk reduction potential

- Experience shows that all risk items with a critical risk index (red area) must be analysed and proposals for risk treatment actions elaborated

- In the end, ideally all risk items should reach a level of justifiable acceptance

- The risk management process should be further developed during the project definition phase in order to refine the risk identification/analysis and provide evidence that all the risks have been effectively controlled.

17.6 Cryo-cooler Reliability and Redundancy Considerations

The NGCryoIRTel mission will have to achieve a high reliability of $R_{mis} \geq 0.85$ at 5 years (see requirement M-SYS-140). One of the main drivers to achieve this requirement will be the cryo-cooling system due to its complexity. For this reason, particular attention needs to be paid to its design.

A preliminary reliability apportionment to the cryo-cooling system yielded a requirement of $R_{cryo} \geq 0.96$ at 5 years. In order to meet this requirement, the cryo-cooling system must include redundancy, either in the form of redundant coolers and/or redundant drive electronics. In addition, electrical and/or heat switches may be needed to access the redundant elements. However, although redundancy protects against possible failures, the increased system complexity and increased cryogenic load may also have a negative impact on reliability that must be studied in detail.

Based on the study performed by RD[31], the following conclusions were drawn:

- The highest reliability is achieved with lightly-loaded, fully redundant coolers with heat interceptors to reduce the parasitic load

- The addition of heat switches can improve the system thermal efficiency, but with a significant increase in failure probability

- The use of redundant electronics only (with an electrical switch) has similar reliability to a system with heat switches, but with lower mass and power

- A single cooler provides the lowest mass, power, and cost, but may have marginal reliability for a long duration mission.

In the case of NG-CryoIRTel, adding heat switches to reduce the number of 2ST coolers could have a significantly negative impact on reliability, unless the reliability of the heat switch is demonstrated to be extremely high.

18 PROGRAMMATICS/AIV

18.1 Requirements and Design Drivers

The main requirements and design drivers for the NG-CryoIRTel Mission from a programmatics point of view are:

- All elements in direct view of the instruments' focal plane detectors shall be cooled to ≤ 6K
- Passive cooling to ≥ 40K (for on-ground thermal system testability)
- Launch from the Tanegashima Space Centre (JP)
- Launch date in 2027 / 2028
- The flight units of the instruments shall be delivered at least 30 months before the start of the launch campaign
- Complex PLM configuration and AIT with main elements from Japan and Europe.

18.2 Assumptions and Trade-Offs

- Phase A/B1 starting mid 2016
- TRL 6 to be achieved before the implementation phase (B2/CD or C/D)
- Expected to be achieved in 2018
- Phase B2/C/D starting not before 2020
- Cryogenic test requirements impacting facilities selection
- AIT Flow driven by modular design.

The product tree in Figure 18-1 shows the assumed responsibility for the various items in the product tree.
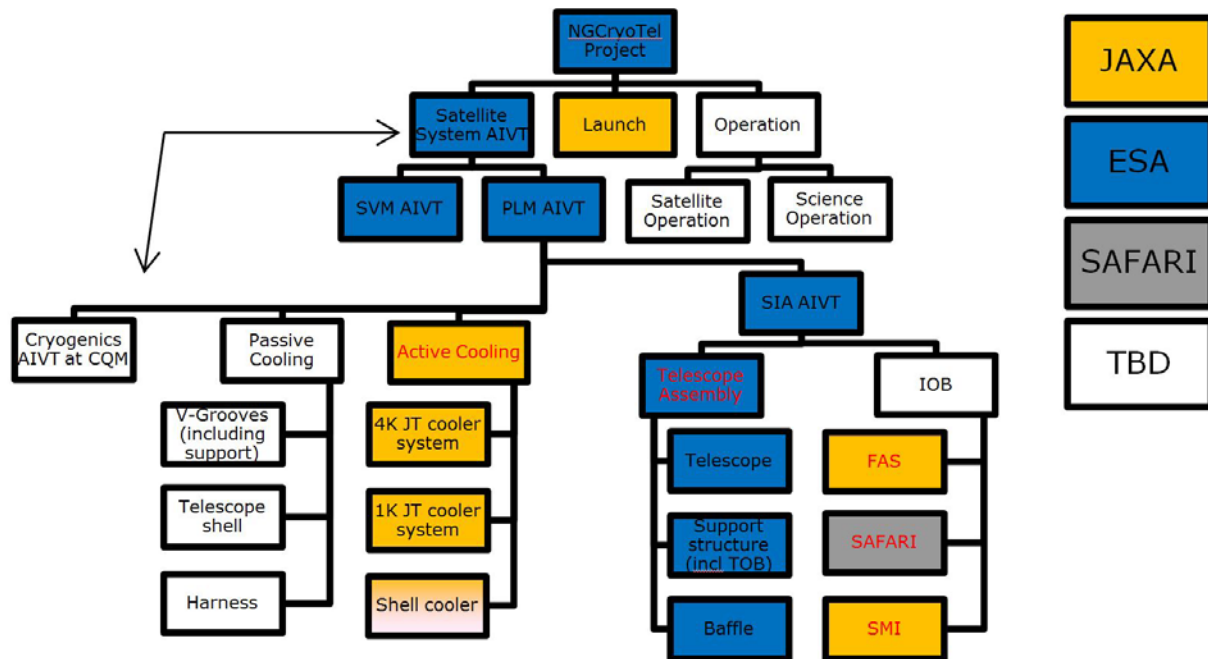
Figure 18-1: Product tree with the assumed workshare for this CDF study

The arrow indicates that Cryogenics AIV and PLM/System AIV are expected to be partly combined as on Planck, i.e. only one Thermal Balance Test at FM, but dedicated Cryogenic Qualification Model test for cryogenic verification.

18.3 Options

No options were considered for the programmatics assessment.

18.4 Technology Requirements

The Technology Readiness Levels (TRL) present a systematic measure, supporting the assessments of the maturity of a technology of interest and enabling a consistent comparison in terms of development status between different technologies.

TRL Summary:

- No equipment TRL are provided
- SAFARI is expected to achieve TRL 6 in 2018
- SMI is expected to achieve TRL 6 in 2018 (tbc)
- FAS (Focal Plane Attitude Sensor) is expected to achieve TRL 6 in 2018.

The different TRL as defined in RD[34] are shown in Table 18-1:

TRL	ISO Definition	Associated Model
1	Basic principles observed and reported	Not applicable
2	Technology concept and/or application formulated	Not applicable
3	Analytical and experimental critical function and/or characteristic proof-of concept	Mathematical models, supported e.g. by sample tests
4	Component and/or breadboard validation in laboratory environment	Breadboard
5	Component and/or breadboard critical function verification in a relevant environment	Scaled EM for the critical functions
6	Model demonstrating the critical functions of the element in a relevant environment	Full scale EM, representative for critical functions
7	Model demonstrating the element performance for the operational environment	QM
8	Actual system completed and "flight qualified" through test and demonstration	FM acceptance tested, integrated in the final system
9	Actual system completed and accepted for flight ("flight qualified")	FM, flight proven

Table 18-1: TRL scale

Table 18-2 shows an indication of the development time depending on the current TRL. According to the European Space Technology Master Plan, to prepare the contractual basis for multi-annual programs it takes about 18 months to reach political agreement on financial ceiling. This has also been included in the table.

TRL	Duration
5-6	4 years + 1.5 year
4-5	6 years + 1.5 year
3-4	8 years + 1.5 year
2-3	10 years + 1.5 year
1-2	12 years + 1.5 year

Table 18-2: TRL – development duration

With the specific critical technologies for this project expected to reach TRL 6 already in 2018, and in view of the envisaged launch date, the technology readiness level is considered not critical. Of course the equipment TRL needs to be assessed in the next phase of the project.

18.5 Model Philosophy

The model philosophy at satellite level, is similar to the model philosophy of the ESA Planck project:

- Structural Model (SM)
- Cryogenic Qualification Model (CQM) – could use a refurbished SM
- Avionics Model (AVM)
- Protoflight Model (PFM)

In addition the following lower level models will be needed:

- Cooling chain development model
- Instrument models
- Flight spares

For the telescope itself a Structural Thermal Model (STM) or Opto-mechanical Structural Thermal Model (OSTM) and a PFM will be needed. The OSTM is recommended before the STM because it allows a more complete qualification of the telescope than the STM.

- Telescope OSTM
- Telescope PFM

18.6 Integration and Verification Approach

Baseline for the study is that the satellite AIV is performed in Europe. The satellite structural qualification is performed with a Structural Qualification Model which is then refurbished to a Cryogenic Qualification Model. The cryogenic tests could be performed in CSL as for Herschel and Planck.

The Protoflight Model will undergo a typical protoflight acceptance test campaign with the tests as described in Table 18-3.

Timely delivery of the elements under the responsibility by JAXA is important and is identified in the schedule. However, if it is considered to refurbish the active coolers which are used on the CQM for the PFM, then this aspect must be revisited. The time between completion of the CQM test campaign and the need date for the cooler integration on the PFM is marginal. Ideally the PFM coolers should be delivered before the CQM test campaign is completed.

The possibility that JAXA might take responsibility for additional/other satellite or PLM level verification activities has not been investigated.

18.6.1 Test Matrix

Test Description	SM	CQM	AVM	PFM
Mech. Interface	R, T			R, T
Mass Property	A, T			A, T
Electr. Performance			T	T
Functional Test			T	T
Propulsion Test			T	T
Thruster Lifetime Test				
Deployment Test	A, T			A, T
Telecom. Link			T	A, T
Alignment	A, T			T
Strength / Load	A, T			T
Shock / Seperation	T			T
Sine Vibration	A, T			T
Modal Survey	A			
Acoustic	T			T
Outgassing		A, I		I (T)
Thermal Balance		T		A, T
Thermal Vacuum		T		T
Micro Vibration		T		
Grounding / Bonding				R, T
Radiation Testing				A
EMC Conductive Interf.		(T)		T
EMC Radiative Interf.				T
DC Magnetic Testing				
RF Testing				T

Abbreviations: I: Inspection,   A: Analysis,   R: Review,   T: Test

Table 18-3: Test Matrix

18.6.2 Test Facilities

Thermal test facilities:

- The baseline at CSL is to develop a dedicated test set-up according to a given specification, i.e. new He-shrouds will need to be developed. The heat dissipation capacity at the specified cryogenic temperatures is a critical parameter for their design
- The highest dimensions so far are the ones used for Herschel in Focal 6.5 (vertical configuration) and for Planck S/W in Focal 5 (Horizontal configuration)
- Both facilities are expected to be available
- For Focal 5 a useful diameter of 4 m - 4.5 m is a first ROM value, i.e. it might just be too small
- For Planck the chamber was divided into a hot zone (LN2 cooled shrouds) and a cold zone (He-shrouds)
- The cold shrouds are generally cooled down to below 20K but not close to 4K. Fine tuning of facility is needed with pre-tests
- The instrument is expected to be tested with stimuli during cryogenic test

<u>Note</u>: The telescope optical verification is still to be defined.
  - o This could be complicated by the horizontal telescope orientation

Other test facilities

- • For the structural and EMC testing all major test centres in Europe, certified according to RD[35], are suitable.

18.6.3 Instrument Level Testing

- • Figure 18-2 shows a reference test sequence for the instrument
  - o The test sequence will be optimised as project develops
  - o "EMC cold" means Conducted EMC in cryogenic
- • Micro-vibration aspects are to be taken into consideration for performance testing and for flight operations:
  - o This aspect requires a design optimisation
  - o The test facility must not introduce disturbances
  - o Analysis of forces exported from cryo-cooler to instrument is required
  - o A Micro-vibration Control Plan is needed.
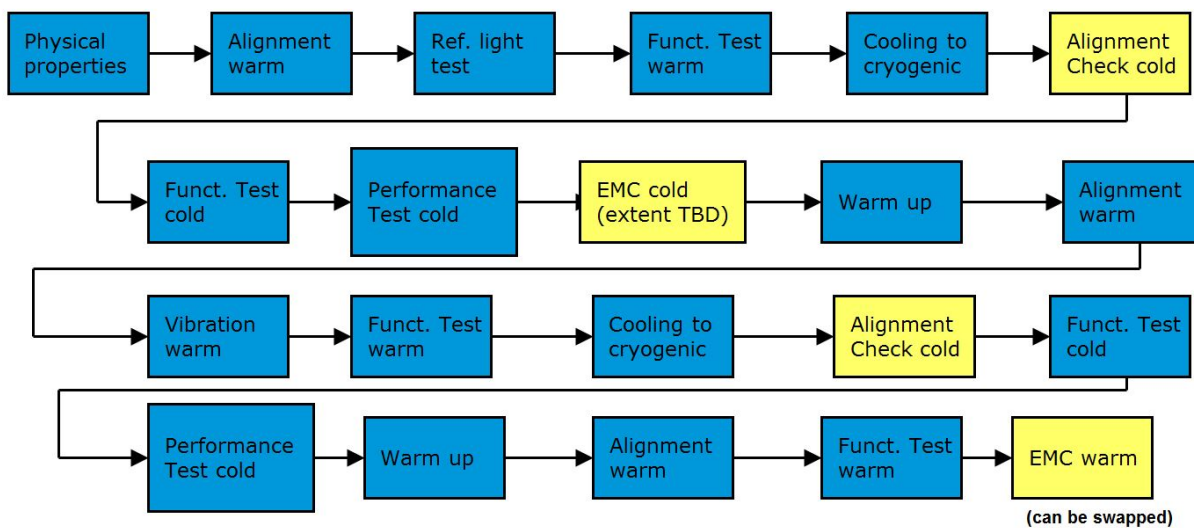
Figure 18-2: Instrument level testing

18.7 Schedule

The Master schedule is shown in Figure 18-3.

- • Phase durations:
  - o Phase A of 24 month (typical are 12 month) to take into account specific requirements of the project
  - o An intermediate phase of 6 months after PRR for Phase B 1 ITT including proposal evaluation and negotiation. Preparation of the ITT might actually

already start at the end of Phase A or in parallel to the PRR, but this is not shown in the schedule

- o Phase B1 of 12 month
- o Another intermediate phase of 9 months after SRR for mission adoption, ITT and Phase B2/C/D proposal evaluation and negotiation
- o Phase B2 of 18 month
- o Phase C & D of 48 month (typical are 30 to 48 months)
- o ESA contingency of 6 month
- o Phase E1 of 3 month

- The above phase durations do not include PRR, SRR, PDR and AR while CDR and QR are included in the Phase C/D bar
- The review durations are based on the average review durations as documented in the ESA Review Portal
- The Instrument schedules need to be aligned with S/C schedule; the FM need date is set to 2.5 years before launch
- The active coolers for CQM integration should be available 6 month before the CQM test campaign
- The active coolers for the PFM are identified to be needed 21 month before the end of Phase C/D assuming that the integration of the PFM starts already in parallel with the CQM test campaign. If refurbished coolers from the CQM should be used on the PFM, they will be available only after QR and feasibility of this needs to be checked
- Technology development activities need to be reviewed to ensure TRL 6 is reached before the phases B2/C/D
- For the telescope models a sub-schedule is shown. The telescope design start is indicated as M1 and M2 design at the beginning of Phase B2
- The manufacturing of the PFM M1 mirror will start right after PDR. It will start before the OSTM M1 mirror because it needs a polishing phase from 14 to 18 month depending on the mirror size. It might be possible to start the M1 procurement already before PDR if the design is sufficiently defined. An 18 month polishing duration is shown in the schedule!
- The OSTM manufacturing is started 4.5 month after the PFM manufacturing. It requires no complete polishing but will include elements for the optical verification
- If instead of the OSTM only an SM is implemented, then it will be necessary to advance the telescope PFM manufacturing to allow its use in the CQM model
- However if instead of the OSTM only an STM is implemented, then the CQM test campaign will be slightly advanced, but it will not allow to verify optical behaviour.

ID	Task Mod	Task Name	Duration	Start	Finish	Predecessors
1		**NG-CryoIrTel**	2930 days	Wed 01/06/16	Tue 24/08/27	
2		Phase A (24 month)	522 days	Wed 01/06/16	Thu 31/05/18	
3		Intermediate Phase (6 month)	132 days	Wed 01/08/18	Thu 31/01/19	12
4		Phase B1 (12 month)	261 days	Fri 01/02/19	Fri 31/01/20	3
5		Intermediate phase (9 month)	197 days	Wed 01/04/20	Thu 31/12/20	13
6		Phase B2 (18 month)	390 days	Fri 01/01/21	Thu 30/06/22	5
7		Phase C/D (48 month)	1043 days	Fri 16/09/22	Tue 15/09/26	14
8		CQM test campaign	195 days	Mon 02/12/24	Fri 29/08/25	29FS+55 days
9		PFM test campaign	195 days	Mon 03/11/25	Fri 31/07/26	33FS+66 days
10		ESA Contingency (6 month)	130 days	Wed 25/11/26	Tue 25/05/27	17
11		Phase E (3 month)	65 days	Wed 26/05/27	Tue 24/08/27	10
12		PRR (2 month)	43 days	Fri 01/06/18	Tue 31/07/18	2
13		SRR (2 month)	42 days	Mon 03/02/20	Tue 31/03/20	4
14		PDR (2.5 month)	55 days	Fri 01/07/22	Thu 15/09/22	6
15		CDR (3 month)	66 days	Fri 15/03/24	Fri 14/06/24	7SS+390 days
16		QR (2.5 month)	53 days	Mon 01/09/25	Wed 12/11/25	8
17		AR (9 weeks)	50 days	Wed 16/09/26	Tue 24/11/26	7
18		Launch	0 days	Tue 24/08/27	Tue 24/08/27	11
19		Instrument TRL6 reached	0 days	Mon 31/12/18	Mon 31/12/18	
20		Mission adoption	0 days	Mon 01/06/20	Mon 01/06/20	13FS+44 days
21		JT-cooler for CQM need date	0 days	Mon 03/06/24	Mon 03/06/24	8SS-130 days
22		JT-cooler for PFM need date	0 days	Wed 18/12/24	Wed 18/12/24	17SF-455 days
23		Instrument FM need date	0 days	Wed 26/02/25	Wed 26/02/25	18SF-650 days
24		**Telescope schedule**	1195 days	Fri 01/01/21	Thu 31/07/25	
25		M1 Design	195 days	Fri 01/01/21	Thu 30/09/21	5
26		M2 Design	130 days	Fri 01/01/21	Thu 01/07/21	25SS
27		M1 OSTM manufuacturing	325 days	Wed 01/02/23	Tue 30/04/24	14FS+98 days
28		M2 OSTM SiC manufacturing	130 days	Thu 16/03/23	Wed 13/09/23	27SS+31 days
29		OSTM integration & alignment	65 days	Mon 17/06/24	Fri 13/09/24	27,15
30		M1 PFM manufacturing	293 days	Fri 16/09/22	Tue 31/10/23	14
31		M1 PFM polishing	391 days	Wed 01/11/23	Wed 30/04/25	30
32		M2 PFM manufacturing, polishing	195 days	Thu 01/08/24	Wed 30/04/25	31FF
33		PFM integration and alignment	66 days	Thu 01/05/25	Thu 31/07/25	31,32

Figure 18-3: Master Schedule

18.8 Summary and Conclusions

- A Model philosophy has been identified
- Suitable thermal test facilities exist, but require adaptation and tuning
- A baseline verification approach has been defined
  - Details, in particular for the optical verification, need still to be refined
  - Potential larger share of JAXA in the verification activities has not been investigated
- Instrument development status
  - SAFARI is expected to achieve TRL 6 in 2018
  - SMI is expected to achieve TRL 6 in 2018 (tbc)
  - FAS (Focal Plane Attitude Sensor) is expected to achieve TRL 6 in 2018
- With a Phase A start mid 2016 and a Phase B2 start early 2021 a launch in the 3rd quarter of 2027 appears feasible.

19 COST

The cost estimate includes costs for the following project elements:

- NG-Cryo spacecraft industrial development and production (Class 4)
- Telescope Module (PLM) development and production (Class 4),
- Project office / AIT / GSE at system and subsystem level (Class 4 & 5)
- Preparations and LEOP
- Cost risk and opportunities
- Mission and science operations *(preliminary assessment to be confirmed respectively by ESOC and ESAC)*
- ESA internal cost
- ESA internal cost-risk margins.

The cost estimate does not include the elements which are assumed to be provided by JAXA in this study, namely:

- Launcher
- Active coolers
- FAS

19.1 Class of Estimate

This cost estimate is classified, according to the ESA Cost Engineering Chart of Services RD[36] as *Class 4* estimate with elements at *Class 5* of a *Major Complexity* project, performed in a *Normal* time frame.

The estimate for the original SPICA concept is classified as *Class 5* estimate (i.e. with declared accuracy +/- 25%) performed in a *compressed* time frame.

19.2 Cost Estimate Methodology

The following methods have been used to derive the point estimates, in descending order of preference:

- Analogy to similar equipment/subsystem/system level costs, taking into account the amount of new development required. In particular relevant recent missions or studies are Herschel, Planck, Euclid and GAIA
- Expert judgment from technical specialists in combination with cost references, in case the amount of new development is extensive
- Parametric models developed in-house by TEC-SYC, in particular equipment CERs, POCoMo v2.0 for detailed PO cost estimate (Mgmt, PA, Eng), the RACE v.10 tool for system level AIT and GSE and the Schedule Model v1.1 for the assessment of the credibility of the schedule. For the estimate of the optics the tool TIW-O v 1.37 has been used after calibration with the Herschel reference
- Equipment and sub-system level in-house developed parametric cost models
- System level parametric cost relationships, based on observed trends for relevant references

- Expert judgment from technical specialists only, if references are not available.

In particular the following table gives in detail the methodology used for each of the different items taken into account within this CDF study:

Cost Element	Estimating method
Payload	Not part of the estimate / assumed to be CFI
Spacecraft HW/SW	Analogy with past mission and estimates (e.g. Herschel, Planck, Euclid, Gaia)
	Equipment level ESA CERs
	RACE 10.3 TEC-SYC Parametric tool
Telescope	TIW-O v 1.37 calibrated with Herschel reference
Cryo-chain	Not part of the estimate, to be provided by JAXA
PO / AIT / GSE	RACE 10.3 TEC-SYC Parametric tool
	POCoMo 2.1 TEC-SYC Parametric tool
Risk Margins	Latin-hypercube simulation using OPERA 2.3 TEC-SYC tool
Launch	Not part of the estimate, to be provided by JAXA
Operations	Analogy with past internal estimates (e.g. Athena)

Table 19-1: Estimating approach

19.3 Main Assumptions

The various requirements and assumptions described in the study documentation apply to the cost estimates. All technical details relevant to the various units have been gathered from the CDF NG-Cryo team, processed by the System team, and reported in the IDM model.

The launch scenario considered for this estimate is the dedicated launch with Japanese launcher H-X (H-II class) from Tanegashima Space Centre in 2027/8.

Risk provisions for schedule delays presented in the risk assessment, account just for typical minor slippages (in the order of few weeks/months) that can be induced by internal or external parties without catastrophic impact.

The industrial set-up presented for the European contribution is based on the so called "3-Tier"or "GEODIS" approach, and is based on the subcontracting of sub-system to external suppliers by running open competition for each subsystem. This allows increased procurement flexibility, with the drawback of increased cost and schedule.

The baseline industrial consortium will then include:

One Prime Contractor, responsible for delivering the whole NG-Cryo spacecraft to ESA/JAXA, and in charge of the Data Handling and the structural subsystem, as well as responsible for the overall assembly integration and verification

One main Sub-Contractor responsible of the development of the Payload Module including the SiC optics, the metering structure and the thermal shields (V-grooves).

Service Module S/S Sub-Contractors, responsible for delivering fully integrated and tested sub-systems: AOCS, EPS, TT&C, Mechanical-Thermal-Propulsion

It is important to underline that in the baseline cost estimate an optimal implementation of this 3-Tier industrial setup has been considered, with limited overlap of activities between the system prime and the various contractors. Nevertheless this approach implies **extremely high risks of cost growth** as will be shown in detail in the following sections presenting the cost-risk assessment.

The development philosophy is based on STM+EFM/AVM+PFM approach, with dedicated tests and EQMs for critical elements such as the cryogenic chain which will require a dedicated "CQM"(Cryo Qualification Model).

To fit the launch in 2028 it could be possible in principle to derive backwards the schedule, leading to significantly overstretched phases, giving more than comfortable margin. Nevertheless this would result in very high costs due to the "marching army" effect, therefore in agreement with the programmatic experts, for the sake of the estimate, realistic durations have been retained:

Phase	Duration [months]
B2	15
CD	48+6
E1	3

Table 19-2: Retained phases duration

The cost estimates are based on economic conditions mid-2014

19.4 Scope of Estimate

The Industrial cost estimate includes:

- Expected industrial price for phase B2,C/D,E1 for Hardware/Software, AIT, GSE and Project Office activities of the platform procurement and payloads integration
- Cost-Risk contingencies at Industry level (CMA, DMM, POE, EPE).

The ESA costs includes:

- ESA Project Team cost
- Cost-Risk contingencies at ESA Project level (CMA, POE)
- Operations setup and implementation, consisting of:
  o Flight Operations Ground Segment (FOS) at ESOC

  o Science Operations Ground Segments (SOC) at ESAC.

The last two have to be considered as preliminary ball-park figures since more accurate estimates will be provided respectively by ESOC and ESAC.

The cost estimate DOES NOT include:

- Cost for phase B1
- Launch Services with H-II x to be provided by JAXA
- Any cost related to the payloads, to be treated by ESA as CFIs from SRON and JAXA.

19.5 NG-Cryo Cost Estimates (Baseline)

19.5.1 Risk Analysis

The methodology used to calculate cost-risk contingencies is described in 0 . The cost estimates are derived as *point* estimates from nominal input parameters, meaning that they represent the best estimate possible with the given information and resources. The Point Estimates do not include any provision for risk of any sort.

A Probability Distribution is added for each cost item as a function of a qualitative risk assessment. The aim is to give a cost assessment based on a *range* between a low and a high value to be expected.

The total probability distribution has four contributors:

- Design Maturity Margin (DMM), to account for cost growth caused by unseen complexities that will be revealed as the design matures into more details. This entropic effect is inherent to the design process and therefore has to be provisioned as part of the core estimate. This contribution is allocated 100% to the industrial price.

- Cost Modelling Accuracy (CMA), to account for uncertainties in the cost estimates. It includes the contribution of the Inherent Quality of the cost Models (IQM) together with contextual factors such as the Degree of Adequacy (DOA) of the cost models used with respect to the specific context of the cost estimate, and the Quality of the Input Values (QIV). Assuming that industry has better and more detailed cost models than ESA because based on internal costs, 25% of the calculated CMA contribution is accounted in the industrial price and 75% in the ESA contingency.

- Project Owned Events (POE), to account for cost risks induced by potential negative events, as well as potential cost reduction opportunities, that may occur or not and that are under the direct responsibility of the Project Manager. POE risks are subject to mitigation measures to be managed at Project level. Without particular indications from the project, the assumed split of the POE contribution is 25% in the industrial price and 75% in the ESA contingency.

- External to Project Events (EPE), to account for cost risks or opportunities that originate from external influences out of the direct control and responsibility of the project manager. The EPE should normally belong 100% to ESA, but ESA regularly transfers the coverage for fair Geo-Return cost impact to Industry. The

EPEs included in the analysis are preliminary provisions only. Depending on the actual constraints put on the program to reach implementation, this amount may turn out to be much higher than accounted for here.

The DMM and CMA cover typically what in industry is identified as Technical Risk. POE and EPE shares cover the expected Management Reserve.

The Point Estimate plus DMM and CMA is identified as Core Estimate and the estimate including all industry share risk contributors is identified as Expected Industrial Price at Contract Award. The value of the contributors is calculated with a Monte Carlo simulation. The total project cost is calculated statistically obtaining a distribution of values. The value extracted and printed in the summary tables represents the 70th percentile value, in other words the value that gives 70% confidence level to complete the project within that given budget.

The value at the 70th percentile is a typical reference point in the compromise between risk and budget containment.

19.5.1.1 Risk Parameters

The following Risk Parameters have been considered for the NG-Cryo spacecraft:

CBS	CMA			DMM	POE
	IQM	DOA	QIV		
	Magn.	Magn.	Magn.	Magn.	Magn.
Subsystem level activities	Medium	Medium	Medium	15%	Low
Primary and Secondary structure	Medium	Medium	Medium	20%	Low
Isolated cryo-coolers panel	Medium	Medium	Medium	20%	Low
Standard Thermal HW	Medium	Medium	Medium	10%	Low
Propulsion Feed Network	Medium	Medium	High	15%	Low
Propellant Tank	High	Medium	High	10%	Low
Thrusters 22N	High	Medium	High	5%	Low
	Medium	Medium	High	20%	Low
Subsystem level activities	Medium	Medium	Medium	20%	Low
Solar Array	Medium	Medium	High	20%	Low
PCDU	High	Medium	High	10%	Low
Battery	High	Medium	High	10%	Low
	Medium	Medium	High	20%	Low
Subsystem level activities	Medium	Medium	Medium	20%	Low
High Gain Antenna	Medium	Medium	Medium	20%	Low
HGA Pointing Mechanism	Medium	Medium	High	15%	Low
HGA HDRM	Medium	Medium	High	5%	Low
APM Electronics	Medium	Medium	High	5%	Low
Low Gain Antennas	Medium	Medium	High	5%	Low
TWTA (incl EPC)	Medium	Medium	High	5%	Low
DST	Medium	Medium	High	5%	Low
RF Distribution Network	Medium	Medium	High	5%	Low

	Medium	Medium	High	20%	Low
Subsystem level activities	Medium	Medium	Medium	20%	Low
AAD (Attitude Anomaly Detector)	High	High	High	5%	Low
Coarse Rate Sensor	High	High	High	5%	Low
Star Tracker	High	High	High	5%	Low
Sun Acquisition Sensors	High	High	High	5%	Low
Reaction Wheels	High	High	High	5%	Low
Gyro	High	High	High	5%	Low
	Medium	Medium	High	5%	Low
Subsystem level activities	Medium	Medium	High	20%	Low
SiC Mirrors manufacturing (incl Brazing)	Medium	Medium	Medium	20%	Low
Mirrors Polishing & Coating	Medium	Medium	Medium	20%	Low
SiC Hexapod	Medium	Medium	Medium	20%	Low
GFRP & CFRP bipods	Medium	Medium	Medium	20%	Low
V-grooves	Medium	Medium	Medium	20%	Low
Telescope Optical bench	Medium	Medium	Medium	20%	Low
Metering structure	Medium	Medium	Medium	20%	Low
Baffle	Medium	Medium	Medium	20%	Low
M2 Refocussing mechanims	Medium	Medium	Medium	20%	Low
Shutter mechanism	Medium	Medium	Medium	10%	Low
Thermal shield	Medium	Medium	Medium	20%	Low
	Medium	Medium	High	20%	Low
CDMU	Medium	High	Medium	10%	Low
Mass Memory	Medium	Medium	Medium	10%	Low
RTU	Medium	Medium	High	10%	Low
	Medium	Medium	High	20%	Low
SVM Harness	Medium	Medium	Medium	20%	Low
PLM Harness	Medium	Medium	Medium	20%	Low
	Medium	Medium	High	20%	Low
Software	Medium	Medium	Medium	20%	Low
ISVV	Medium	Medium	Medium	20%	Low
	Medium	Medium	High	20%	Low
Management & Control	Medium	Medium	High	15%	Low
Product Assurance	Medium	Medium	High	15%	Low
Engineering	Medium	Medium	High	15%	Low
	Medium	Medium	High	15%	Low
Assembly, Integration, Test	Medium	Medium	High	15%	Low
	Medium	Medium	High	15%	Low
Mechanical and Electrical GSE	Medium	Medium	High	15%	Low
	Medium	Medium	High	20%	Low
Phase B2	Medium	Medium	High	20%	Low
PHASE E1	Medium	Medium	High	20%	Low

Table 19-3: Risk Parameters

It is possible to see how the quality of input values is generally medium as typical of this early stages, while in terms of DOA and IQM green "high" settings refer to items estimated through direct reference or appropriate CERs, while yellow "medium" settings are applied to items estimated with extrapolation/adaptation from standard CER.

The DMM as already shown varies between 5% and 25% depending on the development status of the equipment, while POE has been set to *Low* for almost all the items because specific risks have been identified in the risk register of the following Table.

POE		Type	Max	Probability	Split	
	Event Description	Select	impact [%]	%	ESA	Industry
Risks	Unidentified Risk (Max: 10% of Total Point Estimate)	Stochastic	8%	100%	75%	25%
	Schedule Delays Industry (Max: 30% of Total PO Estimate)	Stochastic	30%	90%	25%	75%
	Schedule Delays ESA (Max: 30% of Total PO Estimate)	Stochastic	10%	50%	100%	0%
	Inclusion of more s/s level contractors	Stochastic	30%	50%	75%	25%
Opportunities	Unidentified Opportunities (Max: 5% of Total Point Estimate)	Stochastic	2%	100%	75%	25%
	Experienced Prime	Stochastic	10%	50%	25%	75%
EPE		Type	Max	Probability	Split	
		Select	impact [%]	%	ESA	Industry
Risks	Fair geo-return contingency transferred to industry (Max: 10% of procurements)	Stochastic	6%	100%	0%	100%

Table 19-4: Register based POE and EPE

19.5.2 Industrial Cost

Equipment costs have been estimated mainly with direct recent reference or with equipment level CERs when a delta development was required or references were not available.

Project Office activities have been estimated on the basis of team size assumptions at System and Subsystem level.

GSE, and AIT/V activities are estimated by parametric cost-to-cost models.

The Prime PO activities include the S/C level PO tasks and the S/S design handled by the prime contractor. Please note that the equipment cost includes PO, HW and MAIT of the reference equipment.

The Prime engineering cost is based on an optimistic assumption engineering prime team size with limited activities overlap. It is indeed very likely that to achieve a complete technical capability with regard to the subsystems design, the prime contractor will need to supervise the subcontractors with shadow engineering to contain the risks and to preserve his contract responsibility.

This conservative effort, at Prime level, might lead to a project **cost increase in the order of 30M€,** presented as a standalone cost-risk item at ESA level risk coverage.

19.5.3 Total Cost

Mission and Science Centre and Operations Cost are based on a TEC-SYC model and on recent estimates provided by ESOC and ESAC for similar mission concepts such as Athena L2 (Without need to develop new ground stations). It shall be acknowledged as a provision to be confirmed by ESOC and ESAC. The Project Team and Internal Costs for the Space Segment Development Phase estimate are based on a TEC-SYC model. ESA Internal cost assumptions have been based on the expected values (average) of similar ESA Project team size. It shall be acknowledged as a provision, since it remains a top level figure that does not take into account specific issues.

19.6 NG-Cryo Option 2

19.6.1 Main Assumptions

The main alternative option w.r.t the baseline was a design exercise designed to fully exploit the mass and volume available in the launcher, fitting the largest possible telescope in order to maximise the scientific return of the mission. This design has not

been finalised within this CDF study, with the assessment of the impact only in terms of structure and telescope mirrors.

The service module therefore has not been modified, therefore the estimate for this module can result slightly optimistic (e.g. the need for larger reaction wheels, more thrusters or thicker thrust cone might rise).

With respect to the baseline, the main areas affected are of course the optics (a much larger telescope, with a different construction technique: in fact being the primary mirror elliptical, it is not possible to segment it into many identical segment like in the baseline or in Herschel) and the structure, in order to sustain a larger and heavier telescope (including a larger optical bench).

19.6.2   Risk Analysis

The risk settings are in line with the ones presented in 19.5.1, but applied on a different initial amount and with a slightly higher delays probability due to the larger size of the spacecraft with consequent further increased AIT complexity.

The results of the cost-risk simulation show that on top of high contribution from the Design Maturity (typical of this early stages) it is also possible to identify a large contribution of POEs, due to the complex industrial setup.

19.6.3   Industrial Cost

The same comments of the paragraph 19.5.2 apply, especially the high risk of cost growth linked to the 3-Tier approach.

19.6.4   Total Cost

The estimation of MOC and SOC has not been modified with respect to the baseline.

The main differences are in the HW estimation (both telescope and structure) and consequently on the risk margin and on the system level activities where cost-to-cost models are used.

19.7 Conclusions and Recommendations

The CDF design has presented significant cost optimisation with respect to the original SPICA mission, but still not sufficient to fit within the budget with the current responsibility sharing.

The analysis of the different options shows how it is possible in principle also to get higher scientific return accommodating a much larger telescope, at the cost of several tens of millions of Euro.

Even if a risk provision has been taken into account, the most critical area which may lead to major cost growth is the heavy industrial set-up and related procurement plan together with the Geo-return constraints interesting ESA new member states. A detailed analysis of the procurement plan is recommended before the start of the implementation phase.

In addition of course it is important to keep always in mind the intrinsic risk of inter-agency cooperation scenarios in case these are put in place.

On the other hand it is important to remind that the cost of the operations is a significant slice of the overall programme cost (i.e. more than 20%). Should it be possible to implement a cooperation agreement also in this area (with partial or global operations funding from JAXA) the chances to meet the desired budget cap —at least marginally- would increase dramatically.

This Page Intentionally Blank

20 CONCLUSION

20.1 Satisfaction of Requirements

The study concluded in a feasible mission design compatible with the mission objectives and the requirements presented. This report presents the design outcome.

After an exhaustive telescope architecture trade-off, a mission architecture for the selected telescope design (On-axis Ritchey-Chrétien, with curved image surface) was created in line with the requirements.

The target of fitting the mission into an ESA M-class mission envelope remains a major challenge and requires an increased contribution from JAXA with regards to the study assumptions. Discussions took place between JAXA and ESA after the CDF study, which identified promising solutions (e.g. increased workshare on the PLM and a Japanese contribution to the operations). This scheme, or other potential cooperation schemes, need to be further consolidated in a future study.
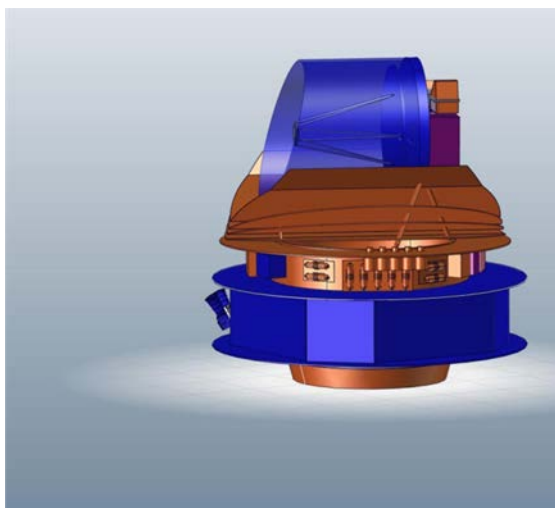
Figure 20-1: Potential future workshare to fit within the M-class envelope for ESA contribution (blue=ESA, brown=JAXA, purple=Member States)

The maximisation of the mirror collecting area within the given S/C configuration and volumetric envelope was the objective of the delta design exercise. Therefore the mirror surface area was increased as much as possible to maximise the science output. The study has shown that a 3m class telescope can be accommodated on top of the V-Groove configuration, but that the resulting thermal load (including instruments) at <6K is not compatible with the existing cooling system from JAXA.

20.2 Further Study Areas

Some areas were identified during the study that require special attention in the future:

- A more detailed share of contributions and responsibilities. Since a physical separation of modules provided by different partners is preferable, this factor might drive the design in the future, since this separation is not possible in the current set-up and design. The high level of system integration of certain sub-

system (e.g. cryogenic chain) will in any case require increased attention. Additionally the share of contributions will impact on the overall cost shares.

- The contribution of micro-vibrations to the pointing stability. The current design foresees the use of standard reaction wheels. With this design, the pointing stability requirement is just met, so any change in requirements, micro-vibration contribution or AOCS design might lead to a potential incompatibility.

- The current thruster configuration does not allow for thrusting in all directions. This implies a heavy penalty on the Δv. Further analysis on the potential plume impingement on the optics and instruments of different thruster configurations to limit the Δv penalty should be carried out.

- The design of the instrument optical bench was not part of this study, since it will heavily depend on the instruments re-design.

- Any update on the configuration and performance of the future H-X launcher should be considered in the design, since the current design is based on the H-II launch vehicle.

- Further areas of cost reduction should be identified to fit within the cost cap.

- The delta design yields more areas of further assessment:
  - An optimisation in telescope design (going completely off-axis?)
  - A reiteration of the structural design to limit the number of bipods
  - A reiteration of the configuration to optimise the available shadow cone and fairing height
  - A reiteration of the PLM thermal design
  - A detailed thermal model of SVM

20.3 Final Considerations

The study demonstrated the feasibility of a joint cryogenic infrared telescope with considerable science output with a 2 m telescope design. It validated the possibility of reusing a considerable part of the Planck SVM equipment, with some additional elements from Herschel or GAIA.

The delta design identified possibilities to increase the collecting area of the telescope and the related system impacts with respect to configuration, structural and thermal design, programmatics, and cost.

The study outcomes provide a good overview of the capabilities of a Planck like passive cooling system for future Scientific Infrared Telescopes, to be considered for future mission calls.

21 REFERENCES

RD[1]   SAFARI Instrument Design Description – SRON-SAFARI-RP-2012-001 Issue 1.0, Dated 30 April 2013

RD[2]   PLATO Consolidated Report on Mission Analysis (CReMA) 1.1, M. Landgraf and F. Renk, Issue 1.2, April 2010

RD[3]   GAIA Consolidated Report on Mission Analysis (CReMA) 4.0 , M. Landgraf and F. Renk, Issue 4.0, April 2010

RD[4]   E-Mail communication, JAXA, Munetaka UENO, 18.11.2014

RD[5]   Euclid System Requirements Document, Euclid Project Team, Issue 1.1, October 2013

RD[6]   http://h2a.mhi.co.jp/en/lineup/h2a/index.html, accessed on 22/01/2015

RD[7]   SPICA Mission Definition Document, JAXA_SPICA_SYS_MDD_001, issue 2.0, 29/09/2010

RD[8]   Criterion to appreciate difficulties of asperical polishing , Conference paper/SPIE 5494-14 – Astronomical Telescopes and Instrumentation, Christian de JEU,Vol 5494, June 2004

RD[9]   Assumed Launcher for SPICA, SPICA Pre-project Team, 10 December 2014

RD[10]   H-IIA User's Manual, JAXA, Second Edition, December 2001

RD[11]   Transducers for sub-micron displacement measurements at cryogenic temperatures, A. Nyilas, Advances in Cryogenic Engineering: Transaction of the International Cryogenic Material Conference –ICMC, 2006.

RD[12]   ASTM E83 - Standard Practice for Verification and Classification of Extensometer Systems, ASTM Standard.

RD[13]   High-precision cryogenic wheel mechanisms for the JWST NIRSPEC instrument, Kai Weidlich, Manfred Fischer, Marc M. Ellenrieder, Torsten Gross, Jean-Christophe Salvignol, Reiner Barho, Christian Neugebauer, Günter Königsreiter, Michael Trunz, Friedrich Müller, Oliver Krause, Spie Advanced Optical and Mechanical Technologies in Telescopes and Instrumentation, 2008.

RD[14]   European Handbook - Electric Motors for Space Applications, Dr. E. Favre, ESMH.401, Issue 4, 2001.

RD[15]   Cryogenic actuator for sub-nanometer positioning, . Huub Janssen, Maurice Teuwena, Ramón Navarrob, Niels Trompb, Eddy Elswijkb, Hiddo Hanenburgb, Spie Modern Technologies in Space- and Ground-based Telescopes and Instrumentation, 2012.

RD[16]   Comparative Study Between Mechanical and Magnetic Planetary Gears, E. Gouda, S. Mezani, L. Baghli, and A. Rezzoug, IEEE, 2010.

RD[17]   Development of a High Temperature Antenna Pointing Mechanism for Bepi-Colombo Planetary Orbiter, Pablo Campo, Aingeru Barrio, Nicolas Puente, Robert Kyle, ESMATS, 2013.

RD[18]   Compliant Parallel Kinematic Machine Design, Compliant Systems Design
         Laboratory, Univ. Michigan, http://csdl.engin.umich.edu/images/kota-cpkm.pdf

RD[19]   ESSB-HB-E-003, ESA Pointing Error Engineering Handbook, 19 July 2011

RD[20]   ECSS-E-ST-60-10C Control Performance, 15 November 2008

RD[21]   Herschel/Planck System Design Report for CDR; TAS-I, July 2004.

RD[22]   Herschel/Planck Reaction Control Subsystem (RCS) Design Report. EADS-
         Astrium, April 2008.

RD[23]   CCSDS 131.0-B-2, CCSDS Recommended Standard for TM Synchronization and
         Channel Coding, Recommended Standard, Issue 2, August 2011,
         ttp://public.ccsds.org/publications/archive/131x0b2ec1.pdf

RD[24]   CCSDS 130.1-G-2, TM Synchronization and channel coding – Summary of
         Concept and Rationale, Informational Report, November 2012,
         http://public.ccsds.org/publications/archive/130x1g2.pdf

RD[25]   ECSS-E-ST-50-05C Rev. 1. Space engineering. Radio frequency and modulation.
         6th March 2006

RD[26]   CCSDS 413.0-G-2, Bandwidth-Efficient Modulations, Summary of Definition,
         Implementation and Performance, Informational Report, October 2009,
         http://public.ccsds.org/publications/archive/413x0g2.pdf

RD[27]   Performance of GMSK for Telemetry and PN Ranging under realistic conditions,
         6th International Workshop on TT&C Systems, ESA-ESOC, 10-13 September 2014

RD[28]   Preliminary Assessment of potential X/K alternatives for PLATO for TTC and
         science data communications, S. Marti, R. Timm, Technical Note, July 2014

RD[29]   CCSDS File Delivery Protocol (CFDP) CCSDS 727.0-B-4 Blue Book January
         2007

RD[30]   Space Project Management, Risk Management, ECSS-M-ST-80C, 31 July 2008.

RD[31]   Ross, R.G. , Cryocooler Reliability and Redundancy Considerations for long-life
         Space Missions, Jet Propulsion Laboratory, California Institute of Technology,
         Pasadena, CA 91109

RD[32]   ECSS-E-ST-10-02C, "European Cooperation for Space Standardisation, Space
         Engineering, Verification", 6 March 2009.
         http://www.ecss.nl

RD[33]   ECSS- E-ST-10-03C, "European Cooperation for Space Standardisation, Space
         Engineering, Testing", 1 June 2012.
         http://www.ecss.nl

RD[34]   "Guidelines for the use of TRLs in ESA programmes", ESSB-HB-E-002, Issue 1,
         Revision 0, 21 August 2013.

RD[35]   ECSS-Q-ST-20-07, "Quality and safety assurance for space test", 1 October2014

RD[36]   TEC-SYC/12/2009/GRE/HJ - ESA Cost Engineering Charter of Services

         TEC-SYC/GRE/SA/2005/021 - TEC-SYC Cost Risk Assessment Procedure

22 ACRONYMS

Acronym	Definition
AAD	Attitude Anomaly Detector
AGN	Active Galactic Nuclei
AIT/V	Assembly, Integration and Test/Verification
AIV	Assembly, Integration and Verification
AIVT	Assembly, Integration, Verification and Test
AKE	Absolute Knowledge Error
AOCS	Attitude and Orbit Control Subsystem
APE	Absolute Performance Error
APM	Antenna Pointing Mechanism
ARAD	Attitude Rate and Anomaly Detection
AVM	Avionics Verification Model
BFL	Back Focal Length
BOL	Beginning of life
BPSK	Binary Phase Shift Keying
C&DH	Command and Data Handling
CaC	Cost at Completion
Can	Controller Area Network
CCSDS	The Consultative Committee for Space Data Systems
CD	Drag Coefficient
CDMU	Command and Data Management Unit
CDR	Critical Design Review
CER	Cost Estimating Relationship
CFDP	CCSDS File Delivery Protocol
CFI	Customer Furnished Instrument
CFRP	Carbon Fibre Reinforced Polymers
CMA	Cost Model Accuracy
CoG	Centre of Gravity
CoM	Centre of Mass
CQM	Cryogenic Qualification Model

Acronym	Definition
CRS	Coarse Rate Sensor
CSL	Centre Spatiale Liège
CTE	Coefficient of Thermal Expansion
DHS	Data Handling Subsystem
DMM	Design Maturity Margin
DOA	Degree of Adequacy of the Cost model
DoF	Degrees of Freedom
EBB	Elegant Breadboard
ECSS	European Cooperation on Space Standardisation
EFL	Effective Focal Length
EFM	Electrical Functional Model
EM	Engineering Model
EMC	Electromagnetic Compatibility
EMI	Electromagnetic Interference
EoL	End of Life
EPC	Electric Power Conditioner
EPD	Entrance Pupil Diameter
EPE	External Project Events
EPS	Electrical Power Subsystem
EQM	Engineering and Qualification Model
ESA	European Space Agency
ESTRACK	European Satellite TRACKing network
EVV	Evacuation Valve
FAS	Fine Attitude Sensor
FDIR	Failure Detection, Isolation and Recovery
FEM	Finite Element Model
FIR	SAFARI Instrument
FM	Flight Model
FOP-SW	Flight Operations Software
FOS	Flight Operations Segment
FoV	Field of View

Acronym	Definition
FTS	Fourier Transform Spectrometer
G/S	Ground Station
GEO	Geosynchronous Equatorial Orbit
GFRP	Glass Fibre Reinforced Polymers
GMSK	Gaussian Minimum Shift Keying
GNC	Guidance, Navigations and Control
GS	Ground Station
GSE	Ground Support Equipment
GSP	General Studies Program
GYR	Gyroscope
HD	Hydrogen-Deuterium
HDO	Hydrogen-Deuterium Oxide (semi-heavy water)
HDRM	Hold-Down and Release Mechanism
HEO	Highly elliptical orbit
HGA	High Gain Antenna
HPC	High Power Command
HW	Hardware
i.a.w.	In accordance with
ICE	Independent Cost Estimate
IEEE	Institute of Electrical and Electronic Engineers
INIT	Initialisation Mode
IOB	Instrument Optical Bench
IQM	Inherent Quality of the cost Model
Isp	Specific Impulse
ITAR	International Traffic in Arms Regulations
JAXA	Japan Aerospace Exploration Agency
JT cooler	Joule-Thomson cooler
LDPC	Low Density Parity Check
LEOP	Launch and Early Orbit Phase
LGA	Low Gain Antenna
LOS	Line Of Sight

Acronym	Definition
LV	Launch Vehicle
LVDT	Linear Variable Differential Transducer
M1	Primary Mirror
M2	Secondary Mirror
MAIT	Manufacturing, Assembling Integration and Testing
MDR	Mission Definition Review
MINT	Mechanical INTegration parts
MIP	Movable Instrument Platform
MLI	Multi-Layered Insulation
MMA	Movable Mirror Assembly
MOC	Mission Operations Centre
MPE	Mean Performance Error
MPS	Micro Propulsion System
N/A	Not Applicable
N_2	Nitrogen gas
N_2H_4	Hydrazine
OBC	On Board Computer
OBCP	On Board Control Procedures
OCM	Orbit Control Mode
OQPSK	Offset Quadrature Phase Shift Keying
OSTM	Opto-mechanical Structural Thermal Model
PA	Product Assurance
PCDU	Power conditioning and distribution unit
PCU	Power Control Unit
PDR	Preliminary Design Review
PEPS	ESA TEC-EP power system modelling and simulation tool
PF	Platform
PFM	Proto-Flight Model
PLM	Payload Module
PMF	Pulse mode Firing
PN	Pseudo Noise

Acronym	Definition
POE	Project Owned Events
PRR	Preliminary Requirements Review
PSK	Phase Shift Keying
PVA	Photovoltaic assembly (solar cells + cover glass + interconnections and diodes)
QIV	Quality of the Input Values
QM	Qualification Model
QR	Qualification Review
R C	Ritchey-Chretien
RCS	Reaction Control Subsystem
RF	Radio Frequency
RFDU	Radio Frequency Distribution Unit
RMS	Root Mean Square
RPE	Relative Performance Error
RSS	Reed Solomon System
RTG	Radio-isotope Thermoelectric Generator
RTU	Remote Terminal Unit
RWA	Reaction Wheel Assembly
RWL	Reaction Wheels
S/C	Spacecraft
S^{3}R	Sequential switching shunt regulator (solar array power regulator)
SA	Solar Array
SAFARI	SPICA Far-Infrared Instrument
SAM	Sun Acquisition Mode
SAS	Sun Acquisition Sensor
SCC	Spacecraft Module
SCM	Science Control Mode
SED	Spin and Ejection Device
SEL2	Sun-Earth Libration Point 2
SFT	System Functional Test
SIA	SPICA Instrument Assembly
SiC	Silicon Carbide

Acronym	Definition
SKA	Square Kilometre Array
SM	Structural Model
SM	Survival Mode
SMBH	Super Massive Black Holes
SMI	SPICA Mid-Infrared Instrument
SNR	Signal-to-Noise-Ratio
SOC	System On Chip
SPICA	SPace Infrared Telescope for Cosmology and Astrophysics
SPW	SpaceWire
SR	Space Research
SRR	System Requirements Review
SRRC	Square-Root Raised Cosine
SSCE	Sun-S/C-Earth angle
SSF	Steady-state Firing
SSMM	Solid State Mass Memory
SSPA	Solid State Power Amplifier
STA	Space Telescope Assembly
STB	Stand-By Mode
STM	Structural Thermal Model
STR	Star Tracker
SVM	Service Module
SVT	System Validation Test
SW	Software
tbc	To be confirmed
tbd	To be defined
TC	TeleCommand
TCM	Transfer Correction Manoeuvre
TES	Transition Edge Sensor
TMA	Tri-Mirror Anastigmat
TOB	Telescope Optical Bench
ToO	Target of Opportunity

Acronym	Definition
TRL	Technology Readiness Level
TRP	Technology Readiness Program
TT&C	Telemetry, Tracking and Command
TWTA	Travelling Wave Tube Amplifier
UV	Ultra Violet
WFE	Wave Front Error

This Page Intentionally Blank

A MISSION AND S/C REQUIREMENTS

ID	Requirement	Note
1. Mission requirements		
1.1 Launch vehicle, site and date		
MR-MIS-010	The S/C shall be compatible with a H-IIA-204 launch from the Tanegashima Space Centre (JP) using the 5S fairing and the 2360SA-equivalent adapter.	Fairing useful diameter is 4600 mm. H-III (new launcher) should also be available.
MR-MIS-020	The mission shall be compatible with a launch date in 2027/2028.	TBC, M5 programmatic constraint.
1.2 Injection, transfer and operational orbits		
MR-MIS-030	The launcher injection orbit shall be an eclipse free (Earth and Moon) direct transfer trajectory to the Sun-Earth L2 point.	
MR-MIS-040	The science operations orbit shall be an eclipse free (Earth and Moon) orbit around the Sun-Earth L2 point.	The exact shape and size of the orbit are to be optimised, taking into account: - the sky accessibility requirements - no eclipses - the ΔV requirements (L2 orbit injection, monthly orbit maintenance and decommissioning) - the Earth-S/C-Sun angle for the design of the power and communications subsystems
1.3 Mission phases		
MR-MIS-050	The mission phases shall be defined as follows, chronologically following each other unless specified otherwise: - 0 Pre-launch Phase (Launch Campaign) - 1 Launch and Early Operations Phase (LEOP) - 2 Transfer Phase - 3 Commissioning Phase - 4 Instrument Performance Verification and Science Demonstration Phase - 5 Nominal Science Operations Phase - 6 Extended Science Operations Phase - 7 Decommissioning Phase - 8 Post-Operations Phase	
1.3.1 Pre-launch phase		
MR-MIS-060	Prior to lift-off the spacecraft shall be in an electrically active state and shall be able to perform the following tasks: - power on/off only via umbilical and without physical access to the spacecraft - receive telecommands - handle telemetry packets - perform on-board monitoring functions - enter launch mode configuration	

1.3.2 LEOP phase		
MR-MIS-070	The LEOP phase shall be from launch to the end of the 1st manoeuvre for launcher dispersion correction.	
MR-MIS-080	From LV separation until Sun acquisition, the S/C shall be in a power mode using on-board batteries with all instruments switched off.	
MR-MIS-090	The S/C shall autonomously detect separation from the LV.	
MR-MIS-100	After separation from the LV, the S/C shall autonomously activate one of its transmitting channels and its 2 receiving channels to allow the ground station network to establish the first contact.	
MR-MIS-110	After separation from the LV, the S/C shall autonomously re-orient itself to a safe attitude in order to: - Start generating Solar power and terminate battery discharge - Protect the payload from the Sun - Allow the ESA ground station network to establish the first contact as specified in MR-MIS-100	This manoeuvre is an attitude correction manoeuvre, not the 1st orbital correction manoeuvre defined in MR-MIS-070.
1.3.3 Transfer, commissioning and performance verification phases		
MR-MIS-120	The transfer phase shall be from the end of LEOP to the insertion into the science operations orbit as defined in MR-MIS-040.	
MR-MIS-130	The commissioning phase can be started during the transfer phase, and shall be completed within 3 months of the LV – S/C separation.	
MR-MIS-140	During the commissioning phase, check-out of the spacecraft functions and verification of all subsystems' performances shall be performed.	
MR-MIS-150	The instrument performance verification and science demonstration phase can be started during the transfer phase, and shall be completed within 8 months of the LV – S/C separation.	After launch, a 6 months (TBC, to be minimised) period is required for the telescope and payload to reach their operational cryogenic temperature. This phase can only be completed after this is achieved.
MR-MIS-160	During the instrument performance verification and science demonstration phase, check-out and verification of the instruments' performances shall be performed.	
MR-MIS-170	Until completion of the instrument performance verification and science demonstration phase, the S/C design and operations shall ensure the direct and reflected Sun light does not cause any irreversible damage to the S/C.	This is particularly important during the launch ascent and during the initial launcher dispersion and perigee velocity correction manoeuvres, when the attitude of the S/C might result in temporary Sun (direct or indirect) illumination on critical

		components, especially at PLM level (i.e. optics, focal plane detectors, thermal hardware etc.). Indirect Sun light could result from reflections on e.g. the S/C baffles or mirrors, or even the Earth. This requirement results in S/C design constraints (e.g. Sun avoidance angles, baffles, deployable/ejectable covers etc.) and/or launch window constraints.
MR-MIS-180	The LEOP and transfer phases shall be completed within 3 months of the LV – S/C separation.	
1.3.4 Science operation phases		
MR-MIS-190	The nominal science operations phase shall start from the end of the instrument performance verification and science demonstration phase.	
MR-MIS-200	The extended science operations phase shall start from the end of the nominal science operation phase.	
MR-MIS-210	The post-operations phase shall start from the end of the extended science operations phase.	
1.3.5 Decommissioning		
MR-MIS-220	The decommissioning phase shall ensure compliance with the Space Debris Mitigation requirements ("ESA/ADMIN/IPOL(2014)2" and "ESA/ADMIN/IPOL(2008)2").	
1.4 Mission lifetime		
MR-MIS-230	The nominal mission lifetime, from LV (upper stage) separation to the end of the nominal science operations phase, shall have a duration of at least 3 years.	According to MR-MIS-150 and 190, this means the nominal science operations phase has a duration of at last 2 years and 4 months.
MR-MIS-240	The extended mission lifetime (the extended science operations phase) shall have a duration of at least 2 years.	
MR-MIS-250	During the nominal science operations phase, all science performance requirements shall be fully met and include all specified margins.	This requirement takes over after MR-MIS-170.
MG-MIS-260	During the extended science operations phase, all science performance requirements should be fully met, without margins.	
MR-MIS-270	All S/C consumables and radiation-sensitive units shall be sized to last from launch till the end of the extended mission lifetime.	
MR-MIS-280	All S/C units shall be designed to include a ground lifetime margin of at least 1 year.	These margins account for e.g. possible launch delays or late delivery of specific units.
MR-MIS-290	The ground lifetime of units which degrade with usage of storage shall include a 50% margin in addition to MR-MIS-280.	

1.5 Delta-V		
MR-MIS-300	The following geometrical ΔVs shall apply: (see table in last spreadsheet). Additional budgets shall include ΔVs for reaction wheels off-loading and safe modes.	
1.6 Operations and modes		
MR-MIS-310	The S/C shall be compatible with the operational space environment (includes Solar flux, radiation, plasmas and micro-meteoroids).	Environment specification document to be written on a later phase.
MR-MIS-320	During all operational modes, the spacecraft shall autonomously avoid "un-safe" attitudes, defined as attitudes where one of the following conditions exists: - Insufficient power is generated for S/C survival - Spacecraft thermal control is compromised - The payload (optics and focal plane detectors) are compromised - Other identified attitudes that impair the S/C and the nominal science operation plan	
MR-MIS-330	**Safe mode:** After a major on-board anomaly or failure from which an autonomous recovery is not possible (see MR-SYS-200), or a violation of the attitude constraints defined in MR-PERF-010 to 030, the S/C shall enter and maintain a safe mode that: - keeps only the minimum number of units that are necessary to the S/C survival switched on - allows a continuous and sufficient supply of power for S/C survival - allows communication with Earth - ensures a survivable thermal environment - prevents damage to the payload (telescope, instruments and any active cryo-cooler)	
MR-MIS-340	**Stand-by mode:** The S/C shall enter / remain in a stand-by mode under the following conditions: - if successive ground contacts are missed during the period defined in MR-OGS-140, or - if minor anomalies are encountered which do not require entering into safe mode as defined in MR-MIS-330 This mode shall ensure: - the same constraints defined in MR-MIS-330 are applied	By keeping the cryo-coolers switched on, this mode optimises the observation efficiency by avoiding unecessary safe modes.

	- any active coolers remain switched on - the attitude constraints defined in MR-PERF-010 to 030 are kept	
MR-MIS-350	**Decontamination mode:** A decontamination mode shall ensure out-gassing and moisture release do not degrade the mission performance at any point during the mission.	This mode is necessary during LEOP and transfer to L2 to prevent contamination of the telescope and focal plane detectors during the initial out-gassing and moisture release of the S/C, but can also be re-used later during the mission lifetime to clean these units from any contaminants that might have accumulated since.
MR-MIS-360	**Coarse pointing mode:** A coarse pointing mode (i.e. without the FAS in the AOCS control loop) shall allow to transition to the Fine pointing mode.	
MR-MIS-370	**Fine pointing mode:** A fine pointing mode (i.e. with the FAS in the AOCS control loop) shall ensure all pointing errors between the science target(s) and all instruments are compliant with the needs imposed by MR-PERF-110 and 120.	
MR-MIS-380	**Scans:** In fine pointing mode (MR-MIS-370), the S/C shall be able to perform the following steps/scans/trackings: (see table in last spreadsheet)	
MR-MIS-390	During the modes defined in MR-MIS-380, the S/C attitude data shall be stored on-board and downloaded to ground for image re-construction.	
2. Science performance requirements		
2.1 Observation requirements		
MR-PERF-010	During phases 4, 5 and 6, the S/C shall have the ability to make a full 360 degree rotation around X_{tel} and observe a science target from any of those attitudes.	
MR-PERF-020	During phases 4, 5 and 6, the S/C shall have the ability to make a 30 degree rotation around Y_{tel} and observe a science target from any of those attitudes.	
MR-PERF-030	During phases 4, 5 and 6, the S/C shall have the ability to make a 2 degree rotation around Z_{tel} and observe a science target from any of those attitudes.	This is not a science need but an AOCS safety margin.
MR-PERF-040	The overall observing efficiency of the S/C during science operation phases 5 and 6 shall be $\geq 85\%$. Instrument calibration shall not be deducated from this budget.	
MR-PERF-050	The S/C shall be able to slew between science targets at a rate of (TBC), including settling time.	This depends on the duration and frequency of observations and their relative angular separation, and impacts the observation efficiency budget. See reference observation plan provided by

		SRON.

2.2 Payload performance requirements		
MR-PERF-060	The S/C shall be able to accommodate and operate the following instruments: - the SAFARI FIR instrument - the SMI MIR instrument - the FAS, to meet the needs of the Fine pointing mode (MR-MIS-370)	SAFARI: SPICA Far-IR Instrument SMI: SPICA Mid-IR Instrument FAS: Focal plane Attitude Sensor, i.e. FGS.
MR-PERF-070	The telescope and instrument fore-optics shall cover the 3μm to 210μm wavelength range.	SAFARI and SMI are both above 20 μm. Lower wavelengths are for the FAS.
MR-PERF-080	The telescope FoV (defined as a circular radius) shall be > 15 arcmin.	
MG-PERF-090	The telescope FoV (defined as a circular radius) should be > 18 arcmin.	
MR-PERF-100	The telescope and instrument fore-optics figure of merit, defined by the product of the effective area and the throughput (A_{eff} x η), shall be ≥ (see table in last spreadsheet) over the entire wavelength range defined in MR-PERF-070 and over the entire FoV defined in MR-PERF-080.	
MR-PERF-110	The telescope and instrument fore-optics shall be diffraction limited at all wavelengths above λ=20 μm within the entire FoV defined in MR-PERF-080.	For optimal spatial resolution.
MR-PERF-120	Background radiation and noise contributions outside of the SAFARI and SMI instruments shall be lower than the astronomical limiting source flux density.	I.e. the complete system should be limited by the astronomical photon noise limit or the instruments noise. This requirement will drive: - the PLM thermal design requirements - the pointing stability requirements - the straylight requirements - etc. These derived requirements are defined at subsystem level.
3. Design requirements		
3.1 Standards		
MR-SYS-010	The SI international system of units shall be used. Radians, degrees, arcmins and arcseconds are acceptable as angular units. All (sub)multiples by factors of 10 of any of the aforementioned units are also acceptable.	
MR-SYS-020	The "Margin philosophy for science assessment studies" shall be applied to the CDF and Phase A/B1 study.	
MR-SYS-030	The list of ESA approved standards, including approved ECSS standards, shall apply throughout the study. Tailoring of specific standards is possible and shall be subject to formal approval by ESA on a case-by-case basis with a	

	detailed rationale.	
3.2 Coordinate systems		
MR-SYS-040	All reference coordinate frames shall be right-handed orthonormal triads.	
MR-SYS-050	The S/C reference frame shall be defined by 3 orthonormal axes ($X_{S/C}$, $Y_{S/C}$, $Z_{S/C}$), with an origin at the geometrical centre of the separation plane between the LV adapter and the S/C.	
MR-SYS-060	The longitudinal axis $+Z_{S/C}$ (roll axis) shall be coincident with the LV symmetry axis, and pointing in the positive direction from the LV − S/C separation plane up to the tip of the S/C.	
MR-SYS-070	The $+X_{S/C}$ axis shall be defined as the orthonormal projection of the telescope pointing axis $+Z_{tel}$ on the LV - S/C separation plane.	These 2 axes are not necessarily parallel to each other, e.g. in case the telescope is not accommodated perfectly "horizontally" but pointed with a small contribution along the $Z_{S/C}$ axis. On the other hand, this is undefined if the telescope is accommodated perfectly vertically.
MR-SYS-080	The $+Y_{S/C}$ axis shall be defined to complete the right-handed orthonormal triad.	
MR-SYS-090	The telescope reference frame shall be defined by 3 orthonormal axes (X_{tel}, Y_{tel}, Z_{tel}), with an origin at the vertex of the telescope's primary mirror.	This is a fictitious point in case of an off-axis telescope.
MR-SYS-100	The telescope's pointing axis $+Z_{tel}$ shall be defined from the reference frame's origin, in the positive direction going towards the centre of the targeted FoV.	
MR-SYS-110	The $+X_{tel}$ axis shall be defined from the reference frame's origin towards the centre of the S/Cs Sun facing side (average Sun direction), projected onto the plane orthogonal to $+Z_{tel}$.	
MR-SYS-120	The $+Y_{tel}$ axis shall be defined to complete the right-handed orthonormal triad.	
3.3 Mass		
MR-SYS-130	The total S/C wet mass (including all margins specified in MR-SYS-020 but excluding the LV adapter) shall be smaller than the LV performance of 3700 kg.	
3.4 Reliability and fault management		
MR-SYS-140	The overall reliability of the mission, from after LV separation till the end of the nominal lifetime, shall be ≥ 85%.	
MR-SYS-150	Single point failures with a severity of catastrophic or critical (as defined in ECSS-Q-ST-30C) shall be eliminated or	

	prevented by design.	
MR-SYS-160	Retention in the design of single point failures of any severity rating is subject to formal approval by ESA on a case-by-case basis with a detailed retention rationale.	
MR-SYS-170	A failure of one component (unit level) shall not cause failure of, or damage to, another component or subsystem.	
MR-SYS-180	The failure of an instrument channel shall not lead to a safe mode of the S/C.	
MR-SYS-190	Any hazardous situation, which will not cause immediate loss of but may develop into the loss of the S/C or instrument, shall be prevented by design or protected against.	
MR-SYS-200	The design shall allow the identification of on-board failures and their recovery by autonomously switching to a redundant functional path. Where this can be accomplished without risk to spacecraft and instrument safety, such switching shall enable the continuity of the mission timeline and performance.	This means the design of fault management systems shall intrinsically be fail-safe.
MR-SYS-210	Where redundancy is employed, the design shall allow operation and verification of the redundant item/function, independent of nominal use.	
MR-SYS-220	For design and analysis purposes, an average of 3 safe mode events of 3 days (plus recovery time) each per year shall be considered.	
4. Operations and ground segment		
4.1 Operations		
MR-OGS-010	The S/C design shall enable operational control by the ground segment during all mission phases and modes in both nominal and contingency situations.	
4.2 MOC		
MR-OGS-020	The mission shall have a single MOC. For the purpose of the CDF, ESOC shall be assumed as the MOC.	JAXA MOC also to be considered.
MR-OGS-030	The MOC shall be responsible for the spacecraft operations after launch, including mission planning, spacecraft monitoring and control, and orbit and attitude determination and control.	
MR-OGS-040	The MOC shall perform all communications with the S/C through the ground stations.	
MR-OGS-050	Orbit determination shall be conducted with the required accuracy to perform all orbital control manoeuvres throughout all mission phases.	

MR-OGS-060	The MOC shall provide all telemetry (science and housekeeping) to the SOC.	
4.3 SOC		
MR-OGS-070	The mission shall have a single SOC. For the purpose of the CDF, ESAC shall be assumed as the SOC.	JAXA SOC also to be considered.
4.4 Ground stations		
MR-OGS-080	All aspects of the mission shall be compatible with the network of ESA and JAXA ground stations.	
4.5 Spacecraft autonomy		
MR-OGS-090	The S/C shall support autonomous (without ground contact) operations according to a mission timeline uploaded from ground.	
MR-OGS-100	The S/C shall support interruption of the mission timeline and re-scheduling of planned events by ground command.	
MR-OGS-110	During LEOP, the S/C shall be able to operate nominally without ground contact for at least 12 hours.	
MR-OGS-120	In all mission phases after LEOP, the S/C shall be able to operate nominally without ground contact for at least 3 days, without any loss of science or housekeeping data.	
MR-OGS-130	In all mission phases after LEOP, the S/C shall be able to survive without ground contact for at least 7 days.	
MR-OGS-140	During the science operations phase, the ground contact duration and frequency shall be 8 hours every day.	
5. Programmatic		
5.1 Technology readiness		
MR-PROG-010	The ISO TRL definitions are applicable.	
MR-PROG-020	All mission related units (LV, space and ground segment) shall have a ISO TRL 6 by the end of the definition phase (Phase A/B1).	
MR-PROG-030	The mission design shall ensure a low development risk for phases B2 and beyond.	
5.2 Schedule		
MR-PROG-040	The flight units of the instruments shall be delivered at least 30 months before the start of the launch campaign.	
5.3 Cost		
MR-PROG-050	The mission shall be compatible with the ESA M5 CaC boundary.	The international contribution is to be defined.

Table A-1: Mission requirements

ID	Requirement	Parent requirement	Note
1. Telescope and instrument fore-optics subsystem specifications			
OR-010	MR-PERF-070	MR-PERF-070	
OR-020	MR-PERF-080	MR-PERF-080	
OG-030	MG-PERF-090	MG-PERF-090	
OR-040	MR-PERF-100	MR-PERF-100	
OR-050	The telescope and instrument fore-optics shall have a WFE ≤ 1.43 μm rms.	MR-PERF-110	Marechal criterion: 20/14.
OR-060	The telescope and instrument fore-optics mirrors' roughness shall be ≤ 143 nm rms.	MR-PERF-110	1) Allocation: 1/10th of OR-050 2) More stringent requirement from FAS (30 nm rms) to be discussed.
OR-070	Stray-light (in- and out of field) levels shall be negligible compared to the astronomical noise floor.	MR-PERF-120	
OR-080	The telescope shall have a mechanism on the secondary mirror for in-orbit adjustment of the focus and the alignment (3 DoF TBC).	MR-PERF-110	3 DoF to be confirmed by further analysis
2. Thermal subsystem specifications			
TR-010	All elements in direct view (or through reflections on mirror surfaces) of the instruments' focal plane detectors shall be cooled to ≤ 6 K.	MR-PERF-120	To limit the thermal background. Includes the complete telescope assembly and baffles. See figure in last spreadsheet.
TR-020	The PLM thermal design shall take into account the heat load from the instruments.	MR-PERF-060	
3. AOCS subsystem specifications			
AR-010	All pointing errors shall follow the temporal interpretation, as defined in "ECSS-E-ST-60-10C".	MR-SYS-030	
AR-020	During the coarse pointing mode, the pointing errors for all instruments shall be (3σ, 0 to peak): - Coarse APE ≤ 30" - Coarse RPE ≤ 3" over 20 min and ≤ 0.5" over 2 sec	MR-MIS-360	
AR-030	During the fine pointing mode, the pointing errors for all instruments shall be (3σ, 0 to peak): - Fine APE ≤ 0.8" (worst case from SMI-Spec) - Fine AKE ≤ 0.03" (worst case from SAFARI)	MR-MIS-370	Around both Xtel and Ytel

	- Fine RPE ≤ see figure in last spreadsheet (worst case from SAFARI)		
4. FAS subsystem specifications			
FR-010	FAS shall provide the attitude estimate to the AOCS control loop with a random error better than 0.036" and bias error of better than 0.5" (3σ) at a frequency of 0.2 Hz.	AR-030	JAXA specification for a 2m class telescope
5. Stray-light requirements			
SR-010	Straylight from out of field astronomical sources scattered onto mirror surfaces into the focal plane instruments shall be ≤ (see table in last spreadsheet).	OR-070	Straylight from in-field S/C thermal background sources is negligible when considering TR-010.

Table A-2: S/C requirements